NOTICE

The quality of this microform is heavily dependent upon the quality of the original thesis submitted for microfilming. Every effort has been made to ensure the highest quality of reproduction possible.

If pages are missing, contact the university which granted the degree.

Some pages may have indistinct print especially if the original pages were typed with a poor typewriter ribbon or if the university sent us an inferior photocopy.

Reproduction in full or in part of this microform is governed by the Canadian Copyright Act, R.S.C. 1970, c. C-30, and subsequent amendments.

AVIS

La qualité de cette microforme dépend grandement de la qualité de la thèse soumise au microfilmage. Nous avons tout fait pour assurer une qualité supérieure de reproduction.

S'il manque des pages, veuillez communiquer avec l'université qui a conféré le grade.

La qualité d'impression de certaines pages peut laisser à désirer, surtout si les pages originales ont été dactylographiées à l'aide d'un ruban usé ou si l'université nous a fait parvenir une photocopie de qualité inférieure.

La reproduction, même partielle, de cette microforme est soumise à la Loi canadienne sur le droit d'auteur, SRC 1970, c. C-30, et ses amendements subséquents.

THE UNIVERSITY OF ALBERTA

HYDROTHERMAL ZONING IN THE KENO HILL Ag-Pb-Zn VEIN SYSTEM: A STUDY IN STRUCTURAL GEOLOGY, MINERALOGY, FLUID INCLUSIONS, AND STABLE ISOTOPE GEOCHEMISTRY.

BY

JOSEPH VINCENT GREGORY LYNCH

A THESIS

SUBMITTED TO THE FACULTY OF GRADUATE STUDIES AND RESEARCH

IN PARTIAL FULFILMENT OF THE REQUIREMENTS FOR THE DEGREE OF

DOCTOR OF PHILOSOPHY

DEPARTMENT OF GEOLOGY

EDMONTON, ALBERTA

Spring, 1989

ISBN 0-315-52849-4

THE UNIVERSITY OF ALBERTA

RELEASE FORM

NAME OF AUTHOR: J. V. Gregory Lynch

TITLE OF THESIS: HYDROTHERMAL ZONING IN THE KENO HILL Ag-Pb-Zn VEIN SYSTEM: A STUDY IN STRUCTURAL GEOLOGY, MINERALOGY, FLUID INCLUSIONS, AND STABLE ISOTOPE GEOCHEMISTRY.

DEGREE: DOCTOR OF PHILOSOPHY

YEAR THIS DEGREE GRANTED: Spring, 1989

Permission is hereby granted to THE UNIVERSITY OF ALBERTA LIBRARY to reproduce single copies of this thesis and to lend or sell such copies for private, scholarly or scientific research purposes only.

The author reserves other publication rights, and neither the thesis nor extensive extracts from it may be printed or otherwise reproduced without the author's written permission.

Gregory Lynch
(Student's signature)

187 4th Ave
(Permanent address)

Ottawa, Ontario
Canada K1S 2L5

Date: 5 Dec 1988

THE UNIVERSITY OF ALBERTA

FACULTY OF GRADUATE STUDIES AND RESEARCH

The undersigned certify that they have read, and recommend to the faculty of Graduate Studies and Research for acceptance, a thesis entitled HYDROTHERMAL ZONING IN THE KENO HILL Ag-Pb-Zn VEIN SYSTEM: A STUDY IN STRUCTURAL GEOLOGY, MINERALOGY, FLUID INCLUSIONS, AND STABLE ISOTOPE GEOCHEMISTRY submitted by JOSEPH VINCENT GREGORY LYNCH in partial fulfilment of the requirements for the degree of DOCTOR OF PHILOSOPHY.

.....
Supervisor

.....

.....

.....

.....

Date: .....

for Teresa

ABSTRACT

High grade Ag-Pb-Zn veins of the Keno Hill district, in central Yukon, occupy sinistral strike-slip faults which formed in association with a broad region of upright shear, overprinting an earlier thrust system. Faults, fractures and veins are lithologically restricted to the graphitic Keno Hill Quartzite unit of Mississippian age. Hydrothermal veining is continuous for 40 km, and is contemporaneous with the Mayo Lake Pluton (81 Ma). Zoning is characterized by quartz-feldspar veins near the pluton, carbonate-Ag-Pb-Zn veins further away, and peripheral deposits of epithermal character.

In the mining district, fluid inclusions were studied from early quartz, and from later siderite which is intergrown with the principal ore assemblage of galena, sphalerite, and tetrahedrite. The dominant components of the fluids are H_2O-CO_2-NaCl in varying proportions. Fault-related depressurization, from approximately 1500 bars during deposition of early quartz to less than 130 bars during deposition of siderite, resulted in boiling and cooling of the fluids from near 310° C, to 250° C, as well as a decrease in CO_2 from X_{CO_2} = 0.25 to < 0.01. Graphite in the host rocks had a strong influence on the system, buffering the fluids to a high CO_2 content and allowing for deep seated boiling to occur. Syn- to post-boiling reactions between graphite and water resulted in high salinities for inclusions in siderite (10 to 15 weight percent NaCl equivalent).

$\delta^{18}O_{SMOW}$ values from vein quartz (+10.6 to +20.0 per mil) indicate that the fluids were largely in equilibrium with the quartzite. Contours of these values outline paths of fluid movement along the 40 km long system. In the mining district $\delta^{18}O_{quartz}$ from Ag-rich deposits is relatively high due to boiling-related cooling, whereas trends of ^{18}O depletion in siderite resulted from post-boiling CO_2 formation. Carbon isotopes in vein carbonates ($\delta^{13}C_{PDB}$ = -12.9 to -4.0 per mil) indicate a reduced carbon source. Meteoric water and mixing are indicated in the late epithermal deposits ($\delta^{18}O_{SMOW}$ for quartz = +10.1 to -7.1 per mil).

ACKNOWLEDGEMENTS

Funding was received from the Northern Affairs Program, Whitehorse, Yukon, and from the Canada-Yukon Economic Development Agreement. The project was initiated by J.A. Morin, formerly Chief Geologist, Northern Affairs Program, who coordinated the interaction between university, government, and industry, and who recognized the need for further geological research in the Keno Hill mining district.

United Keno Hill Mines Ltd. (UKHM) permitted complete access to all mine workings, drill cores, as well as private company files, and generously provided food and lodging for the candidate during field work in the [illegible] nanks are extended to K.W. Watson, Chief Geologist for UKHM in Elsa, and staff, for the invaluable help [illegible] guidance.

I would like to thank members of my thesis committee, in particular my advisor B.E. Nesbitt for many discussions, guidance, and encouragement to strive for a higher scientific level. P. Erdmer directed the candidate to attain a better understanding of the structural controls of the vein system, which has enhanced all aspects of the thesis. The teachings of K. Muehlenbachs in stable isotope geochemistry has greatly influenced the student, and initial isotope analyses obtained from his laboratory established the guidelines for further work.

Acknowledgements are extended to F. J. Longstaffe, for the use of his stable isotope laboratory, for his supervision of laboratory methods and data quality, as well as for his comments on the stable isotope chapter. Also, thanks to Diane Caird for instruction in the use of the stable isotope extraction lines.

Microprobe data acquisition and processing was made possible by the efforts of Steve Launspach, to whom I am grateful. Pierre Vincent provided assistance during field work, and entertainment with the fiddle. Teresa Lynch patiently edited much of the text. Many thanks to both.

TABLE OF CONTENTS

LIST OF TABLES

LIST OF FIGURES

CHAPTER 1

GENERAL INTRODUCTION

The Keno Hill mining district is well known for its high-grade Ag-Pb-Zn mineralization, and is recognized as a classic example of Cordilleran polymetallic, precious metal, vein-type mineralization. The deposits are located in central Yukon, 355 km north of Whitehorse and 45 km north of the town of Mayo (135° 12' west and 63° 56' north). Mining activity in the district has continued almost uninterrupted from the early part of this century to the present day.

To date over 4.54 million tonnes (5 million tons) of ore with an average grade of 1412 g Ag/tonne (41 oz Ag/ton), 7 % Pb, and 4.6 % Zn, have produced in excess of 6.4 billion g Ag (206 million oz Ag) (Watson, 1986). Although historically vein deposits of this type have been an important source of silver and are still an attractive exploration target for some mining companies, their present and future significance as suppliers of Ag has been significantly diminished by the advent of silver production from low-grade, high-tonnage, epithermal and base metal deposits. Nonetheless, mining in the Keno Hill district has been profitable for several companies throughout the years, and the longevity of mining has greatly contributed to the overall social and economic stability of the Yukon territory.

Research on this type of ore deposit has been limited over the past twenty years. Current reports on the geology of the Keno Hill mining district are rare, as they are for this type of deposit in general. This was apparent from recent special volumes published on the geology of ore deposits in the Northern Cordillera (Morin, 1986), and on silver vein deposits in Canada (Andrews, 1986), which do not report on the Keno Hill district, or focus much attention on Cordilleran silver deposits. In general, the overall need for a better understanding of the geology and origin of these deposits, in light of modern theories and techniques of investigation, provided the incentive for undertaking this project

on the Keno Hill mining district. As well as providing an adequate genetic and exploration model, a study of these hydrothermal veins gives further insight into hydrothermal aspects of Cordilleran geology in general.

The Keno Hill mining district is 25 km long by 1.5 to 6.5 km wide. More than 65 ore deposits have been identified within the district, with a cumulative strike length for the veins in excess of 160 km (Watson, 1986). Despite the many years of mining, operations usually proceed with no more than 3 years of proven reserves. This results in part from exploration problems including limited outcrop, and particularly, the fractured nature of the host quartzite which inhibits diamond drilling. Percussion drilling has been very useful, but does not penetrate beyond 60 m, while most deposits have been mined to a depth of 90 - 150 m, with some as deep as 336 m. The underground workings are narrow and contained within incompetent fault zones; timbered stoping is widely employed and open stoping is rare. Open pit mining has been effective in the upper portions of some mines, varying in scale from selective narrow trenches to wider bulk mining in areas of disseminated mineralization.

An account of the history of the region is given by Gaffin (1980), with some of the details of production through the years summarized by Watson (1986). Prospectors originally came to the area in search of placer gold and the earliest mining in the area, at the turn of the century, was a placer-gold operation. The Silver King vein was later discovered in 1906 to the west of Galena Hill, and small scale production began in 1913. A series of discoveries were dispersed over several years, with the last major silver find being the Husky mine, which was found in the mid-1960's. Production from the silver deposits is optimistically expected to continue beyond the turn of the century (Watson, 1986). Placer mining is still active along portions of Duncan Creek, and in the adjacent Thunder Gulch.

Various geological reports and studies on the area have been completed; a bibliography up to 1965 is listed in the report on the deposits by Boyle (1965). Since then

a sulfur isotope study was completed by Boyle et al. (1970). Altered whole rock samples along the veins have been dated by the K-Ar method (Sinclair et al., 1980), and selected elements were analyzed during a geochemical study of the veins (Sinclair and Tessari, 1981). Lead isotope data were obtained from the veins and from various rock types of the region (Godwin et al., 1982). In earlier work a significant contribution was the regional geology map of Bostock (1948), which includes the mining district. Further regional mapping was completed by Kindle (1962), and Green (1971, 1972), with detailed geology of the mining district done by McTaggart (1960).

A detailed geologic map of the mining district and structural analysis of the host rocks and orebodies is provided by McTaggart (1960) who established the thrust and nappe style of deformation. Structural controls on the distribution of mineralized faults in the district, in relation to transcurrent upright shear are considered in Chapter 2 of this thesis.

The most extensive work on the orebodies is that of Boyle (1965), who provides a documentation of the complex vein mineralogy, secondary supergene mineralogy, and geochemical distribution of various elements in the soils from around the orebodies. Since this work, the discovery of new deposits has greatly expanded the field data base, particularly with the discovery of the Husky mine and the Mt. Hinton deposit. These two deposits occur at opposite ends of the mining district and contrast considerably with each other in mineralogy, which has lead to the revelation that the mining district is mineralogically zoned (Chapter 3). Mapping in the course of this study has focussed on the zonal distribution of vein minerals in the district and surrounding region. Several mineralogical subdivisions are now recognized and the large scale nature of the hydrothermal system has been established (Chapter 3). The district scale zoning was corroborated by a microprobe study of tetrahedrite (Chapter 3). Comparisons with other districts show that similar zoning patterns exist in the Slocan district of southern British

Columbia and Coeur d'Alene district of Idaho, which allows for the development of a general zoning model for Ag mineralization in the Omenica Crystalline Belt (Chapter 4).

The study of fluid inclusions (Chapter 5) and stable isotope geochemistry (Chapter 6) from the veins provide valuable information on the genesis of the deposits. Considerable variation in the bulk composition of the hydrothermal fluids is documented, and corresponds to the boiling and fluid mixing events. Fluctuations in temperature, pressure, X_{CO_2}, and salinity help construct a quantitative boiling model, which appears to have been the prime mechanism of ore formation.

Boyle (1965) reported anomalous background values of Ag, Pb, and Zn in the organic-bearing metasediments of the mining district, leading him to conclude that the metals in the orebodies were derived from the host rocks. This hypothesis is examined here (Chapters 5 and 6) by considerations of graphite-water equilibria and the buffering capacity of graphite on hydrothermal fluids, as well as by the carbon isotope signature of vein carbonates. However the mechanism of transfer, by the oxidation of graphite and bulk incorporation of CO_2 into the hydrothermal fluid with accompanying release of metals, contrasts with the slow diffusion processes in a static system proposed by Boyle (1965).

The application of stable isotope geochemistry (Chapter 6) is useful in demonstrating the flow paths of the mineralizing fluids. Sites of boiling are also identified by the isotopic composition of hydrothermal minerals, and may be a potential exploration tool for identifying Ag-rich deposits. Different types of fluids are indicated to have been involved in the mineralizing process as well, including meteoric water in the epithermal deposits (Chapter 6).

REFERENCES

Andrews, A.J., 1986, Silver vein deposits: summary of recent research. Canadian Journal of Earth Sciences, vol. 23, p. 1459-1462.

Bostock, H.S., 1948, Mayo, Yukon Territory. Geological Survey of Canada Map 890A.

Boyle, R.W., 1965, Geology, geochemistry, and origin of the lead-zinc-silver deposits of the Keno Hill-Galena Hill area, Yukon Territory. Geological Survey of Canada Bulletin 111, 302 pages.

Boyle, R.W., Wanless, R.K., Stevens, R.D., 1970, Sulphur isotope investigation of the lead-zinc-silver-cadmium deposits of the Keno Hill-Galena Hill area, Yukon, Canada. Economic Geology, vol. 65, p. 1-10.

Gaffin, J., 1980, "Cashing In". D.W. Friesen & Sons Ltd., Altona, Manitoba, 215 pages.

Godwin, C.I., Sinclair, A.J., Ryan, B.D., 1982, Lead isotope models for the genesis of carbonate hosted Ba-Zn-Pb, and silver-rich deposits in the Northern Canadian Cordillera, Economic Geology, vol. 77, p. 82-94.

Green, L.H., 1971, Geology of Mayo Lake, Scougale Creek and McQuesten Lake map-areas, Yukon Territory. Geological Survey of Canada Memoir 357, 72 pages.

Green, L.H., 1972, Geology of Nash Creek, Larsen Creek, and Dawson map-areas, Yukon Territory. Geological Survey of Canada Memoir 364, 157 pages.

Kindle, E.D., 1962, Keno Hill, Yukon Territory. Geological Survey of Canada, map 1105A.

McTaggart, K.C., 1960, The geology of Keno and Galena Hills, Yukon Territory, Geological Survey of Canada Bulletin 58, 37 pages.

Morin, J.A., (editor), 1986, Mineral Deposits of the Northern Cordillera. Canadian Institute of Mining and Metallurgy, Special Volume 37. 377 pages.

Sinclair, A.J., Tessari, O.J., and Harakal, J.E., 1980, Age of Ag-Pb-Zn mineralization, Keno Hill-Galena Hill area, Yukon Territory. Canadian Journal of Earth Sciences, p.1100-1103.

Sinclair, A.J., Tessari, O.J., 1981, Vein geochemistry, an exploration tool in Keno Hill camp, Yukon Territory, Canada. Journal of Geochemical Exploration, vol. 14, p. 1-24.

Watson, K.W., 1986, Silver-Lead-Zinc deposits of the Keno Hill-Galena Hill Area Yukon Territory. In: Yukon Geology, Vol. 1, Exploration and Geological Services Division, Yukon, Indian and Northern Affairs Canada, p. 83-88.

CHAPTER 2

THRUST TO TRANSCURRENT SHEAR SEQUENCE, AND ITS INFLUENCE ON THE DISTRIBUTION OF MINERALIZED FAULTS IN THE KENO HILL Ag-Pb-Zn DISTRICT, YUKON.

INTRODUCTION

The Keno Hill Mining District of Central Yukon (Fig. 2-1) has been an important silver producer since the early part of this century (Watson, 1986). Due to its economic importance, several geological and mineralogical studies of the region and the vein systems have been undertaken (Cockfield, 1921, 1924; Bostock, 1948; Carmichael, 1957; Kindle, 1962; Boyle, 1965). However, it is not until more recently that a geologic and tectonic framework has been available in which to place the mineralized faults and fractures into structural context (Tempelman-Kluit, 1970, 1979; Green, 1971, 1972).

In the area of central Yukon surrounding the Keno Hill mining district, sedimentary rocks strike east-west, dip to the south, and thrusting appears to have been generally towards the north. In the mining district, detailed structural and geological mapping was carried-out by McTaggart (1960) while mapping along strike east of the district was completed by Green (1971), and earlier by Bostock (1948). To the east a steep north trending fault was mapped, and marks a lateral discontinuity in the thrust belt against which the Keno Hill Quartzite terminates. In this area a structural domain different than that of the mining district was recognized where parallel linear fabrics from an early phase of deformation have been rotated to a new orientation (Green and McTaggart, 1960; Green, 1971). Integrating new field data and structural measurements with previous work, this chapter presents a structural analysis which identifies the region of line rotation as a broad zone of brittle-ductile shear, and relates the mineralized faults of the adjacent mining district to the deformation which generated this shear.

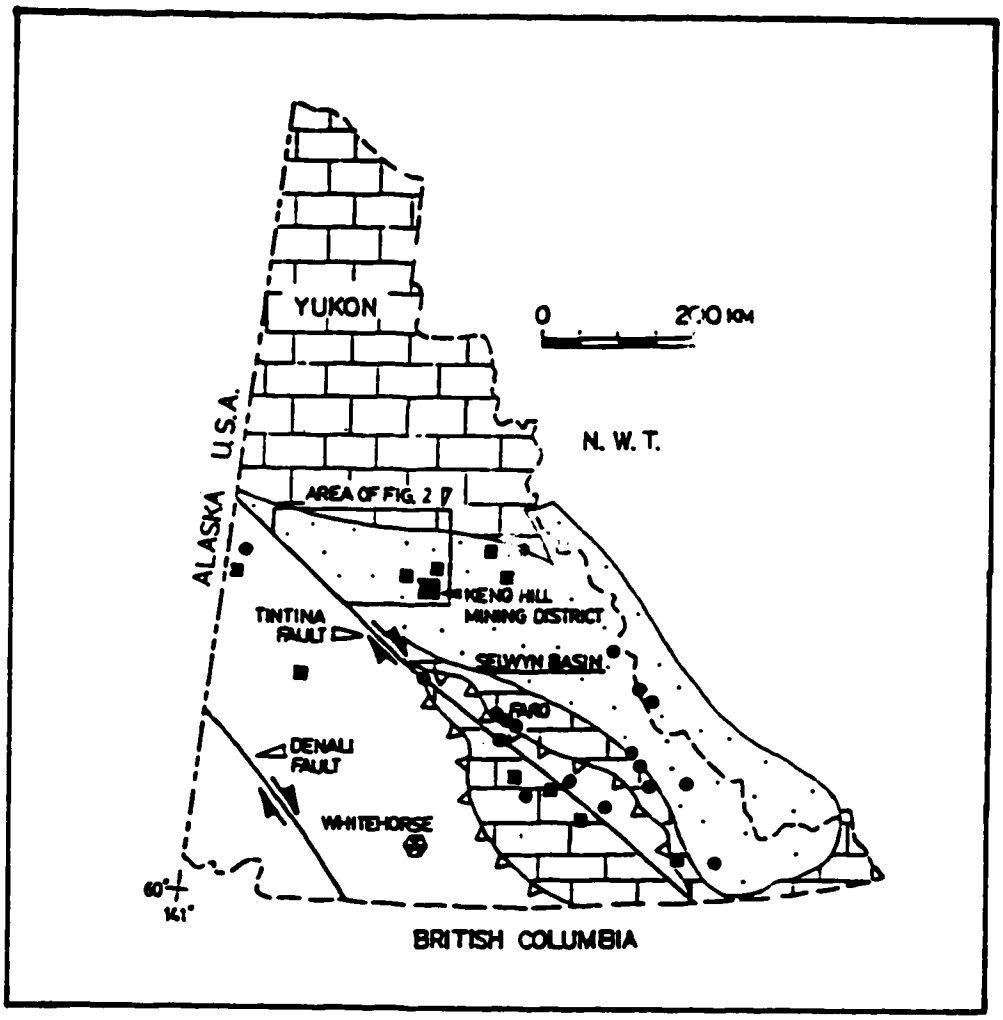

Figure 2-1. Location map of Keno Hill mining district in central Yukon within the Selwyn Basin (stippled pattern). Brick pattern corresponds to the MacKenzie Platform and elements of the Yukon Stable Block (Pugh, 1983) in the north, and largely to the Cassiar Platform to the south. Barbed line shows the position of the Teslin Suture zone separating accreted rocks in the west (unpatterned) from the continental margin strata in the east. Solid blocks are locations of principal epigenetic Ag-Pb-Zn vein systems and circles are syngenetic Pb-Zn-Ag deposits; both types occur in or near the Selwyn Basin (modified from Tempelman-Kluit, 1981)

Within the region of the Keno Hill mining district, a common structural association of many thrust belts is observed; early thrust-related recumbent folds are later refolded or sheared along steeply dipping fabrics (Hobbs et al., 1976, p.417). Two phase deformation sequences in thrust belts are sometimes ascribed to the late break-up of thrust sheets along transcurrent faults, and differential movement of thrust sheets in the direction of thrusting (Sanderson, 1982; Ridley, 1982; Rattey and Sanderson, 1982; Lagarde and Michard, 1986), or to drag along their lateral margins (Coward and Potts, 1983), also variable surging of thrust sheets may be important (Coward, 1982). In some cases "cross-faults", "tear-faults", or "compartmental faults" are generated, to accomodate differential shortening along strike in thrust belts (Cooper et al., 1986; Philcox, 1964). Lagarde and Michard (1986) used the terminology "thrust-wrench shear" for the similar phenomena. Areas of polyphase deformation may be associated with various types of discontinuities along the strike of thrust systems, and these areas are also referred to as "transfer zones" (Aydin, 1988). Other descriptions of such discontinuities include those by Dahlstrom (1969; 1970), Gardener and Sprang (1973), and include the lateral ramp concept of Elliott (1976).

A two phase deformation sequence is documented in the Keno Hill mining district; a upright brittle-ductile shear overprints a moderately dipping regional thrust system. Hydrothermal veining occurs throughout the district, but changes in mineralogy and character according to the various structural domains of the area. Orebodies are shown to be spatially related to brittle deformation and sinistral faulting which forms a conjugate set to earlier brittle-ductile shear. To emphasize controls on mineralization, different styles of faulting are described, and favourable sites of mineralization identified.

In general, brittle as well as brittle-ductile shear zones may fracture vast areas of rock creating passageways for hydrothermal fluids. The association of vein deposits with shear zones has long been established in the geological literature (Newhouse, 1942).

However, their relationship to lateral transfer zones in thrust systems is not widely recorded.

REGIONAL SETTING

The Keno Hill Quartzite is within the ancient continental margin sequence of the Upper Proterozoic to Paleozoic North American miogeocline, near the northern edge of the Selwyn Basin (Abbott et al., 1985) (Fig. 2-1). The region forms the northern extension of the Omineca Crystalline Belt (Monger et al, 1982), and has been affected by late Jurassic to middle Cretaceous metamorphism and igneous activity. In central Yukon, the western extension of the quartzite terminates at the Tintina Trench, which is a prominent dextral fault in the Northern Canadian Cordillera active in Cretaceous and Tertiary time (Gabrielse, 1985). For the Keno Hill Quartzite, recent fossil identifications indicate a middle Mississippian age (Visean age, R. Thompson, pers. comm. 1986).

Mississippian rocks from the ancient continental margin in Yukon are contained mainly within two major groupings: the Imperial sequence in the north, and the Earn sequence in the east of the territory (Gordey et al., 1987). Mississippian rocks also form the lower member of a Mississippian to Triassic sequence which unconformably overlies the Earn Group (Abbott et al., 1986). The Keno Hill Quartzite, situated in the center of the territory, is spatially separate from the Imperial and Earn sequences. Based on lithological similarities, Blusson (1978) correlated the Keno Hill Quartzite with the Imperial sequence. However, the Visean age determination indicates a correlation of the quartzite with the Tsichu Sandstone, which lies unconformably above the Earn Sequence of the Selwyn Basin, in the MacMillan Pass area to the east (Gordey et al., 1987).

The Keno Hill quartzite has been mapped continuously along strike, from east to west, for more than 220 km (Tempelman-Kluit, 1970). The epigenetic Ag-Pb-Zn veins of the Keno Hill Mining district are located within the quartzite, near the eastern extent of this exposure (Fig. 2-2). Strata dip moderately towards the south as a result of northerly

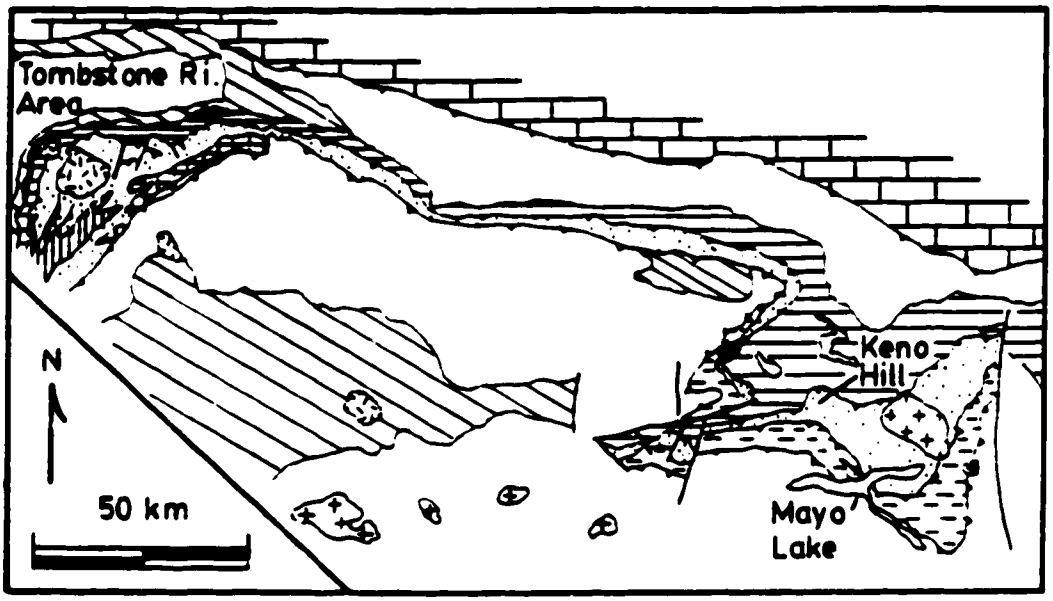

LEGEND

CRETACEOUS
Granodiorite to granite
Granodiorite to syenite
?
Diabase, gabbro, and greenstone
?
'Upper Schist' — graphitic schist, phyllite
JURASSIC
'Lower Schist' —
PERMIAN
Tahkandit Formation, bioclastic limestone
?
Cross laminated siltstone and shale

MISSISSIPPIAN
Keno Hill Quartzite: dark gray orthoquartzite and metaquartzite
ORDOVICIAN AND SILURIAN
'Road River formation: thick bedded chert and shale
?
Undivided, mainly carbonate rock
PRECAMBRIAN
'Grit Unit': gritty micaceous quartzite, phyllite, and schist
Steeply dipping fault
Thrust fault (teeth in direction of dip)

Figure 2-2. Geology of the Tombstone River - Keno Hill region in central Yukon, modified from Tempelman-Kluit (1970).

thrusting, and two major thrusts bound the Keno Hill Quartzite. The quartzite has been thrust to the north (McTaggart, 1960), above the Jurassic "Lower Schist" unit (Poulton and Tempelman-Kluit, 1982). Along much of its length, the Keno Hill Quartzite has been overthrust by "Grit Unit" rocks of the Proterozoic Windermere Supergroup. This contact, the "Robert Service Thrust", is mapped in detail in the Tombstone River area (Tempelman-Kluit, 1970). Another formation in thrust contact with the Keno Hill Quartzite includes Ordovician and Silurian rocks of the Road River formation, which lies above the Keno Hill Quartzite west of the mining district (Fig. 2-2).

The deformed sedimentary rocks are crosscut by bimodal Cretaceous felsic plutons: an extension-related alkalic suite ("A" type), and a compression-related anatectic suite ("S" type) (Anderson, 1987). In the Keno Hill district, the age of deformation postdates the Jurassic Lower Schist unit, and predates the Cretaceous plutons which do not appear to have been affected by deformation.

The Selwyn Basin is host to numerous Paleozoic, syngenetic Pb-Zn-Ag, and Mesozoic epigenetic Ag-Pb-Zn deposits (Fig. 2-1). With high background values of these metals, the basin rocks become a plausible source reservoir to the epigenetic deposits (Boyle, 1965; Blusson, 1978; Goodfellow and Jonasson, 1986), which formed during hydrothermal activity related to the granitic intrusions of the Selwyn Plutonic Suite (Sinclair et al., 1980; Godwin et al., 1982).

LOCAL GEOLOGY

The local geology, described by McTaggart (1960), Kindle (1962), Boyle (1965), and Green (1971), comprises three main units. These are, from a structurally higher to lower position: the Upper Schist unit, the Keno Hill Quartzite, and the Lower Schist unit.

The Upper Schist and Lower Schist units are lithologically similar, areally extensive, and may be stratigraphically equivalent. Graphite-muscovite schist predominates with lesser muscovite schist and chlorite schist. Metamorphic minerals include: muscovite,

chlorite, and graphite with minor chloritoid, stilpnomelane, leucoxene, albite, tourmaline, apatite, carbonates (calcite and dolomite), magnetite, ilmenite, and rutile (McTaggart, 1960).

The Keno Hill Quartzite is a dark grey metamorphosed quartzite with minor graphite, muscovite, chlorite, tourmaline, zircon, and locally up to five percent carbonate. Individual layers of quartzite are typically from 1 to 3 meters thick, with thin layers of graphitic schist in between. In the area of Keno Hill-Galena Hill, the structural thickness of the quartzite is approximately 1 km. Other than bedding, sedimentary structures are not common. The quartzite has been recrystallized during metamorphism and concordant metamorphic quartz segregations are found. In the Tombstone River district west of Keno Hill (Fig. 2-2) the Keno Hill Quartzite has been less affected by metamorphism. Here Tempelman-Kluit (1970) describes the unit as a 550 meter thick succession of submature, massive fine grained orthoquartzite interbedded with black slate. The quartzite is interpreted as a multicycle sandstone deposited under shallow marine conditions, of which the upper part of the formation may be non-marine (Tempelman-Kluit, 1970).

Finely crystalline grey limestone or marble units are widely distributed, but not abundant. One of the larger units is 10 m thick and continuous along strike for 1 km. Limestone occurs with greater frequency in the Upper Schist unit.

Concordant lenses of greenstone are found in the Lower Schist and the Keno Hill Quartzite, but are less abundant in the Upper Schist. The lenses vary from 1m to 30 m in thickness and locally persist along strike for more than a kilometer. They are interpreted to be the metamorphosed equivalents of gabbro and diorite sills (Green, 1971). The most common metamorphic assemblage in the mafic rocks is zoisite-albite-actinolite-chlorite ± stilpnomelane, typical of the greenschist facies (McTaggart, 1960). The greenstone is older than the undeformed granitic bodies (mid-Cretaceous), and possibly cogenetic or younger than the Jurassic rocks.

The Mayo Lake Pluton, which cuts the Keno Hill Quartzite (Fig. 2-3), has been dated by the K-Ar method to be 81 Ma (G.S.C. map 1398A). It is 17 km at its widest part, and ranges in composition from coarse porphyritic granite at the core, with megacrysts of alkali feldspar, black amphibole, and minor sphene, to a finer equigranular granodiorite with green amphibole at the margins. Contact metamorphism extends up to 4 km from the contact. Sillimanite schist at the contact grades into garnet-staurolite-feldspar schist. Greenstones are locally converted to hornblendite. The most distal part of the aureole is characterized by biotite-muscovite schist at low altitudes (700-1220 m) and graphite-andalusite schist at higher altitudes (1525- 1825 m). The presence of andalusite in some portions of the aureole places an upper pressure limit on pluton emplacement, of approximately 3 kilobars, whereas the presence of staurolite indicates that pressures were at least as high as 1 kilobar (Turner, 1980). Coarse andalusite crystals have variable orientations within the schist, and appear to overgrow deformation fabrics. Pressure shadows are not found around garnet crystals. Such features indicate a likely post-kinematic intrusion for the Mayo Lake pluton.

Aplite and pegmatite dykes are common along the margins of the pluton. Quartz-feldspar porphyry dykes, locally with amphibole, extend over a broad area (Boyle, 1965). They have been dated to be 81 ± 5 Ma (Green, 1971), and although they extend into the mining district, they are not abundant. Lamprophyre dykes occur in the district as well; these are rare and of undetermined age.

Hydrothermally altered wallrocks along the margins of the Ag-Pb-Zn veins of the mining district, have been dated (K-Ar) to be mid-Cretaceous (84 ± 4 Ma, Sinclair et al., 1980), which indicates a possible link with the felsic intrusive bodies.

Extensive documentation of the vein mineralogy from the many deposits of the mining district was completed by Boyle (1965). Vein mineralogy is varied and complex, but the dominant ore assemblage throughout the vein system is comprised of galena, sphalerite, and tetrahedrite, with a gangue mineralogy of pyrite, siderite, calcite and quartz.

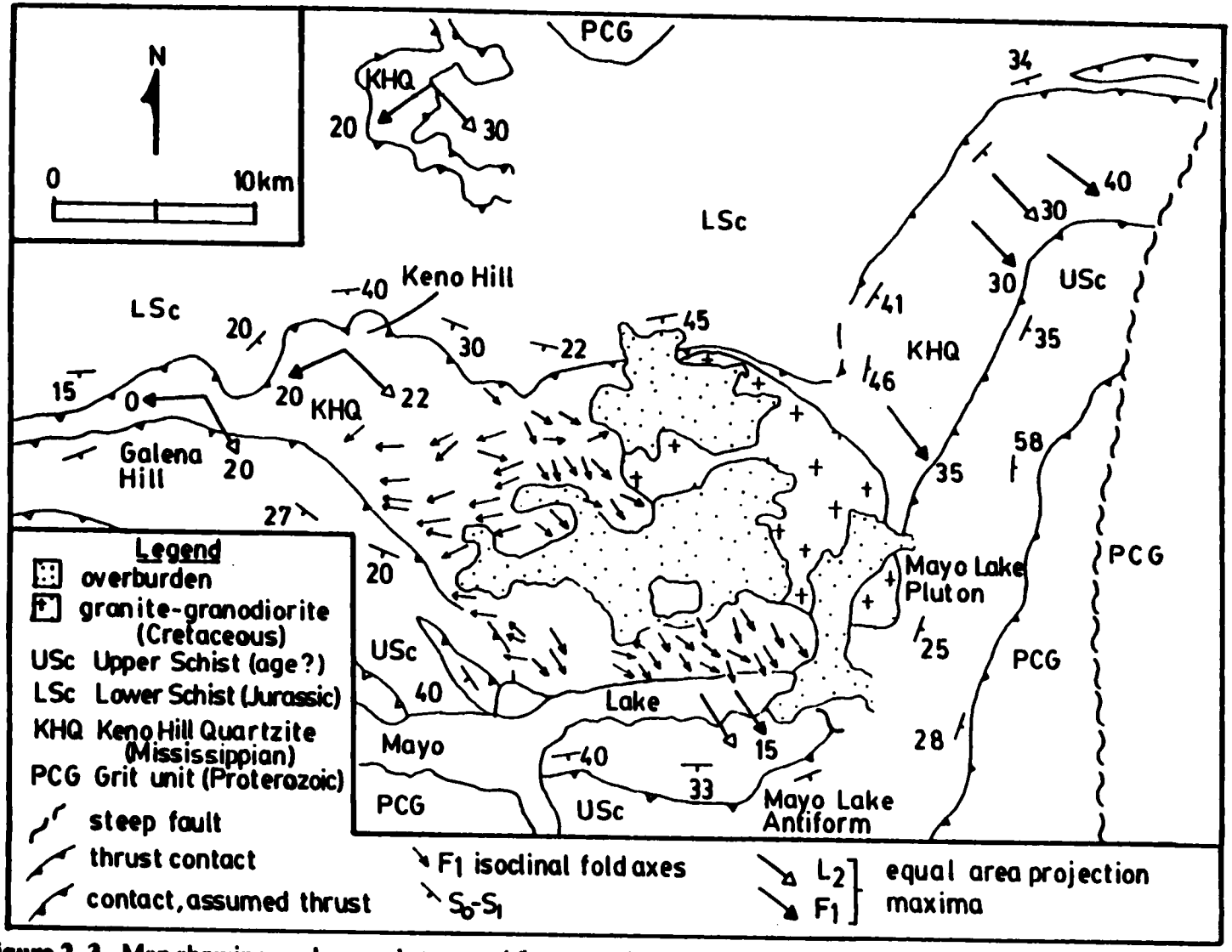

Figure 2-3. Map showing geology and structural features of the region surrounding Keno Hill. Equal area projection maxima on map taken from McTaggart (1960), Green and McTaggart (1960), Green (1971) and this report.

STRUCTURAL GEOLOGY

Structural measurements were taken during geological mapping in the vicinity, and to the east of Keno Hill. These are integrated with the data of McTaggart (1960), Green (1971), and Boyle (1965), and presented in Figures 2-3. Two main phases of penetrative deformation are recognized in the region; an early thrust and nappe phase, followed by a steep transcurrent shear phase, to which the mineralized faults are interpreted to be related.

Thrust and nappe phase, D_1

The earliest recognizable stage of deformation (termed D_1), is characterized by north-verging, isoclinal folds (F_1). Metamorphic quartz segregations, as well as parallel alignment of graphite and mica, define an associated axial-planar schistosity (S_1) which dips moderately to the south (Fig. 2-3, 2-6 A). Large isoclinal folds (F_1) have been outlined on Keno Hill by McTaggart (1960) and in the Davidson Range to the north by Green and McTaggart (1960). Smaller isoclinal folds occur in most rocks. The folds indicate north and northwest movement of the higher units over the lower units on a thrust at the base of the quartzite (McTaggart, 1960). The general northward direction of thrusting is indicated by the overal south dipping attitude of thrusted lithology in the region (Fig. 2-2). Reverse shearing, parallel or at a slight angle to the axial-planar cleavage is common, especially in the hinge zones of isoclinal folds (Fig. 2-4 B).

Shallow-dipping faults are of two types. Most common are (1) thrust faults which occur along graphite-rich layers separating quartzite units; these are called bedding-plane faults. The graphitic layers acted as detachement surfaces and exhibit a well developed anastomosing fabric, as well as containing rootless intrafolial folds, and slivers of detached quartzite (Fig. 2-4 A). (2) The second type consists of low-angle thrust faults where quartzite dominates, with small duplex structures (Fig. 2-5 A). These cross-cut F_1 axial planes and are therefore interpreted as a later feature. Their small scale and form are similar

Figure 2-4. (A) Moderately dipping shear zone with abundant graphitic material and intrafolial folds. Massive quartzite occurs above and below zone. (B) Sawed surface of sheared graphite-muscovite schist displaying tight to isoclinal S_1 fabric.

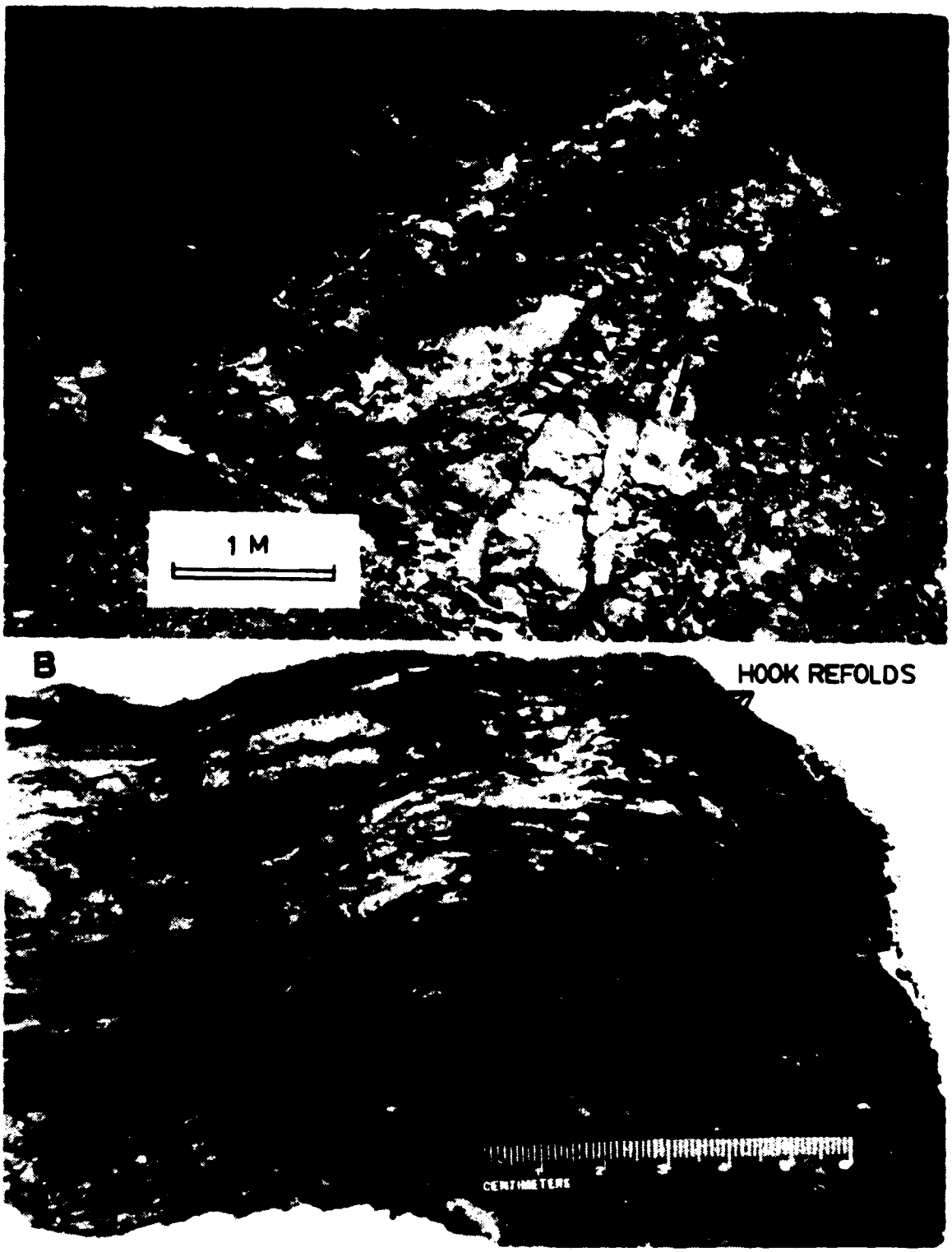

Figure 2-5. (A) Moderately dipping thrust fault in quartzite (type 2). Several small fault horses occur immediately below the roof thrust forming complex outcrop scale duplex pattern. Axial planes of small scale isoclinal folds are locally truncated by thrust faults. (B) Open folds characteristic of F_2 in garnet-staurolite schist, coaxial hook refolds of F_1 are visible in upper right-hand portion of sample.

to the structures described by McClay and Insley (1986) in the Lewis thrust sheet of the Rocky Mountains of Alberta.

The continuity and extensive nature of the thrust faults is made evident by the regional superposition of the Mississippian Keno Hill Quartzite over the Jurassic Lower Schist unit (Fig. 2-3). However, within the Keno Hill Quartzite where stratigraphic markers are lacking, the lateral continuity of thrust faults is difficult to establish, especially within the mining district where exposure is limited.

Transcurrent shear phase, D_2

The second phase of deformation (D_2) is represented in outcrop by small open folds (Fig. 2-5 B) and a widespread well developed crenulation cleavage (S_2) in schist layers. The cleavage is steeply dipping to vertical and strikes northwest (Fig. 2-6 B). Locally, it is seen as a spaced cleavage in the more competent units, appearing as penetrative fracture sets parallel to the axial planes of F_2 folds. A crenulation lineation (L_2) was developed on bedding and S_1 surfaces, and plunges southeast parallel to F_2 fold hinges (Fig. 2-6 C). On a regional scale D_2 produced broad southeast-plunging open folds. The largest of these is the Mayo Lake antiform, having a wavelength of approximately 25 km and an amplitude of about 5 km, it covers most of Figure 2-3. It is not known if the Mayo Lake antiform is cylindrical, and determinations of true thickness along the fold profile are most likely only approximations; however a considerable degree of thickening in the hinge zone is apparent. The fold has either a similar form (type 2), or type 3 form according to the classification of Ramsay (1967, p. 365), as the curvature is greater along the outside of the fold than along the inside (Fig. 2-3). Outcrop scale folds of quartzite beds within the Mayo Lake antiform show different profile types, including type 1, according to the nature and competency contrasts of the interlayered rocks.

F_1 fold axes have been variably affected by D_2 throughout the district. Variations in the orientation of F_1 help define east and west structural domains in the area (Fig. 2-3).

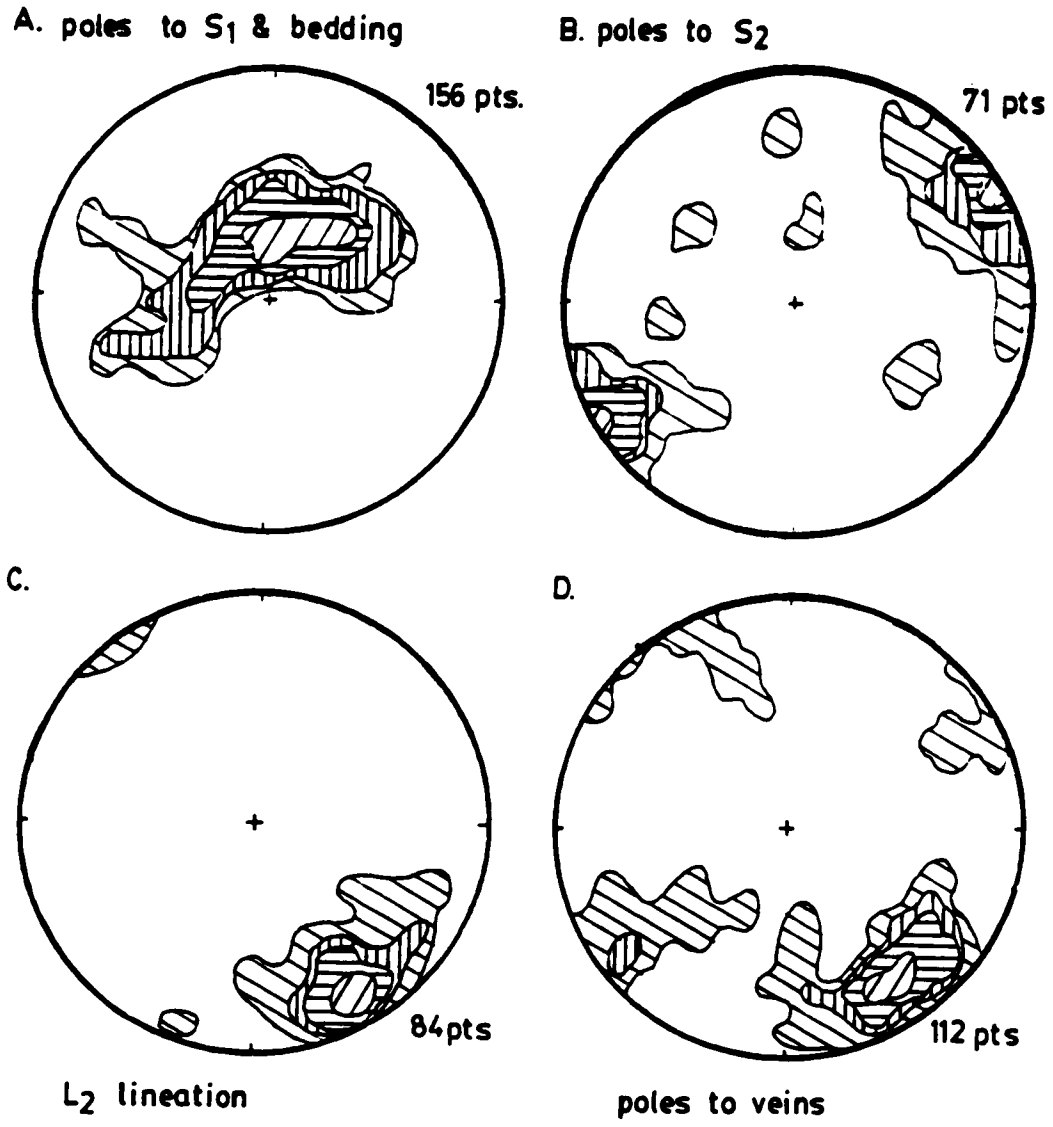

Figure 2-6. Equal area plots of structural measurements in quartzite, taken from area north of Mayo Lake, west of the Mayo Lake Pluton, and east of Keno Hill. Contours are as follows in percentage of total points per one percent total net area: (A) poles to S_1 schistosity and bedding, 1, 2, 4, and 10 %; (B) poles to S_2 cleavage, 1, 2, 5. 10, and 20 %; (C) L_2 lineation, 2, 5, 10, and 20 %; (D) poles to hydrothermal veir 3, 5, and 12 %.

Within the western domain, F_1 axes are near-horizontal to shallow-plunging and trend approximately east-west, forming a high angle with the southeast-plunging crenulation lineation (L_2). The F_2 folds are weakly developed in this area. In the eastern domain, in the area of the Mayo Lake antiform, the isoclinal fold axes (F_1) have been strongly affected by D_2; in this region F_1 is dominantly coaxial with F_2 at an orientation of 143°/14°, and is distributed along a great circle having an attitude of 103°/19° S (Fig. 2-7). The transition between these two domains is irregular and gradual, and within an outcrop the orientation of F_1 may be variable as strain is locally inhomogeneous. On a broader map scale however the boundary roughly trends north (Fig. 2-3, 2-8). The transition occurs on the western limb of the Mayo Lake antiform, where stretching and boudinage of quartzite and greenstone layers is commonly observed. Also, within this limb are sigmoidally-shaped *en echelon* vein arrays. The arrays strike at approximately 330°, are steeply dipping, and display dextral transcurrent shear.

In general, patterns of deformed linear features in shear zones and associated with similar folding are very different than those produced by the buckling process (Ramsay, 1967, p.470). As was pointed out by Green (1971), the distribution of deformed F_1 axes in the area of the Mayo Lake antiform is not compatible with buckle folding; the axes are not distributed along a small circle of an equal area projection (Fig. 2-7). Alternatively, their location along a great circle is an indication that they were deformed principally by similar folding as a result of shear during D_2. In shear zones, pre-shear zone fold axes or linear elements typically are rotated and take up new orientations when passing into a shear zone. The lines become spread along a great circle, and come to approach the direction of shear (Ramsay, 1980).

The presence of the Mayo Lake antiform and deflection of F_1 along a great circle in the eastern domain of Figure 2-3, are representative of higher D_2-associated strain in this area. Since shearing appears to have been an important component of D_2, the eastern

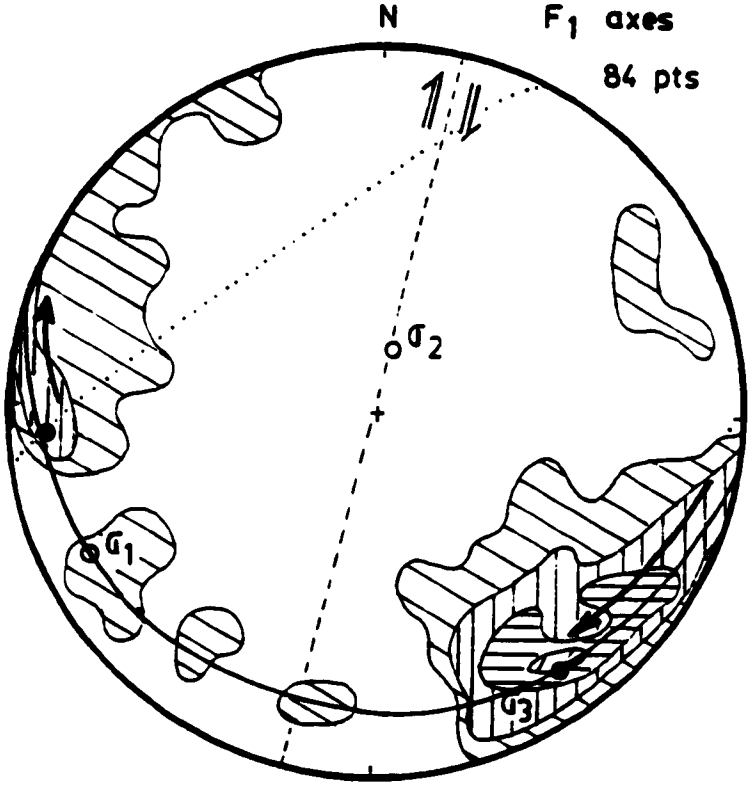

Figure 2-7. Equal area projection of F_1 isoclinal fold axes, with contours in 1, 2, 4, 8, and 9 % of total points per one percent net area. Solid curve is the principal surface along which F_1 is distributed. Bold arrow is an interpretation of the rotation of F_1 along this surface in a simple shear regime between points marked by solid black dots, with corresponding stress directions shown on projection (see text for details). Dashed line is the hypothetical dextral shear plane which would correspond with this model, and approximates the orientation of the mapped line which separates structural domains in Figure 2-8, and corresponds as well to the north striking fault east of the district. The dotted line is the small circle around which F_1 would have been rotated if F_2 was formed by a buckling process, and as can be seen there is no correlation.

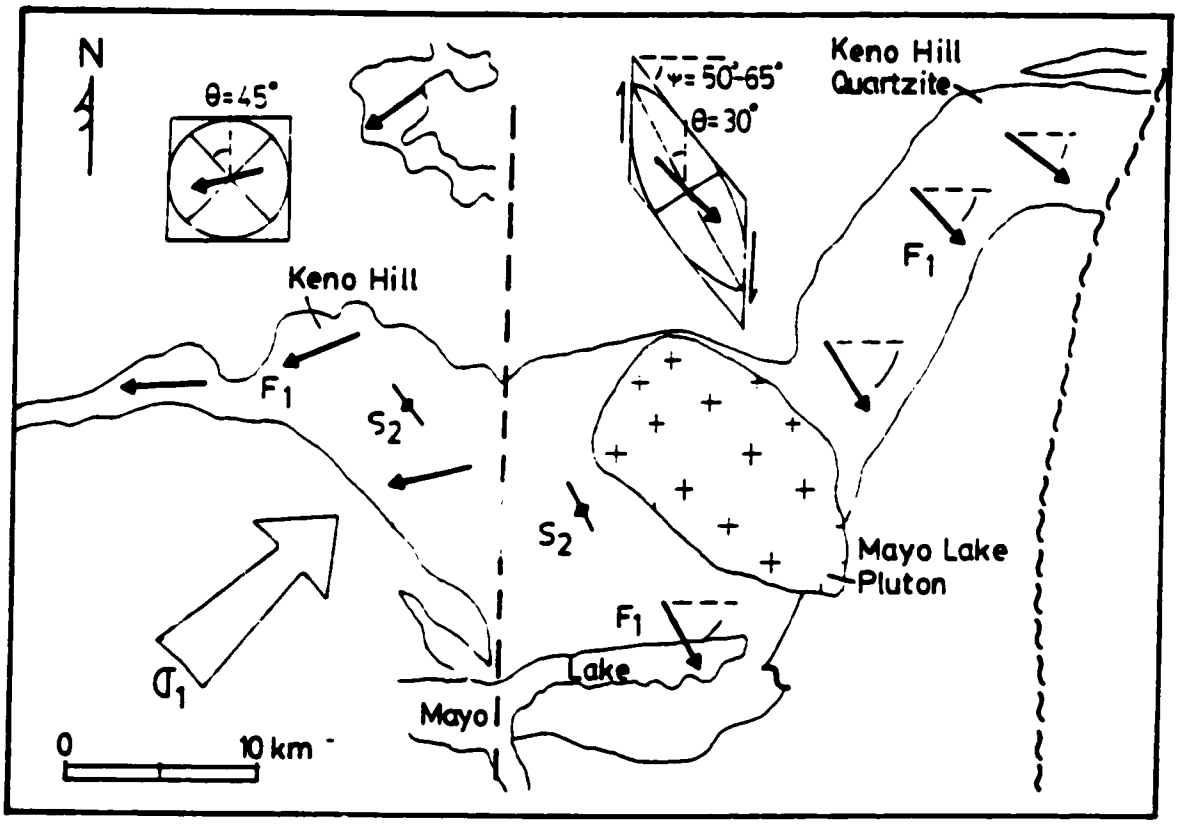

Figure 2-8. Diagram emphasizes variable orientation of F_1 fold axes across the district. Dashed line is the approximate position of the boundary between east and west structural domains. Schematic shear boxes and strain elipses are included; the variable orientation of F_1 may be explained by inhomogeneous simple shear within a dextral brittle-ductile shear zone.

domain may be defined as a dextral brittle-ductile shear zone; however all of the boundaries of the shear zone have yet to be defined.

In using the orientation of F_1 to assess the degree and direction of shear during D_2, assumptions must be made as to the original orientation of F_1 prior to shear. Since the western domain was less strongly affected by D_2, the sub-horizontal east-west orientation of F_1 here possibly approximates its original direction prior to D_2. This is further substantiated by the regional east-west trend of the thrust belt in this portion of the territory (Fig. 2-2). Also, during shear, deflected lines tend to move on a plane locus which connects their initial orientation to the direction of shear (Ramsay, 1980). The initial orientation is then usually represented on the equal area projection. The loci of F_1 along the plane 103°/19° S, extending from the assumed initial F_1 orientation at 268°/4°, to the final position at 143°/ 14°, is interpreted to display a maximum dextral line rotation of 65° (Fig. 2-7, 2-8). Using a simple shear model, the line rotation corresponds to a gamma value of between γ = -1.2 to -2.1. The full degree of flattening and of extension are not known, and it is possible that volume changes or pure shear may have affected the final orientation of F_1 as well.

Veins, faults, and fractures

Veins, faults and fractures are concentrated in the quartzite, and "pinch-out" upwards or downwards where they extend from quartzite into schist units (Boyle, 1965). A regional plot of Ag-Pb-Zn veins shows that none, or very few of the orebodies occur within the eastern structural domain (Fig. 2-9). The entire 25 km long mining district is contained within the western structural domain. Hydrothermal veins are however abundant within the two domains, but they are of a different mineralogy. Both lithologic and structural controls were important in ore formation.

The attitudes of veins, faults, and fractures are illustrated on the map of Figure 2-10 and equal area projection of Figure 2-6 D. In the eastern structural domain, the veins are

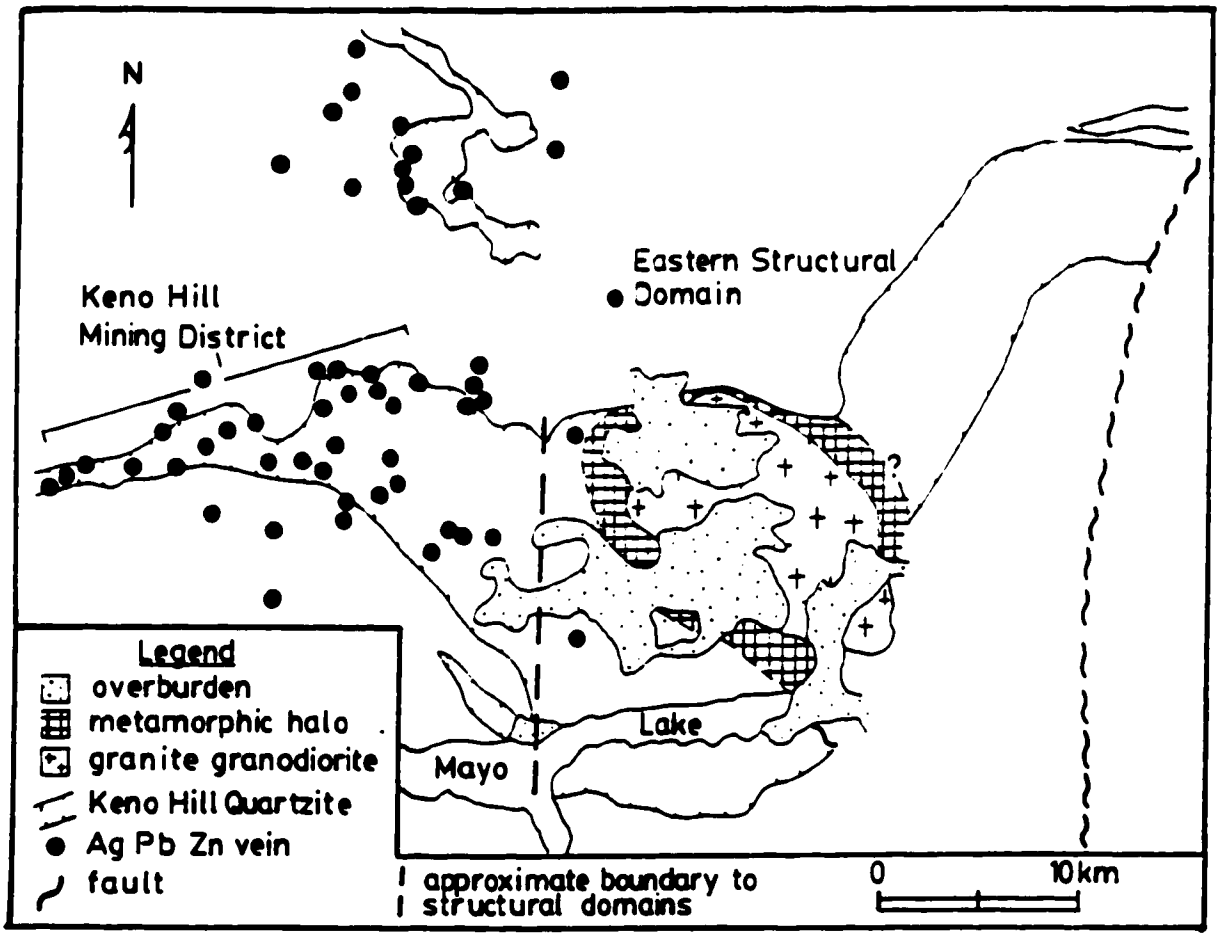

Figure 2-9. Correlation between distribution of Ag-Pb-Zn deposits and structural domains.

coarse grained and vuggy, and are filled predominantly with quartz, as well as feldspar, zoisite, and a variety of accessory minerals (Chapter 3). The feldspars include orthoclase, albite and calcic plagioclase. The veins often occupy tension fractures perpendicular to the F_2 axes ("AC" joints), or are contained along northwest-striking, dextral slip planes which parallel S_2. Most veins formed during a late stage of D_2, since they have not been rotated in the manner that F_1 has. As previously mentioned though, some early sigmoidal vein arrays of quartz only are recorded, but hydrothermal activity appears to have culminated near the end of D_2. Joints measured in the mining ditrict to the west occur perpendicular to F_2 as well, and a second prominent set is vertical and strikes north (McTaggart, 1960).

Northeast-striking sinistral faults are the main hosts to the orebodies (McTaggart, 1960; Boyle, 1965), and form a conjugate set to the eastern region of dextral rotational shear (Fig. 2-10). The faults have been exposed and delineated from extensive mining activity. They trend diagonally across the quartzite unit. Most orebodies strike between east to northeast, and dip steeply to the southeast between 60° to 90°, though a few are steeply dipping to the northwest. Some of the faults are continuous along strike for up to 5 km, and have been mined to depths of 340 m. Left-hand offset of the contact between the Keno Hill Quartzite and Lower Schist is observed along some of the ore bearing faults. As much as 600 meters of offset on some of the faults is recorded from apparent sinistral movement (McTaggart, 1960). Slickensides indicate strike-slip and dip-slip motion.

Ore-bearing fault systems may be straight, branching, or anastomosing (Fig. 2-10, 2-11). The faults often comprise complex stockwork and breccia zones, with the strike and dip directions for slip and fracture planes being quite variable. From a broader perspective however, the overall strike and dip of a fault zone is measured from the attitude of the orebody, or mine workings as a whole. Much fault refraction occurs through the layered sequence of the host lithology. Contrasting degrees of competency between schist, quartzite and greenstone layers in the moderately south dipping sequence has had some control on the dip of the fault structures. Faults passing from quartzite or greenstone into

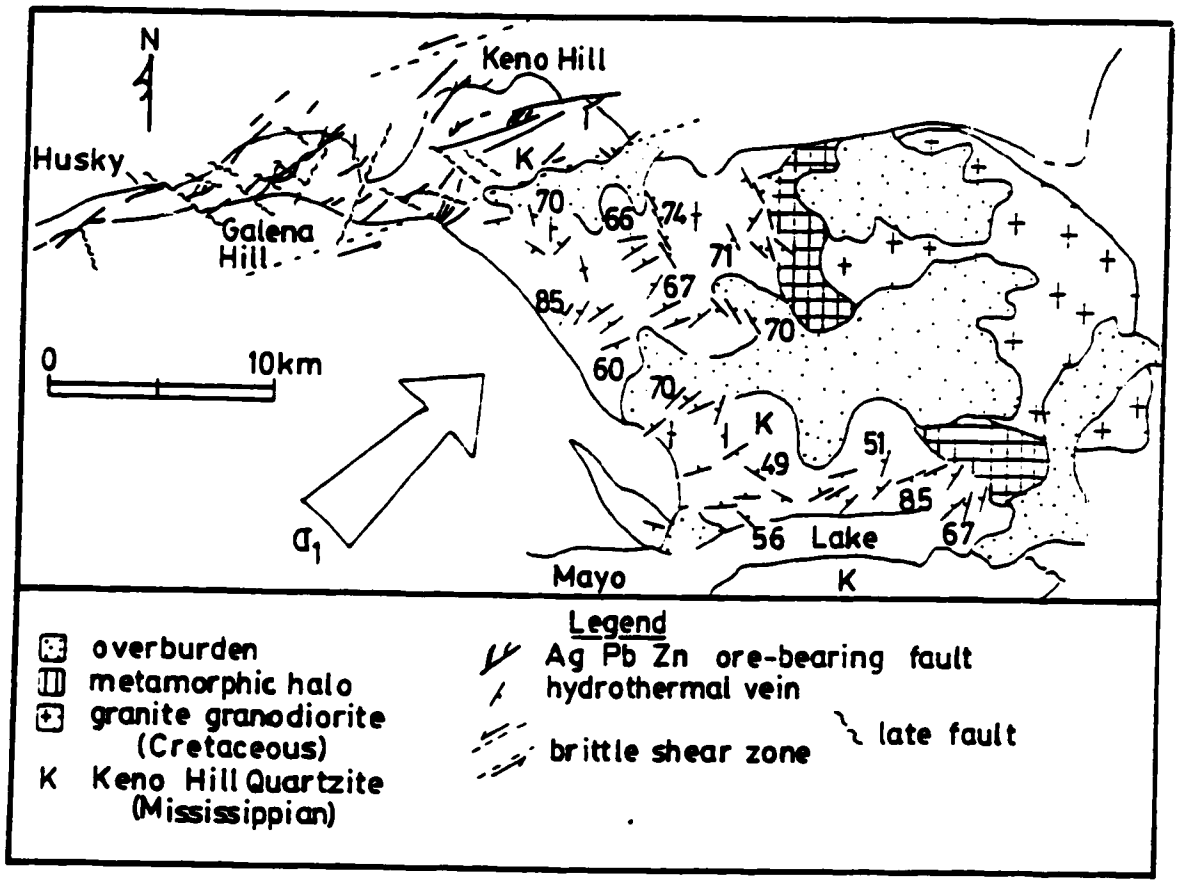

Figure 2-10. Fault and fracture pattern of hydrothermal system. Fine dashed lines outline sinistral shear zone of brittle fault-dominated mining district, which forms a conjugate set to the eastern structural domain.

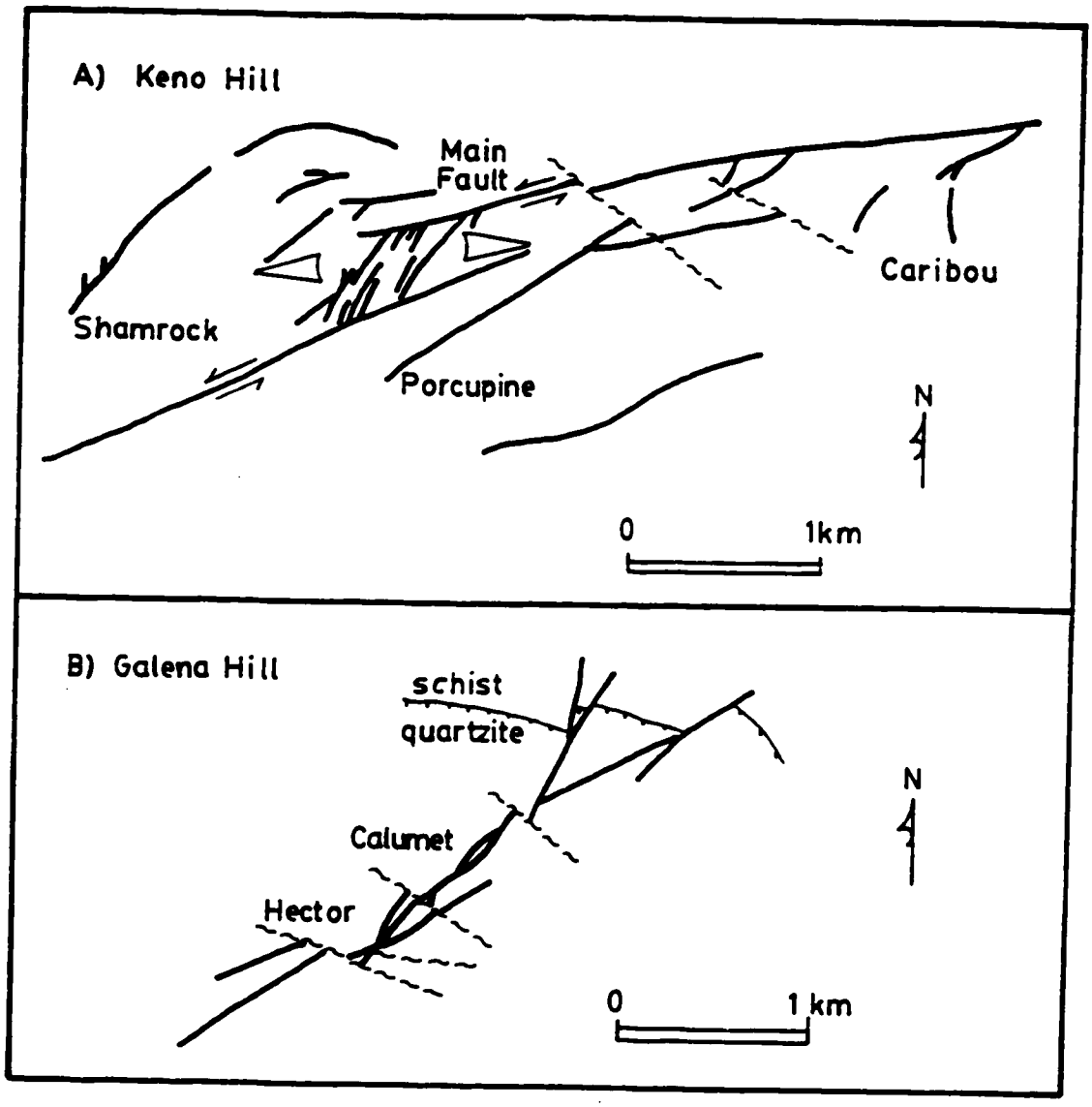

Figure 2-11. Surface trace of important ore-bearing faults (modified from McTaggart, 1960; and Boyle, 1965). Triangular arrows in (A) show zone of tension between overlaping ends of en echelon sinistral faults. Left-hand offset of quartzite is seen in (B), as well as anastomosing and branching nature of fault systems.

schist may be refracted to correspond more closely to the south dipping bedding attitude. In single underground exposures of faults through multilayered outcrops, staircase patterns are sometimes observed for the faults when viewed along strike, as they pass alternately through quartzite and schist. The jagged outline of such faults is thought to result in breccia formation with subsequent fault movement, and then progress to a smoothing of the fault with further displacement. More extensive sections of fault flattening are found as well and have acted as sites for ore deposition. Specifically, Raise-224 of the Husky mine is a 25 meter long tabular oreshoot contained along a section of fault breccia which is roughly concordant to the shallow south-dipping layering. This is a local phenomena, as the dominant orientation of the Husky mine as a whole is steeply dipping and discordant.

High grade oreshoots may be narrow, and are often located at dilational bends in the faults (Boyle, 1965). Fracturing over broader areas on the other hand, which has resulted in stockwork mineralization, is related to regions where the principal slip surfaces have been impeded by antidilational jogs. Obstructions may be large horses within anastamosing vein sets. An example is observed in the Calumet 1 and 15 veins which bound a 40 metre wide zone of disseminated mineralization, amenable to open pit bulk mining methods (Fig. 2-11 B). This style of fracturing may be referred to as "distributed crush brecciation" (Sibson, 1987). Anastomosing fault patterns, such as those present on Galena Hill (Fig. 2-11 B), often develop in strike-slip systems (Naylor et al., 1986; Woodcock and Robertson, 1982). Steeply dipping fault slices, lozenges, or horses, between anastomosing faults have been termed "strike-slip duplexes" by Woodcock and Fischer (1986). The regimes of transtension and transpression that result along these during fault movement, are important in creating openings and zones of crush brecciation for the mineralizing fluids.

Tension fractures, between overlapping ends of *en echelon* strike-slip faults, are favourable sites for hydrothermal mineralization as well (Fig. 2-11 A). On Keno Hill, mineralization in these sections is Au-rich, and mineralogically distinct from bounding Ag-

Pb-Zn strike-slip veins. The difference results from contrasting physical environments; the open nature of the tension fractures form transitory low-pressure channels for the rapid passage of hydrothermal fluids, inducing boiling or carbon dioxide immiscibility (Sibson, 1986, 1987). The mineralized tension fractures, termed "transverse vein faults" in the mining district (Boyle, 1965), are similar in pattern to experimentally derived fractures around overlapping sets of en echelon strike-slip faults (Hempton and Neher, 1986). The correlation may be interpreted to indicate sinistral strike-slip movement for the set of vein faults illustrated in Figure 2-11 A.

Hydrothermal vein material within the faults is locally brecciated and sheared, indicating some post-mineralization strain. Hydrothermal breccias, with hydrothermal material as both clasts and cementing agent, are widespread within the faults. Contemporaneity of hydrothermal activity with fault movement is indicated. Invariably, shearing has affected galena more noticeably than any of the other phases. Excellent examples of sheared ribbon or gneissic galena are seen throughout the mining district; thin strips of coarse galena (1-2 cm) which are unstrained, are separated by slip surfaces where strain has resulted in grain size reduction (<1 mm) and recrystallization (Fig. 2-12). Kink banding is preserved in coarse galena. In the sample of the Keno Hill district, the slip planes regularly splay, creating small scale anastomosing networks with isolated islands of coarse undeformed galena. Atkinson (1976) suggests that grain size reduction and recrystallization of galena during shearing are most effective above temperatures of 200° - 300° C. This was used as an argument by Logan (1986) for sheared vein galena in the Slocan mining district of British Columbia, to indicate a period of high ambient temperature for the host rocks during shear. Similarly, relatively high background temperatures might be inferred to have existed in the Keno Hill district during hydrothermal activity and fault movement.

Sub-vertical northwest-striking faults, which are not mineralized, cut and offset mineralized faults (Fig. 2-3, 2-11) (McTaggart, 1960). They resulted from a later phase of

Figure 2-12. (A) Sheared galena sample from vein-fault in Hector-Calumet mine. Fine grained granular recrystallized galena occurs along shear boundaries between coarser galena, fabric parallels walls of fault zone. (B) Sheared galena sample from Shamrock mine, grain size reduction and recrystallization have affected the galena.

deformation (D_3). Horizontal dextral offsets of up to 700 m are recorded along these. This later period of faulting causes exploration problems, as many orebodies are truncated by these faults.

DISCUSSION

Lineations such as fold hinges are particularly useful in identifying shear zones, since they commonly act as passive markers rotated toward the transport direction (Coward and Potts, 1983). The transition from the mining district into the eastern structural domain is marked by widespread southeast rotation of isoclinal F_1 fold axes. The transition is gradual and irregular, as strain is locally inhomogeneous. The boundary however trends approximately north-south. The counterpart to this boundary, since shear zones have parallel walls (Ramsay, 1980), is possibly a north-trending fault mapped by Bostock (1948), which marks the eastern extent of the Keno Hill Quartzite in the region (Fig. 2-2, 2-3, 2-8). Dextral offset of the Lower Schist unit along this fault is indicated in a map by Green (1971). Geological and structural features further to the east of this fault are not well known however. With these boundaries, the shear has a width of approximately 28 km. The full north to south extent of the shear zone beyond the Keno Hill Quartzite is not known.

The principal component in most shear zones is that of simple shear (Ramsay, 1980). From the sigmoidal vein arrays, F_1 rotation, and similar folding, it appears that simple shear was an important component of D_2 in the eastern structural domain. Structural criteria used for indicating a change in volume, or component of pure shear, was not recognized. Establishing the type of shear is important when interpreting shear zone-related hydrothermal systems, since deformation involving only simple shear is usually isochemical, whereas material influx or expulsion may accompany changes in volume. For example, in a study of the shear zones from the Lewisian complex of Scotland, Beach (1976) reports a metasomatic increase of H_2O, K, and Na into the shear zones, and a

decrease of Fe, Ca, and Mg, immediately prior to and during the intrusion of post-kinematic dolerite dykes. For the Keno Hill district, a similar pattern of metasomatism might be reflected in the hydrothermal vein mineralogy found within and outside of the eastern structural domain; potassium and sodium feldspars are characteristic of the veins within the shear zone, while hydrothermal carbonates of Fe, Ca, and to a lesser degree Mg are found outside of the shear zone and comprise the dominant gangue phases of the Ag-Pb-Zn orebodies. From this correlation, it is hypothesized that a decrease in volume during shear in the eastern structural domain and Mayo Lake antiform, may have established a hydrostatic pressure gradient, resulting in fluid flow and mass transport of material out of the shear zone and into the fault structures of the adjacent Keno Hill mining district. Fluid flow may have been further helped by a heat anomaly generated from the late, to post-kinematic intrusion of the Mayo Lake pluton.

The fault structures which host mineralization in the mining district appear to have been formed during the second phase of deformation, as they form a brittle conjugate set to the shear in the eastern structural domain. To illustrate the structural relationship between D_2 and the ore-bearing faults, a knowledge of the stress field which accompanied D_2 is necessary. The principal stress direction σ_1, the direction of extension σ_3, and the intermediate axis σ_2 are plotted on the stereographic projection of Figure 2-7. The stress directions have been deduced in the following manner; the pole to the extension joints, which parallel F_2 and L_2, correspond to σ_3 at 143°/14°; σ_1 is at 242°/13°, 90° to σ_3, along the great circle of F_1 loci, and perpendicular to S_2; and σ_2 (329°/75°) is 90° to both σ_1 and σ_3, and is contained along the plane of the tension fractures.

The ore bearing fault structures, are only in part compatible with the overall stress field for D_2. Under ideal conditions within an isotropic body of rock, relationships between faults and stress (Anderson, 1951) predict that the sinistral faults of the mining district should strike east to northeast, as they do, but that they should dip steeply to the northwest along σ_2. Most dip steeply to the southeast, or are near vertical. Considerable

departures from the idealized model may occur however in rocks containing a strong fabric. Such is the case for the Keno Hill quartzite; the lithological layering and penetrative schistosity associated with isoclinal folding both dip to the south in the mining district. Fault refraction through the layered sequence greatly influences the overal dip of the orebodies, creating the slight departure from the ideal model and discrepancy between the inferred stress field for D_2 and orientations of the faults.

Green (1971) suggested the possibility that the mineralized faults resulted from late D_2 strain, but a relation of fault system to the second phase of deformation was considered unlikely. The reason for this is that fragments of crenulated and lineated schist were found in breccia within the faults, apparently indicating that faulting postdates D_2 (Green and McTaggart, 1960; McTaggart,1960). This observation corresponds with the formation of the faults as a late stage of D_2; a natural progression of early rock crenulation, followed by brittle failure during a single stage of deformation, may just as easily explain the crenulated breccia fragments. Contemporaneity between fault movement and hydrothermal activity are also indicated from textural evidence; brecciated and slickensided clasts of hydrothermal minerals are cemented by unstrained hydrothermal minerals in the veins of the Keno Hill district. Hydrothermal fluids may have served to lubricate fault surfaces, and fault movement in turn may have assisted local fluid flow, as active faulting typically forms voids along dilational jogs, creating low pressure zones into which fluids migrate and boil.

On a district-wide scale, models of sequential deformation in thrust belts may be used to interpret strain variations within the nappes and thrust sheets of the Keno Hill district. Upright shear zones and wrench faults may be generated during late stages of thrusting as a result of the differential transport of nappes (Sanderson, 1982), or as a result of drag along their lateral margins. In many deep seated thrust systems, the walls of transcurrent shear zones are parallel to the direction of thrusting and tectonic transport (e.g. such as are documented in the Lizard Complex of southwestern Cornwall, England, Rattey and Sanderson, 1982; or in the Irish Variscides, Cooper et al., 1986). The broad north-

directed thrusting and associated east-west fabric of the Keno Hill Quartzite are interpreted as having resulted from an initial north-south directed principal stress direction. After north-trending transcurrent shear was initiated in the east, possibly along a sidewall ramp which limits the Keno Hill Quartzite, the principal stress direction was rotated clockwise by approximately forty-five degrees generating the second phase of deformation. As an analogy, experimental models have shown that upon the generation of a wrench zone, the stress field may be rotated to a new position at 45 degrees to the plane (Naylor et al., 1986), and corresponding strain features will develop in new directions during a second phase of deformation.

SUMMARY AND CONCLUSIONS

The following is a summary of the structural evolution leading to the developement of faults which host the high-grade silver veins in the Keno Hill district. The two principal stages of deformation, named D_1 and D_2, post-date the Jurassic Lower Schist unit, and pre-date final intrusion of the middle Cretaceous Mayo Lake Pluton.

1) The earliest recognized phase of deformation (D_1) resulted from regional northward thrusting. It produced an infrastructure of isoclinal folding with a south-dipping axial planar cleavage, as well as thrusting and shearing along moderately dipping graphitic planes. Greenschist metamorphism accompanied this stage.

2) The second phase of deformation (D_2) is characterized by the developement of a zone, or domain, of upright brittle-ductile shear. The principal features of the zone include apparent clockwise rotation of F_1 isoclinal fold axes along a great circle, folding and thickening of the quartzite, some sigmoidal vein arrays, and widespread development of late tension fractures. A pervasive northwest-striking upright crenulation cleavage occurs throughout the region in association with this stage of deformation. Sinistral strike-slip faults developed in the brittle domain of the quartzite in the western portion of the study area, and form a northeast-striking conjugate set to the eastern structural domain. It is

hypothesized that the eastern structural domain is part of an upright brittle-ductile shear zone that formed from differential surging of thrust sheets during northward tectonic transport.

3) Widespread late to post-D_2 hydrothermal activity precipitated Ag-Pb-Zn minerals within the northeast striking sinistral faults. The ore deposits are lithologically restricted to the brittle Keno Hill Quartzite, and are structurally restricted to the brittle fault zone of the western structural domain. Favorable sites for ore deposition within the sinistral faults include dilational jogs in anastomosing faults, areas of distributed crush brecciation along antidilational jogs and fractured fault horses, extensional veins between overlapping ends of en echelon faults, and brecciated zones along bedding controlled fault refractions.

4) Steep northwest-striking dextral faults post-date mineralization and are interpreted to be associated with a later phase of deformation.

REFERENCES

Abbott, J.G., Gordey, S.P., Tempelman-Kluit, D.J., 1986, Setting of stratiform, sediment-hosted lead-zinc deposits in Yukon and northeastern British Columbia. In, J.A. Morin (editor), Mineral Deposits of the Northern Cordillera, Canadian Institute of Mining and Metallurgy Special Volume 37, p. 1-18.

Anderson, E.M., 1951, The Dynamics of Faulting. Oliver and Boyd, Edinburgh, 206 pages.

Anderson, R.G.,1987, Plutonic rocks of the Dawson map area, Yukon Territory; in Current Research, Part A, Geological Survey of Canada, Paper 87-1A, p. 689-697.

Atkinson, B.K., 1976, Deformation mechanism maps for polycrystalline galena. Earth and Planetary Science Letters, vol. 29, p. 210-218.

Aydin, A., 1988, Discontinuities along thrust faults and the cleavage duplexes. Geological Society of America Special Paper 222, p. 223-232.

Beach, A., 1976, The interelations of fluid transport, deformation, geochemistry and heat flow in early Proterozoic shear zones in the Lewisian complex. Philosophical Transactions of the Royal Society of London, vol. A280, p. 569-604.

Blusson, S.L.,1978, Regional geologic setting of lead-zinc deposits in Selwyn Basin, Yukon. In: Current Research Part A, Geological Survey of Canada Paper 78-1A, P.77-80.

Bostock, H.S., 1948, Mayo, Yukon Territory. Geological Survey of Canada Map 890A.

Boyle, R.W., 1965, Geology, geochemistry, and origin of the lead-zinc-silver deposits of the Keno Hill-Galena Hill area, Yukon Territory. Geological Survey of Canada Bulletin 111, 302 pages.

Carmichael, A.D., 1957, United Keno Hill Mines. In: Structural Geology of Canadian Ore Deposits, vol. 2, p. 66-77.

Cockfield, W.E., 1921, Silver-Lead deposits of the Keno Hill area, Mayo, Yukon. Geological Survey of Canada Summary Reports 1920, pt.A, p. 1-6.

Cockfield, W.E., 1924, Geology and ore deposits of Keno Hill, Mayo District, Yukon. Geological Survey of Canada Summary Reports 1923, pt. A, p. 1-21.

Cooper, M.A., Collins, D.A., Ford, M., Murphy, F.X., Trayner,P.M., and O'Sullivan, M.,1986, Structural evolution of the Irish Variscides. Journal of the Geological Society, London, vol. 143, p. 53-61.

Coward, M.P., 1982, Surge zones in the Moyne Zone of NW Scotland. Journal of Structural Geology, vol.4, p. 247-256.

Coward, M.P., and Potts, G.J., 1983, Complex strain patterns developed at the frontal and lateral tips of shear zones and thrust zones. Journal of Structural Geology, vol. 5, p.383-399.

Dahlstrom, C.D.A., 1969, Balanced cross sections. Canadian Journal of Earth Sciences, vol. 6, p. 743-757.

Dahlstrom, C.D.A., 1970, Structural geology in the eastern margin of the Canadian Rocky Mountains. Bulletin of Canadian Petrolium Geology, vol. 18, p.332-406.

Elliott, D., 1976, The energy balance and deformation mechanisms of thrust sheets. Royal Society of London Philosophical Transactions, ser. A, vol. 283, p. 289-312.

Gabrielse, H., 1985, Major dextral transcurrent displacements along the Northern Rocky Mountain Trench and related lineaments in north central British Columbia. Geological Society of America Bulletin, p. 1-14.

Gardner, D.A.C., Spang, J.H., 1973, Model studies of the displacement transfer associated with overthrust faulting. Bulletin of Canadian Petrolium Geology, vol. 21, p. 534-552.

Godwin, C.I., Sinclair, A.J., Ryan, B.D., 1982, Lead isotope model for the genesis of carbonate hosted Zn-Pb, shale hosted Ba-Zn-Pb, and silver-rich deposits in the northern Canadian Cordillera. Economic Geology, vol. 77, p. 82-94.

Goodfellow, W.D., Jonasson, I.R., 1986, Environment of formation of the Howards Pass (XY) Zn-Pb deposit, Selwyn Basin, Yukon. In, J.A. Morin (editor), Mineral Deposits of the Northern Cordillera, Canadian Institute of Mining and Metallurgy Special Volume 37, p. 19-51.

Gordey, S.P., Abbott, J.G., Tempelman-Kluit, D.J., and Gabrielse, H.,1987, "Antler" clastics in the Canadian Cordillera. Geology, vol. 15, p. 103-107.

Green, L.H., 1971, Geology of Mayo Lake, Scougale Creek and McQuesten Lake map-areas, Yukon Territory. Geological Survey of Canada Memoir 357, 72 pages.

Green, L.H., 1972, Geology of Nash Creek, Larsen Creek, and Dawson map-areas, Yukon Territory. Geological Survey of Canada Memoir 364, 157 pages.

Green, L.H., and McTaggart, K.C., 1960, Structural studies in the Mayo District, Yukon Territory. Proceedings of the Geological association of Canada, vol. 12, p. 119-134.

Hempton, M.R., and Neher, K., 1986, Experimental fracture, strain and subsidence patterns over en echelon strike-slip faults: implications for the evolution of pull-apart basins. Journal of Structural Geology, vol.8, p. 597-605.

Hobbs, B.E., Means, W.D., and Williams, P.F., 1976, An Outline of Structural Geology, John Wiley and Sons, New York, 571 pages.

Kindle, E.D., 1962, Keno Hill, Yukon Territory. Geological Survey of Canada, map 1105A.

Lagarde, J.L., and Michard, A., 1986, Stretching normal to the regional thrust displacement in thrust-wrench shear zone, Rehamna Massif, Morocco. Journal of Structural Geology, vol. 8, p.483-492.

Logan, J.M., 1986, Mineralogy and metal distribution, Hallmac mine, Sandon (82F/14, 82K/3). British Columbia Ministry of Energy, Mines and Petroleum Resources, Paper 1986-1, p. 289-301.

McClay, K.R., Insley, M.W., 1986, Duplex structures in the Lewis Thrust Sheet, Crowsnest Pass, Rocky Mountains, Alberta Canada. Journal of Structural Geology, vol. 8, p. 911-922.

McTaggart, K.C., 1960, The geology of Keno and Galena Hills,Yukon Territory, Geological Survey of Canada Bulletin 58, 37 pages.

Monger, J.W.H., Price, R.A., Tempelman-Kluit, D.J., 1982, Tectonic accretion and origin of the two major metamorphic and plutonic welts in the Canadian Cordillera, Geology, vol. 10, p.70-75.

Naylor, M.A., Mandl, G., Sijpesteijn, C.H.K., 1986, Fault geometries in basement-induced wrench faulting under different initial stress states. Journal of Structural Geology, vol. 8, p.737-752.

Newhouse,W.H., 1942, Ore deposits as related to structural features. Princeton University Press, Princeton, New Jersey, 280 pages.

Philcox, M.E., 1964, Compartment deformation near Buttevant, County Cork, Ireland, and its relation to the Variscan thrust front. Scientific Proceedings of the Royal Dublin Society, 2A, p.1-11.

Poulton, T.P., and Tempelman-Kluit, D.J., 1982, Recent discoveries of Jurassic fossils in the Lower Schist Division of central Yukon. Current Research Part C, Geological Survey of Canada Paper 82-1c, p.91-94.

Pugh, D.C., 1983, Pre-Mesozoic geology in the subsurface of Peel River map area, Yukon Territory and District of MacKenzie. Geological Survey of Canada Memoir 401, 61 pages.

Ramsay, J.G., 1967, Folding and Fracturing of Rocks. McGraw-Hill, New York, 568 pages.

Ramsay, J.G., 1980, Shear zone geometry: a review. Journal of Structural Geology, vol. 2, p. 83-89.

Ratley, P.R., Sanderson, D.J., 1982, Patterns of folding within nappes and thrust sheets: examples from the Variscan of southwest England. Tectonophysics, vol. 88, p. 247-261.

Ridley, J., 1982, Arcuate lineation trends in a deep level, ductile thrust belt, Cyros, Greece. Tectonophysics, vol. 88, p. 347-360.

Sanderson, D.J., 1982, Models of strain variation in nappes and thrust sheets: a review. Tectonophysics, vol. 88, p. 201-233.

Sibson, R.H., 1986, Brecciation processes in fault zones. Pure and Applied Geophysics, vol. 124, p.159-175.

Sibson, R.H., 1987, Earthquake rupturing as a mineralizing agent in hydrothermal systems. Geology, v. 15, p. 701-704.

Sinclair, A.J., Tessari, O.J., and Harakal, J.E., 1980, Age of Ag-Pb-Zn mineralization, Keno Hill-Galena Hill area, Yukon Territory. Canadian Journal of Earth Sciences, p.1100-1103.

Tempelman-Kluit, D.J., 1970, Stratigraphy and structure of the "Keno Hill Quartzite" in Tombstone River-Upper Klondike River map-areas, Yukon Territory (116 B/7, B/8). Geological Survey of Canada Bulletin 180, 102 pages.

Tempelman-Kluit, D.J., 1979, Transported cataclasite, ophiolite and granodiorite in Yukon: evidence of arc continent collision. Geological Survey of Canada Paper 79-14, 27 pages.

Tempelman-Kluit, 1981, Geology and mineral deposits of southern Yukon. In: Yukon Geology and Exploration 1979-80, Northern Affairs Program, Whitehorse, Yukon, 364 pages.

Turner, F.J., 1980, Metamorphic Petrology, Mineralogical, Field, and Tectonic Aspects. McGraw-Hill Book Co., New York, 524 pages.

Watson, K.W., 1986, Silver-Lead-Zinc deposits of the Keno Hill-Galena Hill Area Yukon Territory. In: Yukon Geology, Vol. 1, Exploration and Geological Services Division, Yukon Indian and Northern Affairs Canada, p. 83-88.

Woodcock, N.H., and Robertson, A.H.F., 1982, Wrench and thrust tectonics along a Mesozoic-Cenozoic continental margin, Antalya complex, S.W. Turkey. Journal of the Geological Society of London, vol. 139, p. 147-163.

Woodcock,N.H., and Fischer, M., 1986, Strike-slip duplexes. Journal of Structural Geology, vol. 8, p. 725-733.

CHAPTER 3

LARGE SCALE HYDROTHERMAL ZONING AND TETRAHEDRITE-FREIBERGITE SOLID SOLUTION IN THE KENO HILL Ag-Pb-Zn DISTRICT, YUKON.

INTRODUCTION

This chapter establishes the large scale nature of the Keno Hill hydrothermal system, by documenting a broad and continuous mineral zoning sequence within veins distributed throughout the Keno Hill Quartzite.

The Keno Hill mining district is located in central Yukon, 350 km north of Whitehorse (Fig. 3-1). Since 1913 over 4.54 million tonnes of ore averaging 1412 g/tonne Ag, 6.8 % Pb, and 4.6 % Zn have been mined, and in excess of 6.4 billion g of silver have been produced (Watson, 1986).

The class of deposit to which the Keno Hill veins are assigned is referred to by several designations: "Cordilleran vein type deposits" (Guilbert and Park, 1986), "felsic intrusion associated silver-lead-zinc veins" (Sangster, 1984), "Pb-Zn sulfide Ag-sulphosalt deposits" (Andrews, 1986), or polymetallic veins. Despite the considerable productivity of this type, relatively little research has been directed towards such high grade silver veins in the last decade (Andrews, 1986), and consequently their general characteristics and genesis are poorly understood.

The most extensive geological work completed on the veins of the Keno Hill district is by Boyle (1965), who gave a thorough documentation of the various mineral associations from the district. Boyle recognized separate mineralogically distinct groups of veins throughout the region: cassiterite, wolframite, scheelite and related minerals occur near Cretaceous plutonic bodies, whereas veins containing siderite, galena, sphalerite, and freibergite are separated from the plutons. The two groupings were considered to be

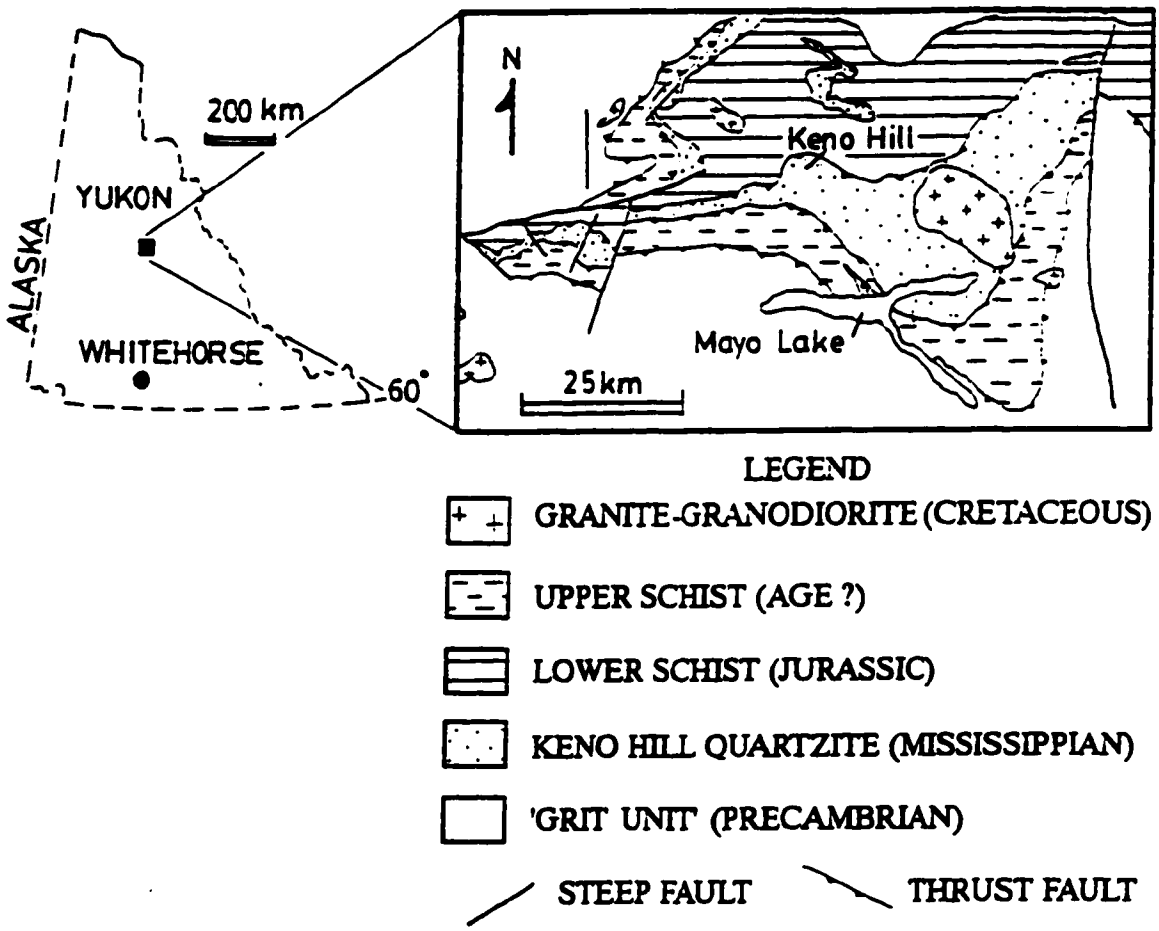

Figure 3-1. Location map and geological setting of Keno Hill mining district in central Yukon.

unrelated, and the silver lodes were thought not to be associated with the plutons, either spatially or genetically (Boyle,1965). Boyle concluded that the metals were emplaced vertically from below through diffusion processes; a flowing hydrothermal medium was not favored. However, hydrothermal features are clearly displayed in the vein system. Also, similar Cretaceous ages for the silver veins and for the felsic plutons of the region indicate the possibility of a genetic link between the two (Sinclair et al., 1980; Godwin et al., 1982).

This chapter describes district-wide mineral zoning within the Keno Hill vein system. Economic and non-economic parts of the district are both considered in documenting the continuity of the zones. The patterns indicate a spatial association between the silver deposits, tin mineralization and the Mayo Lake Pluton. Lateral movement of evolving hydrothermal fluids during mineralization, along the highly fractured Keno Hill Quartzite, is indicated by the mineral zoning sequence. The lateral distribution of minerals allows for the exposure of a complete crossection of the hydrothermal column, at the present level of erosion, from plutonic to epithermal end-members. The documented zoning corresponds to the classic generalized zoning models of Spurr (1907, 1912).

A more quantitative approach to the study of geochemical zoning was pursued through an electron-microprobe investigation of the tetrahedrite-series minerals. Seventy electron-microprobe analyses were performed on tetrahedrite samples from 12 different deposits across the district. Argentian tetrahedrite, the most important silver ore-mineral in the Keno Hill district, occurs throughout a 25-km-long portion of the laterally zoned system. As reported in the literature, zoning tendencies in general are for an increase in Ag/Cu, and Sb/As in the more evolved deposits (Hackbarth and Petersen,1984), as well as Fe/Zn in some cases (Jambor and Laflamme, 1978). Substitutions are generally insensitive to temperature, but are responsive to changing fluid chemistry (Sack and Loucks, 1985). However, in the silver rich end-member, freibergite, there may be a crystallographical restriction to the amount of arsenic present (Johnson and Burnham, 1985). In the Keno

Hill area, the compositional changes in the tetrahedrite correspond well with the broad mineralogical zones.

Data were gathered over the course of two summers of field work that involved local surface mapping at various scales, logging of drill cores, and detailed mapping of underground exposures and open pits. Thin section and polished section petrography was performed in the laboratory during the winter; X-ray diffraction was used to confirm mineral identification.

GEOLOGICAL SETTING

The Mississippian Keno Hill Quartzite, which hosts the high-grade silver deposits, is in the Selwyn Basin in a region that forms the northern extension of the Omineca Crystalline Belt. The Belt is a collision-related, Cordilleran-scale, plutonic-metamorphic welt overlapping accreted terranes and the North American craton (Tempelman-Kluit, 1979; Monger et al., 1982).

The quartzite extends for more than 220 km along strike and is bounded above and below by thrust faults (Fig.3-1). The strata dip moderately towards the south, and thrusting was generally towards the north. The main unit below the quartzite is the Jurassic "Lower Schist" unit (Poulton and Tempelman-Kluit, 1982). Above the quartzite are overthrust "Grit Unit" rocks of the Proterozoic Windermere Supergroup, Siluro-Ordovician Road River formation, and "Upper Schist" unit rocks of undetermined age. This deformed, greenschist facies, sedimentary package is cut by bimodal Cretaceous felsic plutons: an alkalic suite to the west of the district, and a granitic suite in the region near the mining district (Anderson, 1987). The sequence of thrusting and pluton intrusion postdate the Jurassic Lower Schist and terminates with Cretaceous plutonism.

The Keno Hill Quartzite is a dark grey, graphitic quartzite with minor muscovite, chlorite, tourmaline, zircon and usually less than 5% carbonate. Individual layers of quartzite are typically from 1 to 3 m thick and have thin interlayers of graphitic schist. In

the area of Keno Hill-Galena Hill the structural thickness of the quartzite is approximately 1 km. Other than bedding, sedimentary structures are not common. The quartzite has been recrystallized and contains concordant metamorphic quartz segregations. Finely crystalline grey limestone or marble units are widely distributed but are not abundant.

Concordant lenses of "greenstone" are abundant throughout the Lower Schist and in the Keno Hill Quartzite, but are less abundant in the Upper Schist. The lenses are 1 m to 30 m in thick, and locally persist along strike for more than 1 km. They are interpreted to be the metamorphosed equivalents of gabbro and diorite sills (Green, 1971). Their most common metamorphic assemblage is zoisite-albite-actinolite-chlorite ± stilpnomelane (McTaggart, 1960). The lenses are older than the undeformed granitic bodies (mid-Cretaceous), and possibly were cogenetic or younger than the Jurassic rocks.

The Mayo Lake pluton cuts the Keno Hill Quartzite to the east of the mining district (Fig. 3-2). It has been dated by the K-Ar method at 81 Ma (G.S.C. map 1398A). The pluton varies from a core of coarse porphyritic granite containing megacrysts of alkali feldspar, black amphibole, and minor titanite, to a margin of finer equigranular granodiorite with green amphibole. Contact metamorphism extends outwards for up to 4 km. Sillimanite schist at the contact grades outward into garnet-staurolite-feldspar schist. The most distal part of the aureole is characterized by biotite-muscovite schist at low altitudes (700-1220 m) and graphite-andalusite schist at higher altitudes (1525- 1825 m). Texturally, the andalusite crystals have a variable orientation within the schist and overgrew deformation fabrics. Pressure shadows were not found around garnet crystals. Such features indicate a predominantly post-kinematic age for the final emplacement of the Mayo Lake pluton. Greenstone lenses near the pluton have been converted to hornblendite. A tungsten skarn is reported to occurr along the western contact of the pluton (Bostock, 1948), but the remote showing was not visited during the course of this study.

Aplite and pegmatite dykes are common along the margins of the pluton. Quartz-feldspar porphyry dykes, locally with amphibole, extend over a broad area (Boyle, 1965) but are not abundant. They have been dated at 81 ± 5 Ma (Green, 1971). Rare lamprophyre dykes of undetermined age also occur in the district. Micas from hydrothermal alteration surrounding the Ag-Pb-Zn veins of the mining district have been dated (K-Ar) to be mid-Cretaceous (84 ± 4 Ma, Sinclair et al., 1980), showing that they are contemporaneous with the felsic intrusive bodies.

HYDROTHERMAL VEINS, MINERAL ZONING, AND PARAGENESIS

Hydrothermal veins are widespread within the Keno Hill quartzite. The frequency of the veins is variable from outcrop to outcrop; often, only one or two veins are found in an exposure. Nevertheless, the veins are distributed across tens of kilometers, and collectively form a close, complicated network on a larger scale.

Hydrothermal veins of the mineralizing event can usually be distinguished readily from earlier metamorphic quartz segregations of the greenschist metamorphic event. Hydrothermal veins are coarse grained, vuggy, with euhedral to subhedral crystals, display strong banding textures, are structurally discordant and locally have well developed alteration haloes. Metamorphic quartz segregations are concordant, finer grained, massive, usually monomineralic, and exhibit strain features.

Structural control of veins is considered in reports by McTaggart (1960), and Chapter 2. The orebodies are contained within an extensive set of sinistral, strike-slip and dip-slip faults, which strike northeast and dip steeply to the southeast (Fig. 3-2 A). Much of the vein material is unstrained, but parts of some veins contain sheared and deformed crystals; brecciated hydrothermal vein minerals are cemented by later hydrothermal minerals, indicating that faulting and hydrothermal activity could have been contemporaneous. Other types of fractures important in localizing veins are widespread north to northeast striking "AC" tension fractures, and north to northwest striking fractures. Both sets dip steeply.

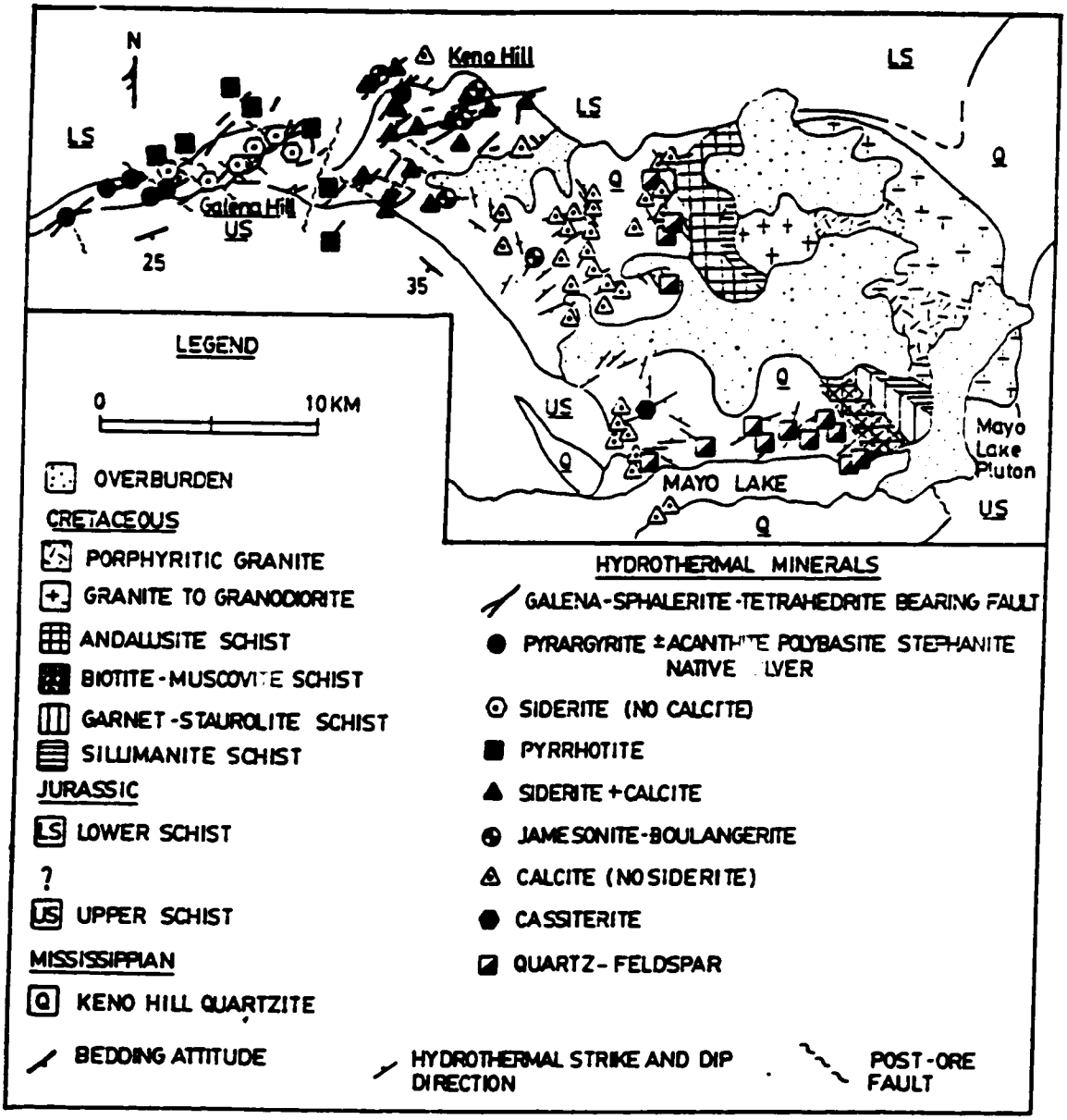

Figure 3-2. Map of pricipal hydrothermal mineral zones within the Keno Hill Quartzite, and relation of veins to the Mayo Lake pluton in the eastern portion of the map. The diagram emphasizes mineralogical differences, though there is considerable overlap between zones.

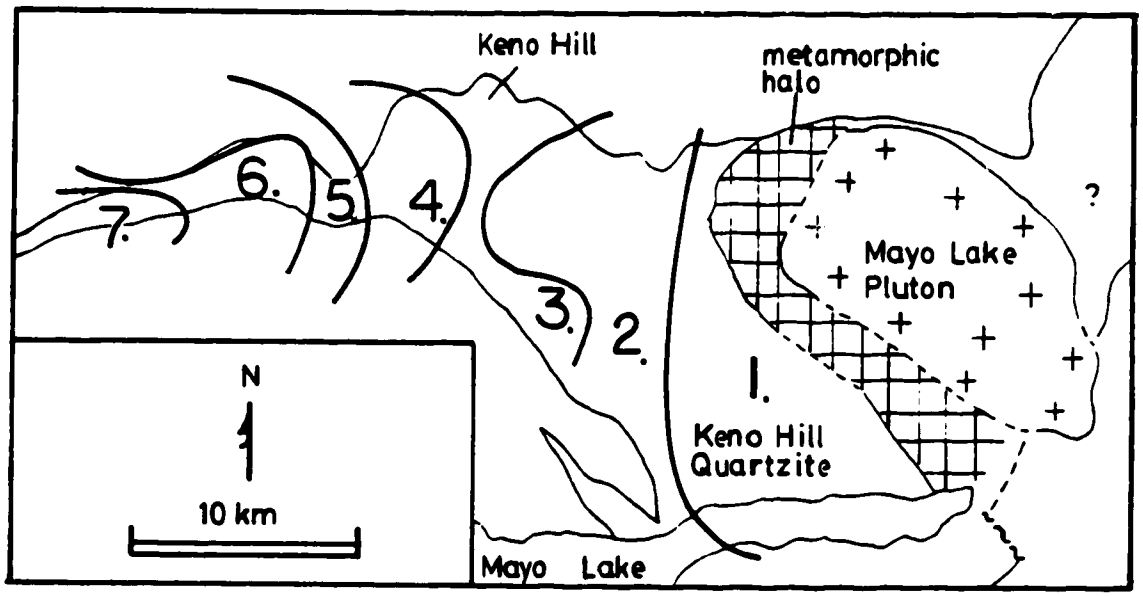

CONTOUR MAP OF HYDROTHERMAL ZONES

BARREN

1. FELDSPAR ZONE: K-feldspar, plagioclase, quartz, epidote ± tourmaline, apatite, pyrite, arsenopyrite, ilmenite, cassiterite, muscovite
2. CALCITE ZONE: calcite, quartz, epidote±pyrite, chalcopyrite, arsenopyrite, galena
3. JAMESONITE ZONE: jamesonite, boulangerite, arsenopyrite, sphalerite, chalcopyrite, tetrahedrite, quartz, calcite, native Au (overlaps with zone 4)

Ag-Pb-Zn ORE

4. SIDERITE-CALCITE ZONE: siderite, quartz, calcite, galena, sphalerite, tetrahedrite, arsenopyrite, pyrite
5. PYRRHOTITE ZONE: siderite, quartz, calcite, galena, sphalerite, tetrahedrite, pyrrhotite, arsenopyrite, pyrite (same as zone 4 with pyrrhotite)
6. SIDERITE ZONE: siderite, quartz, galena, sphalerite, tetrahedrite, pyrite (similar to zones 4 and 5, but without calcite, arsenopyrite, pyrrhotite)
7. EPITHERMAL ZONE: quartz, pyrargyrite, acanthite, polybasite, stephanite, native Ag, pyrite, kaolinite ± marcasite, chalcopyrite, stibnite, barite (overlaps with zone 6).

Figure 3-2 B. Contour map of hydrothermal mineral zones within the Keno Hill Quartzite and Keno Hill mining district. Contours are drawn according to the appearance and disappearance of specific vein minerals away from the Mayo Lake Pluton (see Figure 3-2 A).

Within the system, groups of adjacent veins and deposits have characteristic mineral assemblages that distinguish them from other groups; these groups form mineralogical zones distributed along the length of the hydrothermal system (Fig. 3-2 A and B). Adjacent zones are identified by the appearance or disappearance of specific index minerals, as well as of characteristic assemblages. Other minerals which overlap between zones demonstrate the continuity of the vein system. A summary of the mineral paragenesis for the entire district is presented in Figure 3-3; however the complete listing of minerals is never seen together within a single vein, and the paragenesis diagram is only schematic as timing inferences are made for minerals from adjacent zones by the occurrence of minerals which overlap between the zones.

The veins are texturally quite variable along the length of the belt. Quartz crystals in the region proximal to the pluton are euhedral and up to 20 cm long, and display a comb texture. Crosscutting relations are not complex in this area, though layering within the veins or banded texture is often seen (Fig. 3-4). In the distal region, euhedral quartz crystals are commonly less than 5 mm long and crosscutting relations of various vein sets are considerably more complex. Various types of stockworks and breccias are observed (Figs. 3-5 C, 3-6 A and B). A vuggy texture to the veins, indicative of open space filling, is characteristic of the entire system from east to west.

Figure 3-2 A and B show the mineralogical zoning which is described below.

Feldspar zone

The presence of feldspar in the veins marks the innermost hydrothermal zone around the Mayo Lake Pluton. A variety of feldspars are present: orthoclase, microcline, and plagioclase (albite to labradorite). The potassium feldspar has perthitic texture. Locally, orthoclase forms vermicular intergrowths with quartz.

Many of the feldspar-bearing veins have euhedral yellowish feldspar dominating the vein-wallrock contact, and quartz in the center of the vein (Fig. 3-4 A). Minor constituents

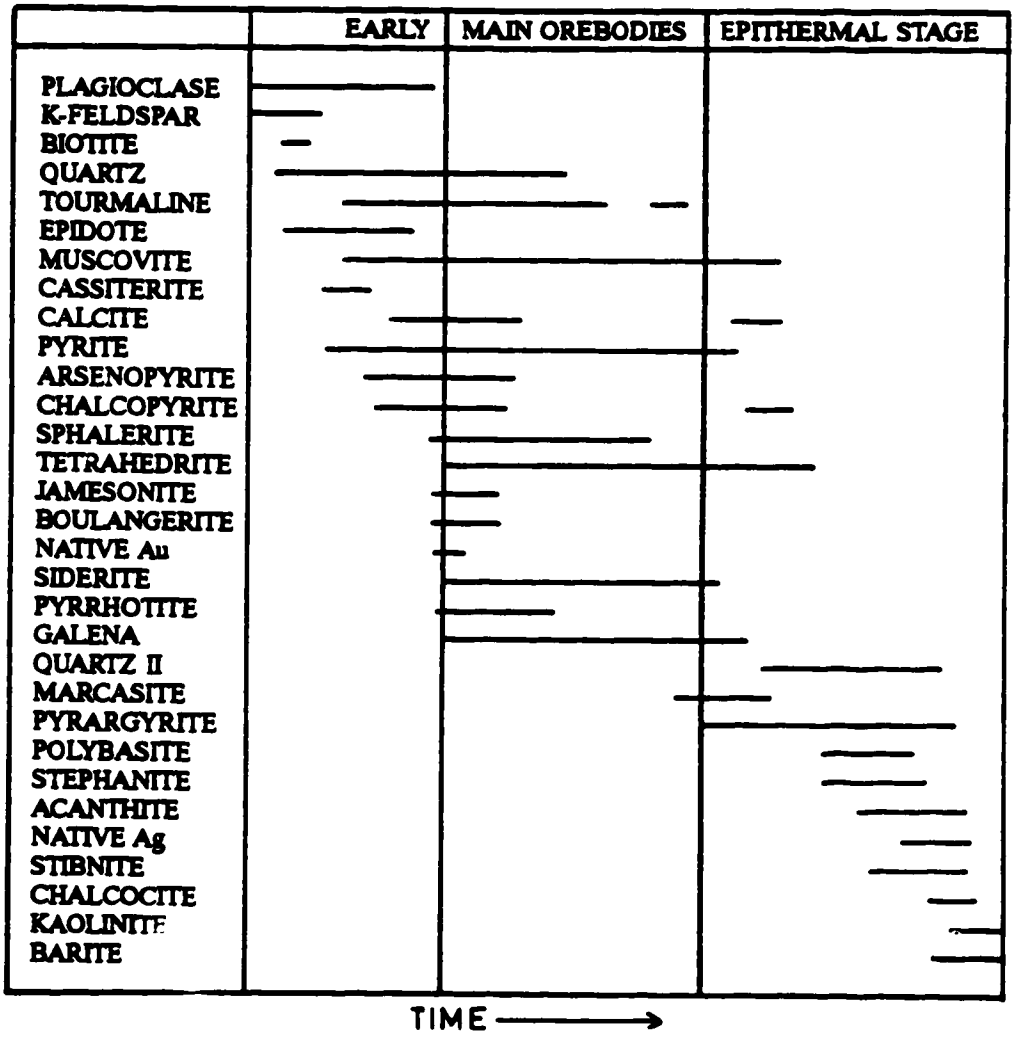

Fig. 3-3 Paragenesis diagram for hydrothermal minerals of the Keno Hill district.

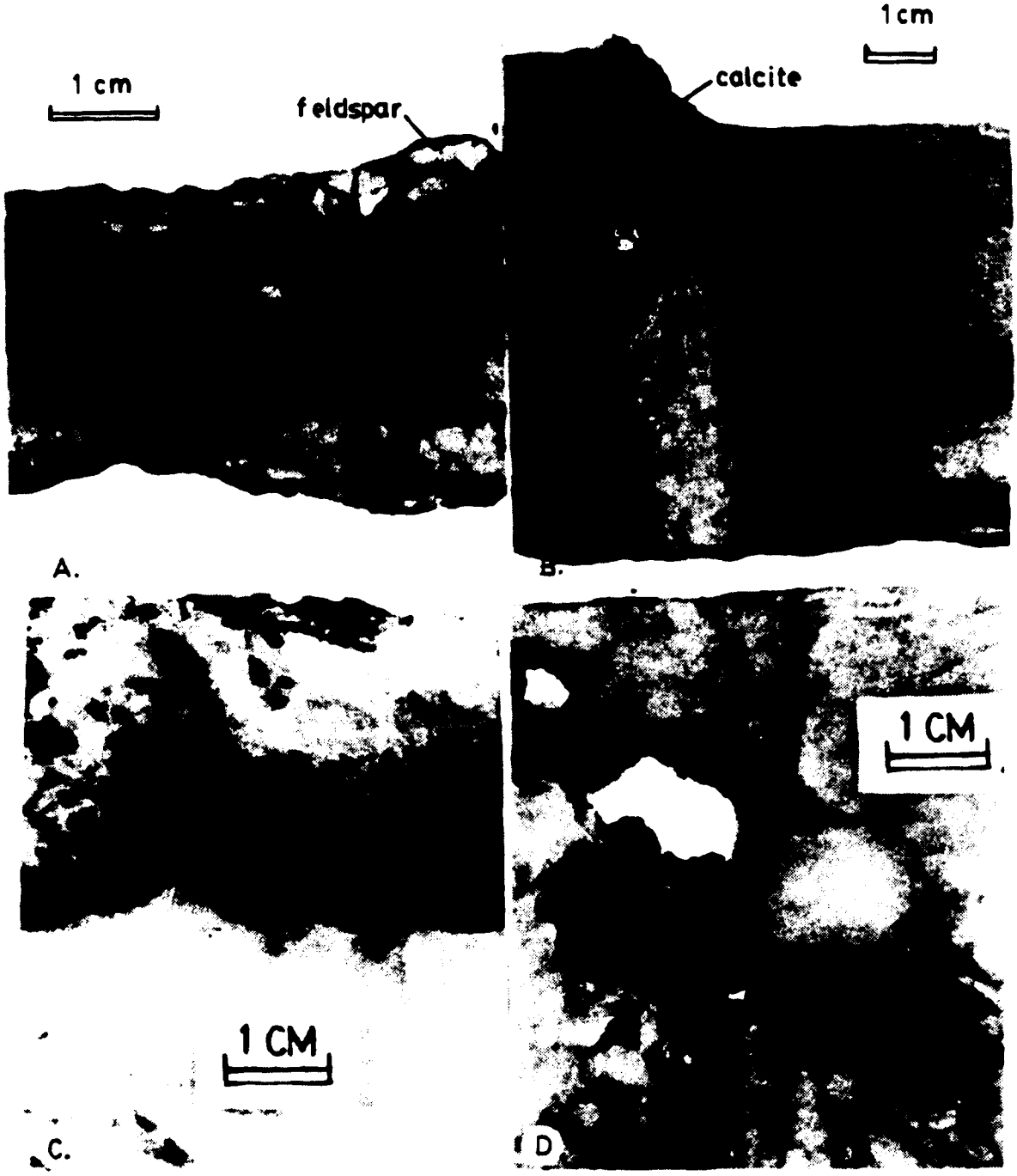

Figure 3-4. Veins east of the mining district near the Mayo Lake Pluton; (A) banded quartz-feldspar vein displaying euhedral light colored feldspar along the upper and lower vein margins; (B) quartz-calcite vein with carbonatization halo in sericitic quartzite; (C) banded calcite and calcite-epidote vein from near margin between calcite zone and feldspar zone; (D) potograph displays coarse vuggy nature of quartz veins, with some interstitial galena.

include zoisite, pyrite, apatite, tourmaline, and rare ilmenite. The alteration of the quartzite is typically weak and may include a small inner halo of feldspathization with outward sericitization. The alteration of greenstones is more complex: chlorite and combinations of anthophyllite, clinizoisite, and fine grained actinolite are typically abundant; also present is a weak alteration containing orthoclase near the vein and biotite farther out. Original feldspars in the greenstones remain unaltered. A late stage of fine grained calcite and siderite fills cracks and microveinlets which cut through earlier vein material.

Cassiterite in quartz veins is uncommon, but serves as a useful index mineral for the near-plutonic environment. The cassiterite-bearing veins occur near the outer margin of the feldspar zone, almost 10 km from the pluton (Fig. 3-2). Coarse flakes and books of muscovite occur along the margins of some of these vuggy quartz veins. Other minerals are rare in these veins, but include pyrite and arsenopyrite. Alteration haloes involve moderate sericitization of the host. It may be significant that the galena of the mining district is reported to have a high tin content (Boyle, 1965), a further link between the cassiterite bearing zone and the Ag-Pb-Zn orebodies.

Calcite Zone

The presence of calcite marks a broad and distinct zone between the silver-rich veins of the mining district to the west and the feldspar-bearing veins in the vicinity of the pluton. Coarse calcite in variable abundances is the most distinguishing feature of this zone (Fig. 3-4 B). Euhedral zoisite and epidote are commonly with the calcite (Fig. 3-4 C), and are important overlap minerals between the feldspar zone and the carbonate zone. Small amounts of pyrite, arsenopyrite and chalcopyrite are usually found in these veins. Multiple banding or layering is a common vein texture (Fig. 3-4 C). Albite intergrown with calcite and quartz was observed in a few samples from near the eastern feldspar zone. The degree of host-rock alteration is more pronounced in the calcite zone and the appearance of sulfides is more frequent. Carbonatization and sericitization haloes surround the veins in

the quartzite, and have a marked bleaching effect due to graphite removal. Chlorite, epidote, carbonate and sericite haloes are more abundant where the greenstone is the host unit. Although these veins have mineralogical features resembling mesothermal precious metal deposits, they have not been extensively explored and their economic potential is uncertain.

Jamesonite-boulangerite zone

The overall mineralogical changes within this zone are considerable. A characteristic feature is the appearance of bladed, medium-grained crystals of jamesonite and boulangerite. The presence of the two in this mining district was established by Boyle (1965); they often occur together but jamesonite appears to be more abundant. Beginning with the jamesonite-boulangerite zone, the overall abundance of opaque minerals in the veins rises sharply (Fig. 3-5 A). The opaque phases include arsenopyrite, pyrite, chalcopyrite, light brown sphalerite, tetrahedrite and traces of fine-grained native gold (Fig 3-5 B). Crosscutting relations increase in complexity in this zone. Thick sphalerite-rich layers alternate with arsenopyrite, pyrite and tetrahedrite layers. Pure quartz zones also occur. Many large euhedral quartz crystals have been brecciated and cemented by felted masses of jamesonite-boulangerite, indicating forceful hydrothermal activity or contemporaneous fault movement. Portions of the veins contain only quartz and calcite with minor pyrite, and are similar to the veins of the previous zone.

Gold is typically microscopic and occurs along the margins of arsenopyrite crystals or with pyrite and tetrahedrite. Placer operations are active in the vicinity of these veins, to which the source of the placer gold is attributed.

Siderite zones

Siderite which is the most widespread and characteristic gangue mineral within the silver orebodies, occurs with pyrite, galena, sphalerite and tetrahedrite. On Keno Hill this

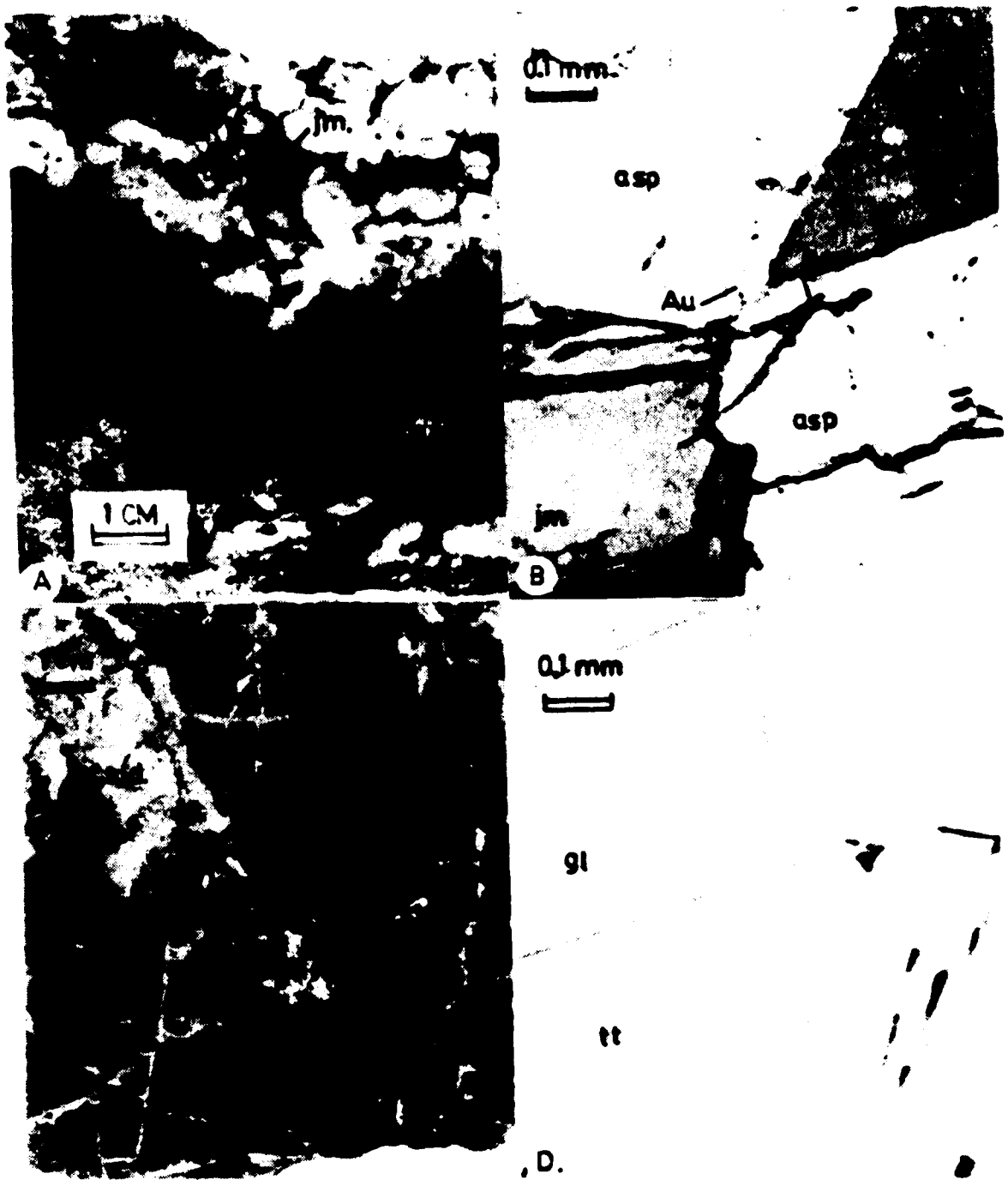

Figure 3-5. Veins from the mining district and central portion of hydrothermal system; (A) banded vein with massive arsenopyrite (asp), and sphalerite (sp) along vein margin, with quartz (white) and jamesonite (jm) towards the vein center; (B) photomicrograph showing position of native gold (Au) between arsenopyrite (asp) and jamesonite (jm) crystals; (C) typical galena (gl)-pyrite-siderite (sid) vein crosscutting early quartz stockwork in dark graphitic quartrzite host; (D) micrograph of tetrahedrite (tt) inclusions in galena (gl).

assemblage is intergrown with quartz, arsenopyrite and calcite. However, arsenopyrite and calcite are less abundant, or more typically absent, in veins to the west on Galena Hill, allowing for the siderite zone to be further subdivided (Fig. 3-2). Texturally, the siderite is coarse to medium grained and massive. It cements breccias and fills stockworks in fault structures. In the upper parts of some veins it is oxidized to iron and manganese hydroxides.

Wallrock alteration is characterized by sericitization with pyrite and minor tourmaline, as well as carbonatization. A more chlorite-rich assemblage typifies the alteration of the greenstone lenses.

Siderite does not generally occur with jamesonite and boulangerite, but is found along strike in some of the same fault structures. Jamesonite and boulangerite also appear in splay faults connecting directly to the main siderite-bearing veins. In some localities siderite veins cut jamesonite-boulangerite-quartz veins (Fig. 3-5 C). The overlap between these two groups is observed only on Keno Hill.

Pyrrhotite zone

Pyrrhotite occurs as an accessory mineral in several of the deeper veins exposed in the low-lying area between Galena Hill and Keno Hill (Fig.3-2). In two of the deposits, Duncan Creek and Flame-Moth veins it is more abundant. At elevations below 900 m altitude, siderite-pyrite-galena-sphalerite-tetrahedrite veins may contain calcite, arsenopyrite and pyrrhotite as well. However, these three minerals disappear at higher elevations on Galena Hill and to the west at low elevations beyond Galena Hill. This is the only clearly established mineral zonation with a distinct vertical component in the district. Most of the other zones adjoin laterally because diagnostic minerals are found at various altitudes. As a group, pyrrhotite-bearing veins form a narrow belt which closely follows contour along the western flank of Galena Hill (Fig. 3-2).

Pyrrhotite is replaced by marcasite along partings in crystals, fractures in aggregates and along grain boundaries. Fresh samples of pyrrhotite commonly have extensive graphic intergrowths with sphalerite. The sphalerite may also have "chalcopyrite disease".

Pyrargyrite zone and veins of "epithermal" character

Pyrargyrite is widespread and contributes significantly to the silver values of the western deposits. However, appreciable amounts of the mineral occurs in the Lucky Queen mine on Keno Hill in the east (localities for the mines referred to are shown in Fig. 3-8). The western zone marks the last stage of the system. It is characterized by other phases as well, which have a more erratic distribution within the zone; these include acanthite, native silver, polybasite, stephanite, stibnite, marcasite, barite, dendritic quartz and kaolinite as an alteration mineral. Such minerals give the deposits a distinctly epithermal character.

Some of the pyrargyrite occurs with galena, freibergite, pyrite, sphalerite, and siderite, but most is intergrown with a late-stage quartz that encrusts vugs in siderite, or in stockwork stringers that cut siderite (Fig. 3-6 A, B). The quartz occurs mainly as fine grained, euhedral, clear crystals, or as radiating bundles of fine-grained, milky white dendrites. The latter show feather-like skeletal patterns in thin section.

At the Husky mine a peculiar form of pyrite can occasionally be seen in the veins. Slender tubes of pyrite project into open vugs (Fig. 3-6 C). The tubes are up to 10 cm long and 1 cm in diameter. All are hollow, and give the appearance of having formed as "chimneys" for hydrothermal fluids seeped into vugs. Vugs also contain coarse world-class specimens of polybasite and stephanite.

Gersdorfite was detected by X-ray diffraction in one sample, with quartz and siderite. This assemblage occurs with marcasite, chalcopyrite and tetrahedrite rimmed by chalcocite. Minor fine-grained sphalerite is also present. Banded textures show that the siderite-

Figure 3-6. Veins from western epithermal system; (A) breccia of dark graphitic quartzite clasts cemented by siderite (light color) and overgrown by quartz (white) with fine grained dark pyrargyrite; (B) subrounded breccia clasts of quartzite (dark) and hydrothermal siderite (light colored) cemented by the late hydrothermal quartz stage (white); (C) coarse wire silver; (D) hollow and spiralling pyrite tubes.

bearing assemblage is typically overgrown by quartz and pyrargyrite, in turn overgrown by cubes of pyrite. Kaolinite fills some of the vugs.

Host-rock alteration includes recrystallization of the quartzite to a fine grained granular mass, within intense stockworks of fine quartz veinlets which are densely interwoven and often not perceptible until the rock has been cut or a thin section made. Sericitization is widespread with minor tourmalinization. Kaolinite occurs locally as an alteration mineral often with disseminated pyrite. Carbonates are not seen in most alteration haloes. Graphite has been removed in altered sections of host rocks, giving the rock a distinct bleached appearance. Coarse barite is occasionally found and appears as a late stage mineral which locally cements brecciated fragments of galena and siderite.

Pyrargyrite also occurs separately with acanthite, coarse wires of native silver and fine-grained euhedral quartz (Fig. 3-6 D). This assemblage is well developed in portions of the Silver King mine.

It was not clearly established in the past whether pyrargyrite and some of its associated minerals are of supergene or hypogene origin (Boyle, 1965). The present interpretation is that minerals of this suite are mainly of hypogene origin. In new mine workings of the Husky orebody, much of the pyrargyrite is associated with pyrite cubes and quartz crystals; the pyrite is fresh, and crystallized quartz does not generally form from low-temperature supergene processes. Also, pyrargyrite in nature is more frequently observed as a hypogene rather than a supergene mineral in vein systems (Guilbert and Park, 1986).

TETRAHEDRITE CHEMISTRY

Analytical methods

Electron microprobe analyses of tetrahedrite samples were performed at the Department of Geology, the University of Alberta, using an ARL-SEMQ microprobe. Quantitative wavelength dispersion analyses (WDS) were done at 15 kv operating voltage,

4 nA probe current and 100 sec counting time. Data were processed with full-matrix (ZAF) corrections using EDATA2 (Smith and Gold, 1979).

Nine elements were analyzed at each point: Cu, Ag, As, Sb, Fe, Te, Cd, Zn, and S. Pure metal standards were used for each element, except that marcasite and arsenopyrite were used for Fe and As. All weight percent totals range between 97 and 101 %.

Analytical results

Texturally, tetrahedrite occurs predominantly as round, bleb-like inclusions, typically < 0.1 mm in diameter, in coarser grained galena (Fig. 3-5 D). A multitude of these inclusions may be contained within a single galena crystal. Tetrahedrite in this form was analyzed from the various deposits of the district to maintain sample consistency. Except for the sheared galena from the Calumet and Shamrock mines, galena used in the microprobe study showed little sign of strain.

Microprobe data are summarized in Tables 3-1 and 3-2. Tetrahedrite chemistry is approximated by the following stoichiometry (Sack and Loucks, 1985): $(Cu,Ag)_6^{TRG}[Cu_{-/3}(Fe,Zn,Cd,Hg,Pb)_{1/3}]_6^{TET}(Sb,As,Bi)_4^{SM}(S,Se)_{13}$, where TRG = trigonal planar, TET = tetrahedral, SM = semimetal sites. However, considerable departures from this ideal formula are widely reported in the literature, particularly in the case of Ag-bearing tetrahedrites (Johnston et al., 1986). Discrepancies are observed both in naturally occurring tetrahedrites and in synthetic tetrahedrite (Mackovicky and Skinner, 1978). In some cases Ag-depleted tetrahedrite does not correspond to the formula as well; Skinner et al. (1972) obtained synthetic tetrahedrite with the composition $Cu_{12+X}Sb_{4+Y}S_{13}$ where $X \leq 1.9$ and $Y \leq 0.3$. Additional metal and semi-metal atoms are reported by Wu and Petersen (1977) for tetrahedrite from Peru.

The composition of tetrahedrite from the Keno Hill district approximates $(Cu,Ag)_{10+X}(Fe,Zn,Cd)_{2+Y}(Sb,As)_{4+Z}S_{13}$, where X = 0.8 to 2.1, Y = 0.1 to 0.5, and Z = 0.3 to 0.8 (Table 3-2). As can be seen, combined Cu and Ag in particular may greatly

Table 3-1. Tetrahedrite microprobe data, in weight percent.

	Cu	Ag	Fe	Zn	Cd	Te	Sb	As	S	TOTAL
Homestake 1	27.21	15.90	3.65	3.20	0.21	0.00	26.70	0.81	21.95	99.65
Homestake 2	26.23	16.41	3.59	3.27	0.23	0.00	26.68	0.78	21.82	99.02
Homestake 2r	26.07	16.64	3.35	3.33	0.23	0.00	26.94	0.85	21.81	99.12
Homestake 3	26.46	15.59	3.81	3.02	0.19	0.00	26.46	0.77	22.13	98.41
Homestake 4	27.24	15.51	3.74	3.15	0.21	0.00	26.41	0.75	22.04	99.06
Homestake 4r	26.81	15.80	3.49	3.18	0.18	0.00	26.52	0.72	21.93	98.62
Homestake 5	27.37	15.67	3.63	3.68	0.16	0.00	26.41	1.35	22.13	100.42
average	26.77	15.93	3.61	3.26	0.20	0.00	26.59	0.86	21.97	
Onek 1	24.84	19.29	4.71	1.86	0.22	0.01	26.72	0.77	21.12	99.53
Onek 1r	25.26	18.93	4.35	2.09	0.22	0.00	26.61	0.78	21.09	99.33
Onek 2	24.68	19.32	4.17	2.45	0.22	0.00	26.41	0.93	21.69	99.88
Onek 2r	24.80	19.00	4.31	2.26	0.20	0.09	26.64	0.83	21.76	99.88
Onek 3	23.99	19.04	4.29	2.35	0.23	0.00	26.70	0.75	21.95	99.31
Onek 4	24.99	19.[illegible]	4.28	2.37	0.23	0.01	26.73	0.70	22.05	100.64
Onek-B 3	23.91	19.13	4.50	1.66	0.15	0.03	27.19	0.55	22.11	99.24
Onek-B 3r	23.82	19.33	4.53	1.66	0.13	0.07	27.27	0.58	22.24	99.64
average	24.54	19.16	4.39	2.09	0.20	0.03	26.78	0.74	21.75	
Sadie 1	19.86	25.00	4.42	1.57	0.25	0.01	26.61	0.15	21.20	99.06
Sadie 2	19.23	27.10	4.63	1.42	0.32	0.09	26.26	0.16	21.11	100.31
Sadie 3	19.61	27.05	4.65	1.37	0.27	0.09	26.54	0.16	21.11	100.85
Sadie 4	19.95	26.21	4.62	1.42	0.23	0.06	26.61	0.15	21.19	100.45
Sadie 5	20.03	26.76	4.22	1.88	0.27	0.07	26.29	0.16	21.14	100.81
average	19.74	26.42	4.51	1.53	0.27	0.06	26.46	0.16	21.15	

Table 3-1 (cont.)

	Cu	Ag	Fe	Zn	Cd	Te	Sb	As	S	TOTAL
Husky 1	20.40	24.90	6.25	0.18	0.37	0.00	25.51	0.76	20.59	98.96
Husky 2	16.59	30.13	5.97	0.36	0.37	0.00	25.36	0.73	19.34	98.84
Husky 3	20.69	24.63	5.51	0.37	0.43	0.00	25.49	0.84	20.61	98.58
Husky 3r	20.37	24.55	5.46	0.41	0.40	0.00	25.45	0.75	20.58	97.97
average	19.51	26.05	5.80	0.33	0.39	0.00	25.45	0.77	20.28	
Shamrock 1	19.82	24.95	3.57	4.28	0.52	0.03	26.87	0.12	21.21	101.36
Shamrock 2	19.99	24.91	3.22	3.74	0.56	0.00	26.94	0.13	20.88	100.39
Shamrock 3	18.23	28.35	3.50	3.21	0.44	0.09	26.88	0.12	20.45	101.26
Shamrock 3r	17.27	29.92	3.43	3.11	0.43	0.08	26.63	0.13	20.00	100.98
average	18.83	27.03	3.43	3.59	0.49	0.05	26.83	0.13	20.64	
Calumet-A 1	19.69	27.74	3.36	2.17	0.47	0.05	24.55	0.51	20.63	99.16
Calumet-A 2	14.89	32.26	2.20	3.99	0.40	0.12	25.86	0.43	18.31	98.45
Calumet-B1	20.20	27.12	3.45	2.52	0.57	0.00	23.91	0.79	19.61	98.18
Calumet-B1r	20.26	26.81	3.53	2.50	0.55	0.00	24.44	0.81	20.51	99.41
Calumet-B2	20.82	24.60	3.43	2.76	0.53	0.00	25.37	0.73	20.15	98.40
Calumet-B3	21.02	23.72	3.65	2.86	0.68	0.00	26.29	0.70	20.50	99.41
Calumet-B4	20.67	24.57	3.55	3.01	0.63	0.00	26.09	0.73	20.32	99.48
average	19.65	26.69	3.31	2.83	0.55	0.02	25.22	0.67	20.00	
Porcupine 1	19.53	26.01	1.22	5.45	0.41	0.00	25.93	0.37	20.17	99.07
Porcupine 2	18.62	25.49	3.37	4.03	0.26	0.00	25.88	0.32	20.50	98.47
Porcupine 3	17.78	28.62	1.03	5.84	0.33	0.00	25.64	0.52	19.76	99.50
Porcupine 4	17.24	28.83	1.35	5.28	0.52	0.00	25.15	0.77	19.81	98.95
Porcupine 4r	18.79	27.77	1.40	5.15	0.57	0.00	26.08	0.66	19.99	100.41
average	18.39	27.34	1.67	5.15	0.42	0.00	25.74	0.53	20.05	

Table 3-1. (cont.)

	Cu	Ag	Fe	Zn	Cd	Te	Sb	As	S	TOTAL
Lucky-Q 1	18.93	27.09	3.71	2.57	0.88	0.00	25.63	0.82	20.33	99.95
Lucky-Q 1r	19.86	26.50	3.75	2.39	0.97	0.00	25.76	0.84	20.39	100.46
Lucky-Q 2	15.86	32.85	4.62	1.51	0.64	0.02	25.64	0.76	19.45	101.33
Lucky-Q 3	16.98	30.66	1.38	5.52	0.53	0.00	25.55	0.74	19.52	100.88
Lucky-Q 4	16.62	30.45	3.12	3.24	0.80	0.00	25.05	0.83	19.47	99.58
Lucky-Q 5	17.07	30.13	1.45	5.54	0.57	0.00	25.21	0.77	19.62	100.37
average	17.55	29.61	3.01	3.46	0.73	0.00	25.47	0.79	19.80	
Ruby 1	16.69	28.74	3.30	2.87	0.28	0.00	26.03	0.32	19.54	97.77
Ruby 2	16.70	28.99	3.42	2.77	0.20	0.00	25.79	0.31	19.33	97.52
Ruby 4	13.64	34.09	5.74	0.21	0.24	0.00	25.76	0.31	18.39	98.39
average	15.68	30.61	4.15	1.95	0.24	0.00	25.86	0.31	19.09	
H-R224-A 1	13.45	33.77	4.40	4.15	0.15	0.00	23.95	0.28	19.16	99.31
H-R224-A 2	17.04	31.09	4.76	1.48	0.09	0.00	26.33	0.52	19.54	100.87
H-R224-A 2r	17.47	29.85	4.73	1.34	0.05	0.00	26.02	0.34	19.33	99.14
H-R224-A 3	15.30	32.54	3.55	2.65	0.18	0.00	25.61	0.32	18.62	98.77
H-R224-A 4	15.75	32.37	4.47	1.56	0.02	0.00	25.56	0.50	19.03	99.26
H-R224-A 4r	14.78	33.40	4.11	2.07	0.06	0.00	25.49	0.36	18.95	99.23
H-R224-B 1	13.78	35.12	4.59	1.56	0.32	0.02	25.23	0.77	18.71	100.09
H-R224-B 2	13.69	35.46	4.75	1.37	0.32	0.01	24.79	1.07	18.66	100.13
H-R224-B 3	12.92	35.46	4.65	1.32	0.38	0.03	24.82	0.73	18.49	98.79
H-R224-B 4	14.90	34.12	4.80	1.29	0.37	0.03	25.33	0.78	18.84	100.47
H-R224-B 5	13.69	34.70	4.67	1.43	0.35	0.01	24.35	0.88	18.61	98.68
average	14.80	33.44	4.50	1.84	0.21	0.01	25.23	0.60	18.90	

Table 3-1 (cont.)

	Cu	Ag	Fe	Zn	Cd	Te	Sb	As	S	TOTAL
Dixie 1	13.50	35.22	4.07	1.71	0.50	0.11	25.87	0.13	18.75	99.87
Dixie 2	13.89	35.27	2.20	4.16	0.59	0.14	25.65	0.12	18.74	100.76
Dixie 2r	14.20	34.37	3.57	2.37	0.58	0.11	25.93	0.13	18.83	100.10
Dixie 3	15.10	33.74	4.36	1.26	0.57	0.12	25.89	0.14	18.94	100.11
Dixie 4	15.39	32.30	5.35	0.48	0.61	0.11	25.63	0.13	19.66	99.67
average	14.42	34.18	3.91	2.00	0.57	0.12	25.79	0.13	18.98	
Silver King 1	14.57	33.86	4.11	2.37	0.38	0.05	25.47	0.78	19.12	100.69
Silver King 2	14.24	34.94	4.15	2.21	0.40	0.05	25.36	0.81	18.80	100.96
Silver King 3	13.38	36.35	4.88	1.47	0.39	0.04	25.06	0.70	18.79	101.05
Silver King 4	13.15	36.91	4.34	1.97	0.43	0.06	24.70	0.76	18.47	100.79
Silver King 5	14.87	33.95	4.04	2.43	0.37	0.09	25.07	0.74	18.96	100.54
average	14.04	35.20	4.30	2.09	0.39	0.06	25.13	0.76	18.83	

Table 3-2. Average tetrahedrite composition, from polished mounts, expressed in number of atoms per 13 S.

	Cu	Ag	Fe	Zn	Cd	Sb	As	S
Homestake	8.0	2.8	1.2	0.9	0.0	4.1	0.2	13.0
Onek	7.4	3.6	1.5	0.6	0.0	4.2	0.2	13.0
Sadie	6.1	4.8	1.6	0.5	0.1	4.3	0.0	13.0
Husky	6.3	5.0	2.1	0.1	0.1	4.3	0.2	13.0
Shamrock	6.0	5.1	1.2	1.1	0.1	4.5	0.0	13.0
Calumet	6.4	5.2	1.2	0.9	0.1	4.3	0.2	13.0
Porcupine	6.0	5.3	0.6	1.6	0.1	4.4	0.1	13.0
Lucky-Queen	5.8	5.8	1.1	1.1	0.1	4.4	0.2	13.0
Ruby	5.4	6.2	1.6	0.7	0.1	4.6	0.1	13.0
HR-224	5.1	6.8	1.8	0.6	0.0	4.6	0.2	13.0
Dixie	5.0	7.0	1.5	0.7	0.1	4.7	0.0	13.0
Silver King	4.9	7.2	1.7	0.7	0.1	4.6	0.2	13.0

exceed the ideal formula. The excess cation content is reflected in the low S weight percent, which varies from 18.32 % to 22.48 % (Table 3-1). Similar low sulfur analyses and excess cation contents are reported from other districts by Petruk et al. (1971) (20.1 weight % S), Riley (1974) (20.4 weight % S), Kvacek et al. (1975) (17.3 weight % S), Pattrick (1978) (20.5 weight % S), Sandecki and Amcoff (1981) (19.6 weight % S), Basu et al. (1981) (20.8 weight % S), Eidsmo et al. (1984) (20.7 weight % S), and others. These are all from Ag-rich tetrahedrite samples and have metals and semi-metals in considerable excess of the ideal formula.

The greatest elemental variations in the analyzed samples presented in Table 3-1 are in Ag, Cu, Fe and Zn. The As and Sb contents, on the other hand, are surprisingly constant in light of zoning studies undertaken in other mining districts (Hackbarth and Petersen, 1984). A plot of Ag versus Cu displays a negative linear correlation (Fig. 3-7 A), indicating direct substitution between Ag and Cu. The trigonal planar sites (TRG) and the tetrahedral sites (TET) are both occupied in part by Ag because of the range in silver values. Within the tetrahedrite series the samples with high silver values (Ag > 20 weight %) of the Keno Hill district are more correctly termed freibergite according to the limits of Riley (1974). A similar linear relation is observed between Fe and Zn in the tetragonal sites (Fig. 3-7 B). Iron increases from 0.4 to 2.3 atoms as zinc decreases from 1.9 to 0.1 atoms per 13 sulfur atoms. The increasing Fe/Zn and Ag/Cu ratios correspond to the spatial distribution of the samples in the district, matching the east to west or "downstream" zoning sequence.

The spatial variation in tetrahedrite chemistry is more fully displayed in Figure 3-8. The map shows the variation of the average Ag/(Cu+Ag) ratio from individual polished mounts according to position in the district. Individual samples may display considerable internal variability (Table 1); however this variability is never as great as the district-wide trend, which shows a distinct increase in the ratio towards the east. The chemical zonation

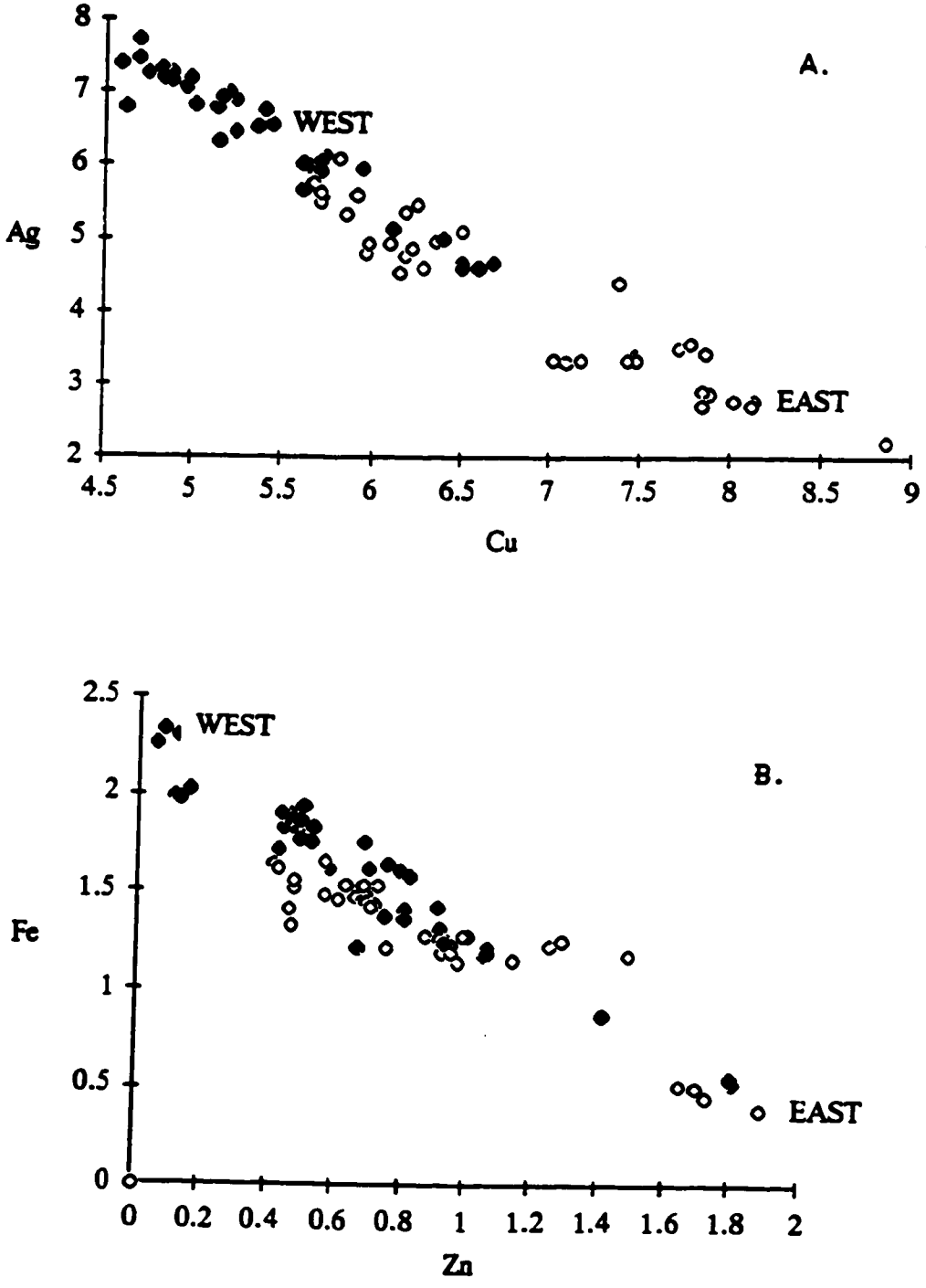

Figure 3-7. (A) Negative linear relation between silver and copper from the tetrahedrite-series minerals. (B) Negative linear relation between iron and zinc in the tetrahedrite-series minerals. Filled pattern are samples from western portion of the district, open are from the east. Values are in number of atoms relative to 13 sulfur atoms.

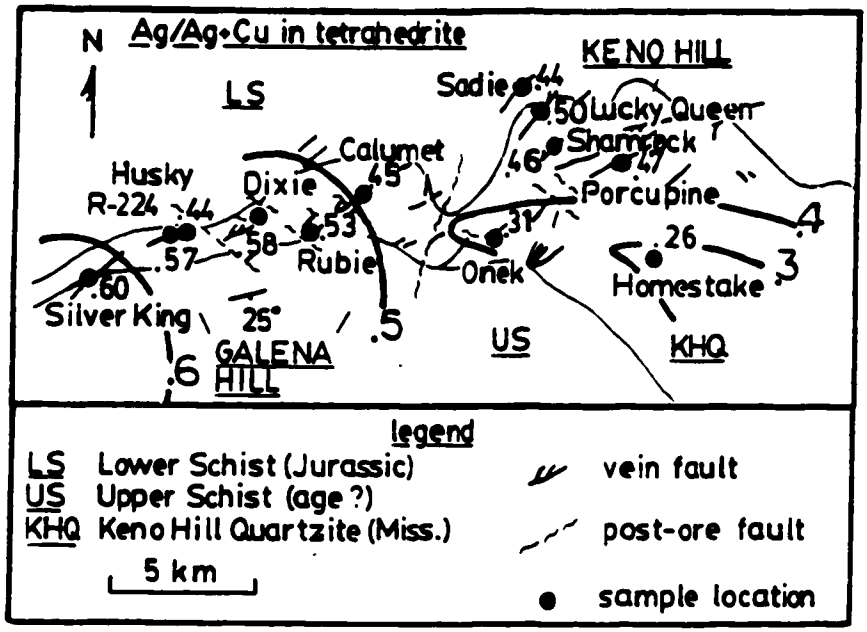

Figure 3-8. Map of spatial variation in Ag/(Cu+Ag) from tetrahedrite-freibergite samples taken across the Keno Hill district. Results plotted are average values from individual polished mounts, in number of atoms relative to 13 sulfur atoms.

stands out clearly, and may suggest a strong component of lateral migration for the mineralizing fluids.

DISCUSSION

The Keno Hill mining district is part of a large, zoned, fossil hydrothermal system. Mineralogical variations within individual orebodies do not generally show any obvious or systematic patterns on a detailed scale. However, regular zonation of mineral distribution is clearly developed on a district-wide scale. Consequently, the district may be viewed as a large continuous deposit formed from one complex hydrothermal system. Mining activities define a multitude of individual orebodies, but the zonal patterns indicate a large uninterrupted system. This system is more completely viewed from a larger scale perspective, allowing the formulation of a useful exploration model.

The veins are confined mainly to the Keno Hill Quartzite and extend laterally for nearly 40 km. Implications are for a vast network of interconnected faults and fractures linking all sectors, during lateral fluid flow. Where mining activity is extensive the continuity across mineralogic zones is clearly shown; however, limited exposure in some areas and lack of mining in the non-economic portions of the system necessitate considerable extrapolation between other mineral zones.

The mineral sequence in the Keno Hill district offers a fairly complete set of classic zoning models (Spurr, 1907, 1912; Emmons, 1936). These are generally pieced together from various districts and are rarely complete in any one system. In this case, veins near the Mayo Lake Pluton are characterized by extensive quartz-feldspar veining with epidote, white mica, and some sulfides, and local Sn-mineralization. Outward from the pluton, in the central portion of the system, Ag-Pb-Zn mineralization and carbonate gangue are present. The outermost part of the sequence has a more epithermal character as is evident from the presence of pyrargyrite, polybasite, stephanite, acanthite and native wire silver, as well as a quartz-dominated gangue with clay alteration.

Mineralogical changes within vein deposits are generally along the inferred direction of fluid-flow. In contrast to other settings, vertical zoning at Keno Hill is less well developed than lateral zoning. The mineral distribution in the area indicates a predominantly unidirectional component of fluid migration from east to west, as controlled by favorable structures. The confinement of the hydrothermal system to the fractured quartzite provides a largely complete section of the hydrothermal system at one erosional level. The permeability and relatively non-reactive nature of the quartzite, as indicated by generally meager alteration haloes, coupled with likely moderate gradients in pressure and temperature in the lateral dimension (relative to the vertical) have allowed for the spatially extensive nature of the system.

The mineralogical zones progress away from the Mayo Lake Pluton in a regular and systematic way, demonstrating a spatial relation to the pluton. However, hydrothermal veins begin outside of both the pluton and its contact metamorphic aureole. The pluton remains for the most part unaltered and no material input from the pluton to the vein system is apparent. The pluton seems to have acted only as a heat source. This probably explains the minor development of Sn and W mineralization relative to Ag-Pb-Zn. Although the source of the fluids remains unknown in the area close to the pluton, stable isotope studies indicate that meteoric waters dominated the distal epithermal domain (Chapter 6).

In order to discuss some of the possible reasons for the mineral zoning, phase diagrams which display portions of the paragenesis have been prepared (Figs. 3-9 and 3-10). The axis parameters fS_2 and pH were chosen for Figure 3-9 since the mineral assemblages indicate that these were variable during hydrothermal mineralization. Oxygen fugacity on the other hand is thought to have been fairly constant during the principal stage of mineralization due to the buffering capacity of graphite (French, 1966). However late stage fluids may have been oxidized as indicated by the presence of barite. Fluid inclusion studies (Chapter 5) indicate that ore formation occurred within the temperature interval 250° - 310° C.

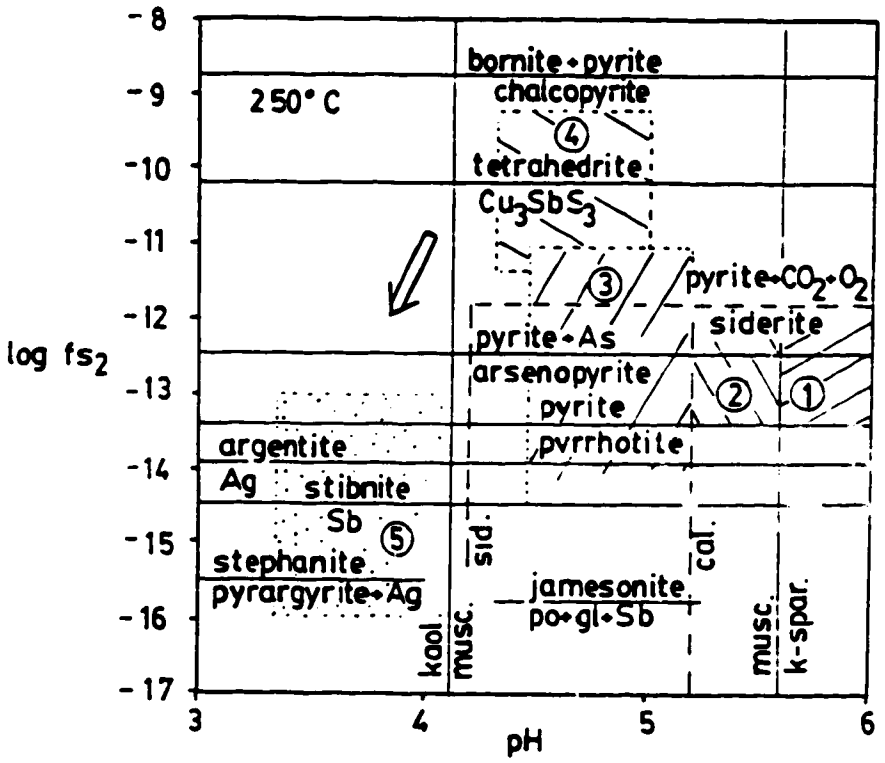

Figure 3-9. A representation of the stabilities of minerals from across the various zones of the Keno Hill mining district at 250° C. The sequence 1 to 5 represents the east to west zonation. Parameters used for the calculations have been estimated from a fluid inclusion study (Chapter 5) and analogy with other types of hydrothermal systems (Barnes, 1979; Ohmoto et al., 1983). A value of log fO_2 = -33.5 was used, which is near the upper stability limit of graphite when boiling began at 1500 bars (Chapter 5). Clathrates which formed in inclusions from siderite provide an estimate of the CO_2 content, log fCO_2 = 1.9.

Siderite saturation established the iron content (log $\alpha_{Fe^{2+}}$ = -4.12), and calcium was set equal to this in order to compare the relative effects of pH on the two types of carbonates at equal concentrations of their divalent metals. The activity of K^+ used is 0.07. The sources of thermodynamic data are Craig and Barton (1973) for the sulfosalts, Barton and Skinner (1979) for the sulfides, and Bowers et al. (1984) for the carbonates and silicates.

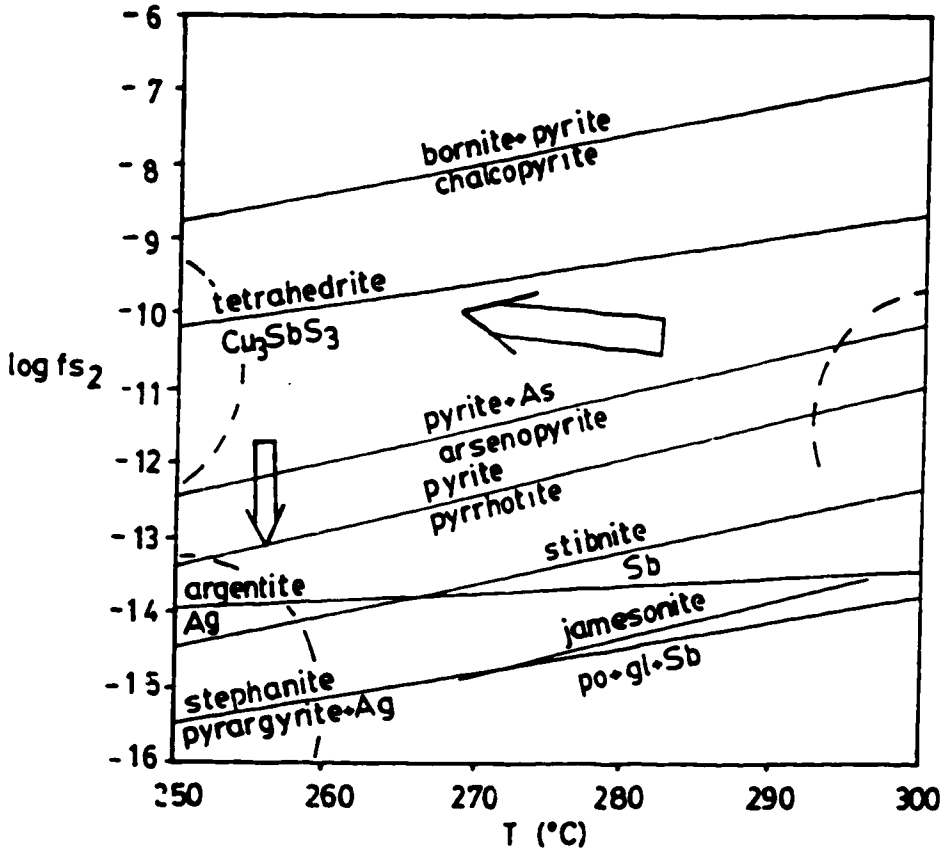

Figure 3-10. Diagram illustrates early paragenesis of arsenopyrite and pyrrhotite evolving to a later tetrahedrite-bearing assemblage upon cooling at a constant sulfur fugacity. Transition may also have occurred with an increase in sulfur fugacity. Late epithermal assemblage appears to have formed from a fluid distinctly depleted in sulfur as indicated by the presence of pyrargyrite, stephanite, native silver and argentite. Source of thermodynamic data is from Craig and Barton (1973).

The most obvious trend in the evolution of the hydrothermal chemistry is that of a decreasing pH from east to west, reflected by the sequence K-feldspar to muscovite to kaolinite. Also the transition from calcite to siderite may have been due to a lowering of the pH, since for similar concentrations of Ca^{2+} and Fe^{2+} in a hydrothermal fluid, siderite is stable under more acid conditions. The increase in acidity was most likely due to the formation of carbonic acid during progressive CO_2 acquisition by the interaction of water and graphite. In the epithermal environment, acid conditions and the formation of kaolinite are usually associated with boiling and the condensation of volatile phases such as CO_2 and H_2S (Knight, 1977). Kaolinite in the western portion of the Keno Hill district may indicate extensive boiling in this area, and the accumulation of CO_2.

In the ore assemblage, the presence of pyrrhotite and arsenopyrite indicate that the mineralizing fluids had a generally low sulfidation state. For tetrahedrite to have followed these in the paragenetic sequence a slight increase in fS_2 or decrease in temperature would have been necessary (Fig. 3-10). Tetrahedrite does not appear to have formed directly with the epithermal stage at the western extremity of the system, where the assemblage of native Ag, pyrargyrite, stephanite, and argentite require sulfidation states which are below the stability of tetrahedrite. A low sulfidation state may have been induced either by extensive H_2S loss during boiling, or by the influx of meteoric water with a low S content, or through oxidation of H_2S to SO_4^{2-}. This last possibility is indicated by the occasional presence of barite in the epithermal assemblage.

Summary and discussion of tetrahedrite chemistry

Tetrahedrite is the dominant silver-bearing phase in the system and is distributed along the entire 25 km length of the mining district. It is present in several of the mineralogical zones. The chemistry of the tetrahedrite series is complex, but offers a more quantitative representation of the zoning and serves to corroborate zoning established by megascopic observations in the field.

In the Keno Hill district the solid solution in the tetrahedrite-series varies from tetrahedrite to freibergite in the more distal assemblages. Elemental variations are characterized by substitutions between Ag and Cu, as well as between Fe and Zn. Substitution within one pair appears to be independent of substitution within the other. A high Sb/As ratio is observed in all samples.

The observed compositional trends are typical of tetrahedrite-bearing hydrothermal veins, with fluid evolution and differentiation interpreted to be due to fractional crystallization of tetrahedrite (Hackbarth and Petersen, 1984); Cu and Zn are partitioned into the mineral at an early stage and enrich the fluid in the Ag and Fe. Small-scale variations result when a mineral grows from more or less evolved fluids at different times. However mixing of different fluids in this district seems to have been important in controlling the chemistry of the tetrahedrite series; a stable isotope study of quartz associated with tetrahedrite shows that meteoric waters were involved in freibergite precipitation (Chapter 6).

Recent studies have shown that substitutions in tetrahedrite between As-Sb, Fe-Zn and Cu-Fe may be considered ideal (Sack and Loucks, 1985), but that Ag-Cu substitution is non-ideal (Johnson et al, 1987). Problems with the general tetrahedrite formula arise in Ag-rich samples and are reported also for synthetic Cu-rich samples, for which an expanded formula is required. Makovicky and Skinner (1978) suggested for synthetically generated Cu-rich tetrahedrite, that the excess "mobile copper" may occupy interstitial cavities within the structure. The expanded formula seems to apply as well to the naturally occurring Ag-rich samples of the Keno Hill district. Sandecki and Amcoff (1981) report on tetrahedrite samples with compositions which are similar to those of the Keno Hill district, where a deficiency in sulfur or excess in cations for Ag-rich samples is recorded. They suggest that since a net charge surplus is impossible, the cation surplus may be due to the presence of cations which are in a reduced state. This could be a possibility as well for

the samples from the Keno Hill district, when considering the reducing nature of the graphitic host rocks.

The low sulfidation state for the mineralizing fluids of the Keno Hill system, as indicated by the presence of pyrrhotite and arsenopyrite, would also have contributed in the formation of S-deficient tetrahedrite. Although 13 S atoms per formula unit is the most widely accepted model (Johnston et al., 1986), some workers still favor a 12 S model (Babushkin et al., 1984).

CONCLUSIONS

The zoned Keno Hill vein system of central Yukon extends in a lateral section from plutonic/metamorphic center and surrounding quartz-feldspar veins to Ag-Pb-Zn deposits and further to peripheral veins having epithermal affinities. The entire sequence is continuous from east to west over a 40 km belt.

The fault and fracture controlled veins are stratabound to the brittle, moderately dipping, 1 km thick Keno Hill quartzite unit of Mississippian age. This unit is graphitic and contains interlayers of schist and greenstone. Regionally extensive impermeable schist units occur above and below the quartzite. The quartzite appears to have acted as a large scale hydrothermal aquifer, restricting fluid flow and mineral zoning predominantly to the lateral direction.

The Mayo Lake Pluton (81 Ma) cuts the quartzite at the eastern end of the district. Hydrothermal veins begin at the outer margin of the contact metamorphic aureole surrounding the pluton. Veins are coarse grained and vuggy. The dominant groups, progressing outward from the pluton, are: 1) quartz-feldspar veins with minor epidote, tourmaline, apatite, pyrite, and rare ilmenite; 2) quartz veins with muscovite and sparse pyrite, arsenopyrite, and cassiterite; 3) quartz-calcite-epidote veins with also pyrite, arsenopyrite and chalcopyrite; 4) veins containing jamesonite, boulangerite, arsenopyrite, sphalerite, pyrite, chalcopyrite, tetrahedrite and native gold in a gangue of quartz and

calcite; 5) siderite veins with calcite, galena, sphalerite, tetrahedrite, pyrite, pyrrhotite, and arsenopyrite; 6) same as (5) but without arsenopyrite, pyrrhotite and calcite; 7) quartz veins containing pyrargyrite, polybasite, stephanite, acanthite and native silver, as well as pyrite, marcasite, freibergite, chalcopyrite, barite, anomalous gold values and clay alteration. Paragenetically, the veins farther from the pluton are also generally younger.

Tetrahedrite is distributed along a 25 km long portion of the system. It has Ag/Cu and Fe/Zn ratios that are highest at the outer extremity of the system, where freibergite dominates over tetrahedrite. The Sb/As ratio is high throughout the district.

REFERENCES

Anderson, R.G., 1987, Plutonic rocks of the Dawson map area, Yukon Territory, in Current Research , Part A, Geological Survey of Canada, Paper 87-1A, p.689-697.

Andrews, A.J., 1986, Silver vein deposits: summary of recent research. Canadian Journal of Earth Sciences, vol. 23, p. 1459-1462.

Babushkin, A.N., Kobelev, L. Ya., Zlokazov, V.B., 1984, Spontaneous deformation in a single crystal of Cu_3AsS_3. Sov. Phys. Cryst. vol. 29, p478-480.

Barton, P.B., Skinner, B.J.,Jr., 1979, Sulfide mineral stabilities. In, H.L. Barnes (editor), Geochemistry of Hydrothermal Ore Deposits, John Wiley and Sons, p. 278-403.

Barnes, H.L., 1979, Solubilities of ore minerals. In, H.L. Barnes (editor), Geochemistry of Hydrothermal Ore Deposits, John Wiley and Sons, p. 404-460.

Basu, K., Bortnykov, N., Mookherjee, A., Mozgova, N., Tsepin, A.I., 1981, Rare minerals from Rajpura-Dariba, Rajasthan, India. III. Plumbian tetrahedrite. Neues. Jahrb. Mineral. Abhand. vol. 141, p. 180-189.

Bostock, H.S., 1948, Mayo, Yukon Territory. Geological Survey of Canada Map 890A.

Bowers, T.S., Jackson, K.J., Helgeson, H.C., 1984, Equilibrium Activity Diagrams. For Coexisting Minerals And Aqueous Solutions Up To 5 kb And 600° C. Springer Verlag, 397 pages.

Boyle, R.W., 1965, Geology, geochemistry, and origin of the lead-zinc-silver deposits of the Keno Hill-Galena Hill area, Yukon Territory. Geological Survey of Canada, Bulletin 111, 302 pages.

Craig, J.R., Barton, P.B., Jr., 1973, Thermochemical approximations for sulfosalts. Economic Geology, vol. 68, p. 493-506.

Eidsmo, O., Foslie, G., Malvik, T., Vokes, F.M., 1984, The mineralogy and recovery of silver in some Norwegian base-metal sulphide ores. In, W.C. Park et al. (editors), Applied Mineralogy, Proc. 2nd ICAM. Metal Soc. AIME, New York, p. 891-910.

Emmons, W.H., 1936, Hypogene zoning in metalliferous lodes. 16th International Geological Congress Report, pt. 1, p. 417-432.

French, B.M., 1966, Some geological implications of equilibrium between graphite and a C-H-O gas phase at high temperatures and pressures. Reviews in Geophysics, vol. 4, p. 223-253.

Godwin, C.I., Sinclair, A.J., Ryan, B.D., 1982, Lead isotope models for the genesis of carbonate hosted Ba-Zn-Pb, and silver-rich deposits in the Northern Canadian Cordillera, Economic Geology, vol. 77, p. 82-94.

Green, L.H., 1971, Geology of Mayo Lake, Scougale Crek and McQuesten Lake map areas, Yukon Territory. Geological Survey of Canada Memoir 357, 72 pages.

Guilbert, J.M., Park, C.F., Jr., 1986, The Geology of Ore Deposits, W.H. Freeman and Co., 985 pages.

Hackbarth, C.J., Petersen, U., 1984, Systematic compositional variations in argentian tetrahedrite. Economic Geology, vol. 76, p. 448-460.

Jambor, J.L., Laflamme, J.H.G., 1978, The mineral sources of silver and their distribution in the Caribou massive sulphide deposit, Bathurst area, New Brunswick, CANMET report 78-14, 26 pages.

Johnson, M.L., Burnham, C.W., 1985, Crystal structure refinement of an arsenic-bearing argentian tetrahedrite. American Mineralogist, vol. 70, p. 165-170.

Johnson, N.E., Craig, J.R., Rimstidt, J.D., 1986, Compositional trends in tetrahedrite. Canadian Mineralogist, vol. 24, p. 385-397.

Johnson, N.E., Craig, J.R., Rimstidt, J.D., 1987, Effect of substitution on the cell dimension of tetrahedrite. Canadian Mineralogist, vol. 25, p. 237-244.

Knight, J.E., 1977, A thermochemical study of alunite, enargite, luzonite, and tenantite deposits. Economic Geology, vol. 72, p. 1321-1336.

Kvacek, M., Novak, F., Drabek, M., 1975, Canfieldite and silver-rich tetrahedrite from the Kutna Hora ore district. Neues. Jahrb. Mineral. Monash., vol. 4, p.171-179.

Makovicky, E., Skinner, B.J., 1978, Studies of the sulfosalts of copper. VI. Low-temperature exsolution in synthetic tetrahedrite solid solution; $Cu_{12+x}Sb_{4+x}S_{13}$. Canadian Mineralogist, vol. 16, p.611-623.

McTaggart, K.C., 1960, The geology of Keno and Galena Hills, Yukon Territory. Geological Survey of Canada Bulletin 58.

Monger, J.W.H., Price, R.A., Tempelman-Kluit, D.J., 1982, Tectonic accretion and origin of the two major metamorphic and plutonic welts in the Canadian Cordillera. Geology, vol. 10, p. 70-75.

Ohmoto, H., Mizukami, M., Drummond, S.E., Eldridge, C.S., Pisutha-Arnond, V., Lenagh, T.C., 1983, Chemical processes of Kuroko formation. In, H. Ohmoto and B.J. Skinner Jr. (editors), The Kuroko and Related Volcanogenic Massive Sulfide Deposits, Economic Geology Publishing Co. Monograph 5, p. 570-604.

Pattrick, R.A.D., 1978, Microprobe analysis of cadmium-rich tetrahedrites from Tyndrum, Perthshyre, Scotland. Mineral. Mag., vol. 42, p. 286-288.

Petruk, W., and Staff, 1971, Characteristics of the sulphides. In, J.L. Jambor (editor), The Silver Deposits of the Cobalt-Gowganda Region, Ontario. Canadian Mineralogist, vol. 11, p. 196-231.

Poulton, T.P., Tempelman-Kluit, D.J., 1982, Recent discoveries of Jurassic fossils in the Lower Schist division of central Yukon. In Current Research Part C, Geological Survey of Canada Paper 82-1c, p. 91-94.

Riley, J.F., 1974, The tetrahedrite-freibergite series, with reference to the Mount Isa Pb-Zn-Ag orebody. Mineralium Deposita, vol. 9, p. 117-124.

Sack, R.O., Loucks, R.R., 1985, Thermodynamic properties of tetrahedrite-tenantites: constraints on the interdependence of the Ag=Cu, Fe=Zn, Cu=Fe, and As=Sb exchange reactions.

Sandecki, J., Amcoff, O., 1981, On the occurrence of silver-rich tetrahedrite at Garpenberg Nora, central Sweden. Neues. Jahrb. Mineral. Abh., vol. 141, p. 324-340.

Sangster, D.F., 1984, Felsic intrusion associated silver-lead-zinc veins. In, Canadian mineral Deposit Types: a Geological Synopsis, O.R. Eckstrand (editor), Geological Survey of Canada Economic Geology Report 36, 66 pages.

Sinclair, A.J., Tessari, O.J., Harakal, J.E., 1980, Age of Ag-Pb-Zn mineralization, Keno Hill-Galena Hill area, Yukon Territory. Canadian Journal of Earth Sciences, vol. 17, p. 1100-1103.

Skinner, B.J., Jr., Luce, F.D., Makovicky, E., 1972, Studies of the sulfosalts of copper. III. Phases and phase relations in the system Cu-Sb-S. Economic Geology, vol. 67, p. 924-938.

Smith, D.G.W., Gold, C.M., 1979, EDATA2: a FORTRAN 4 computor program for processing wavelength and/or energy dispersive electron microprobe analyses. Proceedings of the 14th Annual Conference of the microbeam analysis Society, p. 271-278.

Spurr, J.E., 1907, A theory of ore deposition. Economic Geology, vol. 2, p. 781-795.

Spurr, J.E., 1912, Theory of ore deposition. Economic Geology, vol. 7, p. 485-492.

Tempelman-Kluit, D.J., 1979, Transported cataclasite, ophiolite and granodiorite in Yukon: evidence of arc continent collision. Geological Survey of Canada Paper 79-14, 27 pages.

Watson, K.W., 1986, Silver-Lead-Zinc deposits of the Keno Hill-Galena Hill Area Yukon Territory. In: Yukon Geology, Vol. 1, Exploration and Geological Services Division, Yukon, Indian and Northern Affairs Canada, p. 83-88.

Wu, I., Petersen, U., 1977, Geochemistry of tetrahedrite and mineral zoning at Casapalca, Peru. Economic Geology, vol. 72, p. 993-1016.

CHAPTER 4

SIMILAR ZONING PATTERNS IN THREE Ag-Pb-Zn DISTRICTS OF THE OMENICA CRYSTALLINE BELT

INTRODUCTION

Presented are three maps which display a similar district-scale hydrothermal zoning pattern, which is distinctive of silver mineralization in the Omenica Crystalline Belt. Similarities in terms of mineral distribution, scale of system, and structural-lithologic control are highlighted. Age and tectonic environment are outlined as well; however some discrepancies exist in this area. The three examples are from the most productive silver regions of the Cordillera: the Keno Hill district in Yukon, the Slocan district in southern British Columbia, and the Coeur d'Alene district of Idaho (Fig.4-1). The purpose of this chapter is to compare the zoning pattern documented in Chapter 2 for the Keno Hill district, to other similar regions in the Cordillera; further work could improve the zoning patterns in these other regions, but the existing publications from these areas allow for preliminary. but important, comparative generalizations to be made.

Zoning models serve as useful guides in mineral exploration, and have been the focus of much study, in the past (Spurr,1907; 1912) and to the present day. Classification of deposit, position within system, and genetic insight are gained from their recognition and application. Zoning patterns which recur in various districts and separate systems enhance predictability for the explorationist. In district scale hydrothermal systems, zoning may be a manifestation of a single evolving hydrothermal system in some cases, or may be due to overlap of separate unrelated systems. Where the former is true, the size and large scale nature of some individual hydrothermal networks is displayed; a scale which obscures perception of the continuity between zones, making interpretation subject for considerable debate.

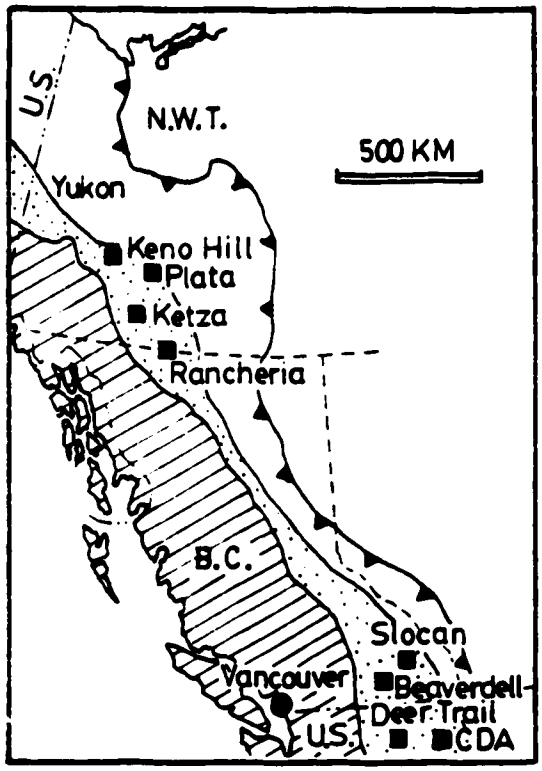

Figure 4-1. Location map of principal Ag-Pb-Zn vein systems (squares) in the Omenica Crystalline Belt (stippled), containing abundant siderite, galena, sphalerite, tetrahedrite, and pyrite. To the east of the belt, the barbed line shows the limit of the cordillera within continental miogeocline. West of the belt are eugeoclinal accreted terranes (rulled pattern). The Keno Hill, Slocan, and Coeur d'Alene (CDA) districts are considered in the text; the Rancheria (Abbott, 1985), Ketza (Abbott, 1986, a), Plata (Abbott, 1986,b), Beaverdell (Godwin et al., 1986), and Deer Trail (Fluet, 1986) also fall within this grouping.

The concentration of high grade Ag-Pb-Zn veins in the eastern belt of the Cordillera, or Omenica Crystalline Belt, has long been recognized (Fyles, 1966). The Omenica Crystalline Belt is a major regional tectonic culmination in the eastern Canadian Cordillera, where intense deformation, regional metamorphism, and granitic magmatism were concentrated (Fig. 4-1). The belt was formed from tectonic overlap and compressional thickening of crustal rocks between the North American craton and large composite allochthonous terrane that was accreted from the west (Monger et al., 1982). Compressional growth of the belt was most intense between mid-Jurassic and Late Cretaceous time. Significant Eocene extension with associated core complexes occurred later in the southern Omenica Crystalline Belt (Parrish et al., 1988), whereas major transcurrent strike-slip faulting affected the northern Omenica Crystalline Belt in Tertiary time (Gabrielse, 1985).

The Omenica Crystalline Belt spans the entire length of the Canadian Cordillera. The southern extension into the United States is largely masked, but projects at least into the northern parts of Idaho and Washington states. The belt is approximately 300 km wide at its northern and southern ends, with a long narrow section in between, commonly less than 50 km wide (Fig.4-1). Correspondingly, significant silver mineralization occurs mainly at these opposite ends, with the narrow band in between displaying marginal economic potential. Accreted terranes to the west have also shown relatively limited silver production, from Ag-Pb-Zn vein deposits.

In summary, large scale Ag-Pb-Zn hydrothermal systems are characteristic of the Omenica Crystalline Belt. The systems are distinctive by their sizes, each is 25-40 km long, and particularly by their horizontal, linear zoning patterns; a plutonic-hydrothermal, to Ag-Pb-Zn, to epithermal silver succession is observed. Through the mining districts the following outward zoning is typical; 1) an early silicate and oxide stage; 2) quartz veins with jamesonite, arsenopyrite, pyrite, sphalerite, pyrite, and chalcopyrite, as well as some gold, calcite, and pyrrhotite; 3) the main orebodies are comprised of siderite, galena,

sphalerite, pyrite, and tetrahedrite; 4) the outer zone may include pyrargyrite, polybasite, acanthite, stephanite, native silver, and late quartz. The zoning is well documented in the Keno Hill district, Yukon, and applies as well to the Slocan district of southern British Columbia, and the Coeur d'Alene district of Idaho.

Keno Hill mining district, Yukon

The Keno Hill mining district is situated in central Yukon, 45 km northeast of Mayo, and 350 km north of Whitehorse. The district has been the largest producer of silver in the northern Canadian Cordillera since mining began in 1913. More than 210 million ounces of Ag have been produced, with recovery of substantial Pb, Zn, and Cd. Average grades over the mining history are: 41 oz Ag/ton , 6.8 % Pb, and 4 % Zn (Watson, 1986). Extensive geological work on the district was completed by McTaggart (1960), and Boyle (1965).

Galena, sphalerite, and tetrahedrite bearing veins are contained within a system of sinistral strike-slip faults. The faults dip steeply to the southeast, and appear to have been active during hydrothermal activity as indicated by sheared galena, as well as multiple stages of brecciation and cementation. The veins are stratabound within the Mississippian Keno Hill Quartzite. The quartzite is brittle, graphitic, and highly fractured. It is approximately 1 km thick in the mining district, was thrust to the north in Late Jurassic-Early Cretaceous time, and dips moderately to the south. Strata of the district were metamorphosed to the greenschist facies, and were later intruded by Cretaceous granitic plutons (80 Ma). Dating of mica within alteration haloes surrounding the veins returned a similar age (Sinclair et al, 1980).

Individual orebodies may have a length of 1 km or more, but have not been explored or developed beyond 300 m depth because of mining tactics and economic restrictions. The district as a whole comprises a multitude of orebodies spread from east to west for 25 km; however a further 10-15 km long eastern extension of the hydrothermal

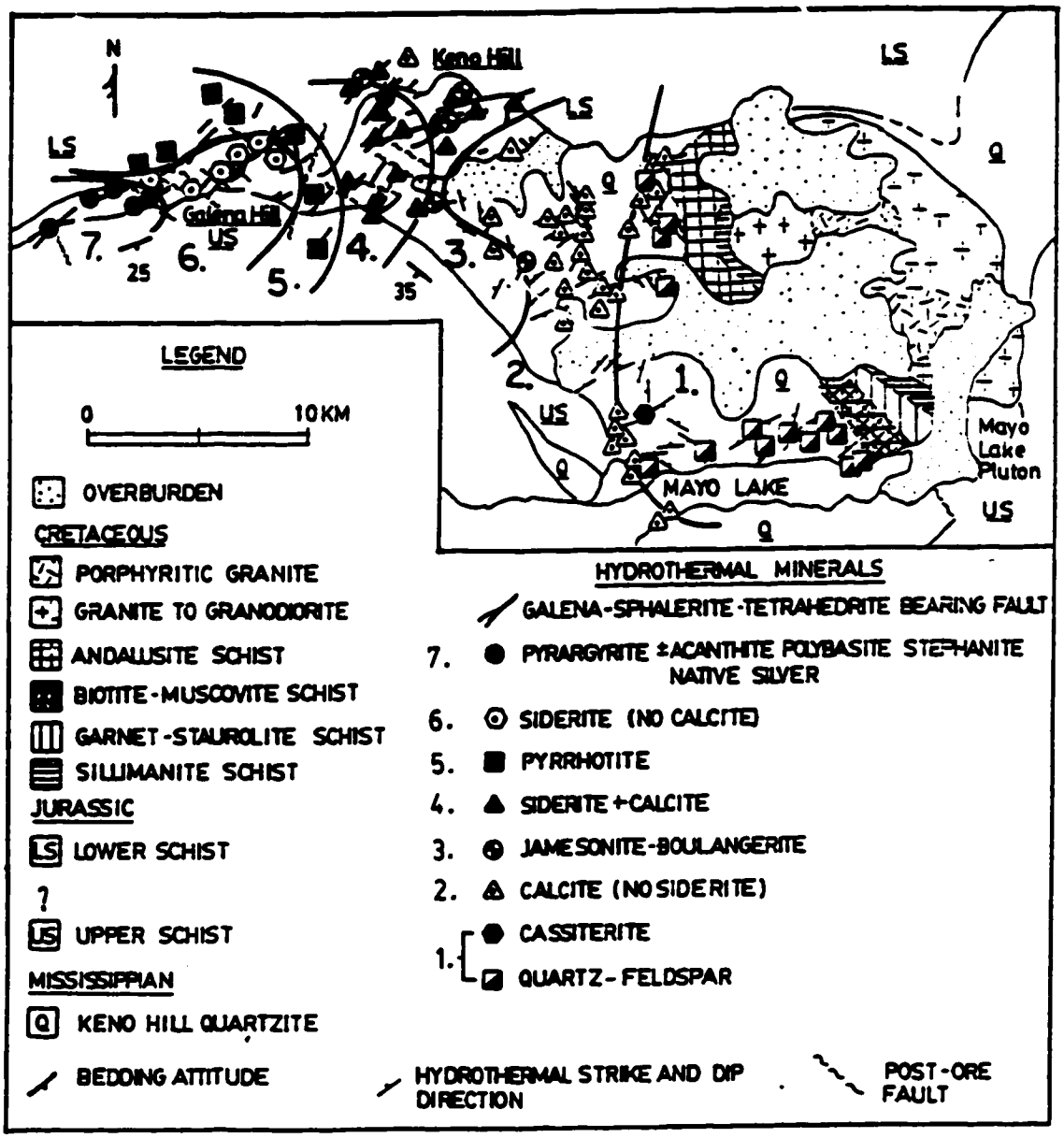

Figure 4-2. Hydrothermal zoning map of the Keno Hill Ag-Pb-Zn mining district, Yukon.

system is added if non-economic veins are included (Fig. 4-2). The system is highly zoned at the district scale, predominantly in the lateral dimension due to its confinement to the Keno Hill Quartzite. Fluid flow was apparently along this highly fractured aquifer during mineralization.

The ore is dominated by galena, sphalerite, and tetrahedrite within a gangue of siderite and quartz. The zones progress systematically from east to west away from the Mayo Lake Pluton. Quartz-feldspar veins characterize the zone closest to the pluton, with subsidiary epidote, apatite, tourmaline, pyrite, and rare wolframite and ilmenite. Quartz-calcite veins occur beyond this, and contain accessory epidote, albite, pyrite, arsenopyrite, and chalcopyrite. A set of cassiterite bearing quartz veins occur between the feldspar and calcite zones. The next zone is marked by the presence of jamesonite-boulangerite, with also an increase in the abundance of sulfides including: sphalerite, pyrite and chalcopyrite, with also some arsenopyrite, tetrahedrite, and native gold, in a gangue of quartz and calcite. Further to the west, siderite becomes the most abundant phase intergrown with galena, sphalerite, tetrahedrite, pyrite, minor quartz and calcite. Pyrrhotite forms a distinctive zone in the mid-section of the mining district, and is seen with the common ore assemblage. Further west calcite disappears from the gangue entirely and siderite dominates. At the fringe of the system, the assemblage furthest from the pluton is distinctly epithermal in character; as marked by the presence of pyrargyrite, polybasite, stephanite, acanthite, native silver, freibergite, as well as pyrite, marcasite, some chalcopyrite, a late quartz stage, anomalous gold values and clay alteration. Galena and sphalerite are less abundant.

Slocan mining district, B.C.

The Slocan mining district is in southern British Columbia, 30 km due north of the town of Nelson. Geological mapping, and extensive descriptions of vein occurrences were completed by Cairnes (1934,1935, 1948). Further studies were done by Hedley (1952),

Fyles (1966), Nguyen et al (1968), Reynolds and Sinclair (1971), Cox (1979), Brame (1979), and Logan (1986).

The vein deposits of the district are fault and fracture controlled, and are contained within sedimentary rocks of the Slocan Series; these are comprised of a thick series of tightly folded Late Triassic (Orchard, 1985) quartzites, slates, argillites, limestones, and volcanic (tuffaceous) units with also some conglomerate (Cairnes, 1934). Intruding the Slocan Series are numerous felsic dikes of uncertain age, but which have been related to the granitic Nelson Batholith (Cairnes, 1934; Hedley, 1952) which is Upper Jurassic in age (Nguyen et al, 1968; Archibald et al, 1983). A granitic pluton of suspected mid-Cretaceous age is present in the northwest portion of the mining district (Parrish et al., 1988). The hydrothermal mineralization of the Slocan system crosscuts all of these suites of granitic rocks.

Tectonically the mining district lies above the northeast flank of the Valhalla core complex of southern British Columbia (Parrish et al., 1988). The orebodies are in the hanging wall of the east dipping Slocan Lake Fault which bounds the mining district to the west. By 54 Ma the fault had dropped middle Jurassic rocks of the Nelson Batholith down onto high-grade metamorphic rocks of the Valhalla core complex (Parrish, 1984, Parrish et al., 1985), with downdip displacement near 10-15 km (Carr, 1986).

Silver, lead and zinc are the principal metals recovered from veins, which are individually up to 2 km long and 1 km deep. The ore bearing fault structures strike principally to the northeast and dip to the southeast. Galena-sphalerite-tetrahedrite with occasional pyrargyrite are the important ore constituents within a gangue of siderite or quartz. However the vein mineralogy is considerably more complex than this and is summarized in a paragenesis diagram by Cairnes (1934). The map distribution of minerals is shown in figure 3, which was compiled from the property descriptions of Cairnes (1934, 1935). The map is simplified to display the presence of the vein minerals which are diagnostic of a particular zone. The district is shown to be clearly zoned in its vein

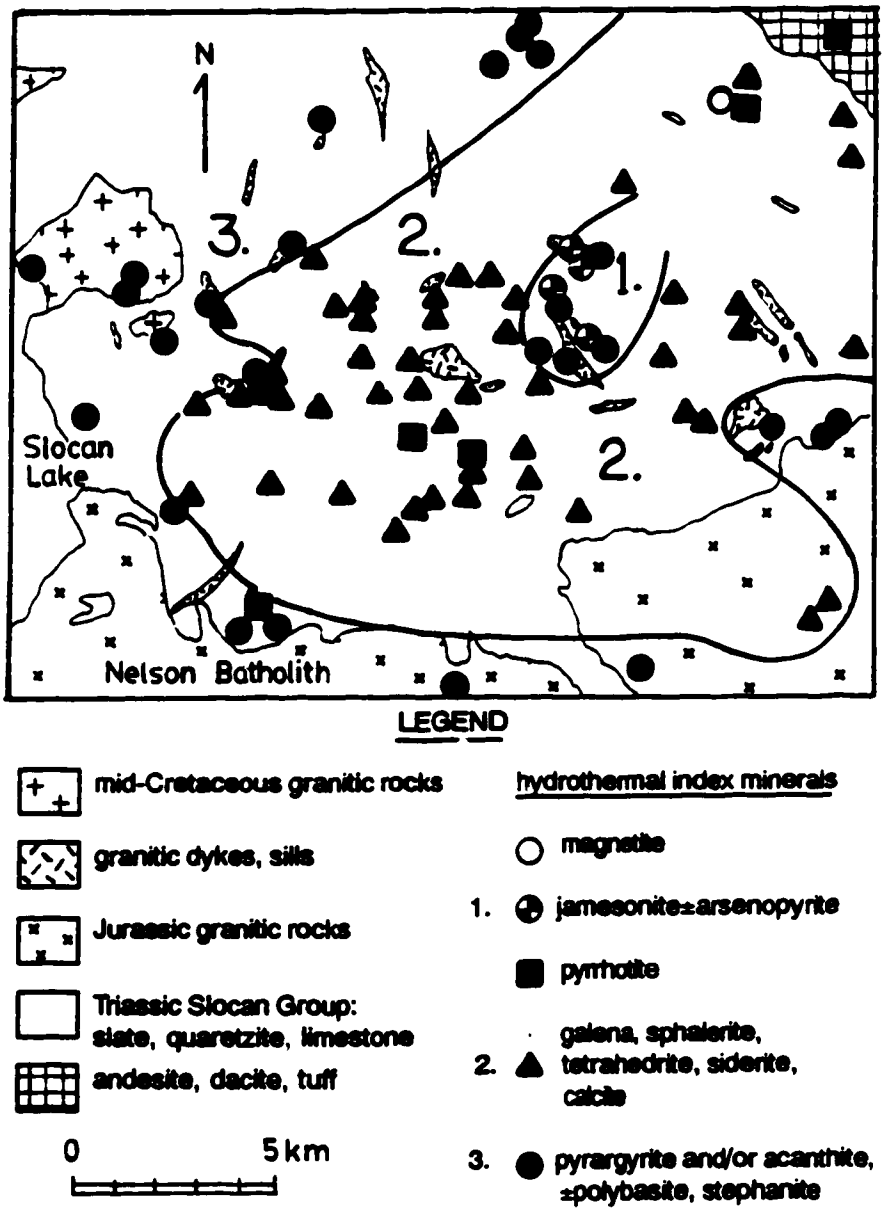

Figure 4-3. General hydrothermal zoning map of the Slocan Ag-Pb-Zn district. Map constructed from Cairnes (1934, 1935).

mineralogy. The zoning pattern is oval in shape with a 25 km long axis trending NE-SW along strike with the vein structures, and a width of approximately 10 km. The mineral distribution is in part concentric. Minerals diagnostic of a less evolved assemblage such as jamesonite-boulangerite, arsenopyrite, and pyrrhotite are in the core area, whereas pyrargyrite, acanthite, native silver, and polybasite in various combinations are mainly along the outer margin of the system with a late quartz stage (Fig. 4-3). These are termed "dry ore" in the mining district due to the general lack of galena, and are distinct in appearance to the veins in the central portion of the district (Cairnes, 1934). It should be noted however that pyrargyrite may be telescoped back to the core of the district. A significant feature of the zoning pattern is that the hydrothermal facies progress outwards in distribution and paragenesis from a core area centered in the Slocan Series, to a marginal facies in the Nelson Batholith. The veining is not zoned away from the batholith but rather in the opposite direction against the batholith. The indications are that the presently exposed margins of the batholith were not the hydrothermal starting point. This interpretation conflicts with past studies which link the veins to the Nelson batholith, and did not consider the district aspect of zoning (Cairnes, 1934; Reynolds and Sinclair, 1971; Cox, 1979; and Andrew et al., 1984). Alternatively, hydrothermal activity may have been related to the many felsic dikes which are distributed throughout the district (Fig. 4-3), or if much younger, to the Eocene extension and emplacement of the Valhalla core complex.

Coeur d'Alene mining district, Idaho

The Coeur d'Alene mining district of Idaho is the world's premier silver producer, with over one billion ounces produced since 1884, as well as significant Pb, Zn, Cu, and Au production (Venkatakrishnan and Bennett, 1988). This prolific area is located in northern Idaho, centered on the town of Wallace, approximately 100 km east of Spokane, Washington.

Host rocks to the mineral deposits are part of the Belt Supergroup which are a 6,400 m thick sequence of regionally extensive Precambrian sedimentary rocks (Hobbs et al, 1965). The St. Regis, Revett, Burke, and Prichard formations are important in localizing ore; these are dominated by clastic sedimentary rocks including mainly quartzite, impure quartzite, argillite, and some carbonate bearing beds (Hobbs et al, 1965). The rocks have been folded and metamorphosed to the greenschist facies.

Plutonic rocks which crosscut the Belt Supergroup in the mining district are known as the Gem and Dago Peak stocks. The intrusions are Late Cretaceous in age and vary from granite to quartz monzonite and granodiorite. The presence of the buried Atlas pluton is inferred from an aeromagnetic survey (Gott and Cathrall, 1980).

Three major northwest striking dextral faults pass through the district. Subsidiary faults to these and joints are important in localizing ore, although much of the movement on the major faults is post-ore. Fault controlled veins are mostly a few meters wide and form extensive planar bodies. As an example, the Star-Morning mine has been mined along strike for 1,372 m and to depths greater than 2,317 m (Bennett and Venkatakrishnan, 1982). The great vertical continuity of the orebodies is characteristic of the district, placing it in a class of its own in terms of productivity. Most of the mineralized veins have similar attitudes to the regional faults. Important ore minerals within the veins are galena, sphalerite, and tetrahedrite in a gangue of quartz, siderite, pyrite, and pyrrhotite. A Cretaceous age of mineralization is favoured by Fryklund (1964), who lists seven mines where mineralized veins crosscut Cretaceous monzonite dykes and intrusions. Crosby (1959) noted that ore in the Success mine crosscuts the Cretaceous monzonite in some places and is earlier in other places, indicating contemporaneity between the two. Leach et al. (1988) on the other hand, present four K-Ar age dates from vein sericite: 829 +/- 40 Ma, 876 +/- 43 Ma, 447 +/- 25 Ma, and 77 +/- 5 Ma. These values and other arguments are used to establish a Proterozoic age of mineralization (Leach et al, 1988); but the range of the four numbers from Proterozoic to Cretaceous time is still somewhat inconclusive,

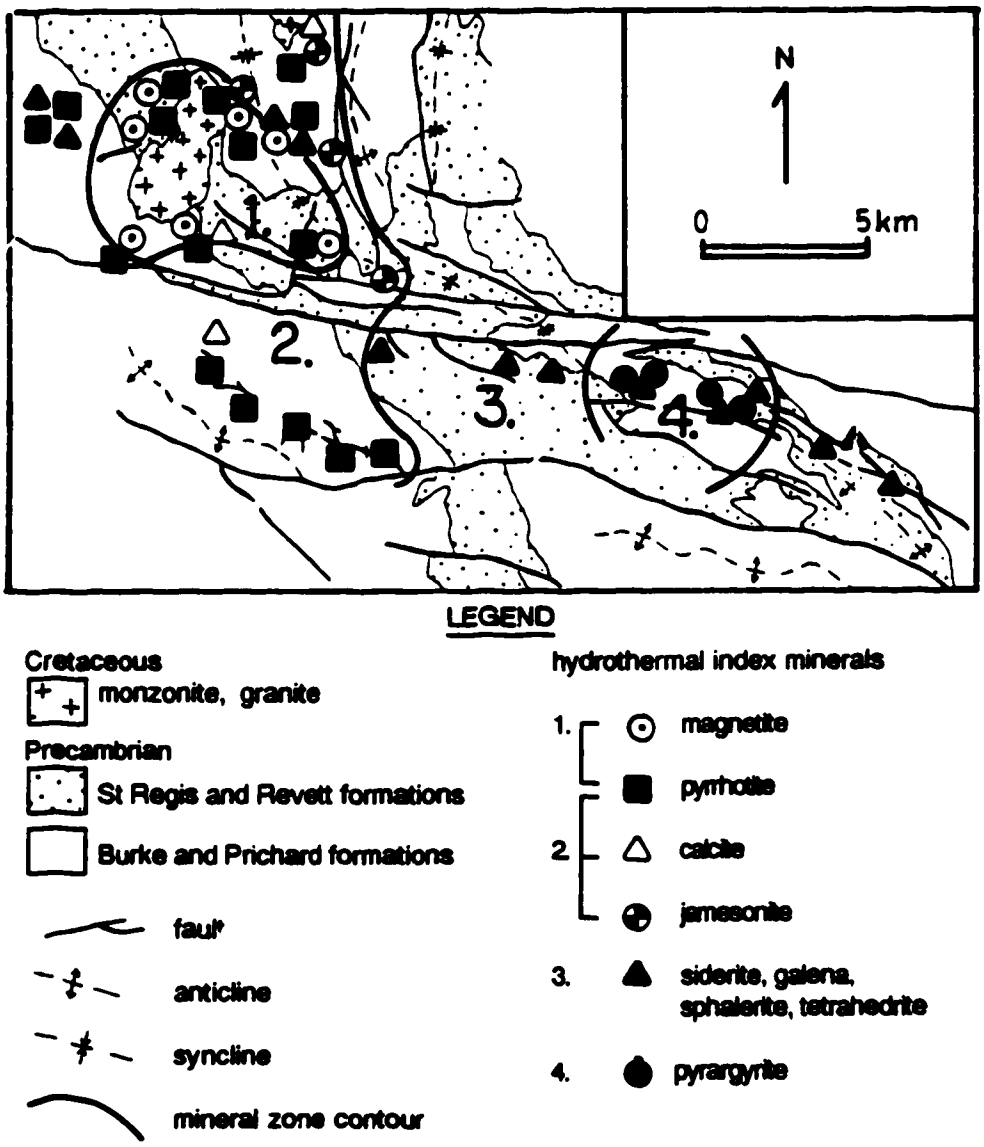

Figure 4-4. General hydrothermal zoning map of the Coeur d'Alene district. Map modified from the mineralogical report of Fryklund (1964), and palinspastic reconstruction of Bennett and Venkatakrishnan (1982).

though critical in a genetic interpretation. Regardless of the association, or lack of association to the plutons, mineralogical zoning of the district is well developed and presented here for comparative use (Fig. 4-4).

Mineralogical zoning within the district was clearly displayed in the report by Fryklund (1964), who also elaborated on geochemical zoning within the ore; zinc, lead, copper with silver zones were represented, and are largely indicative of the changing abundances of sphalerite, galena, and tetrahedrite which increase respectively from northwest to southeast along the district trend.

Post-ore faulting has offset mineralogical zones in the Coeur d' Alene district. A palinspastic reconstruction of the original position of the orebodies has been completed by Bennett and Venkatakrishnan (1982). This reconstruction, together with maps and deposit descriptions by Fryklund (1964), have been combined to form the general mineralogical zoning map of Figure 4-4. Large scale hydrothermal zoning is clearly displayed. The zonation is in part concentric around the Gem stocks, but mainly progresses away from the stocks in a linear fashion, for more than 20 km, to the southeast along the general trend of the preexisting fault structures. The innermost zone to the stocks is characterized by hydrothermal quartz-magnetite veins with grunerite and garnet. This group of veins may be unrelated to the orebodies if the orebodies are Proterozoic in age. However spatial mineralogical zoning progresses outwards beyond this to pyrrhotite and locally jamesonite-boulangerite bearing veins. Calcite-pyrite veins are known to occur in abundance in the area surrounding the stocks. Further from the stocks, siderite appears with also sphalerite, galena, and tetrahedrite. Tetrahedrite increases in importance away from the stocks in deposits such as the Sunshine mine where pyrargyrite, acanthite, and polybasite may also be found (Fig. 4-4). Orebodies completely dominated by epithermal characteristics, however, are not reported.

Mineral zones in the district have in the past been related to stratigraphic formations, partly helping in the palinspastic reconstruction (Bennett and Venkatakrishnan,

1982). But exceptions to this stratigraphic control, where mineral zones transgress formations, indicate that the zones might not be related entirely to stratigraphy (Fig. 4-4) (Bennett and Venkatakrishnan, 1982). Rather, figure 4-4 indicates a proximal to distal flow pattern from northwest to southeast for evolving hydrothermal fluids. With this possibility, and analogies in the Keno Hill and Slocan districts, a possible interpretation is that of Hershey (1916) who proposed that the metals were in the Belt sediments and were remobilized into the veins during the intrusion of the Gem stocks (Fryklund, 1964); an interpretation which hinges on the age of mineralization. This coincides with the documented depletion halo of volatile elements such as antimony and arsenic in the host rocks which surrounds the plutons up to 3 km from the contact (Gott and Cathral, 1980).

DISCUSSION AND SUMMARY

The similarities among the three districts are such that a general model can be applied. All three districts are characterized by thick sequences of predominantly clastic sediments which have been metamorphosed to the greenschist facies. Age of host rocks however are variable, from Proterozoic to Jurassic. Orebodies are structurally controlled along fractures and extensive sets of strike slip faults. Textural evidence exists in all cases, indicating that hydrothermal activity and fault movement have been largely contemporaneous. The hydrothermal systems are typically of a large scale, extending laterally for 25-40 km and display a characteristic zoning sequence. Hydrothermal facies progress from a core area of veins containing various silicates (feldspar, epidote, quartz, or garnet, amphibole etc) and some oxide minerals (cassiterite, magnetite, ilmenite). Carbonates of calcite and/or siderite then appear, locally with the index minerals jamesonite-boulangerite, pyrrhotite, arsenopyrite and variable concentrations of the ore assemblage. Further along the sequence, the typical ore assemblage of galena-sphalerite-tetrahedrite-pyrite-siderite dominates the veins. The outermost zone is marked with pyrargyrite accompanied by acanthite, polybasite, stephanite, and a late quartz stage. This

zone may be telescoped, to overlap to a considerable degree with the inner zones, but commonly contains less galena, sphalerite, and siderite. The linear nature of the zoning appears to be due to the anisotropic and linear distribution of structural features which control the veins. The structures formed independently of pluton intrusion, allowing for an asymmetric distribution of zones about the plutons during hydrothermal activity.

Lateral zoning may be developed over broad areas due to temperature and pressure gradients which are weaker than in the vertical direction. Other features which contributed to the extensive nature of these systems are open space flow, active faulting, and relatively non-reactive host rocks. A certain degree of stratigraphic restriction also enhances lateral distribution. Precipitation mechanisms which are likely more important in such an environment are boiling and fluid mixing, such as are documented in the Keno Hill district (Chapter 5), and in Slocan (Brame, 1979), and immiscibility in the Coeur d' Alene district (Leach et. al., 1988). Genetic implications are not emphasized here, as much work is needed in this area. Rather descriptive similarities are underlined, which themselves have unifying genetic implications for a similar hydrothermal environment established along portions of the Omenica Crystalline Belt.

REFERENCES

Abbott, J.G., 1985, Silver-bearing veins and replacement deposits of the Rancheria district. In, Yukon Exploration and Geology 1983, Exploration and Geological Services Division, Northern Affairs Program, 200 Range Road, Yukon, p.34-44.

Abbott, J.G., 1986 a, Epigenetic mineral deposits of the Ketza-Seagull district, Yukon. In J.A. Morin and D.S. Emond (editors), Yukon Geology, vol. 1, p.56-66.

Abbott, J.G., 1986 b, Geology of the Plata-Inca property, Yukon. In J.A. Morin and D.S. Emond (editors), Yukon Geology, vol. 1, p. 109-112.

Archibald, D.A., Glover, J.K., Price, R.A., Farrar, E., Charmichael, D.M., 1983, Geochronology and tectonic implications of magmatism and metamorphism, southern Kootenay arc and neighbouring regions, southern British Columbia, Pt. 1, Jurassic to mid-Cretaceous, Canadian Journal of Earth Sciences, vol. 20, p. 1891-1913.

Andrew, A., Godwin, C.I., Sinclair, A.J., 1984, Mixing line isochrons: a new interpretation of galena lead isotope data from southeastern British Columbia. Economic Geology, vol. 79, p. 919-932.

Bennett, E.H., Venkatakrishnan, 1982, A palinspastic reconstruction of the Coeur d'Alene mining district based on ore deposits and structural data. Economic Geology, vol. 77, p. 1851-1866.

Boyle, R.W., 1965, Geology, geochemistry, and origin of the lead-zinc-silver deposits of the Keno Hill-Galena Hill area, Yukon Territory. Geological Survey of Canada, Bulletin 111, 302 pages.

Brame, S., 1979, Mineralization Near the Northern Margin of the Nelson Batholith, MSc thesis, The University of Alberta, Edmonton, 146 pages.

Cairnes, C.E., 1934, Slocan mining camp, British Columbia. Geological Survey of Canada, memoir 173.

Cairnes, C.E., 1935, Description of properties, Slocan mining camp, British Columbia. Geological Survey of Canada, Memoir 184.

Cairnes, C.E., 1948. Slocan mining camp, p.200-205, in Structural Geology of Canadian Ore Deposits, Canadian Institute of Mining and Metallurgy, 948 pages.

Carr, S.D., 1986, The Valkyr shear zone and the Slocan Lake fault: Eocene structural development of the Valhalla core complex, southeastern British Columbia [M.Sc. thesis]: Ottawa Ontario, Carlton University, 106 pages.

Cox, J., 1979, The Geology of the Northwest Margin of the Nelson Batholith, British Columbia, MSc thesis, The University of Alberta, Edmonton, 95 pages.

Crosby, G.M., 1959, The Gem stocks and adjacent orebodies, Coeur d'Alene district, Idaho. Mining Engineering, vol. 11, p.697-700.

Fluet, D.W., 1986, Genesis of the Deer Trail Zn-Pb-Ag Vein Deposit, Washington, U.S.A.. Unpublished Masters thesis, University of Alberta, Edmonton Alberta, 129 pages.

Fryklund, Jr, V.C., 1964, Ore deposits of the Coeur d' Alene district, Shoshone county, Idaho. United States Geological Survey professional paper 445, 1^3 pages.

Fyles, J.T., 1966, Lead-zinc deposits in British Columbia. In, Tectonic History and Mineral Deposits of the Western Cordillera. Canadian Institute of Mining Special Volume, p. 231-238.

Fyles, J.T., 1967, Geology of the Ainsworth-Kaslo Area, British Columbia. British Columbia Department of Mines and Petroleum Resources, Bulletin 53, 125 pages.

Gabrielse, H., 1985, Major dextral transcurrent displacements along the Northern Rocky Mountain Trench and related lineaments in north central British Columbia. Geological Society of America Bulletin, p. 1-14.

Godwin, C.I., Watson, P.H., Shen, K., 1986, Genesis of the Lass vein system, Beaverdell silver camp, south-central British Columbia. Canadian Journal of Earth Sciences, vol. 23,p. 1615-1626.

Gott, G.B., Cathrall, J.B., 1980, Geochemical exploration studies in the Coeur d' Alene district, Idaho and Montana. United States Geological Survey professional paper 1116, 63 pages.

Hedley, M.S., 1952, Geology and ore deposits of the Sandon area, Slocan mining camp, British Columbia. British Columbia Department of Energy, Mines and Petroleum Resources, Bulletin 29, 130 pages.

Hershey, O.H., 1916, Origin and distribution of ore in the Coeur d'Alene mining district. Mining Scientific Press, San Francisco, 32 pages.

Hobbs, S.W., Griggs, A.B., Wallace, R.E., Campbell, A.B., 1965, Geology of the Coeur d' Alene district, Shoshone county, Idaho. United States Geological Survey, Professional Paper 478, 139 pages.

Leach, D.L., Landis, G.P., Hofstra, A.H., 1988, Metamorphic origin of the Coeur d'Alene base-and precious-metal veins in the Belt basin, Idaho and Montana. Geology, vol. 16, p. 122-125.

Logan, J.M., 1986, Mineralogy and metal distribution, Hallmac mine, Sandon (82F/4, 82K/3). British Columbia Ministry of Energy, Mines and Petroleum Resources, Paper 1986-1, p. 289-301.

Lynch, G., 1986 , Lateral zoning in the Keno Hill Ag-Pb-Zn mining district, Yukon. North American Conference on Tectonic Control of Ore Deposits, and the Vertical and Horizontal Extent of Ore Systems [abstract volume]. University of Missouri, Rolla, p. 46.

McTaggart, K.C., 1960, The geology of Keno and Galena Hills, Yukon Territory. Geological survey of Canada Bulletin 58.

Monger, J.W.H., Price, R.A., Tempelman-Kluit, D.J., 1982, Tectonic accretion and origin of the two major metamorphic and plutonic welts in the Canadian Cordillera. Geology, vol. 10, p.70-75.

Nguyen, K.K., Sinclair, A.J., Libby, W.G., 1968, Age of the northern part of the Nelson Batholith. Canadian Journal of Earth Sciences, vol. 5, p. 955-957.

Orchard, M.J., 1985, Carboniferous, Permian and Triassic conodonts from the central Kootenay Arc: constraints on the age of the Milford, Kaslo and Slocan Groups. In: Current Research, Part A, Geological Survey of Canada, Paper 85-1A, p. 287-300.

Parrish, R., 1984, Slocan Lake fault: A low angle fault zone bounding the Valhalla gneiss complex, Nelson map area, southern British Columbia. In, Current Research Part A: Geological Survey of Canada Paper 84-1A, p. 323-330.

Parrish, R., Carr, S.D., Brown, R.L., 1985, Valhalla gneiss complex, Nelson map area, southern British Columbia,. In, Current Research, Part A: Geological Survey of Canada Paper 84-1A, p.81-87.

Parrish, R.R., Carr, S.D., Parkinson, D.L., 1988, Eocene extensional tectonics and geochronology of the southern Omenica Belt, British Columbia and Washington. Tectonics, vol. 7, p. 181-212.

Reynolds, P.H., Sinclair, A.J., 1971, Rock and ore-lead isotopes from the Nelson Batholith and the Kootenay Arc, British Columbia, Canada. Economic Geology, vol. 66, p. 259-266.

Sinclair, A.J., Tessari, O.J., Harakal, J.E., 1980, Age of Ag-Pb-Zn mineralization, Keno Hill-Galena Hill area, Yukon Territory. Canadian Journal of Earth Sciences, vol. 17, p. 1100-1103.

Spurr, J.E., 1907, A theory of ore deposition. Economic Geology, vol. 2, p. 781-795.

Spurr, J.E., 1912, Theory of ore deposition. Economic Geology, vol. 7, p. 485-492.

Venkatakrishnan, R., Bennett, E.H., 1988, Structural controls of the Coeur D'Alene ore veins, Shoshone County, Idaho. In, G. Kisvarsanyi and S.K. Grant (editors), North American Conference on Tectonic Control of Ore Deposits and the Vertical and Horizontal Extent of Ore Systems, Proceedings Volume, University of Missouri, Rolla Missouri, p. 125-133.

Watson, K.W., 1986, Silver-Lead-Zinc deposits of the Keno Hill-Galena Hill Area Yukon Territory. In, J.A.Morin and D.S.Emond (editors), Yukon Geology, vol. 1, Northern Affairs Program, Whitehorse Yukon, p. 83-88.

CHAPTER 5

BOILING OF H_2O-CO_2-NaCl FLUIDS IN THE KENO HILL Ag-Pb-Zn VEIN SYSTEM, YUKON: A FLUID INCLUSION STUDY

INTRODUCTION

The Keno Hill mining district is one of the richest polymetallic Ag-Pb-Zn vein systems in western Canada. Situated in central Yukon (Fig. 5-1), the district has produced over 6.4 billion g of Ag since mining began in 1913. Average grades are very high: 1412 g/t Ag, 7 % Pb, and 4.6 % Zn (Watson, 1986). The veins are an excellent example of the many hign grade silver deposits which are located along the eastern portion of the Canadian Cordillera (Fyles, 1966).

Early geological work in the Keno Hill mining district concentrated on documenting the complex mineralogy of the numerous veins (Boyle, 1965). A corresponding mid-Cretaceous age between the veins and granite plutons of the region was established (Sinclair et al., 1980), indicating a possible genetic link between the two. Recent studies of mineral paragenesis in the veins, and mineral zoning in the district display a relationship between the veins of the Keno Hill mining district and the Cretaceous Mayo Lake pluton (Chapter 3).

Although the orebodies have been extensively described, limited information exists concerning the origin of the veins. To investigate the nature of hydrothermal activity in the formation of the orebodies, a fluid inclusion study was undertaken. Samples were collected along the entire length of the 25 km long mining district. Standard heating/freezing techniques were applied using a U.S.G.S. fluid inclusion stage (Werre et al., 1979).

The fluid inclusions demonstrate the correspondence of boiling with ore formation. Because pressure is an important parameter in controlling boiling, methods of pressure

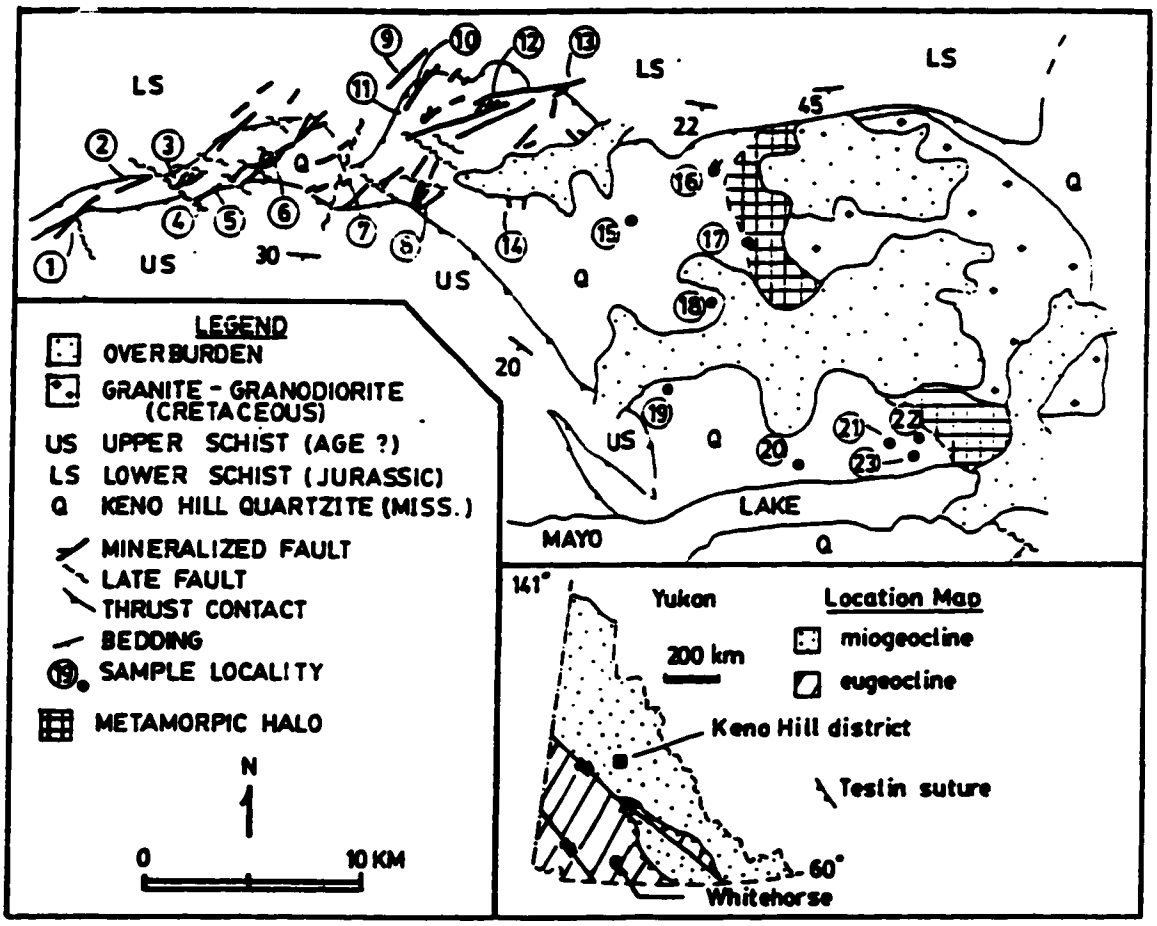

Figure 5-1. Location map of Keno Hill mining district, local geology, and distribution of ore deposits as well as sample localities in district. Numbers correspond to the following deposits: (1) Silver King mine; (2) Husky mine; (3) Dixie mine; (4) Bermingham open pit; (5) Ruby mine; (6) Hector open pit; (7) Flame and Moth vein; (8) Bellekeno mine; (9) Sadie-Ladue mine; (10) Lucky Queen mine; (11) Black Cap open pit; (12) Keno mine; (13) Caribou mine; (14) Homestake vein; (15) vein #243; (16) vein # 152; (17) vein # 165; (18) vein # 221; (19) vein # 310; (20) vein # 49; (21) vein # 25; (22) vein # 15; (23) vein # 60.

estimation from three-phase fluid inclusions were applied (Parry, 1986), and a computer program was developed to perform the calculations (Appendix 2). The results show that large fluctuations in fluid pressure occurred, at various sites within the veins, during mineralization.

Host rocks to the vein system are graphitic. Calculations of water-graphite equilibria are presented. These demonstrate the considerable influence that graphite had on the composition of the fluids. In general graphite has a strong buffering capacity, imparting high $CO_2 \pm CH_4$ contents to hydrothermal fluids (French, 1966; Ohmoto and Kerrick, 1977). Bowers and Helgeson (1983 a,b) have shown that unmixing (boiling) in the system H_2O-CO_2-NaCl may occur at relatively high pressures. The high CO_2 content maintained in the mineralizing fluids of the Keno Hill mining district, due the presence of graphite in the host rocks, increased their susceptibility to boiling. Deep seated high pressure boiling is documented here, in the fluid inclusion record of the Keno Hill mining district, and appears to have been the main mechanism of ore formation. Later mixing of the boiled saline fluids with cooler dilute fluids marked the end of hydrothermal activity.

Geological setting

The mineral deposits of the Keno Hill mining district are contained within the Mississippian, Keno Hill Quartzite of central Yukon. The quartzite has been traced along strike, from east to west, for more than 220 km (Tempelman-Kluit, 1970). Its western extent terminates at the Tintina fault, a Cordilleran scale transcurrent shear which has up to 900 km of right-hand offset (Gabrielse, 1985).

The regional setting consists of sedimentary rocks ranging in age from Proterozoic to Jurassic, which were deposited on the ancient continental margin of North America (Abbott et al., 1986). Stratigraphy in the region has been greatly disrupted by thrusting. Units were thrust to the north in Late Jurassic - Early Cretaceous time (Tempelman-Kluit, 1979).

The Keno Hill Quartzite is a distinctive unit due to its black graphitic nature. In the mining district, it has a structural thickness of approximately 1 km, and is thrust-bound above and below by extensive graphitic schist units. These are informally known as the "Upper" and "Lower" schists (Fig. 5-1). The Lower schist is Jurassic in age (Poulton and Tempelman-Kluit, 1982); the Upper schist is of uncertain age. All three units contain a moderately dipping schistosity related to isoclinal folding and thrusting (McTaggart, 1960). Greenschist metamorphism accompanied deformation. An upright crenulation cleavage overprints the thrust-related fabrics, and is associated with dextral transcurrent shear in the region (Chapter 2).

Concordant greenstone lenses are abundant throughout the Lower Schist and Keno Hill Quartzite. They are interpreted to be the metamorphosed equivalents of gabbro or diorite sills (Green, 1971). The age of the greenstones is uncertain, but they are contemporaneous or younger than the Jurassic Lower Schist unit.

The district is contained within a region which is part of the northern extension of the Omenica Crystalline Belt (Monger et al., 1982). Several felsic plutonic bodies are found throughout the area. These are part of the Cretaceous Selwyn plutonic suite and range in composition predominantly between granite and granodiorite (Anderson, 1987). In association with these are widespread aplite dykes of the same age (Green, 1971). Also in the district are some lamprophyre dykes, which are rare and of undetermined age. Intrusive rocks crosscut all metasedimentary units, as well as deformation fabrics.

Micas from hydrothermal alteration surrounding the Ag-Pb-Zn veins of the mining district have been dated at 84 ± 4 Ma by the K-Ar method, indicating contemporaneity between the veins and granite emplacement (Sinclair et al., 1980).

Mineral deposits

Orebodies are contained within an extensive set of northeast-striking, sinistral strike-slip faults (McTaggart, 1960). These form a conjugate set to the brittle-ductile Mayo Lake

Shear Zone, which is east of the mining district (Chapter 2). Individual ore bearing structures are usually less than 4 km in strike length, but collectively they form the 25 km long mining district. The faults are best developed in the brittle Keno Hill Quartzite; the schist units above and below the quartzite are less fractured and faulted. Both lithologic and structural control are important in localizing orebodies. Zones of dilation due to deflections in the fault planes along anastamosing faults, or between overlapping ends of en echelon faults, are favourable sites for mineralization (Chapter 2). Orebodies are also located along the portions of the faults that pass from the quartzite into the Upper Schist unit (Boyle, 1965). Shearing and brecciation of hydrothermal minerals followed by hydrothermal cementation of broken clasts, indicate a certain degree of contemporaneity between fault movement and hydrothermal activity. Hydrothermal breccias are commonly observed (Chapter 3). A set of northwest striking, dextral faults post-date mineralization, and truncate many of the orebodies.

Although the mining district extends from east to west for 25 km, the entire vein system is continuous within the Keno Hill quartzite for approximately 40 km if non-economic veins are included. Vein mineralogy along the length of the hydrothermal system is zoned relative to the Mayo Lake Pluton (chapter 3). The pluton is situated at the eastern end of the district. A list of hydrothermal minerals and their paragenetic position within the veins is given in Figure 5-2; however the complete set of minerals is never seen together within a single vein, and the paragenesis diagram is only schematic, since timing inferences are made for minerals from adjacent zones which do not occur together by the minerals which overlap between the zones. Quartz-feldspar veins characterize the assemblage nearest to the pluton, with some cassiterite bearing, quartz-muscovite veins at the edge of this zone. Away from the pluton, calcite and then siderite are abundant in the veins. Sulfides become more common with siderite. Extensive mineralogical documentation from within the orebodies is given by Boyle (1965). A typical paragenetic succession consists of early quartz with associated arsenopyrite, jamesonite, boulangerite, sphalerite, some

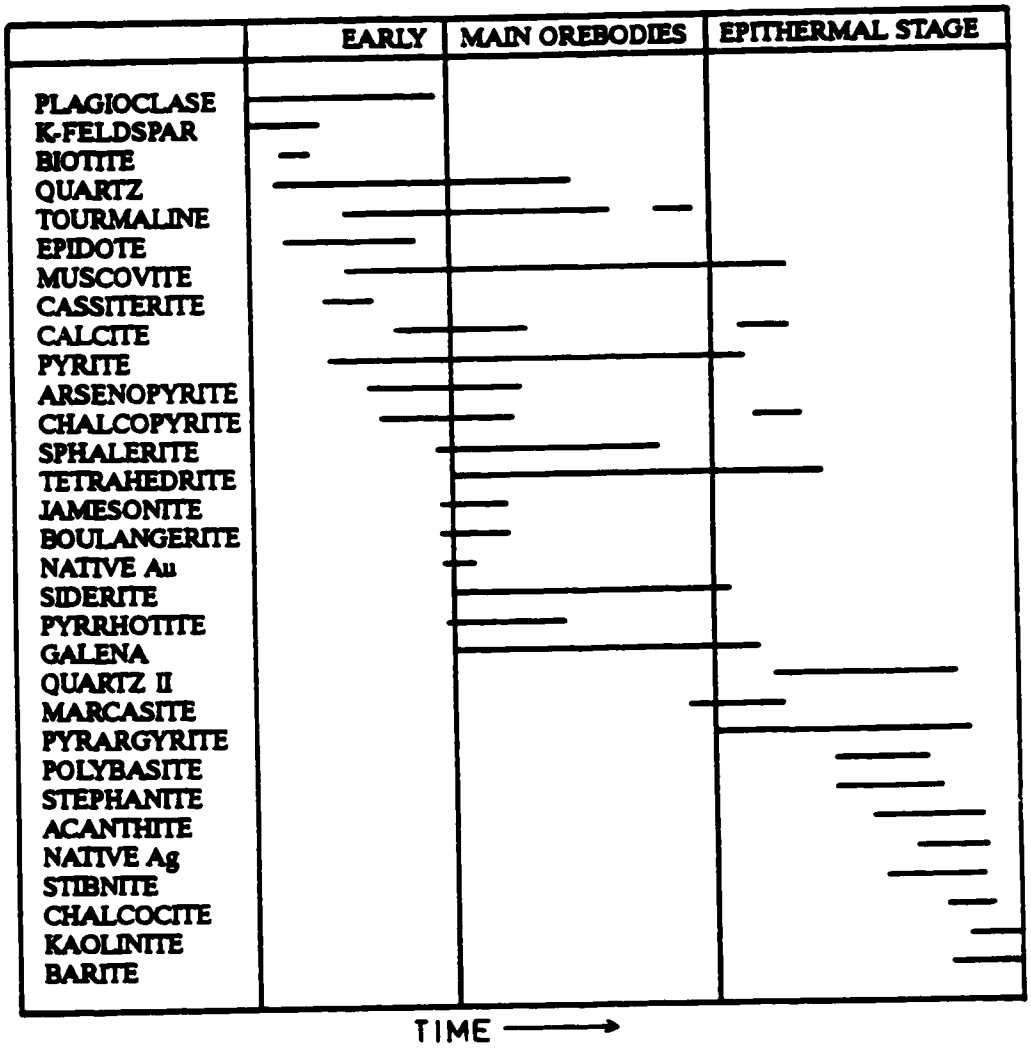

Figure 5-2. Paragenesis diagram of principal hydrothermal vein minerals found in Keno Hill mining district. Quartz, siderite, and late quartz (quartz II) were used in the fluid inclusion study; the relative timing between these is well established. The complete set of minerals, however, from the district is never seen together within a single vein, and the paragenesis diagram is largely schematic, since timing inferences are made for minerals from adjacent zones which do not occur together, by the minerals which overlap between the zones.

chalcopyrite and traces of native gold; followed by the dominant ore stage containing siderite, galena, sphalerite, tetrahedrite, and pyrite. The early ore phase is most abundant on Keno Hill in the eastern portion of the mining district. A third stage which is later than these two, and is found predominantly in the western portion of the district, consists of finer quartz, pyrargyrite, acanthite, native silver, polybasite, stephanite, and freibergite. An exception to this is the Lucky Queen mine on Keno Hill in the east of the district (Fig. 5-1). The late stage is also the furthest from the Mayo Lake Pluton.

FLUID INCLUSIONS

Minerals suitable for fluid inclusion investigation

Of the non-opaque phases in the vein system, quartz and carbonate contain the greatest abundance of fluid inclusions, which are adequate for investigation. Most of the sphalerite is too dark for inclusions to be easily examined. Within the mining district, quartz and carbonates span the entire paragenetic sequence. Siderite is closely intergrown with the opaque mineralogy of the oreshoots, and is thought to contain fluid inclusions representative of the original ore forming fluid. The early quartz stage contains a great abundance of large inclusions, whereas the siderite and late quartz stages contain relatively few, small fluid inclusions. Consequently, the abundance of data is biased to the earlier stage of quartz, but equal importance is given to inclusions from the various stages during the interpretation.

Texturally, considerable contrast can be observed in the gangue mineralogy. The earlier quartz stage is characterized by coarse euhedral crystals with extensive internal growth banding, as defined by multiple, hexagonal, concentric layers of primary inclusions. Siderite on the other hand is generally medium grained, equigranular, and massive. Late stage quartz is fine to medium grained, euhedral to granular, and is often dendritic with single crystals displaying a "feather" pattern in thin section. Overgrown

dendritic quartz may contain very small primary fluid inclusions caught between dendrites; however, these cavities are mostly empty.

Hydrothermal minerals through large sections of the veins have been sheared, from fault movement that was later than, or possibly contemporaneous with hydrothermal activity. But portions of the veins and isolated pods retain unstrained vein minerals; these were used throughout the fluid inclusion study.

The sample distribution spans the entire east-west length of the 25 km long mining district (Fig. 5-1). Sampling transgresses many of the mineralogical zones in an attempt to correlate fluid characteristics with changing mineralogy. Close attention was paid to spatial and temporal distribution of samples. While much of the emphasis was on the orebodies, fluid inclusions were also studied from quartz within the quartz-feldspar veins of the region near the Mayo Lake Pluton. These veins are thought to have been part of, or analagous to, the feeder veins through which the mineralizing solutions passed before ore formation, and may give insight into hydrothemal processes which took place in the source region.

Because of the size of the district and scope of the project, inclusions of obvious secondary nature (along healed fracture planes) were given less attention. Inclusions showing the best evidence of primary origin are those which have formed along growth planes. Fortunately this is a common type in the early quartz stage. However, because rigorous criteria for fluid inclusion origin is more commonly lacking, most of the data were obtained from inclusions of more or less uncertain or ambiguous origin, which are nonetheless representative of one portion of the system's evolving history.

Fluid inclusion types

Fluid inclusion types are distinguished by their phase proportions at room temperature, as well as by their behaviour upon heating/freezing. Six types of fluid inclusions are commonly observed in the gangue mineralogy. Three of these are found in

the early quartz stage, one type predominantly was observed in siderite, and two types were seen in the late quartz stage.

Within early quartz, the inclusions are typically large, from 20-80 microns and contain H_2O-CO_2-NaCl±CH_4. Type I inclusions contain relatively high but variable contents of CO_2 (Fig. 5-3 A). The inner CO_2 bubble volume, at 40° C, varies from 30-50 % of the total inclusion volume, but may be as high as 80%. Distinctive of type I inclusions is the tendency of the innermost CO_2 (g) bubble to homogenize at low temperature by bubble shrinkage to liquid CO_2, between 23°-26° C. Correspondingly, at room temperature, the CO_2 (g) bubble is very small and near its homogenization point (Fig 5-3 A). Type I inclusions within quartz crystals are sometimes distributed along growth planes, and are thought to be mostly primary in origin. Morphologically, the inclusions often form hexagonal negative crystals, but also can be quite irregular. Within the veins, type I inclusions are found both in compact anhedral early quartz, or in coarse euhedral early quartz which appears to have grown into open portions of veins. Locally, quartz interlocked with siderite contains type I inclusions.

Type II inclusions are also three phase inclusions within early quartz, similar in appearance to type I except that their CO_2 content is significantly less (Fig. 5-3 B, C). Here the internal bubble is dominated by gaseous CO_2, with only a thin rim of liquid CO_2. The most definitive means of distinguishing type I from type II inclusions, is by the CO_2 inner bubble homogenization characteristics. The inner $CO_{2(g)}$ bubble of type II inclusions homogenizes by bubble expansion to gas, instead of by bubble shrinkage to liquid. Because the third dimension of the fluid inclusion is not usually seen, the volume percent estimate of the bubble relative to the whole inclusion is not always accurate; however, estimates range from 20-70 %. The size and shape of type II inclusion are similar to that of type I. Type II inclusions are located in the same quartz crystals as type I inclusions, and microscopically they may occur in the same field of view. Type II inclusions of primary origin do exist, but they can be frequently observed along secondary planes as well.

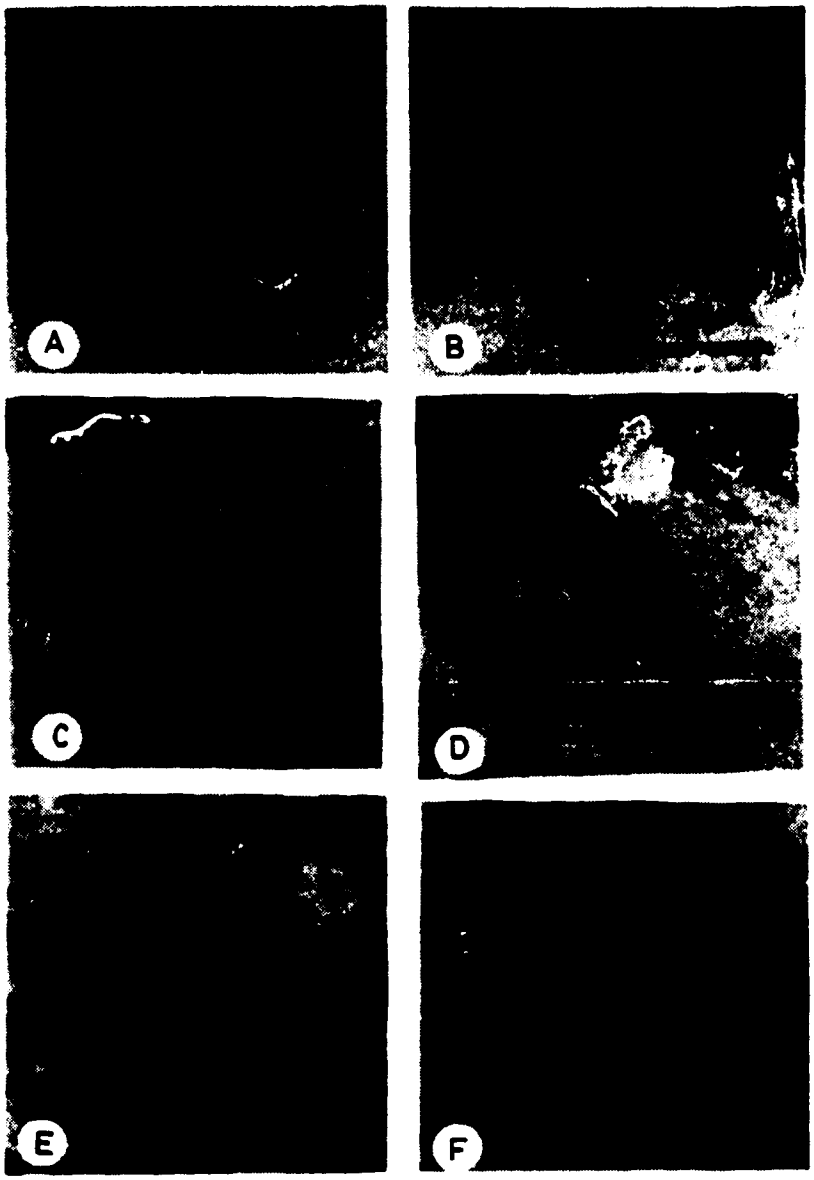

Figure 5-3. Micrographs of main fluid inclusion types: a) 3 phase type I inclusion, inner $CO_{2(g)}$ bubble homogenizes first by bubble shrinkage, followed by total inclusion homogenization by bubble expansion at high temperature; b) 3 phase type II inclusion, inner $CO_{2(g)}$ bubble homogenizes first by bubble expansion to gaseous CO_2, followed by total inclusion homogenization at high temperature by bubble shrinkage to liquid; c) Type II inclusion with thin rim of liquid CO_2 along margin of inner bubble; d) two phase type III inclusions; e) type IV inclusions in siderite; f) type V inclusion in late quartz.

Type III inclusions, common in early quartz, are characterized by two phase liquid/vapor inclusions (Fig. 5-3 D). These are often smaller in size, from < 5-30 microns and do not usually form negative crystals, but are elliptical in form. At room temperature the vapor/liquid ratio is 15 %-50 % by volume, notably less than in inclusion types I and II. Water dominates type III inclusions, but the presence of carbon dioxide is indicated in many inclusions by the formation of clathrates in the freezing experiments. Isolated, possibly primary, type III inclusions may be found in portions of some quartz crystals, but they are also observed along healed fractures.

Within the same veins, siderite is paragenetically later than the early quartz. Fluid inclusions within siderite (type IV) are small, 5-15 microns across, irregular in form, and show two phases at room temperature (Fig. 5-3 E). They are water dominated and contain a gas bubble which makes up 15-30 % of the inclusion volume. Carbon dioxide within the gas phase is indicated in some of the inclusions, by the formation of clathrates during freezing runs. Type IV inclusions are generally rare, and difficult to work with due to poor optics in the oxidized siderite. Many fractures, small inclusions, and double refraction also cause difficulties. Doubly polished chips must be cut thin, are fragile, and often tend to crumble because of the perfect rhombohedral cleavage. Consequently relatively few data were obtained from these. However substantial effort was dirrected towards finding inclusions in siderite suitable for study, since siderite is closely intergrown with the ore, and is thought to contain inclusions representative of the ore forming fluids. Within siderite a few vapor dominated inclusions were observed at room temperature, but because of leakage during heating it remains unknown if they are representative of the fluids in its originally trapped state.

The late stage quartz contains fluid inclusions (type V) which are very small, less than 10 microns, dilute $H_2O_{(l)}$-$H_2O_{(v)}$ inclusions (Fig. 5-3 F). The vapor bubble at room temperature is small, comprising between 15 % - 25 % of the inclusion volume. The

inclusions are most often trapped within overgrowths to quartz dendrites, and are representative of the fluids which precipitated the latest stage of quartz.

A few pure CO_2 inclusions (type VI) were found within the late stage quartz, as well as a few within the early quartz stage. The purity of these inclusions is indicated by melting temperatures very near -56.6° C, and by the lack of clathrate formation. Total homogenization is to vapor, between +25.8° to +27.8° C. Their origin is uncertain, but they may indicate the complete immiscibility between H_2O and CO_2 under low pressure conditions.

Heating/freezing data

The heating and freezing measurements for all inclusions are summarized in Appendix 1. Type I inclusions contain variable proportions of CO_2 and H_2O. Correspondingly, upon heating total homogenization is either by CO_2 bubble shrinkage for inclusions with lesser amounts of CO_2, or by CO_2 bubble expansion for inclusions with higher gas contents. Both homogenize within the range 285°-345° C, with a histogram peak distribution at 305° C (Fig. 5-4 A). The contemporaneous entrapment of liquid-dominated and gas-dominated fluids at the same temperature is typically interpreted to indicate boiling fluids (Roedder, 1984).

Variable liquid/gas ratios are observed in type II inclusions. At high temperature, characteristics of homogenization vary widely. Inclusions homogenize to either liquid by bubble shrinkage, or to gas by bubble expansion, both within the same temperature bracket. Occasional supercritical behaviour, such as bubble margin "fade-out" is recorded as well (Roedder, 1984). Almost all type II inclusions homogenize between 300° to 310° C, similar to type I inclusions (Appendix 1, Fig. 5-4 A). Type II inclusions are interpreted to have been trapped during boiling.

In both type I and type II inclusions, the melting temperature for CO_2 is usually between -56.6° C and -57.5° C, indicating the presence of relatively pure CO_2 (Hollister

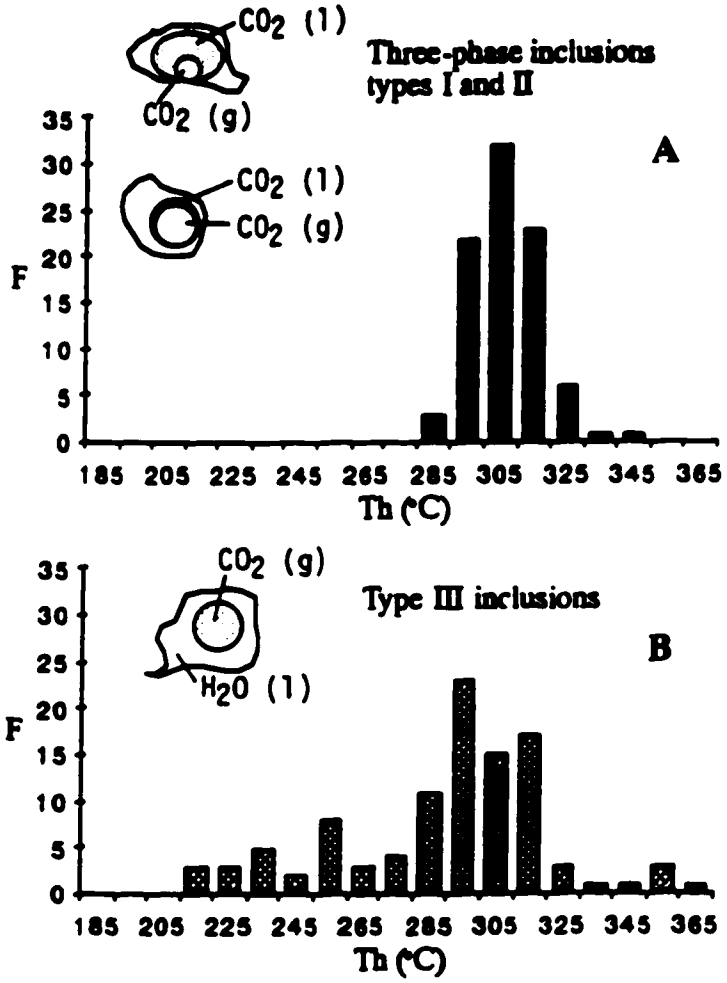

Figure 5-4. (A) Frequency diagrams of total homogenization temperatures (Th) for inclusion types I and II. Ten degree intervals are used on the x axis, with the median temperature to these intervals shown on the diagram. (B) Homogenization temperature histogram for type III inclusions.

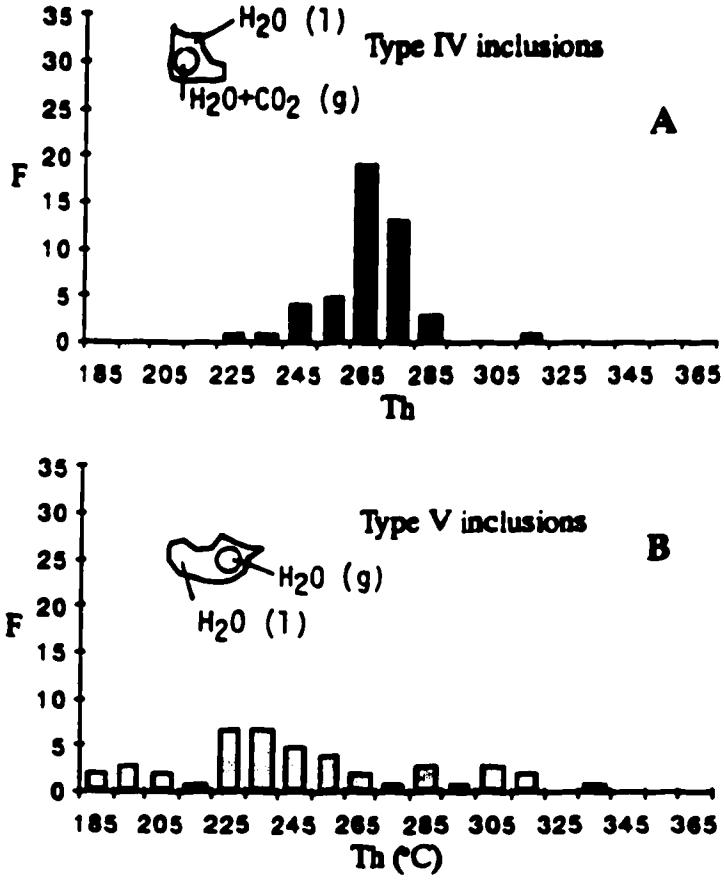

Figure 5-5. Frequency diagrams of total homogenization temperatures for inclusion types IV (A) and V (B). Ten degree intervals are used on the x axis, with the median temperature to these intervals shown on the diagram.

and Burruss, 1976). However the presence of other gases in small quantities, likely CH_4 and/or N_2, is indicated in some inclusions by slightly depressed CO_2 melting temperatures, down to -59.2° C (Hollister and Burrus, 1976).

Type III inclusions generally homogenize by bubble shrinkage. A wide range of homogenization temperatures are recorded, from 210° C to 365° C, but tend to cluster near 290° C, slightly lower than types I and II (Fig. 5-4 B). A few type III inclusions homogenize to gas, at similar temperatures to surrounding inclusions which homogenize to liquid, indicating that some boiling occurred during quartz precipitation from type III fluids.

In siderite, homogenization of inclusions (type IV) is to liquid, mainly between temperatures of 260°-280° C (Fig. 5-5 A). Supercritical phenomena were observed in one specimen. During heating, siderite and its weathering products tend to oxidize, reducing visibility; the problem was somewhat alleviated by using N_2 gas instead of air.

Type V inclusions from late quartz homogenize to liquid. A wide range of temperatures is recorded, from 152° to 335° C, but a faint clustering of data is observed near 220°-250° C (Fig. 5-5 B).

Salinity

Salinity determinations are reported in weight percent NaCl equivalent relative to water. Although other salts are likely present as well, this notation is the widely used index of the overall amount of dissolved salts in the fluids, when salinity is determined from ice and clathrate melting temperatures. For inclusion types I, II, III, and IV, clathrate melting temperatures were measured and salinity was estimated using the equation of Bozzo et al. (1973). For type V inclusions, as well as some type IV inclusions which did not form clathrates due to low CO_2 contents, ice melting temperatures were inserted into the equation of Potter et al. (1978) for salinity determinations.

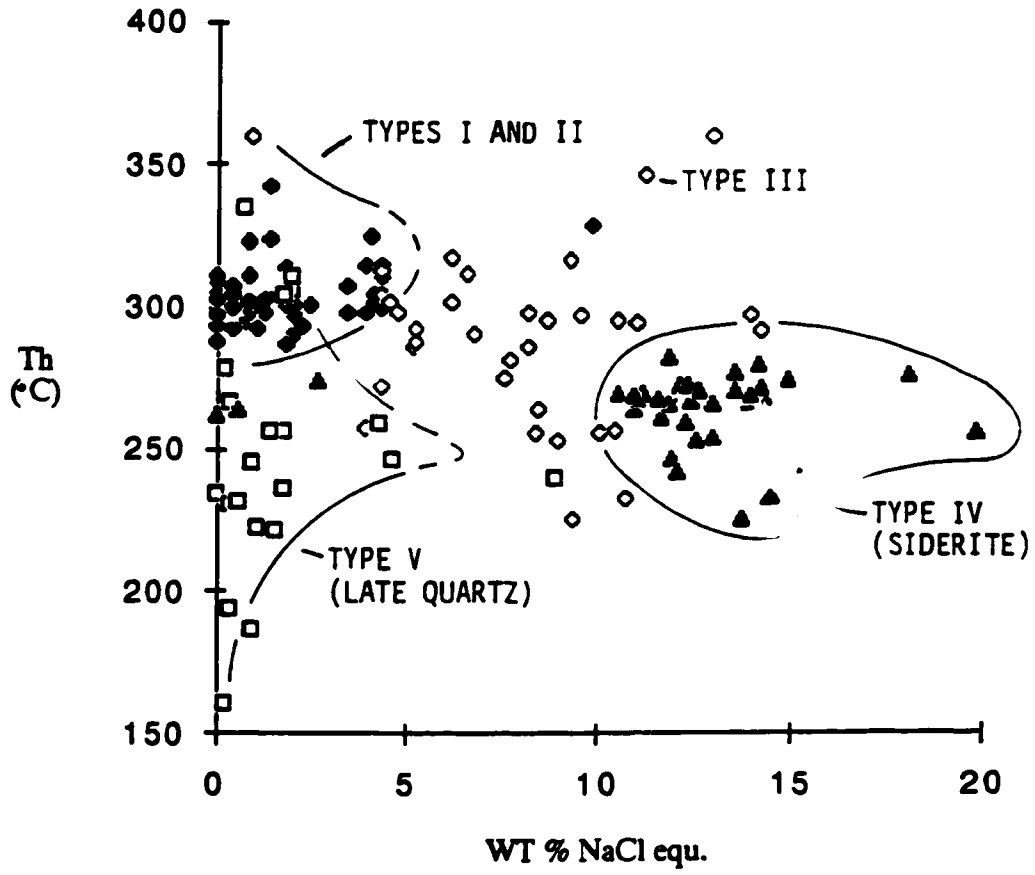

Figure 5-6. Plot of total homogenization temperatures (Th) versus salinity in weight percent NaCl equivalent, for fluid inclusion types I, II, III, IV, and V.

Results of salinity determinations are displayed in Figure 5-6. Types I and II inclusions have a salinity range between 0 and 7.1 weight percent NaCl equivalent, corresponding to clathrates melting between +10.0° to +6.2° C, though salinity is usually less than 4 weight percent. The salinity estimates are slightly lower than the actual salinity in some inclusions due to the presence of minor accessory gases other than CO_2, as indicated by depressed melting temperatures for CO_2 below -56.6° C (Burruss, 1981). For type III inclusions in early quartz, melting temperatures indicate a wide range of salinities, from 0 to 17.3 weight percent NaCl equivalent. An even greater range of results is observed from type IV inclusions in siderite, from 0 to 19.8 weight percent NaCl equivalent, but most of the results fall between 10 to 15 weight percent NaCl equivalent (Fig. 5-6).

A characteristic feature of fluid inclusions within late quartz is the generally low salinity, most often less than 1.5 weight % NaCl equivalent. Higher salinities, up to 8.8 and 13.3 weight % NaCl equivalent, are occasionally recorded.

Figure 5-6 is a plot of homogenization temperature versus salinity. Type I and II inclusions have temperatures mostly between 300°-310° C and a salinity range of 0 to 5 weight percent NaCl equivalent. Fluid inclusions from siderite are distinctive due to their high salinity and slightly lower homogenization temperatures. Homogenization temperatures and salinities recorded in type III inclusions from early quartz overlap between the characteristics of the inclusions in siderite, and the characteristics of type I and II inclusions. The late stage quartz has distinctive inclusions in that they are low temperature, low salinity inclusions (Fig 5-6).

Inclusions of type I, II, III, IV, and V maintained consistent heating/freezing properties from east to west along the length of the mining district (Fig. 5-1 and Appendix 1). However early quartz, and consequently fluid inclusion types I, II, and III, are more abundant in the east, whereas late quartz is more widespread in the west. Siderite, paragenetically between these two, extends completely from east to west.

Quartz-feldspar veins

Although not presently of economic interest, quartz-feldspar veins within the Keno Hill hydrothermal system form a distinctive zone, nearer to the plutonic bodies than the ore deposits (chapter 3). Some fluid inclusion data were gathered from vein minerals in the ion of quartz-feldspar veining near the Mayo Lake Pluton to help characterize the full extent of the system (sites 15 to 23 on Figure 5-1). Eight different veins were sampled, and 110 inclusions in quartz were studied.

Five relatively high temperature inclusions were observed (Appendix 1). These are two phase inclusions, which homogenize to the vapor phase between 450° and 535° C. At room temperature the vapour/liquid ratio is approximately 50 % by volume. No freezing point determinations were obtained from these, even after cooling the chips down to -120° C. Consequently, they are of undetermined composition.

The majority of inclusions viewed however, homogenize to liquid between 300° and 400° C. Both two phase and 3 phase H_2O-CO_2±CH_4 inclusions occur. The presence of some gases other than CO_2 is noticeable in these inclusions, as clathrate melting temperatures often exceed +10° C, and the CO_2 melting point has been depressed to values usually near -59° C. Because of these extra components, salinity determinations are minimum values when using the clathrate melting temperature. Estimates are generally less than 3 weight percent NaCl equivalent.

Within the three phase inclusions, a particularly distinctive feature is the low homogenization temperature recorded for many of the inner CO_2 bubbles; these homogenize to liquid at temperatures as low as +12.6° C. The depressed temperatures may be interpreted to be due to the presence of CH_4, which has the effect of lowering the critical point of CO_2 to temperatures below 31° C (Hollister and Burruss, 1976). Higher pressure conditions of fluid entrapment, and a high density CO_2 fluid within the inclusions may also contribute to the lower hogenization temperatures for CO_2.

X_{CO_2} and pressure determination

Fluid composition in the system CO_2-H_2O-NaCl is typically estimated in fluid inclusions from the CO_2/H_2O volume measurements (Burruss, 1981; Poty et al., 1974; Hollister and Burruss, 1976), and from the clathrate melting temperature for salinity (Bozzo et al., 1973). An inherent problem is not being able to observe the form of the fluid inclusion in the third dimension (Bodnar, 1983). This introduces a great deal of uncertainty when estimating the volume percentage that the CO_2 bubble occupies in the inclusion, since inclusions can have irregular forms and variable depth.

Parry (1986) outlined an alternate method for the estimation of X_{CO_2} and pressure in three phase H_2O-CO_2-NaCl fluid inclusions, which requires only accurate heating-freezing data. The method may be applied to inclusions which have been trapped on the two phase boundary. A restriction of the method is that methane must be negligible or absent from the inclusion, a condition which can be verified by the freezing point determinations on CO_2 (Burrus, 1981).

For pressure determinations, calculations are performed using the Redlich-Kwong equation of state, with parameters proposed by Bowers and Helgeson (1983). A computer program written in BASIC was designed during the course of this study, and is included in Appendix 2.

Many type I and II inclusions are appropriate for calculating X_{CO_2} and pressure. Type I inclusions vary in composition from X_{CO_2} = 0.13 to 0.28, and were trapped in a pressure range from 1514 bars to 1767 bars. Type II inclusions are relatively depleted in CO_2, with X_{CO_2} = 0.05 to 0.08, and were trapped at a lower pressure, between P = 486 bars to P = 675 bars.

Type III, IV and type V inclusions are two phase inclusions to which the pressure determination method cannot be applied. However, the formation of clathrates upon freezing, brackets the CO_2 content to: $0.01 < X_{CO_2} < 0.03$ (Hedenquist and Henley, 1985). And, for the inclusions that did not form clathrates, the CO_2 content is low , less

than 0.01 mole fraction. Pressure determinations for these low CO_2 inclusions cannot be made using the above method, which requires three phase fluid inclusions.

The contrasts in pressure and XCO_2 which are recorded for type I and II inclusions, are spatially distributed on a small scale, within individual veins and individual hand samples. It is evident from the data and inclusion distribution that a significant pressure drop occurred at local sites. The resulting immiscibility from pressure drop, boiling, and loss of CO_2 coincide with ore deposition within individual fault zones.

INTERPRETATION OF FLUID INCLUSION DATA: A BOILING MODEL FOR THE KENO HILL Ag-Pb-Zn HYDROTHERMAL SYSTEM

Depressurization, cooling, and loss of CO_2 during early stages of boiling

Boiling of fluids in the Keno Hill system is demonstrated in fluid inclusion types I, and II, and to a lesser degree in type III. Inclusions from these three groupings homogenize at high temperature by either bubble expansion, or bubble contraction, within a limited temperature interval. Because CO_2 is lost during boiling, the low CO_2 content of type III and IV inclusions may be the result of a fluid which formed as an end product of boiling. This is further substantiated by the lower temperature, higher salinity, and later paragenesis of these inclusions.

Figure 5-7 is a plot of fluid inclusion homogenization temperature versus XCO_2 content of the fluid inclusion. A calculated boiling curve was generated from the method of Henley et al. (1984), and is included on the diagram. A close correlation is observed between the boiling curve and distribution of inclusion types I, and II from early quartz, and type IV from siderite. Type III inclusions would correspond approximately to the position of type IV inclusions on the diagram if plotted, but were omitted from the diagram to ensure clarity of representation. The boiling curve provides an estimation of the amount

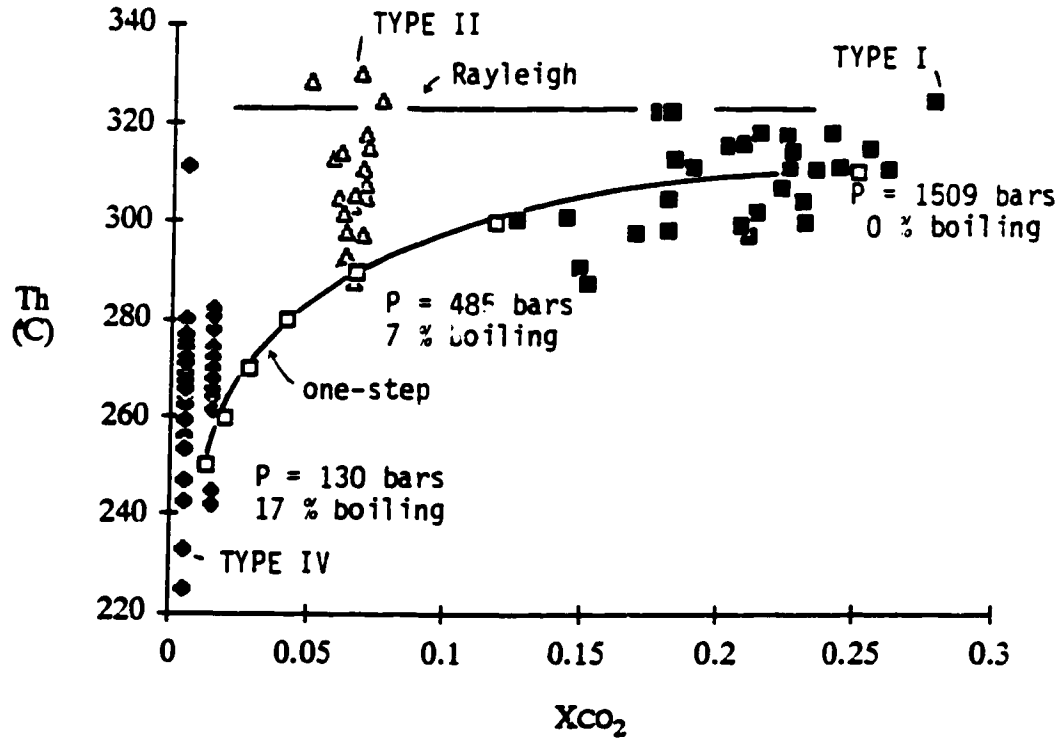

Figure 5-7. Plot of total homogenization temperature (Th) versus estimates of X_{CO_2} for inclusion types I, II, and IV. Inclusions from the type III grouping are omitted due to their predominantly secondary nature. Thick lines display evolution path of boiling fluids, for Rayleigh (upper line) and one-step (lower line) models. Pressure and percent boiling are also represented along portions of the curve. The lower line matches much of the data, suggesting that type I fluids evolved to type IV fluids after a total of about 17 % water boiling, which requires a drop in pressure from 1509 bars to 130 bars during vein opening (see text for explanations and discussion).

of steam separation, and a determination of the fluid pressure at the time of trapping, as well as showing the cooling effects of boiling and loss of CO_2.

Calculations used in boiling curve determinations are described by several authors (Giggenbach, 1980; Henley et al., 1984; Drummond and Ohmoto, 1985; Hedenquist and Henley, 1985). However, unlike the Keno Hill system, most of these are applied to epithermal systems where initial carbon dioxide contents are lower, less than 3 molal, and boiling is initiated at relatively low pressures.

Boiling is a dynamic event in hydrothermal systems, resulting in significant chemical and physical changes within the fluid (Drummond and Ohmoto, 1985). Principal among these is the cooling effect. The molal enthalpy of $H_2O_{(v)}$ is significantly higher than $H_2O_{(l)}$, or any of the other common gases in the fluid. Loss of $H_2O_{(v)}$ results in a cooler residual liquid. Even with significant loss of CO_2, which has a relatively small enthalpy of exsolution and negligible effect on heat loss, cooling is principally the result of water vapor formation (Drummond and Ohmoto, 1985). The fraction of water converted to steam (Y), which is necessary for a particular degree of cooling, may be calculated from the following formula:

$$H_{(l),T1} = (1\text{-}Y)H_{(l),T2} + (Y)H_{(v),T2} \qquad (1)$$

where $H_{(l)}$ and $H_{(v)}$ are the enthalpy of $H_2O_{(l)}$ and $H_2O_{(v)}$ in saline solutions (Haas, 1976), and T1 is the temperature at the beginning of boiling while T2 is the temperature at the end of boiling.

Two types of fluid separation are commonly modelled when calculating [illegible] composition after boiling. The first, single-step boiling which is also known as [illegible] system boiling, assumes that the steam separates adiabatically and remains in [illegible] the liquid over the boiling interval. It can be expressed as follows:

$$C_l = C_o/(1+Y(B-1)) \qquad (2)$$

where C_o is the initial concentration of the species in the liquid, and C_l is the concentration after boiling. The fraction of steam formation, Y, is calculated from (1), and B is the partition coefficient (Giggenbach, 1980; Henley et al., 1984). During steam separation, dissolved gases typically partition into the volatile phase. The partition coefficient B is defined as the concentration of gas in vapor divided by the concentration of gas in liquid. The coefficient is temperature dependent, and shows a decrease for the following gases (in decreasing order of B): H_2, CH_4, CO_2, H_2S, SO_2 (Drummond and Ohmoto, 1985; Giggenbach, 1980). Because of the preferential loss of reduced gases such as H_2 and CH_4, boiling tends to have an oxidizing effect on the fluid.

The second type of boiling commonly referred to is known as continuous steam separation or Rayleigh boiling. This form of boiling assumes that the separating steam fraction does not remain in contact with the liquid and is immediately removed upon exsolution, represented by:

$$C_l = (Y)C_o\, e^{-B'} \qquad (3)$$

where B' is the average distribution coefficent for the temperature interval considered (Henley et al., 1984).

Truesdell et al. (1977) found that in active geothermal systems, closed system boiling in sequential batches, or what may be termed multiple-step, steam separation (Henley et al., 1984), best explains the observed phenomena in boiling systems. In Figure 5-7, the calculated curve for closed system boiling in 10° C cooling intervals, closely approximates much of the observed data. After 17 percent water vapor formation, the temperature of the liquid is lowered from 310° C to 250° C. Also, the CO_2 content is lowered from X_{CO_2} = 0.25 at the beginning of boiling to X_{CO_2} = 0.01 at 250° C, effectively reproducing the

different fluid types recorded in the fluid inclusions. As can be seen in Figure 5-7 carbon dioxide is rapidly lost at the beginning of boiling, with X_{CO_2} decreasing by half to X_{CO_2} = 0.12 after only 4 percent water vaporization. The initial effects on temperature are minimal, even though significant portions of CO_2 have separated. This is because of the low heat content of CO_2. It is not until much water has vaporized that the residual fluid is markedly cooled.

During Rayleigh boiling, nearly all of the CO_2 separates into the volatile phase after only small degrees of vapor formation and limited cooling. Some of the higher temperature inclusions with low CO_2 contents, which fall on the upper curve of Figure 5-7, may have formed in this manner.

Also obtained from the boiling model is an estimate of the variation in pressure with progressive boiling. Total pressure in the fluid is equal to the sum of partial pressures exerted by the various gas phases. In this case, with H_2O and CO_2 dominating:

$$P_{total} = P_{H_2O} + P_{CO_2} \qquad (4)$$

The partial pressure of water (P_{H_2O}) at specific temperatures may be determined from the steam tables of saline solutions, such as those of Haas (1976). The table corresponding to 5 weight percent NaCl was chosen for use in this model. The partial pressure of CO_2, in a water dominated fluid, may be determined from Henry's law constant (K_H) using the relation:

$$P_{CO_2} = K_H(X_{CO_2}) \qquad (5)$$

Ellis and Golding (1963) have determined Henry's law constant for CO_2 in saline waters having a salinity range of 0 - 5 weight percent NaCl. The variation in pressure along the boiling path is displayed in parts of Figure 5-7; first boiling begins at 1509 bars

and X_{CO_2} = 0.25 where quartz precipitates, and ends at approximately 130 bars and X_{CO_2} = 0.01 where siderite forms.

Individual samples may contain a variety of fluid inclusions which collectively span the entire boiling curve, indicating that depressurization occurred in place. The estimated changes in pressure cannot be explained by a simple lithostatic to hydrostatic depressurization, but were more likely due to expansion from active faulting similar to the mechanisms described by Sibson (1987) for other areas. This is consistent with the textural evidence presented in Chapter 2 indicating contemporaneity between fault movement and hydrothermal activity.

The pressures of the boiling curve correspond well with the earlier fluid inclusion pressure determinations. Type I inclusions were trapped at approximately 1550 bars, and the model estimates 1509 bars; type II inclusions were trapped at approximately 500 bars, and the model estimates 485 bars. Fluid inclusion pressure determinations for the two phase inclusions in siderite were not possible by the method of Parry (1986), but the model indicates that they were trapped between 130 and 327 bars.

Siderite precipitation as a result of boiling

To better identify the causes of mineral precipitation and ore formation, calculations on the solubility of siderite have been made (Fig.5-8). Siderite was chosen because of its close association with the ore minerals, and because the fluid inclusion data yield direct information on the principal parameters which affect carbonate solubility: P, T, and X_{CO_2}. Although high temperature and pressure experimental information is not available for siderite, approximations of its behaviour during boiling may be made by the use of thermodynamic data (Bowers et al., 1984) and the equations listed in Fournier (1985).

As an analogy to siderite, experimental investigations on calcite solubility by Ellis (1963) have shown that carbonate solubility is lowered in a hydrothermal fluid by decreasing the partial pressure of CO_2 and that carbonate solubility increases with

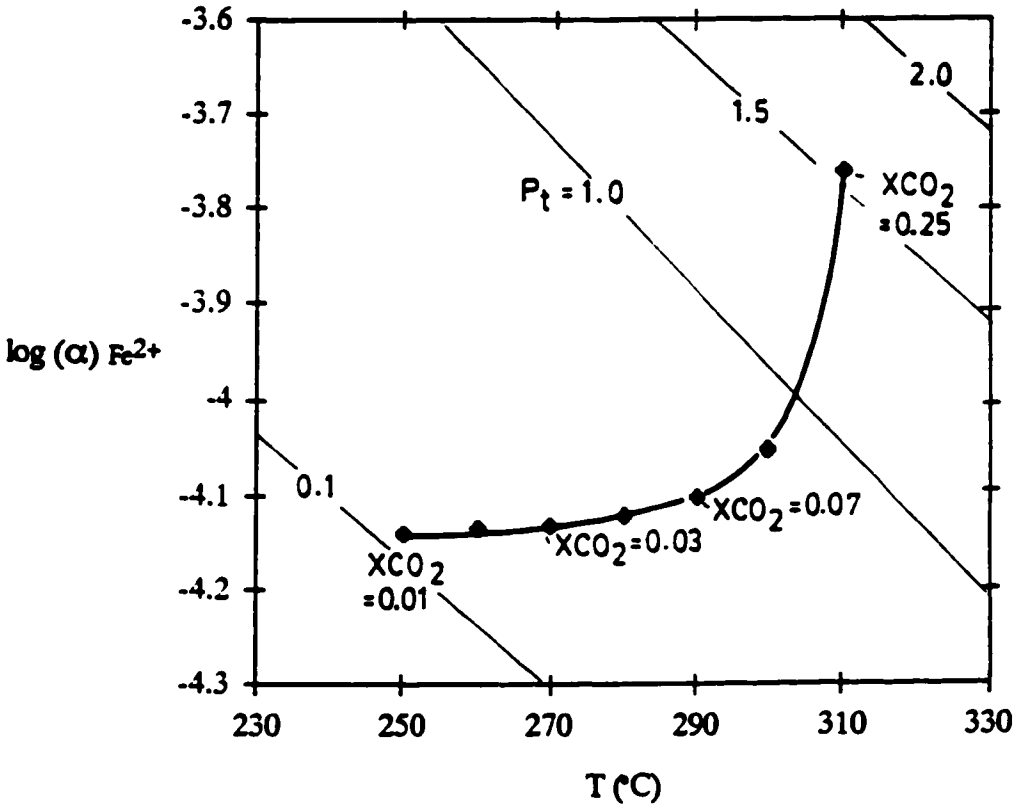

Figure 5-8. Solubility curves for siderite under conditions of 2.0, 1.5, 1.0, and 0.1 kilobars pressure. Thick line depicts saturation curve for siderite under the boiling conditions estimated for the Keno Hill system (see figure 7 for parameters), a decrease in solubility with loss of CO_2 is indicated. Calculations were made in the manner described by Fournier (1985),using the high pressure and temperature equilibrium constants of Bowers et al. (1984).

decreasing temperature. In a boiling hydrothermal fluid these two effects counteract each other, as CO_2 is lost and temperature is lowered. More recent determinations (Fein and Walther, 1987) confirm this, and further indicate that carbonate is least soluble at both extremes of XCO_2 in H_2O-CO_2 mixtures. Increasing salinity, another consequence of boiling, also increases calcite solubility (Ellis, 1963).

The activity of iron in a hydrothermal solution at the point of siderite saturation was calculated for various conditions of pressure, temperature, and fCO_2, in accordance to the conditions of the boiling curve established from the fluid inclusion study (Fig. 5-7). A plot of log $\alpha\ Fe^{2+}$ versus temperature is presented in Figure 5-8. The diagram shows that the solubility of siderite decreases rapidly during the initial stages of boiling, when most of the CO_2 is lost. The solubility then remains constant near a minimum during further boiling. At this point, cooling and a decreased rate of CO_2 loss counteract each other to maintain a constant solubility level for siderite. It is evident from Figure 5-8 that the initial stage of boiling is most significant in causing siderite precipitation, the decreasing PCO_2 being the prime factor. The minimum in siderite solubility is maintained between temperatures of 250° to 285° C, a bracket which corresponds well with the recorded fluid inclusion homogenization temperatures for siderite (Fig. 5-5 A).

A few vapour-rich inclusions were observed in siderite. However, fluid inclusion characteristics indicative of boiling are not obvious. It is believed that boiling did however continue into this stage because of the position of type IV inclusions at the end of the boiling curve (Fig. 5-7). Gas-rich fluids are not always trapped in carbonates precipitated from boiling fluids; for example, in the active geothermal fields of New Zealand, carbonates precipitated directly from boiling fluids contain fluid inclusions which show no evidence of boiling (Hedenquist and Henley, 1985).

Large salinity increases from boiling of fluids in an excess enthalpy reservoir, and from reaction of gas depleted fluids with graphite

The large increases in salinity, recorded in the fluid inclusion record, may have been attained in deep boiling hydrothermal systems in two ways: 1) by excessive boiling where heat was gained through conduction from hot reservoir rocks (Truesdell et al., 1982); 2) by water loss through the reaction of water with the host rocks, either continuously during boiling and/or during post-boiling reequilibration (Yardley and Bottrell, 1988; Tromsdorff and Skippen, 1986).

Evidence for an excess enthalpy reservoir

The boiling model proposed adequately accounts for many of the observed properties of the evolving fluids, as recorded in the fluid inclusions. These include a decrease in temperature, pressure, X_{CO_2}, and carbonate solubility. However, the boiling model, as is, does not account for the salinity increase from the early quartz stage to the siderite stage. With the 20 % boiling or less calculated in the present model, the salinity increase is only from approximately 5 to 6 weight percent NaCl equivalent. This greatly underestimates the observed values, which are up to 10 to 15 weight percent NaCl equivalent within the siderite stage (Fig. 5-6). Approximately 70 to 80 percent boiling is required to attain such high salinities. This discrepancy arises because the first estimate of boiling was limited by the degree of cooling, as calculated from equation (1). Such a model may be representative of the initial stages of boiling which is accompanied by fluid cooling, but is a minimum estimate of total boiling. In active geothermal systems, additional heat may be absorbed by the fluids from hot reservoir rocks, and anomalously high chloride concentrations are attained through excessive boiling without the usual cooling, in what are termed "excess enthalpy wells" (Henley et al., 1984).

Useful for interpreting excess enthalpy wells and geothermal systems in general are enthalpy-chloride diagrams (Fournier, 1979). These are widely used for showing the relationships between boiling, mixing, changes in temperature, and concentrations of dissolved species within geothermal fluids (Truesdell and Fournier, 1977), and may be applied as well to fluid inclusion data (Robinson and Norman, 1984). An enthalpy-chloride diagram has been constructed for the Keno Hill system (Fig. 5-9 A), using some representative fluid inclusions from the various groupings, and enthalpy tables for saline fluids of Haas (1976). Figure 5-9 (B) is a schematic representation taken from Henley et al. (1984), displaying the various trends caused by boiling, mixing, and salinity increases during boiling under excess enthalpy conditions labelled "excess enthalpy shift". It can be seen in Figure 5-9 (A) that cooling accompanied the initial boiling in the Keno Hill system, but that large salinity increases and extensive boiling (or water loss) occurred at a constant enthalpy corresponding to a water temperature near 250° C. Such extensive boiling at a constant temperature requires additional heat to have been gained by the fluids from the host rocks. It is interesting to note that White et al. (1971) and James (1968) suggest that the maximum enthalpy of steam in steam dominated systems, buffers these systems at temperatures near 240° C, closely matching the lower end of the cooling trend for the fluids precipitating siderite in the Keno Hill system (Fig. 5-5 A). For fluid inclusions from the late stage quartz, mixing is indicated from inclusions of intermediate salinity and temperature, which plot at the lower left hand portion of Figure 5-9 A. Although texturally the quartz which contains these inclusions is paragenetically late, some overlap in time with the siderite stage would have been necessary for the fluid mixing to have occurred. The temperatures and enthalpy for this stage, represented on Figure 5-9 A, are possibly below the real values because unlike the other inclusion types, boiling was not observed in inclusions from this stage, and a pressure correction of homogenization temperatures may be necessary.

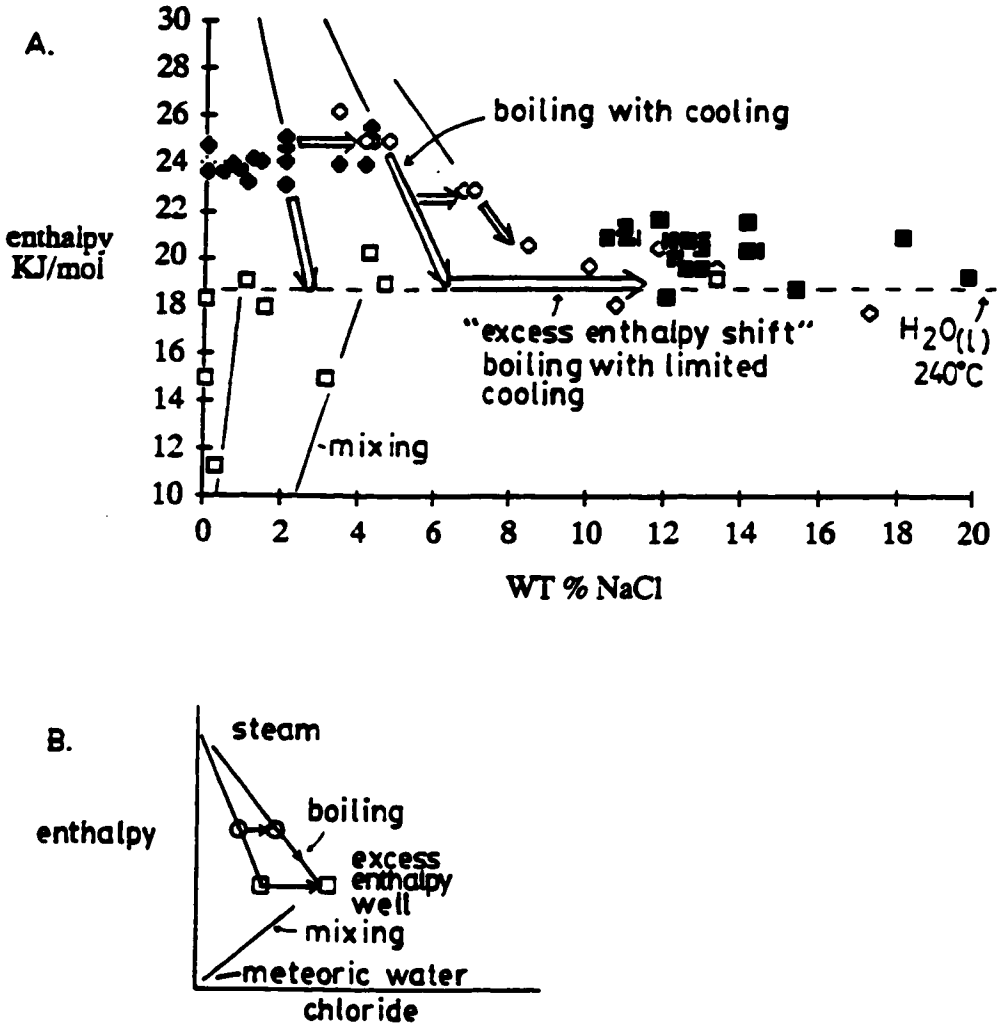

Figure 5-9. (A) Enthalpy-salinity diagram for selected fluid inclusions from type I and II (solid diamonds), type III (open diamonds), type IV (solid squares), and type V (open squares) groupings. (B) Schematic representation of trends caused by boiling under excess enthalpy conditions, and mixing with meteoric water.

With the above data, it seems apparent that extensive boiling occurred due to heat acquired from the host rocks. However, a degree of 80 % boiling is quite high, and three points argue against the attainment of such a level; 1) sustained low pressures would have been necessary as most of the CO_2 would have escaped, and the boiling pressure of water at 250° C is only 40 bars; 2) a significant CO_2 content is recorded for the fluids which precipitated siderite, by the presence of clathrates during freezing experiments; 3) vapor-rich inclusions are rare in siderite. Consequently water-rock reactions need to be also considered when interpreting fluctuations in fluid salinity, since hydration reactions may contribute to an increase in dissolved components.

Graphite as a CO_2 buffer, and its role in the formation of saline fluids

Graphite is widespread in the Keno Hill Quartzite. Fault planes are filled with black, pasty, graphite-rich gouge through which the hydrothermal fluids infiltrated. Graphite likely had an important role in controlling fluid composition. Graphite cannot coexist with pure H_2O (Frost, 1979) under typical hydrothermal or greenschist metamorphic conditions, since the reaction

$$2C + 2H_2O = CO_2 + CH_4 \qquad (17)$$

(Ohmoto and Kerrick, 1977), maintains the mole fraction of water to less than X_{H_2O} = 0.85 (French, 1966). The presence of graphite may also control oxygen fugacity in the fluids, according to:

$$C + O_2 = CO_2 \qquad (18)$$

(Zen 1963; Miyashiro, 1964; French, 1966; Nockleberg, 1973; Ohmoto and Kerrick, 1977; Frost, 1979), keeping the fo_2 generally low in the fluids. A small amount of

graphite in the rocks is sufficient to act as an internal oxygen buffer (French, 1966), since a unit volume of graphite has nearly 17 times more buffering capacity than an equal volume of magnetite (Frost, 1979). If other oxygen buffering minerals are not present in the rock, or are exhausted through reaction, then the oxygen fugacity of the fluid is generally buffered to, or just above the upper stability limit of graphite (Nockleberg, 1973).

Calculations for the distribution of species in equilibrium with graphite are given in several papers (Frost, 1979; Ohmoto and Kerrick, 1977; Nockleberg, 1973; French, 1966). Equations and equilibria used in the construction of Figure 5-10 A and B are summarized in Ohmoto and Kerrick (1977). A computer program was written to perform the calculations, and is presented in Appendix 3. Figures 5-10 A and B display the relative concentrations of species versus fo_2, at pressure and temperature conditions approximating the beginning and ending of boiling in the Keno Hill hydrothermal system. Although several different gases may be present, the system is overwhelmingly dominated by CO_2, H_2O, and CH_4. Other gases such as CO and H_2 are of minor importance (Frost, 1979), and are not shown here. In general, a condition of decreasing pressure has the effect of expanding the mole fraction of CO_2 and CH_4 fields, w. the mole fraction of H_2O decreases. The opposite is true for temperature, the maximum water content is increased by a decreasing temperature. For the Keno Hill system, the upper stability limit of graphite is pushed to lower values of fo_2 upon both cooling and depressurization.This can be seen by comparing Figures 5-10 A and B.

It is not known if the low pressure environment was maintained over a long enough period of time in the faults. If reaction rates are rapid though, graphite would have had a strong reducing effect on the fluid during boiling. The resulting reduction of the system would have contrasted with the instantaneous effects of boiling which tend to oxidize the fluids due to the preferential partitioning of reduced gas, such as CH_4 and H_2, into the volatile phase (Drummond and Ohmoto, 1985).

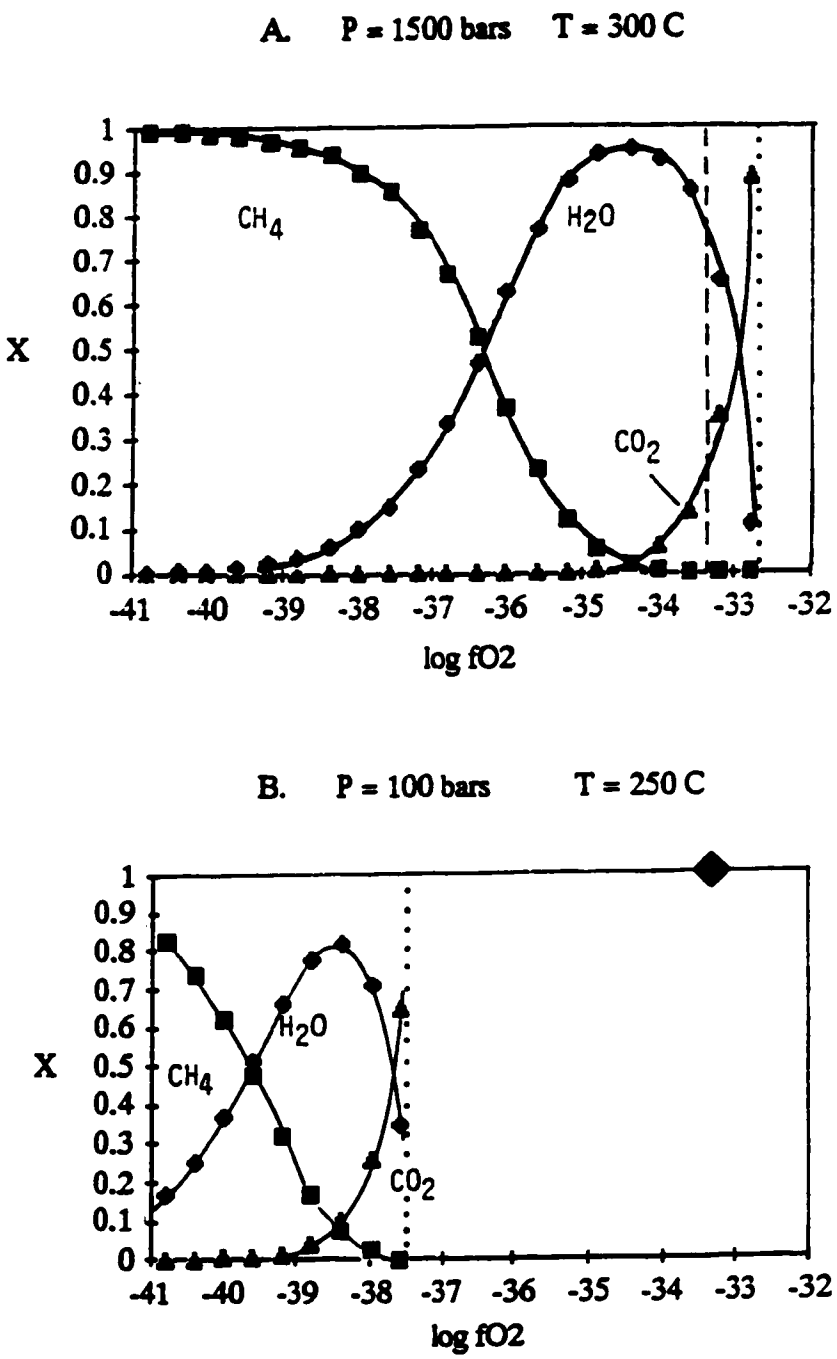

Figure 5-10. Water-graphite equilibria under conditions simulating beginning (A) and ending (B) of boiling. Dotted lines show upper stability limits of graphite. Dashed line in Figure A is the original composition of the fluid in equilibrium with graphite at the beginning of boiling, at a log fO_2 = -33.4, and XCO_2 = 0.25. The large diamond in figure B represents the relatively pure, slightly oxidized water as a post-boiling residual fluid, now in disequilibrium with the graphitic host rocks. Diagrams generated from the equations of Ohmoto and Kerrick (1977).

At 1500 bars, 310° C, and X_{CO_2} = 0.25, the initial fluid in the Keno Hill system in equilibrium with graphite, had an oxygen fugacity of approximately log fo_2 = -33.4 (Fig. 5-10 A). The upper stability limit of graphite under these conditions is at log fo_2 = -32.8. Under a pressure of 100 bars and temperature of 250° C, the upper stability limit of graphite is reduced to log fo_2 = -37.5. After boiling, the fluid had lost most of its CO_2 and CH_4, and had an fo_2 above the upper stability limit of graphite. The water content may have been lowered to values between X_{H_2O} = 0.8 to X_{H_2O} = 0.3 (Fig. 5-10), while carbon dioxide increased to between X_{CO_2} = 0.2 to 0.7. Such high CO_2 contents are above the miscibility limit for CO_2-H_2O mixtures in the faults, and unmixing is enhanced because of the saline conditions (Bowers and Helgeson, 1983), possibly establishing continuous disequilibrium.

DISCUSSION

Boiling is clearly indicated to have been an important process in the formation of the Keno Hill Ag-Pb-Zn deposits. Generally in polymetallic Ag-Pb-Zn veins, boiling is widely recognized through fluid inclusion studies to have coincided with ore precipitation (Barton et al., 1977; Brame, 1979; Godwin et al., 1986; Kerrich et al., 1986; Leach, et al., 1988). The quantitative chemical effects of boiling on hydrothermal systems have been investigated by Drummond and Ohmoto (1985), as well as Reed and Spycher (1985). In these studies it is shown that the most significant consequence of boiling on fluid chemistry is associated with the separation of CO_2 and H_2S from water. Drastic increases in pH may accompany CO_2 loss, while a tendency towards higher oxidation states may be due to H_2S separation. As a result, metals which are complexed by chloride, such as Ag, Pb, and Zn (Seward, 1976, 1984), are deposited due to the decreasing proton concentration. This can be seen in the following reactions for galena and argentite:

$$PbCl_2 + H_2S_{aq} = PbS_{(s)} + 2Cl^- + 2H^+ \quad (19)$$

$$2AgCl + H_2S_{aq} = Ag_2S_{(s)} + 2Cl^- + 2H^+ \quad (20)$$

The loss of the hydrogen ion is likely more significant than the concomitant decrease in H_2S during boiling, because of its exponential effect on the equilibrium constant. Also, boiling was found to be particularly effective near 300° C, and increases in efficiency as temperature is lowered (Drummond and Ohmoto, 1985).

At Keno Hill, the salinity of the fluids indicates that chloride complexes of Ag, Pb, and Zn were likely important in metal transport. The complexes which were in solution initially near 300° C, were destabalized during boiling and cooling due to CO_2 exsolution and accompanying rise in pH, resulting in ore precipitation. The loss of CO_2 is clearly documented in the fluid inclusion record. Salinity on the other hand is shown to increase with boiling, an effect that would have the consequence of increasing metal solubility, except that the metal concentration increases due to boiling as well.

Graphite in the host rocks of the Keno Hill mining district appears to have had an important role in the genesis of the hydrothermal orebodies. Its widespread distribution had the effect of buffering a high CO_2 content in the fluid. Such high volatile contents rendered the fluids susceptible to immiscible phase separation and boiling at relatively high pressure. Furthermore an increase in XCO_2 may increase fluid pressures (Ramboz and Charef, 1988), providing a driving mechanism for the hydrothermal system. Large pressure variations appear to have occurred during vein opening, a decrease in pressure by a factor of up to eleven is indicated. Typically, pressure variations within hydrothermal systems are reported to fluctuate beween lithostatic and hydrostatic, which are separated by a factor of three (Kern and Weisbrod, 1967, p. 92). In dynamic hydrothermal systems however, significant fluid overpressures are inferred in regions of hydrothermal geopressuring and breccia formation (Ramboz and Charef, 1988), whereas suction and low pressures result in dilational portions of active faults with resulting implosion breccias reported (Sibson, 1987). In passive hydrothermal systems, pressure determinations of the fluid may be used to adequately estimate depth as well. If the pressure estimate of 1500 bars measured from the fluid inclusions is representative of lithostatic pressure, then the

depth of the Keno Hill system is estimated to have originally been at approximately 5 km. This corresponds well with the pressure estimates from similar veins in the Coeur d' Alene district of Idaho (Leach et al., 1988). Large pressure variations at individual sites are likely characteristic of dynamic flowing systems, and as in this case are likely related to active faulting.

The alteration of organic material in the host rocks is of particular significance when considering the source of the metals for the mineralizing fluids; black shales and organic-rich sedimentary rocks are widely recognized as being enriched in a variety of metals relative to most rock types (Peltola, 1960; Vine and Tourtelot, 1970; Levinson, 1974; Bell, 1979), and are considered to be the source of many Ag-rich polymetallic vein deposits after remobilization (Morton and Changkakoti, 1987; Boyle, 1968). More specifically, silver is associated directly with carbonaceous material such as graphite, and with sulfides which may be present in the metasediments (Boyle, 1968). In the Keno Hill district graphitic schist lies above, below, and is interlayered with the graphitic quartzite which hosts the orebodies. Fault gouge through which the fluids passed contains much graphite. In the district the graphitic schists contain on the average 0.5 ppm Ag, 15 ppm Pb, 19 ppm As, 30 ppm Cu, 60 ppm Zn, and 8100 ppm S (Boyle, 1965). Boyle (1965) consequently ascribed these as the source rocks for the ore deposits. This is consistent with the water-graphite equilibria discussed above; the continuous and selective alteration of graphite by the hydrothermal fluids, due to CO_2 separation, may have resulted in the incorporation of significant quantities of metals after much fluid migration.

The origin of the early mineralizing fluids in the Keno Hill system remains uncertain. Typically, under conditions of medium grade metamorphism the three major volatiles are commonly H_2O, CO_2, CH_4, in that order of abundance with also some dissolved chloride species (Roedder, 1984; Ferry and Burt, 1982). The early fluids in the Keno Hill system have these compositional characteristics, and may on this basis be described as having a metamorphic character. The carbon in the fluids appears to have been derived from the

graphite of the host rocks; water however was not necessarily derived from metamorphic dehydration reactions, but may have been introduced from external sources (i.e. meteoric water). A true definition of the fluid is ambiguous at this stage; further work is needed in this area.

Inclusions within the late quartz stage are dilute and homogenize to a lower temperature. Boiling was not indicated for this stage. These are thought to represent the late incursion of meteoric water, as substantiated by stable isotope data (Chapter 6). This late quartz stage is more abundant in the west and contributes to the district scale mineralogical zoning. It is unclear to what extent the meteoric water interacted with the early fluid, but a certain degree of mixing appears to have occurred.

CONCLUSIONS

Mineralization in the Keno Hill Ag-Pb-Zn mining district was coincident with, and a direct result of CO_2 immiscibility and boiling. Depressurization during faulting, on the order of from 1500 bars to 130 bars, resulted in a decrease in CO_2, from $X_{CO_2} = 0.25$ to 0.013. Accompanying steam separation lowered the temperature from approximately 310° C to 250° C. Simple numerical representations using a single-step vapor separation model adequately reproduces the observed fluid inclusion data.

The presence of graphite in the host rocks and fault gouge was important in the evolution of the hydrothermal system due to its buffering effect on the fluid, establishing a generally high CO_2 content. Boiling had the effect of separating CO_2 from H_2O, creating momentary disequilibrium and a transition in hydrothermal mineralogy from a quartz dominated to siderite dominated gangue. Ore deposition resulted from a rise in pH. Boiling and the reaction of water with graphite both contributed in establishing the high salinities of the fluids, up to 10-15 weight percent NaCl equivalent.

The incursion of a late stage dilute fluid, of likely meteoric origin, marks the terminal stage of ore formation, and contributed to the zoned mineralization pattern of the district.

REFERENCES

Abbott, J.G., Gordey, S.P., Tempelman-Kluit, D.J., 1986, Setting of stratiform, sediment-hosted lead-zinc deposits in Yukon and northeastern British Columbia. In, J.A. Morin (editor), Mineral Deposits of the Northern Cordillera, Canadian Institute of Mining and Metallurgy Special Volume 37, p. 1-18.

Anderson, R.G., 1987, Plutonic rocks of the Dawson map area, Yukon Territory, in Current Research , Part A, Geological Survey of Canada, Paper 87-1A, p.689-697.

Barton, P.B., Jr., Bethke, P.M., Roedder, E., 1977, Environment of ore deposition in the Creede mining district, San Juan Mountains, Colorado: Part III. Progress toward interpretation of the chemistry of the ore-forming fluid for the OH vein. Economic Geology, vol. 72, p. 1-24.

Bell, R.T., 1979, Uranium in black shales-a review. In M.M. Kimberley (editor), Uranium Deposits: Their Mineralogy and Origin. Mineralogical Association of Canada, Short Course Handbook, vol. 3, p. 307-329.

Bodnar, R.J., 1983, A method of calculating fluid inclusion volumes based on vapor bubble diameters and P-V-T-X properties of inclusion fluids. Economic Geology, vol. 78, p. 535-542.

Bowers, T.S., Helgeson, H.C., 1983, Calculation of the thermodynamic and geochemical consequences of nonideal mixing in the system H_2O-CO_2-NaCl on phase relations in geologic systems. Equation of state for H_2O-CO_2-NaCl fluids at high pressures and temperatures. Geochimica et Cosmochimica Acta, vol. 47, p. 1247-1275.

Bowers, T.S., Helgeson, H.C., 1983, Calculation of the thermodynamic and geochemical consequences of nonideal mixing in the system H_2O-CO_2-NaCl on phase relations in geologic systems. Metamorphic equilibria at high pressures and temperatures. American Mineralogist, vol. 68, p. 1059-1075.

Bowers, T.S., Jackson, K.J., Helgeson, H.C., 1984, Equilibrium Activity Diagrams, For Coexisting Minerals And Aqueous Solutions Up To 5 kb And 600° C. Springer Verlag, 397 pages.

Boyle, R.W., 1965, Keno Hill-Galena Hill lead-zinc-silver deposits, Yukon territory. Geological Survey of Canada Bulletin 111, 302 pages.

Boyle, R.W. 1968, The geochemistry of silver and its deposits. Geological Survey of Canada, Bulletin 160, 264 pages.

Bozzo, A.T., Chen, J.R., Barduhu, A.J., 1973, The properties of the hydrates of chlorine and carbon dioxide. International Symposium on fresh water from the sea, Heidelberg Sept. 9-14, 1973, vol. 3, p. 437-451.

Brame, S., 1979, Mineralization Near the Northern Margin of the Nelson Batholith, MSc thesis, The University of Alberta, Edmonton, 146 pages.

Burruss, R.C., 1981, Analysis of phase equilibria in C-O-H-S fluid inclusions. In L.S. Hollister and M.L. Crawford (eds.), Fluid Inclusions: Applications to Petrology, Mineralogical Association of Canada short course, vol. 6, p. 39-74.

Drummond, S.E., Ohmoto, H., 1985, Chemical evolution and mineral deposition in boiling hydrothermal systems. Economic Geology, vol. 80, p. 126-147.

Ellis, A.J., 1963, The solubility of calcite in sodium chloride solutions at high temperatures. American Journal of Science, vol. 261, p. 259-267.

Ellis, A.J., Golding, R.M., 1963, The solubility of carbon dioxide above 100° C in water and sodium chloride solutions. American Journal of Science, vol. 261, p. 47-60.

Fein, J.B., Walther, J.V., 1987, Calcite solubility in supercritical CO_2-H_2O fluids. Geochimica et Cosmochimica Acta, vol. 51, p. 1665-1674.

Ferry, J.M., Burt, D.M., 1982, Characterization of metamorphic fluid composition through mineral equilibria. In J.M. Ferry (editor), Characterization of Metamorphism Through Mineral Equilibria. Mineralogical Society of America, Reviews in Mineralogy volume 10, p. 207-262.

Fournier, R.O., 1985, Carbonate transport and deposition in the epithermal environment. In, B. R. Berger, and P.M. Bethke (eds.), Geology and geochemistry of epithermal systems, Society of Economic Geologists, Reviews in Economic Geology, vol. 2, p. 63-72.

Fournier, R.O., 1979, Geochemical and hydrologic considerations and the use of enthalpy-chloride diagrams in the prediction of underground conditions in hot-spring systems. Journal of Volcanology and Geothermal Research, vol. 5, p. 1-16.

French, B.M., 1966, Some geological implications of equilibrium between graphite and a C-H-O gas phase at high temperatures and pressures. Reviews in Geophysics, vol. 4, p. 223-253.

Frost, B.R., 1979, Mineral equilibria involving mixed volatiles in a C-O-H fluid phase: the stabilities of graphite and siderite. American Journal of Science, vol. 279, p. 1033-1059.

Gabrielse, H., 1985, Major dextral transcurrent displacements along the Northern Rocky Mountain Trench and related lineaments in north central British Columbia. Geological Society of America Bulletin, p. 1-14.

Giggenbach, W.F., 1980, Geothermal gas equilibria. Geochimica et Cosmochimica Acta, vol. 44, p. 2021-2032.

Godwin, C.I., Watson, P.H., Shen, K., 1986, Genesis of the Lass vein system, Beaverdell silver camp, south-central British Columbia. Canadian Journal of Earth Sciences, vol. 23,p. 1615-1626.

Green, L.H., 1971, Geology of Mayo Lake, Scougale Creek and McQuesten Lake map areas, Yukon Territory. Geological Survey of Canada Memoir 357, 72 pages.

Haas, J.L., Jr., 1976, Physical properties of the coexisting phases and thermochemical properties of H_2O component in boiling NaCl solutions. U.S. Geological Survey Bulletin 1421-A, 73 pages.

Hedenquist, J.W., Henley, R.W., 1985, The importance of CO_2 on freezing point measurements of fluid inclusions: evidence from active geothermal systems and implications for epithermal ore deposition. Economic Geology, vol. 80, p. 1379-1406.

Henley, R.W., Truesdell, A.H., Barton, P.B., Jr., Whitney, J.A., 1984, Fluid-Mineral Equilibria in Hydrothermal Sysytems. Reviews in Economic Geology Volume 1, Economic Geology Publishing Co., 267 pages.

Hollister, L.S., Burruss, R.C., 1976, Phase equilibria in fluid inclusions from Khtada Lake metamorphic complex. Geochimica et Cosmochimica Acta, vol. 40, p. 163-175.

James, R., 1968, Wairakei and Larderello; geothermal power systems compared. New Zealand Journal of Science and Technology, vol. 11, p. 706-719.

Kern, R., Weisbrod, A., 1967, Thermodynamics for Geologists. Freeman Cooper and Company, 304 pages.

Kerrich, R., Strong, D.F., Andrews, A.J., Owsiacki, L., 1986, The silver deposits at Cobalt and Gowganda, Ontario. III: Hydrothermal regimes and source reservoirs - evidence from H, O, C, and Sr isotopes and fluid inclusions. Canadian Journal of Earth Sciences, vol. 23, p. 1519-1550.

Leach, D.L., Landis, G.P., Hofstra, A.H., 1988, Metamorphic origin of the Coeur d'Alene base- and precious-metal veins in the Belt basin, Idaho and Montana. Geology, vol. 16, p. 122-125.

Levinson, A.A., 1974, Introduction to Exploration Geochemistry. University of Chicago Press, Chicago, IL, 614 pages.

Lynch, G., Longstaffe, F.J., Nesbitt, B.E., 1987, Stable isotopic indications of large scale fluid flow, boiling and fluid mixing in the Keno Hill Ag-Pb-Zn district, Yukon. [abst.] Geological Society of America Abstracts with Programs.

McTaggart, K.C., 1960, The geology of Keno and Galena Hills, Yukon Territory. Geological survey of Canada Bulletin 58.

Miyashiro, A., 1964, Oxidation and reduction inthe earth's crust with special reference to the role of graphite. Geochimica et Cosmochimica Acta, vol. 28, p. 717-729.

Monger, J.W.H., Price, R.A., Tempelman-Kluit, D.J., 1982, Tectonic accretion and origin of the two major metamorphic and plutonic welts in the Canadian Cordillera. Geology, vol. 10, p.70-75.

Morton, R.D., Changkakoti, A., 1987, The possible roles of Precambrian biota in the origin of magmatogene and hydrothermal silver-bearing vein deposits. Canadian Journal of Earth Sciences, vol. 24, p. 291-295.

Nockleberg, W.J., 1973, CO_2 as a source of oxygen in the metasomatism of carbonates. American Journal of Science, vol. 273, p. 498-514.

Ohmoto, H., Kerrick, D., 1977, Devolitization equilibria in graphitic systems. American Journal of Science, vol. 277, p. 1013-1044.

Parry, W.T., 1986, Estimation of XCO_2, P, and fluid inclusion volume from fluid inclusion temperature measurements in the system NaCl-CO_2-H_2O. Economic Geology, vol. 81, p. 1009-1013.

Peltola, E., 1960, On the black schists in the Outkumpu region in eastern Finland. Finland Commission on Geology, Bulletin 192.

Potter, R.W., Clynne, M.A., Brown, D.L., 1978, Freezing point depression of aqueous sodium chloride solutions. Economic Geology, vol. 73, p. 284-285.

Poty, B., Stalder, H.A., Weisbrod, A.M., 1974, Fluid inclusion studies in quartz from fissures of western and central Alps. Schweizer. Mineralog. Petrog. Mitt., vol. 54, p. 717-752.

Poulton, T.P., Tempelman-Kluit, D.J., 1982, Recent discoveries of Jurassic fossils in the Lower Schist division of central Yukon. In Current Research Part C, Geological Survey of Canada Paper 82-1c, p. 91-94.

Ramboz, C., Charef, A., 1988, Temperature, pressure, burial history, and paleohydrology of the Les Malines Pb-Zn deposit: reconstruction from aqueous inclusions in barite. Economic Geology, vol. 83, p. 784-800.

Reed, M.H., Spycher, N.F., 1985, Boiling, cooling, and oxidation in epithermal systems: numerical modelling aproach. In, B. R. Berger, and P.M. Bethke (eds.), Geology and geochemistry of epithermal systems, Society of Economic Geologists, Reviews in Economic Geology, vol. 2, p. 249-272.

Robinson, R.W., Norman, D.I., 1984, Mineralogy and fluid inclusion study of the southern Amethyst vein system, Creede mining district, Colorado. Economic Geology, vol. 79, p. 439-447.

Roedder, E., 1984, Fluid Inclusions. Mineralogical Association of America Reviews in Mineralogy, vol. 12, 644 pages.

Seward, T.M., 1976, The stability of chloride complexes of silver in hydrothermal solutions up to 350° C. Geochimica et Cosmochimica Acta, vol. 40, p. 1329-1341.

Seward, T.M., 1984, The formation of lead (II) chloride complexes to 300° C. A spectophotometric study. Geochimica et Cosmochimica Acta, vol. 48, p. 121-134.

Sibson, R.H., 1987, Earthquake rupturing as hydrothermal mineralizing agent. Geology, vol. 15, p. 751-754.

Sinclair, A.J., Tessari, O.J., Harakal, J.E., 1980, Age of Ag-Pb-Zn mineralization, Keno Hill-Galena Hill area, Yukon Territory. Canadian Journal of Earth Sciences, vol. 17, p. 1100-1103.

Tempelman-Kluit, D.J., 1970, Stratigraphy and structure of the "Keno Hill Quartzite" in Tombstone River-Upper Klondike River map-areas, Yukon Territory (116 B/7, B/8). Geological Survey of Canada Bulletin 180, 102 pages.

Tempelman-Kluit, D.J., 1979, Transported cataclasite, ophiolite and granodiorite in Yukon: evidence of arc continent collision. Geological Survey of Canada Paper 79-14, 27 pages.

Trommsdorff, V., Skippen, G., 1986, Vapour loss ("boiling") as a mechanism for fluid evolution in metamorphic rocks. Contributions to Mineralogy and Petrology, vol. 94, p. 317-322.

Truesdell, A.H., Nehring, N.L., Thompson, J.M., Janik, C.J., 1982, A review of Progress in understanding the Fluid Geochemistry of the Cerro Prieto Geothermal System: 4th Symposium on the Cerro Prieto Geothermal field, Guadalajara, 1982.

Truesdell, A.H., Fournier, R.O., 1977, Procedure for determining the hot water component in a mixed water using a plot of dissolved silica vs. enthalpy. U.S. Geological Survey, Journal of Research, vol. 5, p.49-52.

Vine, J.D., Tourtelot, E.B., 1970, Geochemistry of black shale deposits-a summary report. Economic Geology, vol. 65, p. 253-272.

Werre, Jr., R.W., Bodnar, R.J., Bethke, P.M., 1979, A novel gas-flow fluid inclusion heating/freezing stage (abstract). Geological Society of America Abstracts with Programs, vol. [illegible]9.

White, D.E., Muffler, L.J.P., Truesdell, A.H., 1971, Vapor-dominated hydrothermal systems compared with hot water systems. Economic Geology, vol. 66, p. 75-97.

Yardley, B.W.D., Bottrell, S.H., 1988, Immiscible fluids in metamorphism: implications of two phase flow for reaction history. Geology, vol. 16, p. 199-202.

Zen, E-an, 1963, Components, phases and criteria of chemical equilibrium in rocks. American Journal of Science, vol 261, p. 929-942.

CHAPTER 6

STABLE ISOTOPIC INDICATIONS OF LARGE SCALE HYDROTHERMAL PALEOFLOW, BOILING, AND FLUID MIXING IN THE KENO HILL Ag-Pb-Zn DISTRICT, YUKON.

INTRODUCTION

Historically, the Keno Hill Ag-Pb-Zn mining district has been a significant producer of Ag, Pb, Zn, and Cd from high grade, polymetallic, hydrothermal veins (Watson, 1986). A variety of deposit types occur in the region, and include in addition to the Ag-Pb-Zn deposits, Sn, W, and gold bearing veins (Boyle, 1965; Lennan, 1986). Collectively, these deposit types form broad mineralogical zones which overlap, and appear to be continuous from zone to zone (Chapter 3). In fossil hydrothermal systems, stable isotopes are often applied in reconstructing the geometry of the systems, to help in making hydrologic or fluid dynamic inferences (Criss and Taylor, 1986). In this paper a contour diagram of $\delta^{18}O$ values from widely distributed vein quartz is presented for the Keno Hill district. The diagram demonstrates the large scale nature of the system and outlines regions of concentrated fluid movement. The contours produce the image of a large flow net.

The effects of boiling on isotopic signatures in the Keno Hill district are also investigated. In the veins of the mining district, widespread CO_2 exsolution and boiling during mineralization have been documented from fluid inclusions (Chapter 5). Stable isotope signatures of the veins are interpreted here by considering the possible fractionation and thermal effects due to boiling. Degrees of boiling are quantified, and sites of boiling within the flow system are identified.

In general, carbon dioxide is an important component of many ore forming fluids, including W-Sn deposits (Campbell et al., 1984), mesothermal gold deposits (Nesbitt et al., 1986), Archean lode gold deposits (Kerrich,1987), and polymetallic Ag-Pb-Zn

systems (Leach et al., 1988; Godwin et al., 1986; Hedenquist and Henley, 1985). In all of these examples, boiling is cited as an important ore forming process. As a volatile component, CO_2 is preferentially exsolved during boiling (Giggenbach, 1980). Isotopically, CO_2 is a distinctive compound because of its strong tendency to partition the heavy isotope of oxygen, ^{18}O (Bottinga, 1968). Isotopic values of water are strongly fractionated if involved in CO_2 producing reactions, or during cooling of CO_2-H_2O mixtures (Truesdell et al., 1977). In hydrothermal systems, the loss of water vapor may accompany CO_2 exsolution during boiling. Water vapor contrasts isotopically with CO_2 by preferentially partitioning the light isotope of oxygen, ^{16}O. On the one hand, these opposing tendencies of fractionation may potentially mask each other in boiling CO_2-H_2O systems. On the other hand, the opposing effects may be used to identify and quantify the various processes which constitute dynamic boiling systems. This paper presents results of an oxygen and carbon isotope study, which investigates the effects that boiling of H_2O-CO_2 mineralizing fluids had on the isotopic signature of quartz and carbonates in the Keno Hill, Ag-Pb-Zn vein system. The veins of the district are suitable for such a study, since the presence of large amounts of graphite in the host rocks buffered the mineralizing fluids to a high CO_2 content, allowing for boiling, and for much of the fluid evolution to have proceeded along the two phase, H_2O-CO_2 boundary (Chapter 5).

The origin of the primary mineralizing fluids remains uncertain, due to a considerable degree of isotopic equilibration with the host rocks. However, relatively pristine meteoric water can be identified in some late stage quartz, which mineralogically and texturally appears to mark the end of the mineralization event.

Geological setting and characteristics of mineral deposits

Detailed accounts of the local geology in the Keno Hill area are given by McTaggart (1960), and Green (1971), with extensive descriptions of mineral deposits by Boyle (1965). The Keno Hill mining district is situated in central Yukon (Fig. 6-1 A). Host

rocks to the orebodies are part of a miogeoclinal stratigraphic succession, which formed the ancient continental margin of North America (Abbott et al., 1986). The mining district has produced over 6.4 billion grams of silver since production began in 1913, and is still a significant producer today (Watson, 1986).

The stratigraphy of the region was disrupted in Jurassic-Cretaceous time by widespread thrusting and deformation from tectonic accretion (Tempelman-Kluit, 1979). This is most evident in the mining district by the northward thrusting of the Mississippian Keno Hill Quartzite on top of the Jurassic "Lower Schist" unit (Poulton and Tempelman-Kluit, 1982). Above the quartzite is the "upper Schist" unit of unknown age, but which is similar in appearance to the graphite-muscovite schist of the Lower Schist unit. Proterozoic rocks from the 'Grit' unit of the Windermere Supergroup underlie much of the region. In the mining district, rocks were metamorphosed to the greenschist facies during deformation, and were then intruded by Cretaceous granitic plutons. These plutons are a part of the Selwyn Plutonic Suite (Anderson, 1987), within the northern extension of the Omenica Crystalline Belt (Monger et al., 1982). From this suite, the large Mayo Lake Pluton (81 Ma) crosscuts the Keno Hill Quartzite, at the eastern end of the Keno Hill mining district (Fig. 6-2). The pluton ranges in composition from granite to granodiorite (Green, 1971). A contact metamorphic aureole extends outwards for up to four kilometers from the pluton, with an inner sillimanite facies followed by a staurolite-garnet-biotite facies. Hydrothermal veining begins at the margin of the contact metamorphic aureole surrounding the pluton. An extensive vein system, which contains the orebodies, extends laterally from the plutonic/metamorphic center and associated quartz-feldspar veins, to the Ag-Pb-Zn deposits, to peripheral veins having epithermal characteristics (Chapter 3). The entire zoned sequence is continuous from east to west in a 40 km long hydrothermal belt. The fault and fracture controlled veins are stratabound mainly to the brittle, moderately dipping, 1 km thick, Keno Hill Quartzite unit of Mississippian age. The unit is graphitic and contains interlayers of schist and metamorphosed greenstone (McTaggart, 1960).

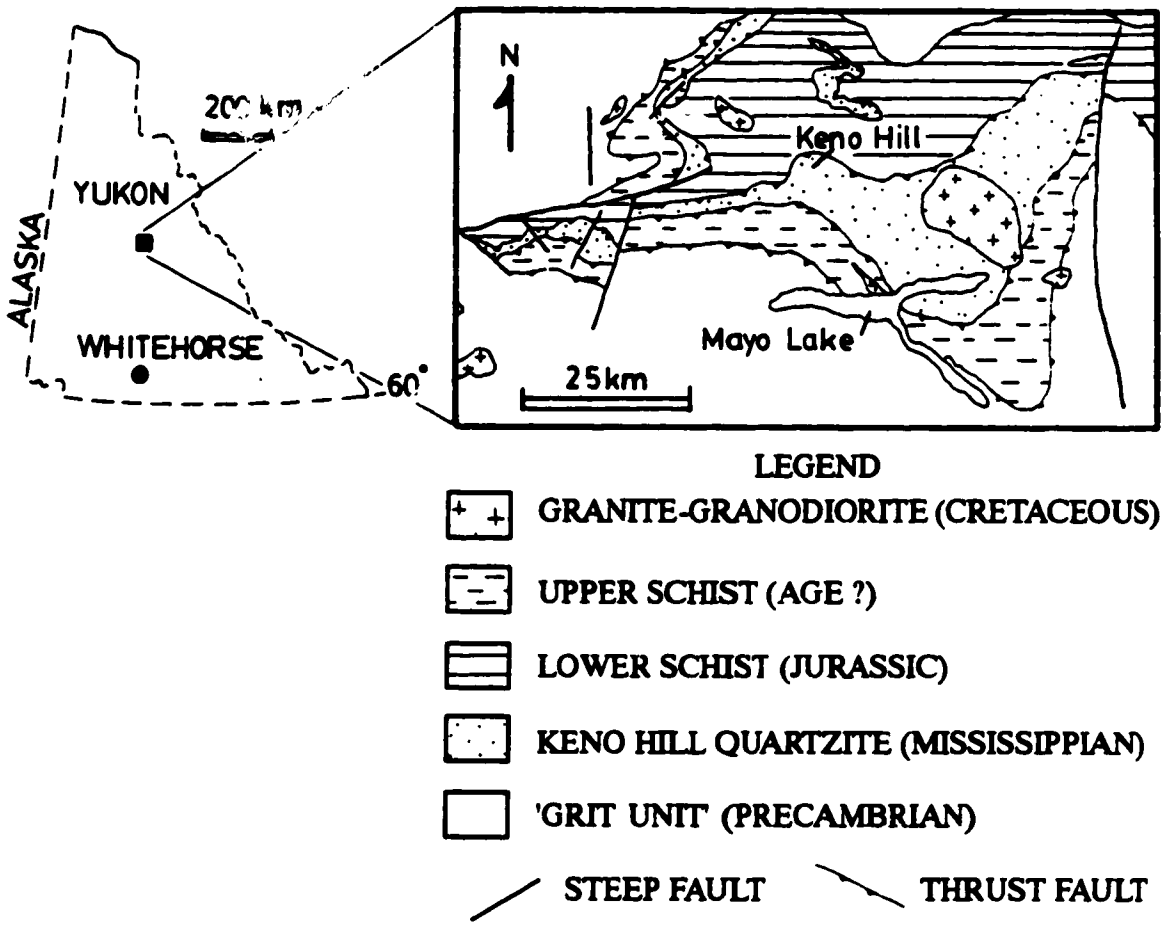

Figure 6-1 (A). Location map of the Keno Hill area in central Yukon, and geological setting of mining district, as modified from Tempelman-Kluit (1970), and Green (1971).

Figure 6-1B has been removed due to the unavailability of copyright permission.

Figure 6-1 (B). Location map of principal orebodies, from Watson (1986).

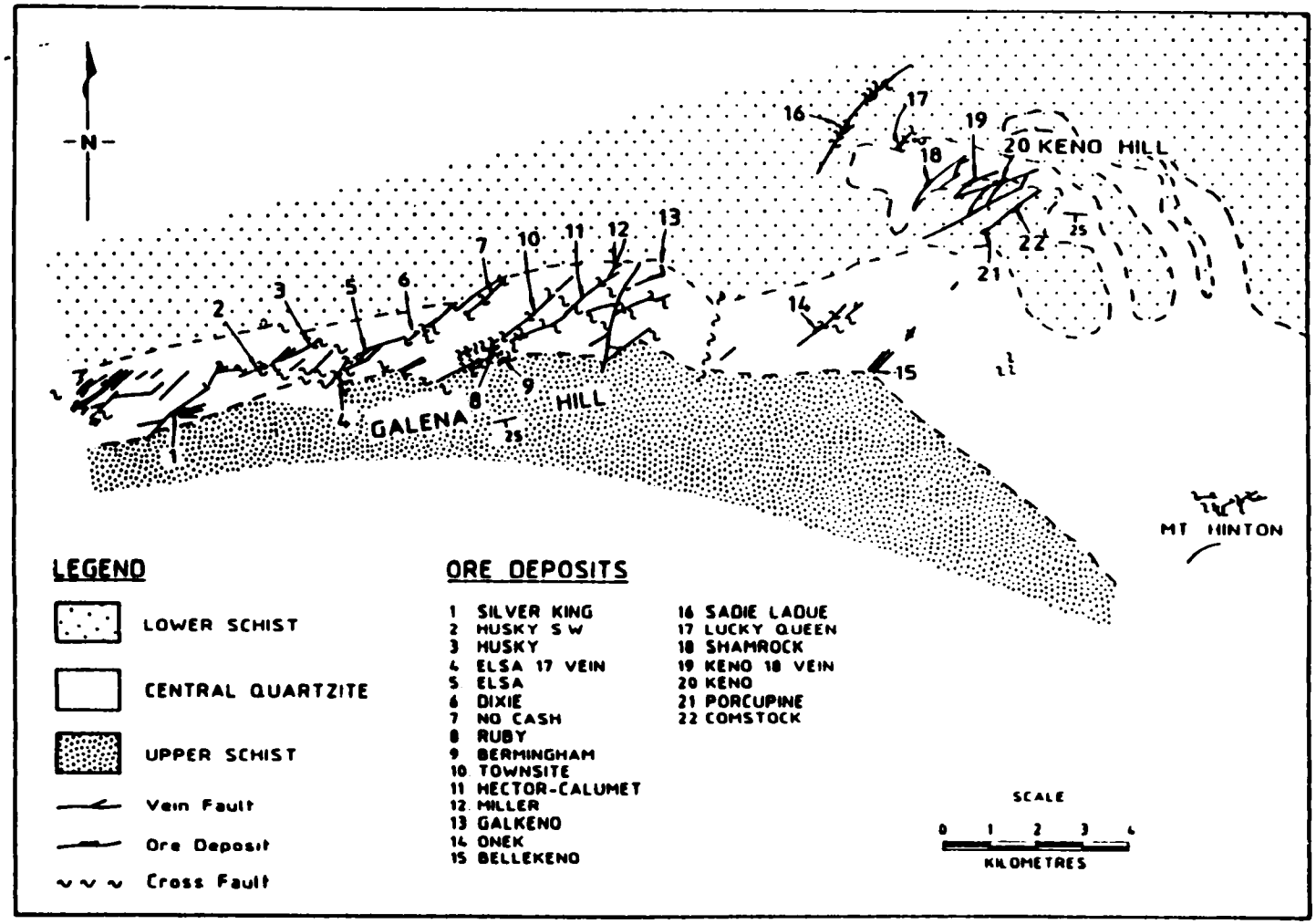

Figure 6-1 (B). Location map of principal orebodies, from Watson (1986).

Regionally extensive schist units occur above and below the quartzite. The orebodies are contained along an extensive set of steeply dipping, northeast striking, sinistral faults (McTaggart, 1960; Boyle, 1965). Hydrothermally altered rocks along the vein walls has been dated at 84 Ma by the K-Ar method (Sinclair et al., 1980), indicating that hydrothermal activity was contemporaneous with the Selwyn plutonic suite. The hydrothermal zonation which extends away from the pluton records an evolving environment of mineral deposition and fluid chemistry in a fractured hydrothermal aquifer. The principal mineral zones, outwards from the pluton, are described in Chapter 3, and briefly are: quartz-feldspar±epidote veins with minor local quartz-cassiterite-muscovite veining, followed by quartz-calcite veins with some sulfides including pyrite, chalcopyrite, and arsenopyrite, further away to veins comprised of early quartz with arsenopyrite and jamesonite as well as local pyrrhotite, followed by texturally intergrown galena, sphalerite, tetrahedrite, pyrite, and siderite, and ending at the outer edge of the system with late quartz veins containing pyrargyrite, acanthite, polybasite, stephanite, and native silver, as well as local argillic alteration and some barite.

Summary of observations from fluid inclusions

In order to better understand and interpret stable isotope measurements, a knowledge of the hydrothermal fluid characteristics is essential. Of particular importance are thermal properties, as well as estimates of compositional fluctuations of H_2O/CO_2 ratios. Such data were obtained from the study of fluid inclusions within the veins (Chapter 5), and are summarized below.

Fluid inclusions from the orebodies were studied from the three principal stages of gangue mineralogy, which are (1) early coarse grained quartz, (2) siderite intergrown with the ore and (3) late stage finer grained quartz. The transition from early quartz to the carbonate stage is characterized by boiling of H_2O-CO_2 mixtures, and exsolution of CO_2. The influx of dilute water typifies the late quartz stage.

Pressure determinations obtained on the two phase boundary in the system H_2O-CO_2-NaCl, indicate that fluid pressure dropped in situ during vein opening, from approximately 1500 bars in early quartz to as low as 130 bars or less in siderite. Initial boiling produced an estimated 15-20 % water vaporization. This had the effect of decreasing the fluid temperature from 310° C in early quartz to 250° C in siderite and quartz, because of high enthalpy steam loss. Boiling also caused a decrease in dissolved CO_2, from $X_{CO_2} = 0.25$ in early quartz to $X_{CO_2} < 0.01$ in siderite, stabilizing carbonates and precipitating the ore minerals.

From the early quartz stage to the siderite stage, the fluids increased in salinity from a range of 1-5 weight percent NaCl equivalent, to 10-15 weight percent NaCl equivalent. The total salinity increase requires a loss of up to 80 percent of the water. Large increases in salinity accompanied by limited cooling in hydrothermal systems are indications of boiling within excess enthalpy reservoirs. Hot host rocks prevented the fluids from cooling below 250° C, even with extensive boiling. Hydration reactions also contributed to the increase in salinity. Mineral equilibria considerations between water and graphite indicate that further water consumption was attained through post-boiling reaction between water and graphite in replenishing the lost CO_2, and contributing to the increased salinity.

Relative to the orebodies, very little fluid inclusion data are available from the quartz-feldspar veins in the area near the pluton. Homogenization temperatures for some of the inclusions range between 450° and 535° C; the majority of inclusions, however, homogenize to liquid between 300° and 400° C. Some boiling was also indicated in this region. Both two phase and three phase H_2O-$CO_2 \pm CH_4$ inclusions occur. Freezing determinations indicate the presence of significant amounts of gases other than CO_2, probably CH_4 or N_2. Because of these extra components, salinity determinations are minimum values when using the clathrate melting temperature. Estimates are generally less or equal to 3 weight percent NaCl equivalent.

Analytical methods

The quartz separates were analyzed using the BrF_5 method of Clayton and Mayeda (1963). The data are reported in the usual δ notation relative to SMOW (Craig, 1961), using a National Bureau of Standards quartz sample (NBS-28) as a reference sample. A CO_2-H_2O fractionation factor of 1.0412 was used.

Carbon dioxide extraction from calcite, for isotopic analysis, was performed by the technique of reacting the calcite with phosphoric acid at 25° C (McCrea, 1950). For siderite, a modification of this method was used to ensure 100% yields, as siderite is relatively unreactive at low temperatures. Rosenbaum and Sheppard (1986) found that at 150° C, siderite reacts completely with phosphoric acid within one hour. They experimentally determined the fractionation factor at this temperature to be 1.00771. Hence, for high temperature reactions, 30-40 mg of siderite was placed in the main tube of a reaction vessel while the side arm was filled with 3 cc of phosphoric acid. The tube was then evacuated, and both the sample and acid degassed overnight on a high vacuum line. Evacuated tubes were then placed in a 150° C ± 1° C oven where they were allowed to reach thermal equilibrium. The acid was then poured onto the sample and the two reacted for an hour at 150° C. To tip the samples, the oven door had to be momentarily opened, creating a slight thermal perturbance; however, thermal reequilibration was monitered to have been established within 3-4 minutes, and then was maintained for the rest of the hour long reaction time. Yields were typically better than 99%, and values reproducible to within 0.07 per mil. Data for the carbonate minerals are reported in δ notation relative to the PDB standard for carbon, and SMOW for oxygen.

STABLE ISOTOPE MEASUREMENTS

Quartz

The sample distribution and $\delta^{18}O$ values for vein quartz from the district, including the orebodies, are summarized in Figure 6-2. The names and distribution of orebodies are

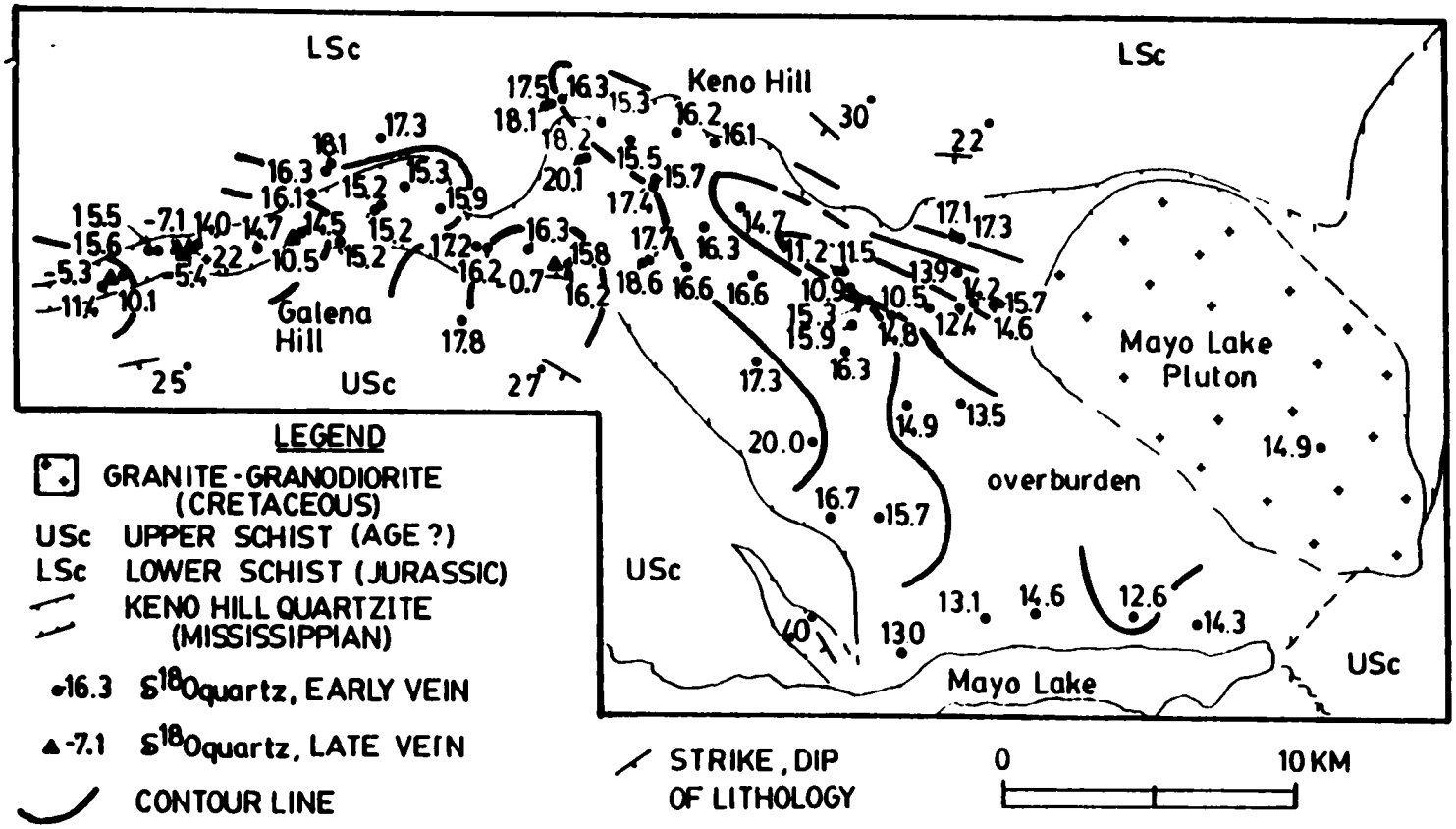

Figure 6-2. Contour map of $\delta^{18}O_{quartz}$ values from hydrothermal veins within the Keno Hill quartzite. Sample distribution shows the east-west spatial extent of the Keno Hill hydrothermal system and its relationship to the Mayo Lake pluton. The Ag-Pb-Zn orebodies are in the west of the system extending between Keno Hill and Galena Hill.

shown in Figure 6-1 (B), and isotopic data for these are listed in Table 6-1. Samples from the early quartz stage, which is paragenetically earlier than the carbonates, and the late quartz stage are both represented. Veining is confined predominantly to the Keno Hill Quartzite. Some of the veins from the adjacent schist units were also analyzed. Sample distribution extends east to west from the end of the district to the margin of the Mayo Lake Pluton, across a total distance of approximately 40 km.

Data on the map have been contoured in 2 per mil intervals (Fig. 6-2). Considerable, systematic variation along the strike length of the vein system is observed. The isotopic map pattern approximately matches the large scale east to west hydrothermal mineral zoning sequence documented in the district. Moving away from the pluton, values increase gradually from $\delta^{18}O_{quartz}$ = +10.5 per mil near the pluton, to +15.3 - +20.1 per mil on Keno Hill, 15 km away. Proceeding further west, values then decrease to approximately +10.1 per mil in the early quartz stage, near the end of the system (Fig. 6-2). The late quartz stage is most abundant at the western end of the system, where values as low as -7.1 per mil are recorded. The orebodies are located at the western end of the system as well, principally along this outward trend of decreasing $\delta^{18}O$ values.

At individual sample locations, specimens were collected and analyzed from different parts of single veins, from vein walls to vein centers. Only slight variations in $\delta^{18}O$ values (< 2 per mil) on a small scale are normally observed within the early quartz stage (Table 6-1). In contrast, the late quartz stage which is spatially restricted to the western end of the district, displays larger variations in $\delta^{18}O$ within single veins (Table 6-1, Fig. 6-2).

In the mining district, at the western end of the system, deposits may be grouped into either high Ag/Pb or low Ag/Pb deposits, according to bulk tonnage mining records (United Keno Hill Ltd., proprietary files). Deposits of the first group have produced ore with Ag/Pb weight ratios between 0.02 to 0.11, whereas the other deposits have produced below 0.02. Both high and low Ag/Pb deposits occur adjacent to one another, and are

Table 6-1. $\delta^{18}O$ of vein quartz from orebodies, different samples from same vein numbered -1, -2 etc..

High Ag/Pb deposits

Early quartz	$\delta^{18}O_{SMOW}$	Late quartz stage	$\delta^{18}O_{SMOW}$
DUNCAN CREEK	17.8		
FLAME AND MOTH -1	17.2		
FLAME AND MOTH -2	16.2		
HUSKY-208	14.0	HUSKY R-208 -1	2.1
HUSKY S.W. -1	15.5	HUSKY R-208 -2	2.3
HUSKY S.W. -2	15.6	HUSKY R-224 -1	-7.1
BLACK CAP -1	20.1	HUSKY R-224 -2	-5.4
BLACK CAP -2	18.2	HUSKY R-224 -3	-4.9
LUCKY QUEEN	15.3		
ELSA	14.7		
SILVER BASIN	16.2		
McQUESTEN Rd. -1	18.1		
McQUESTEN Rd. -2	16.3		
YUKENO	17.3		
NO CASH	16.1		
HOMESTAKE -1	18.6		
HOMESTAKE -2	17.7		
SADIE -1	17.4		
SADIE -2	18.1		
SADIE -3	16.3		
SILVER KING -1	10.5	SILVER KING	-5.2
SILVER KING -2	11.4		
VANGUARD	15.7		

Low Ag/Pb deposits

DIXIE	14.5	DIXIE	10.5
GALKENO	15.9		
BERMINGHAM	15.2		
HECTOR -1	15.3		
HECTOR -2	15.2		
CALUMET	15.3		
BELLEKENO -1	15.8	BELLEKENO	-0.7
BELLEKENO -2	16.2		
KENO -1	15.7		
KENO -2	17.5		
TOWNSITE	15.2		
ONEK	16.3		

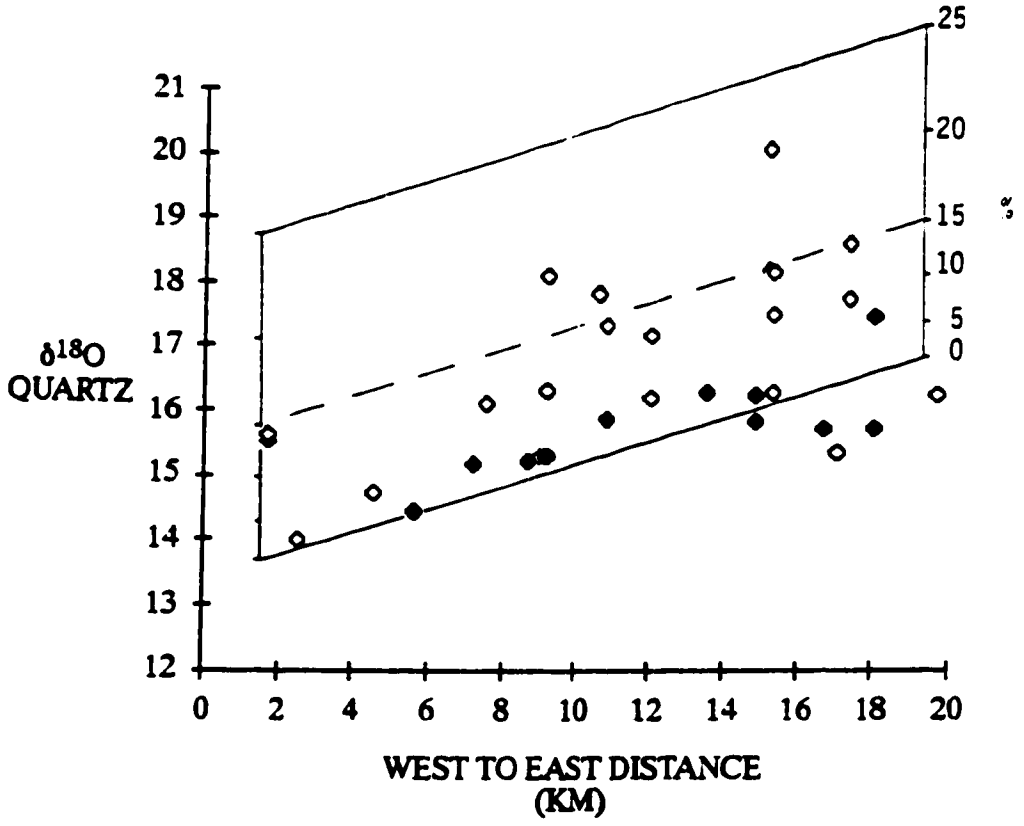

Figure 6-3. $\delta^{18}O$ quartz values from Ag-Pb-Zn orebodies along east to west trend of the mining district, between Keno Hill and Galena Hill. High Ag/Pb orebodies (open pattern) are enriched in ^{18}O relative to adjacent low Ag/Pb grouping (solid pattern). A general east to west decrease is observed. Superimposed on the data is a boiling model, the series from 0 % to 25 % represents the percentage of water converted to steam (boiling), and the corresponding isotopic shift within quartz that would result.

spread along the length of the 25 km long mining district. Mineralogically the two groupings are very similar, except for an increase in the overall tetrahedrite content of the high Ag/Pb deposits. These two groupings may be distinguished by their isotopic signatures as well. The $\delta^{18}O$ values of early quartz from high Ag/Pb deposits is up to about 4 per mil enriched relative to the quartz in the low Ag/Pb group (Fig. 6-3); however the spread is usually less than 1 or 2 per mil. Both groupings display an east to west decrease in $\delta^{18}O$ for quartz by approximately 3 per mil (Fig. 6-3).

Siderite

In the western portion of the system, siderite is distributed in veins along the 25 km length of the mining district (Fig. 6-4). Texturally, siderite is the gangue most closely intergrown with the ore minerals and sulfides. Veins near the Mayo Lake pluton in the eastern portion of the system do not contain siderite.

Oxygen-isotope values for siderite within the mining district show a similar east to west decrease as observed in the quartz analyses (Fig. 6-4). The $\delta^{18}O$ values for siderite range mostly from +12.3 to +19.1 per mil, with two anomalous low values at -8.7 and +0.9 per mil (Table 6-2). $\delta^{13}C$ values range from -7.9 to -11.3 per mil. A plot of $\delta^{18}O$ versus $\delta^{13}C$ is given in Figure 6-5. As with quartz, different isotopic groupings are observed in siderite for samples from high Ag/Pb deposits to those from low Ag/Pb deposits (Fig. 6-5). A positive linear correlation between $\delta^{13}C$ and $\delta^{18}O$ is observed for samples from the low Ag/Pb grouping. Also, the distribution of deposits along this line corresponds well with their spatial position within the district; eastern deposits are enriched in ^{18}O and ^{13}C, whereas western deposits are depleted. For the high Ag/Pb deposits, considerable isotopic variability is observed within individual veins; a negative correlation between $\delta^{18}O$ and $\delta^{13}C$ is recorded in three separate deposits (Fig. 6-5). The isotopic values of siderite are up to 2 per mil heavier in $\delta^{13}C$, and depleted by as much as 4

Table 6-2. Stable isotope data from siderite, different samples from same vein numbered -1, -2 -3, etc..

High Ag/Pb deposits	$\delta^{13}C_{PDB}$	$\delta^{18}O_{SMOW}$	Low Ag/Pb deposits	$\delta^{13}C_{PDB}$	$\delta^{18}O_{SMOW}$
DUNCAN CREEK	-10.8	15.2	DIXIE	-11.1	14.8
FLAME	-10.6	16.4	SUGYAMA	-10.3	16.6
LUCKY QUEEN -1	-9.1	15.5	RICO ADIT	-11.1	15.4
LUCKY QUEEN -2	-10.6	16.9	RICO	-11.0	15.5
LUCKY QUEEN -3	-10.6	17.2	BERM	-10.9	15.2
LUCKY QUEEN -4	-10.2	17.5	BELLEKENO	-10.7	16.5
LUCKY QUEEN -5	-8.6	16.1	KENO -1	-10.3	18.0
LUCKY QUEEN -6	-7.9	17.2	KENO -2	-9.6	17.2
LUCKY QUEEN -7	-8.4	15.6	TOWNSITE	-10.7	15.9
ELSA	-10.1	14.3	COMSTOCK1	-9.7	17.9
HUSKY -1	-10.5	13.0	COMSTOCK2	-9.7	17.7
HUSKY -2	-10.2	12.3	PORCUPINE	-9.6	17.8
HUSKY -3	-11.3	15.9	CARIBOU -1	-8.5	19.1
HUSKY -4	-10.8	14.3	CARIBOU -2	-8.8	18.8
HUSKY-R-224 -1	-9.8	0.9	ONEK	-10.5	16.1
HUSKY-R-224 -2	-8.1	-8.64			
NO CASH -1	-11.0	16.1			
NO CASH -2	-11.1	16.1			
RUBY -1	-10.4	13.8			
RUBY -2	-11.1	15.9			
HOMESTAKE	-10.2	16.2			
SADIE LADUE -1	-8.5	16.9			
SADIE LADUE -2	-8.0	17.1			
SADIE LADUE -3	-8.0	17.1			
SADIE LADUE -4	-8.5	17.0			
SADIE LADUE -5	-8.4	17.1			
SILVER KING -1	-11.1	14.9			
SILVER KING -2	-11.1	15.4			

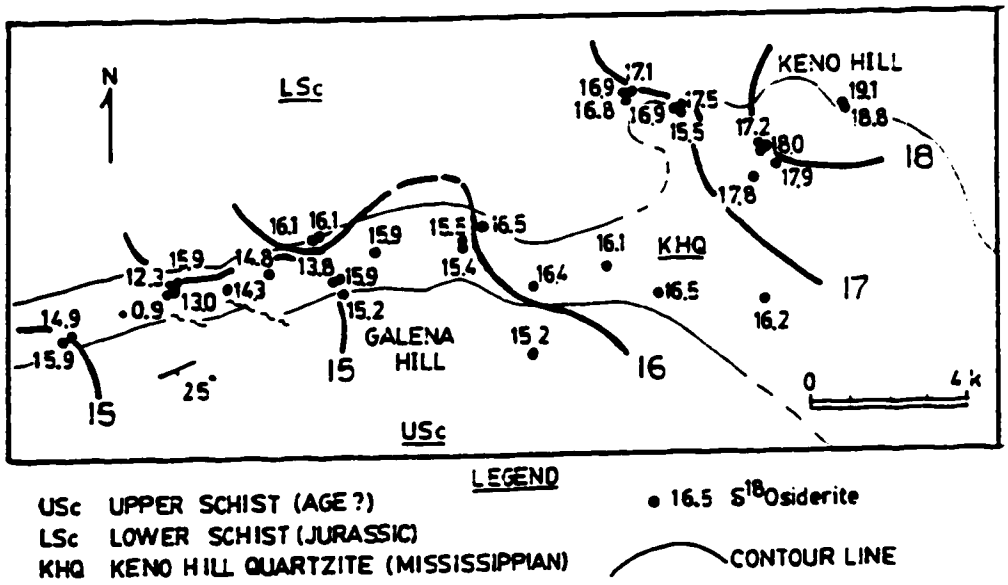

Figure 6-4. Contour map of $\delta^{18}O_{siderite}$ values from orebodies.

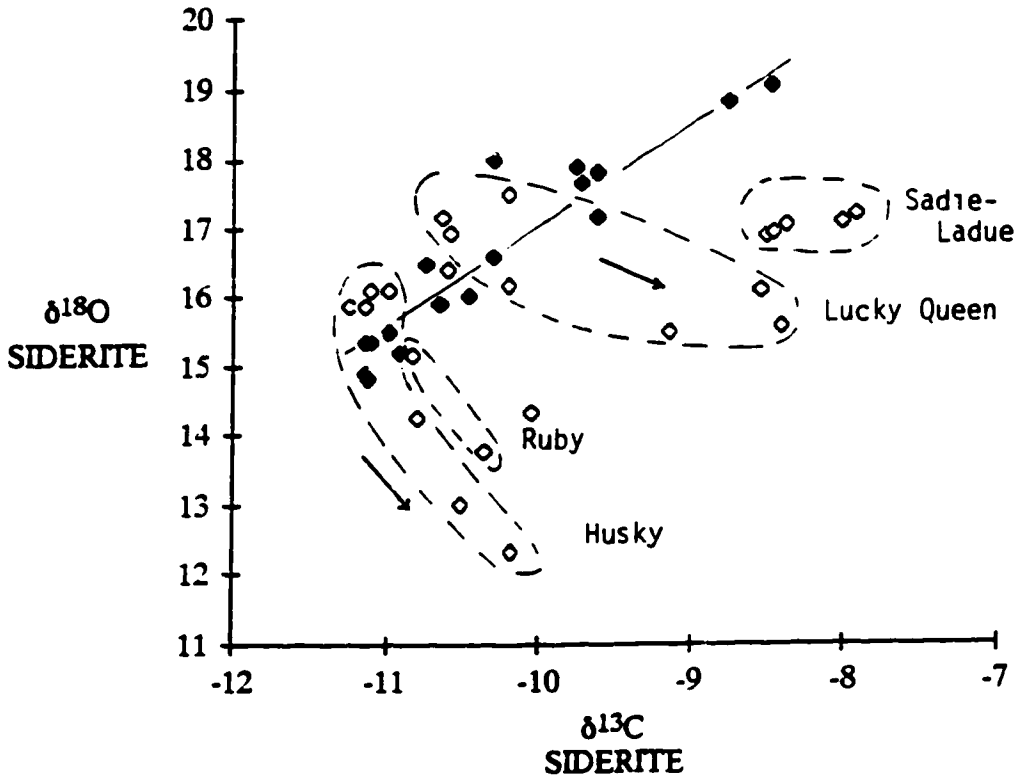

Figure 6-5. Plot of $\delta^{18}O$ versus $\delta^{13}C$ for siderite samples taken from the orebodies. Data are separated into two groupings; low Ag/Pb deposits are shown by solid pattern, high Ag/Pb deposits are shown by open pattern. Dashed lines envelope samples taken from individual deposits. Arrows indicate the fractionation trend that would result from the reaction of water and graphite in the formation of CO_2 and CH_4.

per mil in $\delta^{18}O$ relative to other portions of the same vein, and relative to adjacent orebodies of the low Ag/Pb grouping (Fig. 6-5).

Quartz-siderite pairs occasionally show clear isotopic disequilibrium, particularly in the low Ag/Pb grouping of deposits. For example the sample entitled DIXIE in tables 6-1 and 6-2 has $\delta^{18}O_{quartz} = +14.4$ and $\delta^{18}O_{siderite} = +14.8$. Typically the siderite values are heavy in ^{18}O, indicating its lower temperature of formation.

Calcite

Calcite occurs in veins situated between the Mayo Lake pluton and the mining district, and in the eastern part of the mining district, where calcite occurs with siderite and ore minerals (Fig. 6-6). The east to west transition in hydrothermal carbonates progresses from calcite dominated to siderite dominated.

Because calcite occurs mostly outside of the mining district, fewer samples and records are available for these veins, and a more detailed characterization of the fluids which precipitated calcite is not possible. Nevertheless, for the eastern part of the study area, the oxygen-isotope contour diagram (Fig. 6-6) is similar in pattern to that for quartz in the same area (Fig. 6-2 A). Values increase away from the pluton, from $\delta^{18}O = +9.8$ to +14.5. Further west, within the mining district, isotopic values for calcite are much more irregular and difficult to contour; $\delta^{18}O$ values range from +14.8 to -8.3 per mil (Fig. 6-6, Table 6-3).

$\delta^{13}C$ results for calcite are quite negative, from -12.9 to -4.0 per mil (Table 6-3). No correlation was established between carbon- and oxygen- isotope values within calcite, or between the carbon-isotope values of calcite and the mineral's distribution on the map.

Table 6-3. Stable isotope data from calcite, different samples from same vein numbered, -1, -2.

Calcite from orebodies	$\delta^{13}C_{PDB}$	$\delta^{18}O_{SMOW}$
McQUESTEN RD.	-7.8	-5.3
RICO	-9.7	14.1
MT. HINTON	-6.8	14.2
CREAM	-5.5	14.8
YUKENO	-7.0	-8.3
LUCKY QUEEN	-7.6	-7.8
BELLEKENO -1	-8.3	2.0
BELLEKENO -2	-8.2	1.3
SILVER SPRING	-6.6	3.1
HOMESTAKE -1	-5.7	-3.0
HOMESTAKE -2	-6.1	-1.4
KENO -1	-5.7	-4.0
KENO -2	-5.4	-3.4
Calcite east of mining district		
vein #46	-8.4	13.2
vein #72	-12.9	10.5
vein #152	-7.4	11.3
vein #155	-4.0	10.3
vein #158	-10.4	13.3
vein #160	-7.8	10.5
vein #204	-8.4	14.5
vein #243	-11.3	9.9

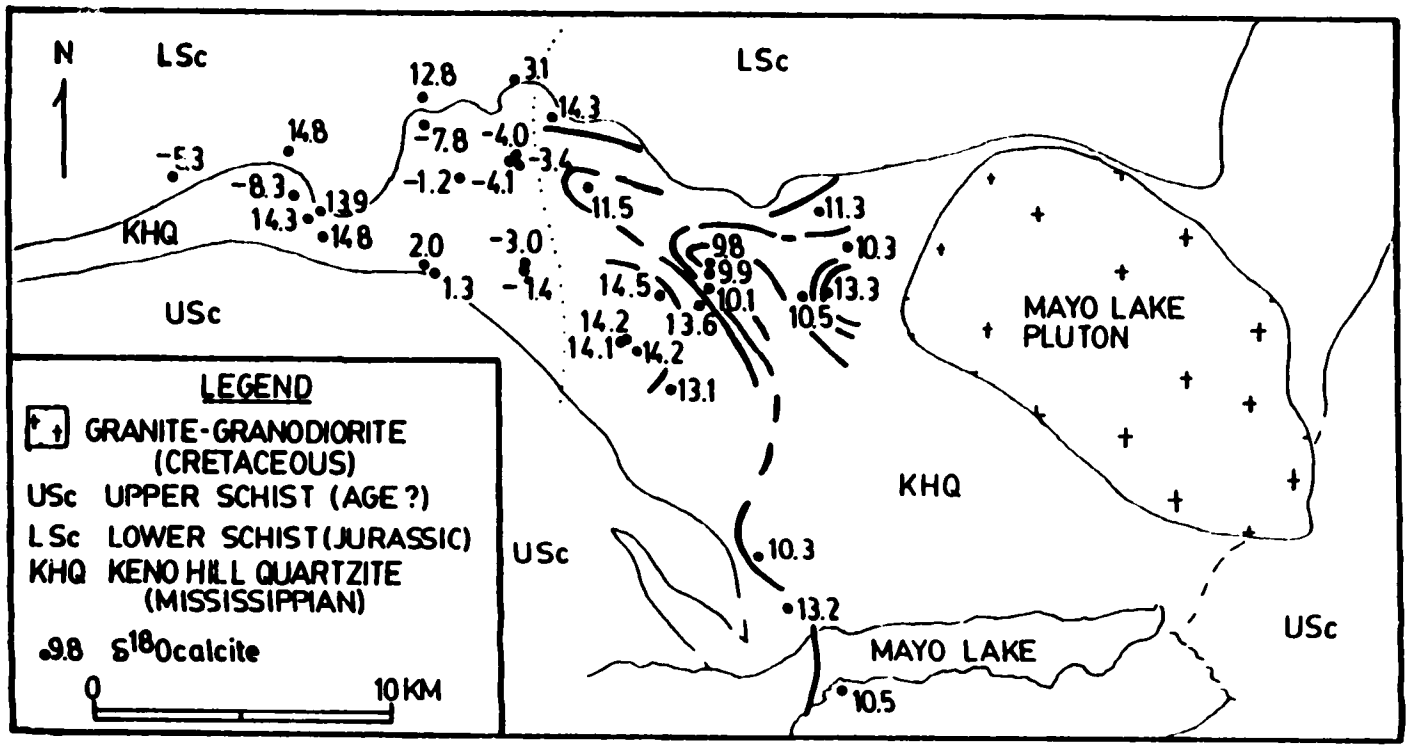

Figure 6-6. Contour map of $\delta^{18}O_{calcite}$ from hydrothermal veins in Keno Hill Quartzite.

INTERPRETATION OF STABLE ISOTOPE DATA

Stable isotope indications of boiling from $\delta^{18}O$ variations in quartz

In hydrothermal systems boiling is widely recognized as an important mechanism for ore formation (Drummond and Ohmoto, 1985). Boiling may be identified with the use of stable isotopes, since boiling results in quartz with higher ^{18}O contents due to fractionation of water, and because of the cooling effect which boiling has on hydrothermal fluids. In the Keno Hill mining district, ore veins with the highest Ag/Pb contents generally contain quartz with greater ^{18}O values as well; both of these effects may be reconcilled to a boiling event.

Fluid inclusion characteristics indicate that the mineral deposits of the mining district were formed under boiling conditions (Chapter 5). Observations and calculations from the fluid inclusion data indicate that during the initial boiling, between 15-20 % vaporization of water may have occurred within some ore shoots. Because CO_2 is relatively volatile, the content in the fluid decreased during boiling from approximately $X_{CO_2} = 0.25$ to less than 0.01. Loss of high enthalpy steam also had the effect of lowering the temperature of the ore fluid from about 310° C to 250° C. In high temperature, flowing geothermal systems, cooling by conduction is minimal, and most heat is lost by boiling or dilution with cooler water (Truesdell et al., 1977). Further effects of boiling in the Keno Hill system include a change in the dominant gangue mineralogy, from quartz at the beginning of boiling to siderite at the end of boiling.

The effects of boiling on isotopic signatures of hydrothermal fluids in active subsurface geothermal fields are documented by Craig (1963) and Truesdell et al. (1977). Fractionation results because the escaping vapor is depleted in ^{18}O, resulting in an ^{18}O-enriched residual water. For deeper CO_2-rich systems, such as the fluids which precipitated the Keno Hill veins, the effects of CO_2 loss must also be considered. Carbon dioxide is a volatile substance which strongly partitions ^{18}O (Bottinga, 1968).

CO_2 may lower the bulk $\delta^{18}O$ of the overal fluid. However, escaping CO_2 has negligeable fractionation effects on the water, as exsolved CO_2 is isotopically similar to aqueous CO_2 (Vogel et al., 1970). However reactions which produce CO_2 during post boiling equilibration of fluids and host rocks may have a strong fractionation effect on the water.

In the deeper portions of hydrothermal reservoirs, multiple step closed system steam separation is considered to be the most important form of boiling, in which batches of steam seperate from the system in isotopic equilibrium with the water (Truesdell et al., 1977). For very small batches, the model is equivalent to Rayleigh boiling, for large batches it is equivalent to single step boiling. Calculations for heat loss and isotopic fractionation during boiling are given in Truesdell et al.(1977). Results of calculations performed for 5 % boiling increments are presented in Figure 6-7, and are useful in the interpretation of the isotopic variability recorded within the Keno Hill system. In this example, it can be seen that the isotopic fractionation of water is quite small; the water is enriched in $\delta^{18}O$ by 0.3 per mil after 20 % vaporization of the water. However considerable cooling occurs due to separation of steam, modelled temperatures drop from 310° C to 243° C after 20 % boiling. Quartz $\delta^{18}O$ values consequently increase by 3.1 parts per mil (Fig. 6-7). Hence the increase in quartz $\delta^{18}O$ is principally the result of cooling. The redistribution of isotopes between $H_2O_{(l)}$ and CO_2 from cooling during the boiling event is not considered to have been an important factor because most CO_2 loss occurs at the onset of boiling before much cooling has happened (Chapter 5).

The model has been applied to the quartz $\delta^{18}O$ data from the Keno Hill mining district, and the results are displayed in Figure 6-3. The increase in ^{18}O in quartz from the high Ag/Pb deposits relative to the low Ag/Pb deposits may be interpreted as the result of boiling and cooling. Most of the oxygen isotope values fall within the 15 - 20 % boiling lines, consistent with the thermal range 250° - 310° C and the percentage boiling estimate reported for the fluid inclusions within quartz.

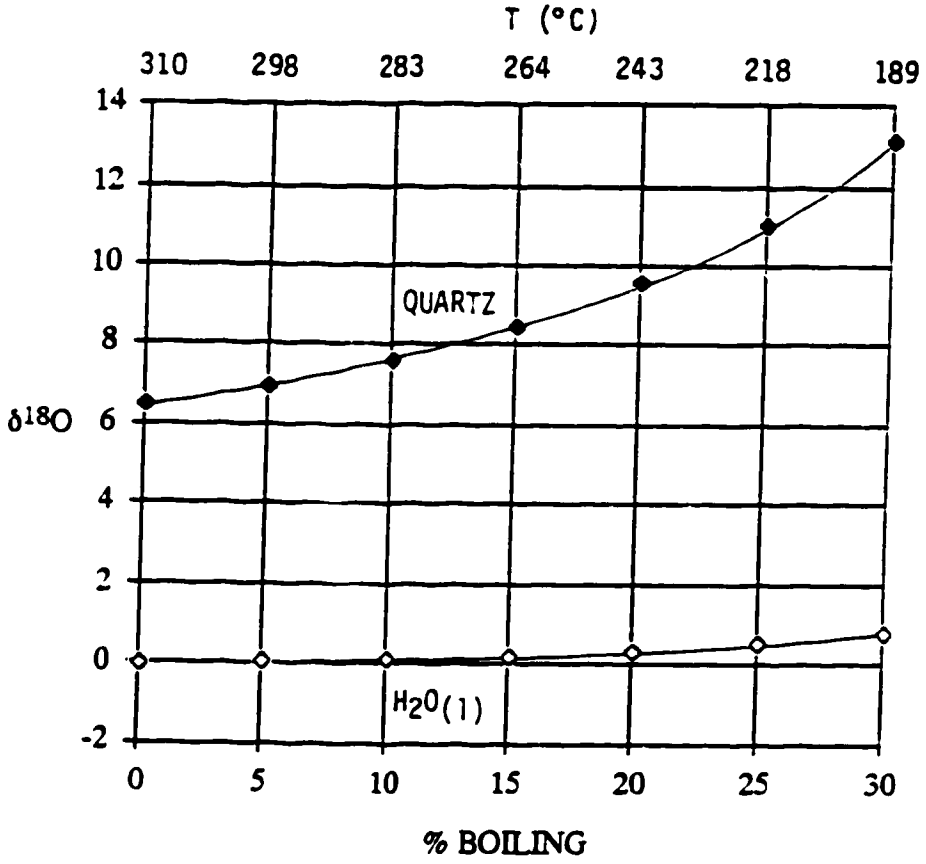

Figure 6-7. Diagram models oxygen isotope fractionation of water in a closed boiling system. Equilibrium $\delta^{18}O$quartz values are shown, these increase with progressive boiling due to fractionation of water, but mainly due to cooling effect of boiling shown at top of diagram. Fractionation factors taken from Matsuhisa et al (1979) for quartz-water pair, and Friedman and O'Neil (1977) for water liquid-vapor pair.

Both high Ag/Pb and low Ag/Pb deposits display a 2 - 3 per mil east to west decrease in $\delta^{18}O$ of quartz (Fig. 6-3). Two interpretions of this trend are: (1) a greater interaction of water and graphite to the west resulted in the formation of more CO_2, decreasing the $\delta^{18}O$ of water, or (2) increased westward mixing of H_2O-CO_2 fluids with isotopically light meteoric water generated the decreasing trend. A third possibility, increasing temperature towards the west, is not favoured because the deposits are furthest from the Mayo Lake Pluton, and fluid inclusion data does not substantiate increasing temperature in this direction (Chapter 5).

In the first hypothesis, saturation and loss of CO_2 during flow towards the west may have resulted in the reaction of water and graphite:

$$2C + 2H_2O = CO_2 + CH_4 \qquad \text{(Ohmoto and Kerrick,1977).} \qquad (1)$$

Exsolution of CO_2 and CH_4, with the progression of the above reaction (1) to the right may have generated water depleted in ^{18}O. Graphitic rocks typically buffer hydrothermal fluids to high CO_2 contents (French, 1966; Nockleberg, 1973), and in an environment of fluctuating pressure and phase separation, a substantial amount of water may be converted in part to CO_2. The fractionation effects on the oxygen-isotope composition of water when it has been partially converted to CO_2 are shown in Figure 6-8. At 300° C, a decrease of 3 parts per mil in the $\delta^{18}O$ content of water is generated after conversion of 25 % of the original water mass. The calculations presented are based on a closed system. Localized areas of intense boiling superimposed on the saturated H_2O - CO_2 mixtures, resulted in the positive $\delta^{18}O$ shifts of the isolated Ag-rich "ore shoots", a feature controlled by active faulting and structural geometry (Chapters 2 and 5).

In the case for the second hypothesis the presence of meteoric water is indicated in the late quartz stage at the western end of the district where $\delta^{18}O$ for quartz is as low as -7.1 per mil. At 250° C this value translates to a water with $\delta^{18}O$ = -16.0 per mil, which must be meteoric in origin as present day meteoric water in the Yukon is isotopically light, at $\delta^{18}O$ = -23 per mil (Hitchon and Krouse, 1972). Only slight increments of this water,

mixed with the early H_2O-CO_2 fluids, would have been necessary to establish the decreasing westward trend of $\delta^{18}O$ in the early fluid.

Post-boiling reequilibration of fluids with graphitic host rocks, isotopic evidence from siderite

Formation of siderite is closely related to the boiling event. The paragenetic position of siderite in the veins, its fluid inclusion characteristics, and calculations of carbonate solubility all indicate that siderite precipitated as an end product of boiling at a temperature near 250° C (Chapter 5). The precipitation of hydrothermal carbonates because of boiling is frequently the result of CO_2 loss, and accompanying raise in pH (Fournier, 1985). Oxygen-isotope values for siderite show a similar east to west decrease as in quartz from the mining district. However the quartz-siderite mineral pairs are in isotopic and thermal disequilibrium, since siderite formed from a more advanced stage of boiling. As a result, mineral-pair isotope-thermometry yields unreasonable temperatures.

Many factors may have contributed to variations in the $\delta^{13}C$ of the hydrothermal carbonates, including different sources of carbon, changes in temperatures, and variations in the oxidation state of the fluid (Rye and Ohmoto, 1974). Indications are that most of the carbon in the hydrothermal fluid was likely obtained from a reduced organic source, such as the graphitic host rocks. The $\delta^{13}C$ for siderite ranges from -11.3 to -7.9 per mil (Table 6-2). High temperature experimental measurements of the fractionation factor for $\delta^{13}C$ between siderite and other carbon bearing species are not available. However, assuming that the fractionation factor for siderite is similar to that of other carbonates, at 250° C, siderite would have been approximately 2 per mil heavier in $\delta^{13}C$ than CO_2, indicating $\delta^{13}C$ values for CO_2 of -8.8 to -6.5 per mil. Such values would have been in equilibrium with graphite having $\delta^{13}C$ of approximately -25 per mil. This value is typical of reduced or organic carbon from sediments which normally have $\delta^{13}C_{PDB}$ values of less than -15 per mil (Rye and Ohmoto, 1974).

The oxidation state of the hydrothermal fluids has a considerable effect on the distribution of carbon isotopes between various carbon bearing compounds. In graphite buffered hydrothermal fluids, the dominant carbon species are CO_2 and/or CH_4 (Ohmoto and Kerrick, 1977). The ratio of these two gases may vary drastically within the fluids with changing conditions of oxidation according to:

$$CO_2 + 2H_2 = CH_4 + O_2 \qquad (2)$$

This in turn may have a significant impact on the distribution of carbon isotopes in the hydrothermal fluids since the isotopic fractionation between CO_2 and CH_4 is large: at 250° C, $1000 \ln \alpha_{CO_2\text{-}CH_4} = +28.7$ per mil (Bottinga, 1969). Also, variations in the content of the gas species may arise due to their contrasting volatility (Giggenbach, 1980). Boiling is recognized as having an oxidizing effect on hydrothermal fluids because of the more volatile nature of reduced gaseous species such as H_2, CH_4, and H_2S (Drummond and Ohmoto, 1985). Phase separation may have the effect of increasing the CO_2/CH_4. As well, the downward influx of high level oxidizing fluids may result in the production of CO_2, from:

$$C + O_2 = CO_2 \qquad \text{(Zen, 1963)} \qquad (3)$$

The general east to west decrease in $\delta^{13}C$ of siderite (Fig. 5) is a possible indication of an increasing oxidation state with subsequent increase in the CO_2/CH_4 ratio of the fluid. This may have been attained in two manners, either by an increased interaction of the mineralizing fluids with the late stage meteoric water, assuming that the meteoric water is relatively oxidized, or by a greater loss of the more volatile H_2 and CH_4 during phase separation towards the west. Definitive criteria for distinguishing between the two are not presently available.

Within the high Ag/Pb deposits, siderites from individual ore deposits display a linear increase in $\delta^{13}C$ coupled with a decrease in $\delta^{18}O$ (Fig. 6-5). This negative shift in $\delta^{18}O$ is in direct contrast with the positive boiling shift observed for early quartz from the same deposits (Fig. 6-3). The fluids which precipitated siderite were depleted in CO_2

relative to the fluids at the beginning of boiling, which were in equilibrium with graphite. Because of the buffering effects of graphite the natural tendency for these gas depleted fluids was to regain the lost CO_2. Production of CO_2 from water and graphite resulted in the lower ^{18}O water. Also, production of equal proportions of CO_2 and CH_4 according to reaction (1) increased the overall CH_4/CO_2 ratio resulting in ^{13}C-enriched carbonates. A closed system model in which 20-25 % of the water is consumed during CO_2 and CH_4 production can account for the observed 3-4 per mil $\delta^{18}O$ depletion (Fig. 6-8).

After much water consumption, from the begining of boiling in quartz to the end of reequilibration of the fluids with graphite during the formation of siderite, fluid salinity increased drastically; the total depletion of water may have been greater than 50% for the entire cycle, resulting in the observed salinity increase from approximately 5 weight percent NaCl equivalent to 10-15 weight percent NaCl equivalent relative to water, as measured in the fluid inclusions (Chapter 5).

Considerable amounts of graphite as well as rapid rates of reaction are required for the reactions to have been complete. However, the absence of a shift in the O and C isotopic values of siderite from the low Ag/Pb group of deposits (Fig. 6-5) indicates that graphite may not have been as readily available in these.

Hydrothermal paleoflow, sources of water, and water-rock exchange of oxygen

The contour diagram for $\delta^{18}O$ values of quartz (Fig. 6-2) bears a strong resemblance to a hydrological flow net, and may be interpreted as depicting areas of higher permeability and fluid migration. It may be used as such because changes in the isotope values of quartz are a function of water/rock interaction, cooling, boiling, and degrees of fluid mixing, which generally are all in part a function of permeability and the distance travelled by the hydrothermal fluid. The acute northwest trending linear anomaly at the center of the map indicates a region of fluid focussing and concentrated hydrothermal flow, evidently

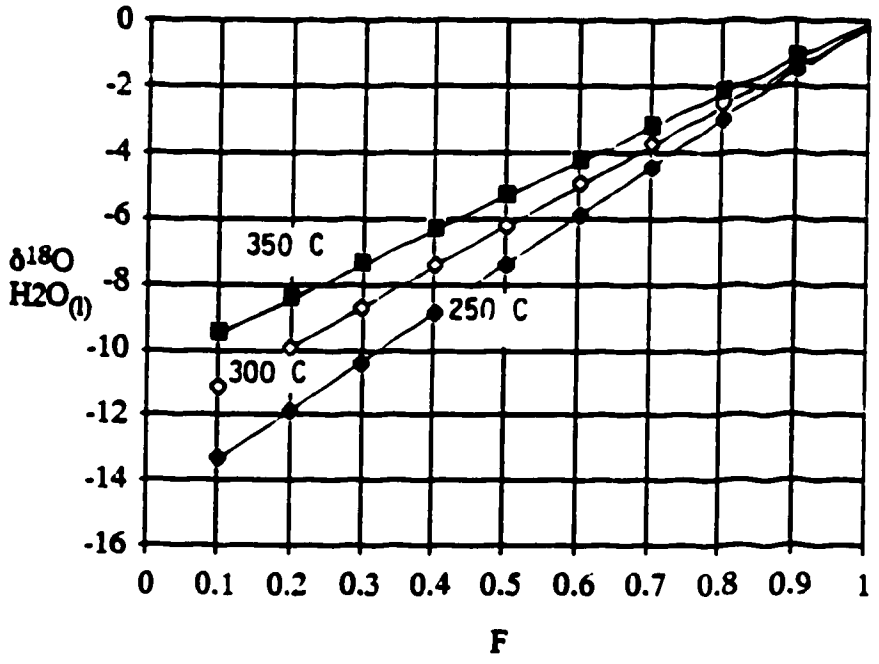

Figure 6-8. Fractionation of $\delta^{18}OH_2O$ from conversion of water to CO_2, represented for 250°, 300°, and 350° C. F is the fraction of water remaining. Model is based on equilibrium conditions in a closed system, fractionation factors taken from Truesdell (1974).

along a permeable major fault structure. The direction of the anomaly corresponds with vein attitude measurements in this region, which strike to the northwest and are steeply dipping to vertical (Chapter 2). The thickness of the quartzite decreases to the west in the mining district, where flow appears to have been more evenly distributed through the many fault structures and a more restricted aquifer.

Using temperature determinations from fluid inclusions (Chapter 5) and oxygen isotope measurements from quartz, $\delta^{18}O_{water}$ have been estimated. In the area near the pluton (Fig. 6-2), hydrothermal temperature estimates are as high as 535° C, but lower temperature determinations, to near 300° C, are more common. Depending on temperature, the water which precipitated quartz having $\delta^{18}O_{SMOW} = +10.5$ would have had an oxygen-isotope composition of $\delta^{18}O_{SMOW} = +3.6$ to +8.5 per mil (Matsuhisa et al., 1979). At the center of the district, on Keno Hill, quartz precipitated within a more restricted temperature interval, between approximately 250° - 310° C. From a discussion earlier in this paper, quartz precipitated near 310° C at the start of boiling, with $\delta^{18}O_{quartz}$= +16 per mil, and would have been in equilibrium with a water having $\delta^{18}O = +9.5$ per mil. These calculations indicate that water increased in $\delta^{18}O$ away from the pluton by a minimum of 1 per mil, and by as much as 6 per mil.

The origin of these fluids is somewhat ambiguous. However, if a hydrothermal temperature near 310° C was representative of conditions in the fluids near the pluton, then these fluids were light with $\delta^{18}O_{water} = +3.6$. On one hand, this composition is below values for typical magmatic waters, which are usually greater than +5 per mil (Taylor, 1974). On the other hand, the oxygen isotope values for metamorphic waters can range from +3 to +20 per mil (Sheppard, 1986), to which the hydrothermal fluids near the Mayo Lake pluton may be assigned. Another possible source for the fluids is a highly exchanged meteoric water. Such a model seems favourable in light of widespread documentation of the interaction between deeply circulating meteoric waters with the margins of granitic plutons and batholiths (Taylor, 1974, 1977), and the spatial relationship here between the

Mayo Lake pluton and Keno Hill hydrothermal system (Fig. 6-2). The introduction of an oxidizing meteoric water into the graphitic host is also indicated by the observed dominance of CO_2 over CH_4 as the principal accessory gas phase throughout the system. Connate or formation waters are not thought to have been important in contributing water to the system because of geological reasons; isoclinal folding and recrystallization of the host rocks, and the regional greenschist metamorphism would have expelled most pore fluids.

Even if a higher temperature regime is favoured for the hydrothermal fluids near the pluton (up to 535° C as recorded in some fluid inclusions), an east to west increase in the $\delta^{18}O$ of water is still suggested by the calculations. The increase likely resulted from water-rock exchange. The solubility of quartz, an important consideration in exchange reactions with quartzite, is greatly dependent on temperature (Holland and Malinin, 1979; Kennedy, 1950). Exchange between the Keno Hill Quartzite and the hydrothermal fluids was likely more extensive in the high temperature regime near the pluton. Below 300° C the solubility of quartz is relatively diminished, and exchange of oxygen between the hydrothermal fluids and the quartzite in the mining district would have been less significant. To assess the degree of equilibration between the fluids and the host rock, seventeen whole-rock samples of the Keno Hill quartzite were analyzed for $\delta^{18}O$. Their $\delta^{18}O$ values range from +11.8 to +19.2 per mil, with an average at +16.1 per mil (Table 6-4). A single analysis of a greenstone sample from a concordant lens measures +6.7 per mil, typical of gabbroic rocks. Hydrothermal quartz from veins on Keno Hill with $\delta^{18}O$ = +16, similar to the average for the quartzite, is interpreted to indicate a large degree of isotopic equilibrium between the fluids and the quartzite, and a generally low water/rock ratio. Quantifying the water/rock ratio by standard means (Taylor, 1974; Nabelek, 1987) is complicated in this case by the effects of isotopic fractionation between CO_2 and H_2O. Both cooling of H_2O-CO_2 mixtures, and production of CO_2 have the tendency of lowering $\delta^{18}O_{H_2O}$, in direct opposition to isotopic exchange with the host rocks. In Figure 6-9 it is shown that cooling of an H_2O-CO_2 mixture with X_{CO_2} = 0.25, from 535° C to 310° C,

Table 6-4. Whole rock $\delta^{18}O$ from Keno Hill Quartzite unit.

Sample #	$\delta^{18}O_{SMOW}$	Sample #	$\delta^{18}O_{SMOW}$
HUSKY R-224	16.1	#150	17.2
HUSKY R-121	15.5	#151	15.3
SILVER KING 2	19.2	#7	16.8
CARIBOU	17.0	#288	17.0
HECTOR	16.7	#36	16.9
MT.ALBERT	19.1	#95	11.8
MT. HINTON	15.7	#103	14.4
#172	14.7	#1	15.3
#32	14.4	average:	16.1

fractionates water by -1.5 per mil, whereas cooling of a mixture with $X_{CO_2} = 0.10$ fractionates water by -0.6 per mil. Also, Figure 6-8 demonstrates that at 350° C, the conversion of 10 - 20 % of the water to CO_2 and CH_4 by reaction with graphite would have depleted the water by approximately -1 to -2 per mil. Because of these competing effects on the fractionation of water, small increases calculated for $\delta^{18}O_{H_2O}$ are representative of greater decreases in the water/ rock ratio than would normally be estimated from pure water systems.

It is not certain to what degree the late meteoric fluids interacted with the primary mineralizing fluids. However the late stage quartz is most abundant in the western portion of the district at the end of the system, where the mineralogy of the veins is epithermal in character (Chapter 3). The coincidence that the early mineralizing fluids decrease in ^{18}O gradually toward the west in the mining district may be interpreted to have been the result of mixing with the meteoric water, and that the two fluids did overlap in time. Isotopic values for hydrothermal quartz and siderite (Table 6-1, 6-2) which are intermediate to the end members, are an indication that the fluids were contemporaneous and did mix. Assuming present day meteoric values were applicable, a meteoric component of approximately 9 % would have been sufficient to cause the 3 per mil decrease from east to west (Fig. 6-3). The decrease corresponds with the ore zone, and mixing is often cited as an effective mechanism for ore formation (Barnes, 1979).

Interpretation of stable isotope data from calcite

The $\delta^{18}O$ values for calcite increase away from the Mayo Lake pluton, from +9.8 to +14.5 (Fig. 6-6), likely reflecting cooler hydrothermal temperatures away from the pluton and a lower water/rock ratio. Although calcite produces a similar contour map pattern as quartz in this portion of the system, quartz-calcite mineral pair temperature determinations consistently yield unrealistic temperatures, indicating disequilibrium

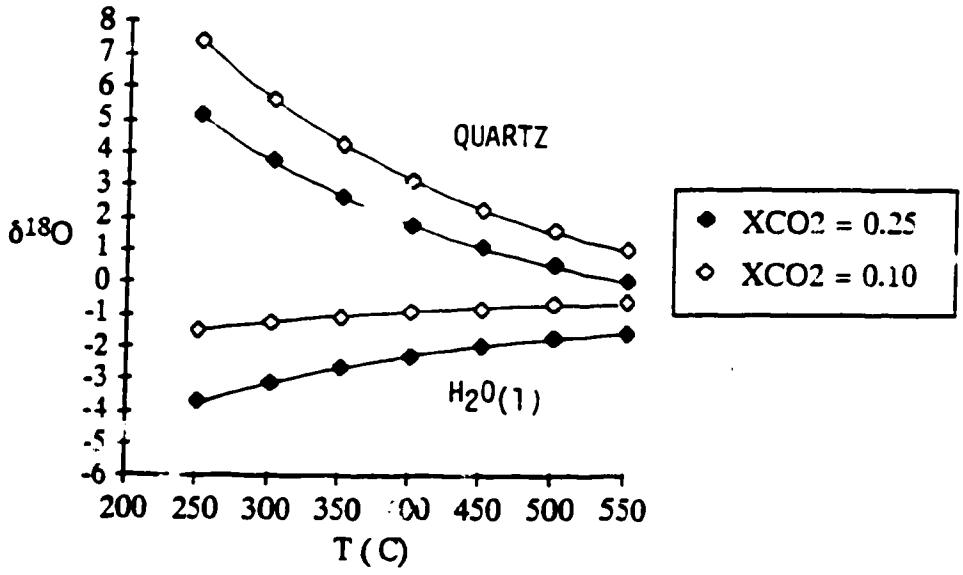

Figure 6-9. Diagram displays redistribution of $\delta^{18}O$ in water from H_2O-CO_2 mixtures, upon cooling from 550° C to 250° C. Quartz in equilibrium with the water is also shown.

between the two. As with siderite, this is likely a result of calcite having precipitated as an end-product of boiling, in disequilibrium with higher temperature quartz.

Calcite with low or negative $\delta^{18}O$ values (-8.3 to +2.0 per mil, Fig. 6-6), is restricted to the mining district. These likely reflect precipitation from meteoric waters. While it is possible that the influx of meteoric water post-dated ore deposition completely, the observation that these negative values from calcite are confined entirely to the mining district, indicates that meteoric water likely influenced ore formation. None of the calcite in the eastern portion of the system have negative isotope values for oxygen or reflect any effects of later exchange with surface waters, possibly because pristine meteoric water was involved only in the ore-forming process to the west.

The low $\delta^{13}C$ values of calcite are probably derived from the graphitic host rocks. The wide variation in values (2.9 to -4.0 per mil) may indicate that a portion of the carbon was derived from carbonate units as well, or may reflect fluctuating CO_2/CH_4 ratios in a dynamic boiling system.

Comparison of O and C isotope data with published S isotope data

Boyle et al. (1970) conducted an extensive study on sulfur isotope ratios of host rocks and vein sulfides from the Keno Hill mining district. Averages of the tabulated data for vein galena, from Boyle et al. (1970), were plotted on a map and contoured (Fig. 6-10) for comparison with the oxygen and carbon isotope data. Within the mining district a strong correlation is observed; galena from the eastern deposits is relatively enriched in the heavy isotope, with $\delta^{34}S_{galena}$ = 0.0 parts per mil using a meteoritic troilite standard, whereas galena from the western deposits is depleted having values near -10 parts per mil. The transition from one end of the 25 km long district to the other is quite regular and gradational. A 275 meter vertical section in the Calumet mine was sampled and analyzed, with no regular pattern in the vertical dimension observable at this scale. The sulfur isotope study demonstrates the unidirectional nature of the zoning, and produces a contour

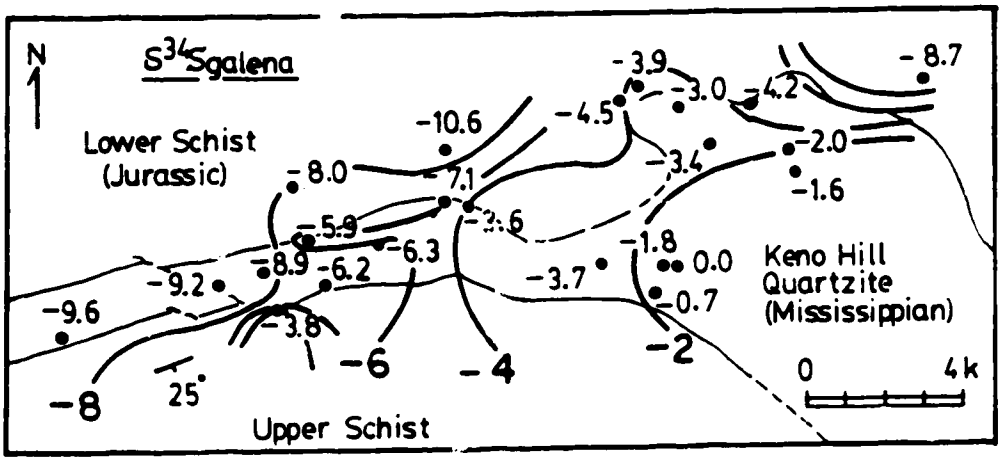

Figure 6-10. Contour diagram showing general decrease of average $\delta^{34}S_{galena}$ from east to west in Keno Hill mining district. Averages for galena sam taken from individual vein deposits obtained from tabulated data of Boyle et al., 1970).

pattern similar in form to that for oxygen isotopes from quartz (Fig. 6-2) and siderite (Fig. 6-4).

Sulfur isotope ratios measured for pyrite obtained from the metamorphosed sedimentary rocks of the district, vary in an irregular manner across the district, from +14.9 to -5.1 parts per mil (Boyle et al., 1970). The average for these however is $\delta^{34}S_{pyrite} = +1.7$ and is possibly representative of the sulfur source reservoir for the hydrothermal fluids. For vein galena, even large variations in temperature will not generally cause changes in the sulfur isotope value by ten parts per mil. Systematic mixing of different sulfur reservoirs from east to west across the district is not indicated either, in light of the irregular distribution of measured values from pyrite in the host rocks. On the other hand , a slight increase in pH and/or in the oxidation state of the fluids under hydrothermal conditions can easily account for a decrease of 10 parts per mil in galena (Ohmoto and Rye, 1979; Rye and Ohmoto, 1974). The east to west sulfur trend is likely representative of an increasing oxidation state, which created sulfate ions in the western [illegible] into which partitioned ^{34}S, resulting in lighter sulfides. The presence of Kaolinite in some of the western deposits is an indication of decreasing pH towards the west, and not of increasing pH as would be required by the sulfur isotope trend.

DISCUSSION

Boiling is widely recognized as an important mechanism of hydrothermal ore deposition (Drummond and Ohmoto, 1985; Reed and Spycher, 1985). It is most frequently considered to be important in shallow epithermal systems where low pressures allow for vapor escape (Larson and Taylor, 1987). When carbon dioxide is a significant constituent of the mineralizing fluids, however, deeper seated boiling may occur (Bowers and Helgeson, 1983, a,b). Boiling is also recognized as an effective means of hydrothermal differentiation in metamorphism, where CO_2 loss generates water - rock reactions and higher salinities, which in turn promotes increased CO_2 immiscibility,

pushing fluid evolution along the two phase boundary to hypersaline conditions (Yardley and Bottrell, 1988; Trommsdorff and Skippen, 1986).

Central to the processes discussed here is the availability of graphite required for the initial formation of CO_2 and for the replenishment of lost CO_2. The carbon isotope values for siderite and calcite indicate that reduced or organic carbon is the principal source of carbon in the fluids. Such a graphite reservoir is provided by the black graphitic Keno Hill Quartzite, and the fault gouge with which the fluids interacted. Graphite buffered the fluids to a high fCO_2, thus maintaining the volatile content of the fluids (French, 1966).

The selective reaction with graphite also has considerable implications for release of metals into the fluids. Organic materials in sediments are known to be an effective sink, or reservoir, of metals (Vine, 1970; Morton and Changkakoti, 1987). Measured values of Ag, Pb and Zn from the Keno Hill Quartzite and Lower Schist units of the mining district are generally anomalous (Boyle, 1965). The importance of graphite in the ore forming process may then have been twofold: (1) as a metal source which is highly reactive with hydrothermal fluids, graphite may have been a principal source of metals for the ore deposits: (2) graphite buffered the fluids to a high partial pressure of CO_2 allowing boiling to occur, the principal mechanism of ore precipitation.

The distribution of stable isotope values throughout the district places considerable constraints on the geometry of the hydrothermal system (Fig. 6-2). The large scale nature of the system becomes evident when the values are contoured. Of particular significance is the apparent dominance of lateral as opposed to vertical fluid migration, a feature which coincides with the geological observations that fractures are most abundant within the brittle moderately dipping quartzite.

The identification of meteoric water involved in the formation of late quartz, siderite, and calcite is also of genetic significance, as mixing is known as well to be another important process associated with ore deposition (Taylor, 1974). Pristine meteoric water

was not identified in the eastern portion of the system near the pluton, but only in the west coincident with the orebodies (Figs. 6-2 and 6-6).

Finally, the potential use of stable isotopes in mineral exploration has been displayed for the Keno Hill district by the isotopic characterization of high Ag/Pb deposits. Boiling, mixing, and flow patterns are identified, all of great importance in exploration. Presently, stable isotopes measured from quartz or siderite encountered in a newly found vein in the Keno Hill district could be used to predict wether the overall Ag/Pb ratio of the deposit is of the high or low grouping even if no mineralization is encountered, allowing for further exploration decisions to be made from limited sampling.

CONCLUSIONS

The Keno Hill vein system of central Yukon is restricted predominantly to the highly fractured, graphitic Keno Hill Quartzite unit of Mississippian age. Hydrothermal mineral zoning is spatially related to a Cretaceous granitic pluton which intrudes the quartzite. During mineralization, the quartzite acted as a district scale aquifer, apparently restricting flow mostly to the lateral direction. Subsequent erosion has exposed a 40 km long vein system, from its plutonic roots, outwards to polymetallic Ag-Pb-Zn veins, and further to assemblages of epithermal character.

The $\delta^{18}O$ values for vein quartz near the pluton increase outwards from +10.6 per mil to +20.1 per mil, due to cooling of the hydrothermal fluids, and exchange with the quartzite. Contours of isotope values outline broad paths of fluid movement within the quartzite. Proceeding still further from the pluton, $\delta^{18}O_{quartz}$ then decreases from +20.1 to +10.1 per mil to the outer edge of the system. The presence of meteoric water is indicated at the outer edge of the system, where a late quartz stage has oxygen isotope values near $\delta^{18}O$ = -7.1 per mil. The outward decreasing trend appears to have been established in one of two manners; 1) by mixing of fluids with isotopically light meteoric water; or 2) by fractionation due to CO_2 formation.

Boiling of fluids also had an effect on the isotopic signature of quartz and carbonates. Considerations of fluid-mineral equilibria indicate that graphite buffered the hydrothermal fluids to a high CO_2 content ($XCO_2 = 0.25$), allowing for boiling to have occurred at considerable depths. Superimposed on the outward decreasing $\delta^{18}O_{quartz}$ trend are local isotopically anomalous zones, which are also silver-rich. The quartz from these zones has been shifted to higher $\delta^{18}O$ values, by up to 4 per mil, due to a minimum 10 - 25 % boiling of fluids and fractionation dominated by water vapourization and cooling. Carbonates formed as a late stage product of the boiling event, and the oxygen isotope boiling shift was reversed during precipitation of this phase, due to the equilibration of graphite and water in replacing exsolved CO_2.

A closed system boiling model, together with calculations of water consumption during post-boiling CO_2 formation, indicate that greater than 50% of the original water involved in the ore-forming process was removed. Relatively saline mineralizing fluids resulted. The involvement of organic carbon from the wallrocks is indicated by the negative $\delta^{13}C_{PDB}$ values for the carbonates, from -12.9 to -4.0 per mil. Variations in the carbon isotopes are due to fluctuating CO_2/CH_4 ratios in the boiling system, reflecting the contrasting volatility of the gas pair.

REFERENCES

Abbott, J.G., Gordey, S.P., Tempelman-Kluit, D.J., 1986, Setting of stratiform, sediment -hosted lead-zinc deposits in Yukon and northeastern British Columbia. In, J.A. Morin (editor), Mineral Deposits of the Northern Cordillera, Canadian Institute of Mining and Metallurgy Special Volume 37, P. 1-18.

Anderson, R.G., 1987, Plutonic rocks of the Dawson map area, Yukon Territory, in Current Research , Part A, Geological Survey of Canada, Paper 87-1A, p.689-697.

Barnes, H.L., 1979, Solubilities of ore minerals. In, H.L. Barnes (editor), Geochemistry of Hydrothermal Ore Deposits, second edition, John Wiley and Sons, p. 404-460.

Bowers, T.S., Helgeson, H.C., 1983, Calculation of the thermodynamic and geochemical consequences of nonideal mixing in the system H_2O-CO_2-NaCl on phase relations in geologic systems. Equation of state for H_2O-CO_2-NaCl fluids at high pressures and temperatures. Geochimica et Cosmochimica Acta, vol. 47, p. 1247-1275.

Bowers, T.S., Helgeson, H.C., 1983, Calculation of the thermodynamic and geochemical consequences of nonideal mixing in the system H_2O-CO_2-NaCl on phase relations in geologic systems. Metamorphic equilibria at high pressures and temperatures. American Mineralogist, vol. 68, p. 1059-1075.

Bottinga, Y., 1968, Calculation of fractionation factors for carbon and oxygen isotopic exchange in the system calcite-carbon dioxide-water. Journal of physical Chemistry, vol. 72, p. 800-808.

Bottinga, Y., 1969, Calculated fractionation factors for carbon and hydrogen isotope exchange in the system calcite-CO2-graphite-methane-hydrogen and water vapor. Geochimica et Cosmochimica Acta, vol. 33, p. 49-64.

Boyle, R.W., 1965, Keno Hill-Galena Hill lead-zinc-silver deposits, Yukon territory. Geological Survey of Canada Bulletin 111, 302 pages.

Boyle, R.W., Wanless, R.K., Stevens, R.D., 1970, Sulphur isotope investigation of the lead-zinc-silver-cadmium deposits of the Keno Hill-Galena Hill area, Yukon, Canada. Economic Geology, vol. 65, p. 1-10.

Campbell, A., Rye, D., Petersen, U., 1984, A hydrogen and oxygen isotope study of the San Cristobal mine, Peru: implications of the role of water to rock ratio for the genesis of wolframite deposits. Economic Geology, vol. 79, p. 1818-1832.

Clayton, R.N., Mayeda, T.K., 1963, The use of bromine pentafluoride in the extraction of oxygen from oxides and silicates for isotopic analysis. Geochimica et Cosmochimica Acta, vol. 27, p.43-52.

Craig, H., 1961, Isotopic variations in meteoric waters. Science, vol. 133, p.1702-1703.

Craig, H., 1963, The isotopic geochemistry of water and carbon in geothermal areas. In, E. Tongiorgi (editor), Nuclear Geology on Geothermal Areas - Spleto 1963, p. 17-53.

Criss, R.E., Taylor, H.P. Jr., 1986, Meteoric hydrothermal systems. In, J.W. Valley, H.P. Taylor Jr., J.R. O'Neil (editors, Stable Isotopes In High Temperature Geological Processes, Mineralogical Society of America, Reviews in Mineralogy, Volume 16, p. 373-423.

Drummond, S.E., Ohmoto, H., 1985, Chemical evolution and mineral deposition boiling hydrothermal systems. Economic Geology, vol. 80, p. 126-147

Fournier, R.O., 1985, Carbonate transport and deposition in the epithermal environment. In, B. R. Berger, and P.M. Bethke (eds.), Geology and geochemistry of epithermal systems, Society of Economic Geologists, Reviews in Eco Geology, vol. 2, p. 63-72.

French, B.M., 1966, Some geological implications of equilibrium between graphite and a C-H-O gas phase at high temperatures and pressures. Reviews in Geophysics, vol. 4, p. 223-253.

Friedman, I., O'Neil, J.R., 1977, Compilation of stable isotope fractionation factors of geochemical interest. In, M. Fleisher (editor), Data of Geochemistry, Sixth edition, U.S. Geological Survey Profesional Paper 440-KK, p. KK1-KK12.

Giggenbach, W.F., 1980, Geothermal gas equilibria. Geochimica et Cosmochimica Acta, vol. 44, p. 2021-2032.

Godwin, C.I., Watson, P.H., Shen, K., 1986, Genesis of the Lass vein system, Beaverdell silver camp, south-central British Columbia: Canadian Journal of Earth Sciences, vol. 23,p. 1615-1626.

Green, L.H., 1971, Geology of Mayo Lake, Scougale Creek and McQuesten Lake map areas, Yukon Territory. Geological Survey of Canada Memoir 357, 72 pages.

Hedenquist, J.W., Henley, R.W., The importance of CO2 on freezing point measurements of fluid inclusions: evidence from active geothermal systems and implications for epithermal ore deposition. Economic Geology, vol. 80, p. 1379-1406.

Hitchon, B., Krouse, H.R., 1972, Hydrogeochemistry of surface waters of the Mackenzie River drainage basin Canada, III. Stable isotopes of oxygen, carbon and sulfur. Geochimica et Cosmochimica Acta, vol. 36, p. 1337-1358.

Holland, H.D., Malinin, S.D., 1979, The solubility and occurrence of non-ore minerals. In, H.L. Barnes, Geochemistry of Hydrothermal Ore Deposits, John Wiley and Sons Ltd., p. 461-508.

Kennedy, G.C., 1950, A portion of the system silica-water. Economic Geology, vol. 45, p. 629-653.

Kerrich, R., 1987, The stable isotope geochemistry of Au-Ag deposits in metamorphic rocks. In, T.K. Kyser (editor), Mineralogical Association of Canada Short Course in Stable Isotope Geochemistry of Low Temperature Fluids, vol. 13, p. 287-336.

Larson, P.B., Taylor, H.P. Jr., 1987, Solfataric alteration in the San Juan mountains, Colorado: Oxygen isotope variations in a boiling hydrothermal environment. Economic Geology, vol. 82, p. 1019-1036.

Leach, D.L., Landis, G.P., Hofstra, A.H., 1988, Metamorphic origin of the Coeur d'Alene base- and precious-metal veins in the Belt basin, Idaho and Montana.Geology, vol. 16, p. 122-125.

Lennan, W.B., 1986, Ray Gulch tungsten skarn deposit, Dublin Gulch area, central Yukon. In, J.A. Morin, Mineral Deposits of the Northern Cordillera, Canadian Institute of Mining and Metalurgy, Special Volume 37, p. 245-254.

Lynch, G., 1986, Mineral zoning in the Keno Hill Ag-Pb-Zn mining district, Yukon. In, Yukon Geology Volume 1, Exploration and Geological Services Division, Yukon, Indian and Northern Affairs Canada, p. 89-97.

Matsuhisa, Y., Goldsmith, J.R., Clayton, R.N., 1979, Oxygen isotopic fractionation in the system quartz-albite-anorthite-water. Geochimica et Cosmochimica Acta, vol. 43, p. 1131-1140.

McCrea, J.M., 1950, On the isotopic chemistry of carbonates and a paleotemperature scale. Journal of Chemical Physics, vol. 18, p. 849-857.

McTaggart, K.C., 1960, The geology of Keno and Galena Hills, Yukon Territory. Geological survey of Canada Bulletin 58.

Monger, J.W.H., Price, R.A., Tempelman-Kluit, D.J., 1982, Tectonic accretion and origin of the two major metamorphic and plutonic welts in the Canadian Cordillera. Geology, vol. 10, p. 70-75.

Morton, R.D., Changkakoti, A., 1987, The possible roles of Precambrian biota in the origin of magmatogene and hydrothermal silver-bearing vein deposits. Canadian Journal of Earth Sciences, vol. 24, p. 291-295.

Nabelek, P.I., 1987, General equations for modelling fluid/rock interaction using trace elements and isotopes. Geochimica et Cosmochimica Acta, vol. 51, p. 1765-1769.

Nesbitt, B.E., Murowchick, J.B., Muehlenbachs, K., 1986, Dual origins of lode gold deposits in the Canadian Cordillera. Geology, vol. 14, p. 506-509.

Nockleberg, W.J., 1973, CO_2 as a source of oxygen in the metasomatism of carbonates. American Journal of Science, vol. 273, p. 498-514.

Ohmoto, H., Kerrick, D., 1977, Devolitization equilibria in graphitic systems. American Journal of Science, vol. 277, p. 1013-1044.

Ohmoto, H., Rye, R.O., 1979, Isotopes of sulfur and carbon. In H.L. Barnes (editor), Geochemistry of hydrothermal ore deposits. John Wiley and Sons, New York, p. 509-567.

Poulton, T.P., Tempelman-Kluit, D.J., 1982, Recent discoveries of Jurassic fossils in the Lower Schist division of central Yukon. In Current Research Part C, Geological Survey of Canada Paper 82-1c, p. 91-94.

Reed, M.H., Spycher, N.F., 1985, Boiling, cooling, and oxidation in epithermal systems: numerical modelling aproach. In, B. R. Berger, and P.M. Bethke (eds.), Geology

and geochemistry of epithermal systems, Society of Economic Geologists, Reviews in Economic Geology, vol. 2, p. 249-272.

Rosenbaum, J., Sheppard, S.M.F., 1986, An isotopic study of siderites, dolomites and ankerites at high temperatures. Geochimica et Cosmochimica Acta, vol. 50, p.1147-1150.

Rye, R.O., Ohmoto, H., 1974, Sulfur and carbon isotopes and ore genesis: a review. Economic Geology, vol. 69, p. 826-842.

Sheppard, S.M.F., 1986, Characterization and isotopic variations in natural waters. In, J.W. Valley, H.P. Taylor Jr., J.R. O'Neil (editors), Stable Isotopes In High Temperature Geological Processes, Mineralogical Society of America, Reviews in Mineralogy, Volume 16, p. 165-184.

Sinclair, A.J., Tessari, O.J., Harakal, J.E., 1980, Age of Ag-Pb-Zn mineralization, Keno Hill-Galena Hill area, Yukon Territory. Canadian Journal of Earth Sciences, vol.17, p. 1100-1103.

Taylor, H.P. Jr., 1974, The application of oxygen and hydrogen isotope studies to the problems of hydrothermal alteration and ore deposition. Economic Geology, vol. 69., p. 843-883.

Taylor, H.P. Jr., (1977), Water/rock interactions and the origin of H_2O in granitic batholiths. Journal of the Geological Society of London, vol. 133, p. 509-558.

Tempelman-Kluit, D.J., 1970, Stratigraphy and Structure of the "Keno Hill Quartzite" in Tombstone River-Upper Klondike River Map Areas, Yukon Territory (116 B/7, B/8). Geological Survey of Canada, Bulletin 180, 102 pages.

Tempelman-Kluit, D.J., 1979, Transported cataclasite, ophiolite and granodiorite in Yukon: evidence of arc continent collision. Geological Survey of Canada Paper 79-14, 27 pages.

Trommsdorff, V., Skippen, G., 1986, Vapour loss ("boiling") as a mechanism for fluid evolution in metamorphic rocks. Contributions to Mineralogy and Petrology, vol. 94, p. 317-322.

Truesdell, A.H., 1974, Oxygen isotope concentrations and activities in aqueous salt solutions at elevated temperatures: consequences for isotope geochemistry. Earth and Planetary Sciences Letters, vol. 23, p. 387-396.

Truesdell, A.H., Nathenson, M., Rye, R.O., 1977, The effects of subsurface boiling and dilution on the isotopic compositions of Yellowstone thermal waters. Journal of Geophysical Research, vol. 82, p. 3694-3704.

Vine, J.D., Tourtelot, E.B., 1970, Geochemistry of black shale deposits-a summary report. Economic Geology, vol. 65, p. 253-272.

Vogel, J.C., Grootes, P.M., Mooke, W.G., 1970, Isotopic fractionation between gaseous and dissolved carbon dioxide. Zeit. Physik, vol. 230, p. 225-238.

Watson, K.W., 1986, Silver-lead-zinc deposits of the Keno Hill - Galena Hill area, central Yukon. In, Yukon Geology , Volume 1; Exploration and Geological Services Division, Yukon, Indian and Northern Affairs Canada, p. 83-88.

Yardley, B.W.D., Bottrell, S.H., 1988, Immiscible fluids in metamorphism: implications of two phase flow for reaction history. Geology, vol. 16, p. 199-202.

Zen, E-an, 1963, Components, phases and criteria of chemical equilibrium in rocks. American Journal of Science, vol 261, p. 929-942.

CHAPTER 7

GENERAL DISCUSSION, SUMMARY, AND CONCLUSIONS

DISCUSSION AND SUMMARY

Different aspects of the orebodies from the Keno Hill district have been investigated through field and laboratory methods. The topics covered include structural controls of veins, mineralogical zoning, fluid inclusion characteristics of quartz and siderite, as well as stable isotope geochemistry. In this section, these different aspects of the deposits are examined collectively, to expand upon what has already been said concerning the nature and the origin of the deposits. Areas of study which need more research are also indicated. A comparison of fluid inclusion characteristics between similar Ag-Pb-Zn vein systems from various districts is also included in this section.

Shear zones are widely recognized as being important in localizing mineral deposits (Newhouse, 1948). Not only do large volumes of fractured rock create passageways for mineralizing fluids, shear zones may also establish fluid pressure gradients because of volumetric changes. Changes in shear zone volume may cause expulsion or attraction of fluids, providing a driving mechanism for flowing systems (Sibson et al., 1975). Brittle shear zones are naturally most important in high level epithermal systems (Sibson, 1987); whereas, brittle-ductile shear zones are more characteristic of deeper mesothermal systems (Roberts, 1987; Sibson et al., 1988). Metasomatism and material transfer across shear zone boundaries (Beach, 1976) likely contribute to ore-forming processes as well.

In the Keno Hill district, two conjugate shear zones of a contrasting nature affected the overall hydrothermal evolution of the system; the ore deposits are contained within an upright fault dominated shear zone, whereas the core of the system is within a zone of brittle-ductile transcurrent shear which is characterized by similar folding and the rotation of early thrust-related fold axes. District scale mineral zoning corresponds in part to the

structural domains; quartz-feldspar veins are contained within the region of brittle-ductile shear; carbonate veins appear at the margin of this zone and extend into the brittle domain of the mining district where sulfides and sulfosalts abound. Textural evidence indicates that precipitation of hydrothermal minerals coincided with brittle faulting, but largely post-dated ductile rotational shear. Brittle faulting and fracturing formed later than the ductile deformation, in a sequential manner which is typical of conjugate shear sets (Ramsay, 1980). The intrusion of the Mayo Lake Pluton appears to have been largely post-kinematic with respect to ductile deformation, but further work is required to determine its full relationship to the deformation event.

The district-scale mineral zoning is thought to reflect chemical evolution and fluid flow in a fossil hydrothermal system. Possible mechanisms for fluid flow, outlined below, include structural-related volume changes, a pluton-related heat anomaly, and fluid pressure gradients established from the formation of CO_2. The mineral zoning may actually be viewed in two manners, either as being zoned away from the Mayo Lake Pluton, or as being zoned away from the eastern structural domain of rotational shear. Both views are in part correct, and the question arises then as to which feature was more important in influencing the hydrothermal system. The late timing for the hydrothermal activity and the Mayo Lake pluton argue for the pluton as having been the principal driving mechanism for the system, coupled with active faulting. However, the large scale of the hydrothermal system corresponds more closely to the scale and distribution of the structural domains, and the mineral zoning may alternatively be interpreted as being associated to broad hydrothermal metasomatism related to deformation, with the intrusion of the pluton as a further late stage consequence. Another hypothesis as to why large scale fluid movement occurred, is that the system may have been driven by chemical reactions; because of the high partial pressure of CO_2, the production of CO_2 at different rates in different parts of the system could have established fluid pressure gradients resulting in

fluid flow. Additional study is needed to more fully assess the true driving mechanism of the system.

A nearly complete cross-section of the classic hydrothermal zoning sequence is preserved in the Keno Hill district. This is due mainly to the lateral distribution of the zones, and the stratigraphic restriction of the system to the moderately dipping Keno Hill Quartzite unit. Mineral zones, which are most often thought to be stacked vertically, are spread laterally here. The feldspar veins near the pluton and the few cassiterite-bearing quartz veins are characteristic of deeper systems; the quartz-calcite veins with minor epidote, tourmaline, and sulfides are similar in appearance to mesothermal precious metal deposits. The zoning progresses further to the Ag-Pb-Zn orebodies, and ends with the "epithermal" assemblage which occurs within the same altitude range as all of the other zones, in contrast to the traditional sense of the terminology. Zoning models in general are most often intended for the vertical extrapolation of mineralogical assemblages to depth, but in this case the models apply as well to the lateral direction. From a lateral perspective, the position of the Ag-Pb-Zn orebodies in the Keno Hill district matches the early vertical models of Spurr (1907, 1912) with a position between the 'higher' epithermal veins and 'lower' mesothermal and plutonic assemblages. More work is needed on refining the mineralogical zonation in terms of solid solutions and compositions of phases from microprobe analyses. Initial work on tetrahedrite composition shows a clear zonation, and might be established as well in other minerals such as sphalerite and carbonates.

The identification of similar zoning patterns in the Slocan and Coeur d'Alene mining districts, at a similar scale, indicate that the zoning model has widespread applicability and is thus useful for exploration.

Fluid inclusion data are available from other silver districts in the Omenica Crystalline Belt, to which the fluid inclusion data of the Keno Hill district can be compared. From the Beaverdell mining camp of Southern British Columbia, Godwin et al. (1986) report on fluid inclusions in quartz and sphalerite samples from two generations.

The early assemblage has inclusions which homogenize near 285° C, contain variable amounts of CO_2, and have a generally high salinity up to 15 weight percent NaCl equivalent. The transition to the ore stage is thought to have been through boiling and mixing, producing inclusions with a lower salinity near 7 weight % NaCl equivalent, negligible CO_2, and a lower homogenization temperature of approximately 225° C. In the Coeur d'Alene district of Idaho, Leach et al. (1988) have studied fluid inclusions from quartz. Their type 1 inclusions have X_{CO_2} = 0.05 to 0.15 with minor N_2, CH_4, and other light chain hydrocarbons, 5 to 10 weight percent NaCl equivalent, and homogenize in the range 225° - 300° C. Type 2 inclusions are gas dominated and may coexist with type 1, and are interpreted to indicate boiling in the system. Minimum pressure estimates are on the order of 1500 bars. Type 3 are dilute water dominated secondary inclusions. In the Deer Trail vein of Washington State, Fluet (1986) report on inclusions mainly from quartz. In the pre-ore stage, inclusions homogenize near 300° C, have salinities of approximately 8 weight percent NaCl equivalent and have a CO_2 content of up to X_{CO_2} = 0.10. Pressure is thought to have been within the interval 500 to 1000 bars. In the ore stage, inclusions homogenize between 150° - 250° C, have a lower salinity near 6 weight percent NaCl equivalent and a variable but lower CO_2 content. Inclusions from a post-ore stage of fluids are cooler (<150° C), dilute (<3 wt. percent NaCl equivalent) with negligible CO_2. Boiling was not indicated. From the Slocan district of Southern British Columbia, Brame (1979) reports on fluid inclusions in quartz which homogenize over the range 157° - 277° C. Most have high to very high salinity, up to 40 weight percent NaCl equivalent has been estimated, and daughter crystals of halite, sylvite and an unspecified sulfate are reportedly common. Some CO_2 in the inclusions has been identified. Variable gas ratios and the homogenization of some inclusions to vapor are cited as clear evidence of boiling (Brame, 1979).

In the ore veins of the Keno Hill district, quartz contains inclusions which homogenize mostly between 250° - 310° C, have CO_2 up to X_{CO_2} = 0.25, and have a

variable salinity between 1 to 14 weight percent NaCl equivalent. Coexisting gas-rich inclusions which homogenize to vapor indicate boiling conditions. Pressure determinations show that boiling began near 1500 bars. Boiling resulted in the precipitation of siderite which contains inclusions that homogenize mostly between 250° - 280° C, have $X_{CO_2} < 0.01$, and are generally saline with between 10 to 15 weight percent NaCl equivalent. Late stage quartz contains lower temperature, dilute inclusions with minor CO_2.

A considerable degree of consistency is seen in the fluid inclusion data from the various districts. The high temperature end of the spectrum for homogenization temperatures falls within the relatively narrow range of 277° - 310° C. A moderate to high salinity is reported from all of the districts, with very high salinities recorded in the Slocan veins only. Variable but often substantial quantities of CO_2 is a common trait. Boiling is cited as an important ore-forming process in all districts except for the Deer Trail vein. High pressures at the beginning of boiling have been determined from the Keno Hill district (1500 bars) and the Coeur d'Alene district (1500 bars minimum). Influx of a cooler late stage dilute water is recorded in all systems except for the Slocan veins. Mixing with this late stage fluid is thought to have been an important process in the Deer Trail, Beaverdell, and Keno Hill vein systems, but later in time and unrelated in the Coeur d'Alene veins.

All of these vein systems likely formed at considerable depth; this is indicated because in general high pressure conditions are required for saline water solutions to dissolve even small quantities of CO_2 (Bowers and Helgeson, 1983), otherwise boiling would occur. Boiling would seem to be almost inevitable for such fluids because of their high volatility, and because of their natural tendency to migrate to lower pressure areas such as fault zones.

Another common trait of all of these districts is the dominance of clastic sedimentary rocks as host rocks to the deposits. In the Keno Hill district it was demonstrated that

organic material or graphite from the host rocks was important in maintaining a high CO_2 content to the fluids, and that the high salinities achieved were likely generated through boiling as well as through reactions between water and graphite. With similar fluid characteristics recorded in all districts, it seems likely that reduced carbon in the host rocks from all of these districts may have had a similar influence on the mineralizing fluids. Furthermore organic carbon is recognized as a general metal "sink", and the selective alteration of such material over broad areas in large scale hydrothermal systems may account for the source of the metals in the orebodies.

The fluid inclusion data from the Keno Hill mining district provides further information about the importance of active faulting during the mineralizing process through the pressure determinations. At local sites the pressure drop is estimated to have been by at least a factor of eleven times, from near 1500 bars to less than 130 bars. This certainly would have caused a great deal of suction on the fluids, likely influencing and driving fluid migration. The hypothesis of considerable fluid pressure drops during active faulting (Sibson, 1987) appears to apply here, and is consistent with the textural data presented in the structural analysis indicating the overlap in time between hydrothermal activity and faulting.

Measurements of carbon isotopes from siderite and calcite indicate that organic or reduced carbon such as graphite was the principal source of carbon in the fluids. Fluctuations in isotopic signatures likely reflect variations in oxygen fugacity. The dominance of CO_2 over CH_4 as observed in the fluid inclusions indicates that relatively oxidizing conditions predominated. This may have been established in the fluids because of the presence of magnetite in the host rocks reported from the quartzite and greenstone lenses (McTaggart, 1960). Another factor which may have contributed in maintaining $CO_2 > CH_4$ is the greater volatility of the reduced species H_2 and CH_4, which helps in maintaining oxidizing conditions in the residual fluids (Drummond and Ohmoto, 1985). Furthermore, if meteoric water was relatively oxidized, the influx of deeply circulating

meteoric waters is another means in which CO_2 may have been produced in excess of CH_4; this would appear to have been a real possibility as $\delta^{18}O$ values for late quartz indicate that meteoric waters were a significant component of at least the late stage mineralization.

Broad variations in $\delta^{18}O_{quartz}$ recorded in the Keno Hill veins correspond to a large degree with the mineralogical zonation of the district. Contour patterns also display a likely fault structure which was not detected in its full extent during the field work, and may be interpreted to have acted as a major conduit for circulating fluids.

CONCLUSIONS

Orebodies of the Keno Hill mining district are closely constrained by structure. Mineralized Ag-Pb-Zn veins occupy northeast striking, sinistral strike-slip faults. These form a conjugate set to the brittle-ductile shear of the "eastern structural domain". The upright shear overprints early, shallow dipping thrust-related fabrics, and appears to have formed in association with a lateral discontinuity in the thrust system. The eastern structural domain is characterized principally by the rotation of early isoclinal fold axes along a great circle, by a widespread upright crenulation cleavage, and by similar folding. Faulting and joint formation typify the later stages of shear. As well as being structurally controlled, faults, fractures and veins are lithologically restricted, mainly to the the graphitic Keno Hill Quartzite unit of Mississippian age.

The entire vein system is mineralogically zoned, and is continuous along the quartzite for 40 km. Veining is contemporaneous with and zoned away from the Mayo Lake Pluton (81 Ma). The pluton and surrounding quartz-feldspar veins post-date rotational shear. Some overlap is apparent though in the timing of brittle strike-slip faulting, and hydrothermal activity in the mining district. Veining progresses further outwards from the pluton to carbonate-Ag-Pb-Zn veins in the mining district, and end with distal epithermal veins.

Seven mineralogical zones have been defined. Key index minerals are underlined below for emphasis. The dominant groups, progressing outward from the pluton, are: 1) quartz-feldspar veins with minor epidote, tourmaline, apatite, pyrite, and rare ilmenite; 2) quartz veins with muscovite and sparse pyrite, arsenopyrite, and cassiterite; 3) quartz-calcite-epidote veins with also pyrite, arsenopyrite and chalcopyrite; 4) veins containing jamesonite, boulangerite, arsenopyrite, sphalerite, pyrite, chalcopyrite, tetrahedrite and native gold in a gangue of quartz and calcite; 5) siderite veins with calcite, galena, sphalerite, tetrahedrite, pyrite, pyrrhotite, and arsenopyrite; 6) same as (5) but without

arsenopyrite, pyrrhotite or calcite; 7) quartz veins containing pyrargyrite, polybasite, stephanite, acanthite and native silver, as well as pyrite, marcasite, freibergite, chalcopyrite, stibnite, anomalous gold values, some barite and clay alteration. Paragenetically, the veins farthest from the pluton are also generally younger.

Tetrahedrite is distributed throughout the mining district, along the 25 km long outer portion of the hydrothermal system, and is the principal Ag-bearing ore mineral. Both Ag/Cu and Fe/Zn ratios increase in tetrahedrite towards the outer extremity of the system, where freibergite dominates over tetrahedrite. The Sb/As ratio is high in all samples.

In the orebodies, three stages of gangue mineralogy were used in a fluid inclusion investigation, comprising (1) early coarse grained quartz, (2) siderite intergrown with the ore and (3) late stage finer grained quartz from the veins of epithermal character. Fluids are distinct in all three stages, but a considerable degree of overlap is also observed. Boiling, a loss of CO_2, and an increase in salinity characterize the transition from early quartz to siderite; mixing and the influx of dilute meteoric water typifies the late quartz stage.

Pressure determinations obtained on the two phase boundary in the system H_2O-CO_2-NaCl, indicate that fluid pressure dropped during vein opening, from approximately 1500 bars in early quartz to less than 130 bars in siderite. Initial boiling with 15-20 % water vaporization decreased the liquid temperature from 310° C to 250° C. The boiling also caused a loss of CO_2, from $X_{CO_2} = 0.25$ to $X_{CO_2} = 0.01$, which produced a higher pH, stabilized carbonates and destabilized chloride-metal complexes. Increases in salinity indicate that heat gained from the host rocks allowed for extensive boiling to have occurred with limited cooling. High salinities are recorded in the fluid inclusions within siderite, near 10 to 15 weight percent NaCl equivalent, up from 1 to 5 weight percent in the early high temperature fluids.

Graphite in the host rocks had a strong influence on the hydrothermal system, buffering the initial fluids to a high CO_2 content, allowing for deep seated boiling to have occurred. Post-boiling equilibration of water with the graphitic host, producing CO_2 and

CH_4, may also have been a significant factor in increasing the salinity of the fluids. Furthermore, widespread selective alteration of graphite in large quantities, as indicated by the abundance of CO_2 in the fluids and depletion of graphite from some alteration haloes, is thought to have been an effective means of releasing metals into the solutions.

Both the mineralogical zoning and fluid inclusion characteristics of the Keno Hill mining district are similar to those other Ag districts from the Omenica Crystalline Belt. Other similarities between the various districts include host rock types and structural controls.

Stable isotopes were used during the course of this study to help in identifying fluid sources, assess water-rock interaction, establish continuity between mineralogical zones, and to help in identifying dynamic hydrothermal processes such as boiling, mixing, and fluid flow. The $\delta^{18}O_{quartz}$ from veins near the pluton increases outwards from +10.6 per mil to +20.0 per mil, due to cooling of the hydrothermal fluids, and exchange with the quartzite. Contours of isotope values outline broad paths of fluid movement within the quartzite, and outline a suspected permeable fault or fracture zone. Proceeding still further from the pluton, $\delta^{18}O_{quartz}$ then decreases from +20.0 to +10.1 per mil to the outer edge of the system where the orebodies are found. The presence of meteoric water during vein formation is indicated in the veins furthest from the pluton, where late stage quartz has oxygen isotope values as low as $\delta^{18}O_{SMOW} = -7.1$ per mil. The outward decreasing trend for quartz appears then to have been established in one of two ways; 1) by mixing of isotopically light meteoric water with the exchanged fluids that were in isotopic equilibrium with the quartzite; 2) extensive reaction of water and graphite during the formation of CO_2 and CH_4 may have fractionated the water to a greater degree in the outer portion of the system.

Cooling due to boiling of the fluids had an effect on the isotopic signature of quartz and carbonates. Superimposed on the outward decreasing $\delta^{18}O_{quartz}$ trend are local isotopically distinct veins, which are also silver-rich. The quartz from these veins is higher

in $\delta^{18}O$ values by up to 4 per mil, due to a minimum of 10 to 25 percent boiling of the fluids and associated cooling. Siderite formed as a late stage product of the boiling event, during production of CO_2 and CH_4, resulting in trends of ^{18}O depletion and ^{13}C enrichment in siderite.

A closed system boiling model, together with estimates of water loss from reaction with graphite, indicate that greater than 50% of the original water in the ore fluid was removed. Relatively saline mineralizing fluids resulted. The reaction of water with a reduced organic carbon source is indicated by the negative $\delta^{13}C_{PDB}$ values for the hydrothermal carbonates, from -12.9 to -4.0 per mil. Variations in the carbon isotopes are likely due to fluctuating CO_2/CH_4 ratios in the boiling system, reflecting the contrasting volatility of the gas pair.

REFERENCES

Beach, A., 1976, The interelations of fluid transport, deformation, geochemistry and heat flow in early Proterozoic shear zones in the Lewisian complex. Philosophical Transactions of the Royal Society of London, vol. A280, p. 569-604.

Bowers, T.S., Helgeson, H.C., 1983, Calculation of the thermodynamic and geochemical consequences of nonideal mixing in the system H_2O-CO_2-NaCl on phase relations in geologic systems. Equation of state for H_2O-CO_2-NaCl fluids at high pressures and temperatures. Geochimica et Cosmochimica Acta, vol. 47, p. 1247-1275.

Brame, S., 1979, Mineralization Near the Northern Margin of the Nelson Batholith: [MSc thesis], The University of Alberta, Edmonton Alberta, 146 pages.

Drummond, S.E., Ohmoto, H., 1985, Chemical evolution and mineral deposition in boiling hydrothermal systems. Economic Geology, vol. 80, p. 126-147.

Fluet, D.W., 1986, Genesis of the Deer Trail Zn-Pb-Ag Vein Deposit, Washington, U.S.A.. Unpublished Masters thesis, University of Alberta, Edmonton, Alberta, 129 pages.

Godwin, C.I., Watson, P.H., Shen, K., 1986, Genesis of the Lass vein system, Beaverdell silver camp, south-central British Columbia: Canadian Journal of Earth Sciences, vol. 23,p. 1615-1626.

Leach, D.L., Landis, G.P., Hofstra, A.H., 1988, Metamorphic origin of the Coeur d'Alene base- and precious-metal veins in the Belt basin, Idaho and Montana. Geology, vol. 16, p. 122-125.

McTaggart, K.C., 1960, The geology of Keno and Galena Hills, Yukon Territory. Geological survey of Canada Bulletin 58.

Newhouse,W.H., 1942, Ore deposits as related to structural features. Princeton University Press, Princeton, New Jersey, 280 pages.

Ohmoto, H., Rye, R.O., 1970, The Bluebell mine, British Columbia: 1. Mineralogy, paragenesis, fluid inclusions, and the isotopes of hydrogen, oxygen and carbon. Economic Geology, vol. 65, p. 417-437.

Ramsay, J.G., 1980, Shear zone geometry: a review. Journal of Structural Geology, vol. 2, p. 83-89.

Roberts, R.G., 1987, Ore deposit models # 11. Archean lode gold deposits. Geoscience Canada, vol. 14, p. 37-52.

Sibson, R.H., 1986, Brecciation processes in fault zones. Pure and Applied Geophysics, vol. 124, p.159-175.

Sibson, R.H., 1987, Earthquake rupturing as a mineralizing agent in hydrothermal systems. Geology, v. 15, p. 701-704.

Sibson, R.H., Moore, J.M., Rankin, A.H., 1975, Seismic pumping-a hydrothermal fluid transport mechanism. Journal of the Geological Society of London, vol. 131, p. 653-659.

Sibson, R.H., Robert, F., Poulsen, K.H., 1988, High-angle reverse faults, fluid pressure cycling, and mesothermal gold-quartz deposits. Geology, vol. 16, p. 551-555.

Spurr, J.E., 1907, A theory of ore deposition. Economic Geology, vol. 2, p. 781-795.

Spurr, J.E., 1912, Theory of ore deposition. Economic Geology, vol. 7, p. 485-492.

APPENDIX 1

FLUID INCLUSION HEATING/FREEZING DATA

Fluid inclusion heating/freezing measurements: P, fluid inclusion of primary origin; S, secondary origin; A, uncertain or ambiguous origin; vol, volume percent of gas bubble in inclusion at room temperature (R), or at 40° C (40); Th_T, total homogenization temperature to liquid (L), or to vapor (V); Th CO_2, homogenization temperature of CO_2 inner bubble, to liquid (L), or to vapor (V); Tm cl, clathrate melting temperature; Tm ice ice melting temperature; Tm CO_2, CO_2 melting temperature; NaCl, weight percent NaCl equivalent relative to water; XCO_2, mole fraction CO_2 in H_2O-CO_2 mixture; P, pressure estimate in bars.

SAMPLE	origin	type	vol %		Th_T (°C)		Th CO_2 (°C)		Tm cl (°C)	Tm ice (°C)	Tm CO_2 (°C)	NaCl (wt %)	XCO_2	P (bars)
HOMESTAKE-1	A	I	35	R	300.0	D	23.8	L	11.0		-57.4			
HOMESTAKE-2	A	II	31	R	297.4	L	26.8	V	10.2		-57.1		0.07	487
HOMESTAKE-3	A	II	31	R	305.0	L	27.0	V	10.8		-57.1		0.07	586
HOMESTAKE-4	A	I	30	R	309.7	L	26.0	L	10.3		-57.2			
HOMESTAKE-5	A	II	32	R	310.8	V	26.2	S	10.3		-57.1		0.07	575
HOMESTAKE-6	A	I	15	R	297.2	L	25.3	L	10.4		-57.4			
HOMESTAKE-7	A	II	15	R		D	26.7	V	10.9		-56.9			
HOMESTAKE-8	A	I	20	R		D	23.5	L	10.4		-57.4			
HOMESTAKE-9	A	I	20	R		D	25.8	L	11.4		-57.2			
HOMESTAKE-10	A	I	20	R		D	25.7	L	10.8		-57.0			
HOMESTAKE-11	A	II	25	R	305.5	L								
HOMESTAKE-12	A	II	32	R	294.6	L								
HOMESTAKE-13	A	II	35	R	306.0	L								
HOMESTAKE-14	S	I	35	R	314.4	V								
HOMESTAKE-15	A	II	30	R	287.9	L								
HOMESTAKE-16	A	II	20	R	294.1	L								
HOMESTAKE-17	A	I	43	R	309.6	L								
HOMESTAKE-18	A	I	35	R	306.3	L								
HOMESTAKE-19	A	I	30	R	314.1	L								
HOMESTAKE-20	A	I	35	R	313.0	L								

SAMPLE	origin	type	vol %		Th_T (°C)		Th CO_2 (°C)		Tm cl (°C)	Tm ice (°C)	Tm CO_2 (°C)	NaCl (wt %)	XCO_2	P (bars)
HOMESTAKE B-1	P	I	30	R	293.6	L	24.8	L	10.2		-58.6	0.0		
HOMESTAKE B-2	P	I	40	R	292.8	L	24.8	L	9.8		-58.3	0.4		
HOMESTAKE B-3	P	I	25	R	294.8	L	24.2	L	9.6		-58.5	0.8		
HOMESTAKE B-4	P	I	25	R	305.1	L	24.8	L	9.0		-58.3	2.0		
HOMESTAKE B-5	P	I	48	R	311.3	L	24.9	L	9.0		-58.1	2.0	0.23	1556
HOMESTAKE B-6	P	I	25	R	297.0	L	25.2	L	9.0		-58.2	2.0		
HOMESTAKE B-7	P	I	30	R	297.5	L	25.1	L	9.7		-58.1	0.6		
HOMESTAKE B-8	P	II	29	R	303.3	L	26.1	V	9.3		-58.2	1.4	0.06	582
HOMESTAKE B-9	P	I	25	R	299.0	L	24.7	L	9.4		-58.1	1.2		
HOMESTAKE B-10	P	II	27	R	292.7	L	26.0	V	9.5		-57.9	1.0	0.06	512
HOMESTAKE B-11	P	II	28	R	298.0	L	26.1	V	9.6		-57.6	0.8	0.06	540
SADIE A-2	A	I	36	40	291.0	L	26.2	L	9.0		-56.8	2.0	0.15	1527
SADIE A-3	A	I	33	40	300.6	V	28.6	L	9.1		-57.0	1.8	0.13	1515
SADIE A-4	A	I	36	40	287.5	V	25.6	L	9.1		-56.6	1.8	0.15	1527
SADIE A-5	A	I	48	40	307.0	V	24.4	L	9.0		-57.0	2.0	0.22	1558
SADIE A-6	A	I	55	40	324.7	V	22.1	L	8.0		-56.7	4.0	0.28	1767
SADIE A-7	A	I	48	40	300.0	V	22.7	L	7.8		-56.9	4.3	0.23	1546
SADIE A-8	A	I	46	40	297.6	V	23.9	L	10.0		-57.0	0.0	0.21	1556
SADIE A-9	A	I	50	40	310.6	V	24.7	L	9.6		-57.1	0.8	0.23	1553
SADIE A-10	A	I	53	40	311.0	V	23.9	L	9.6		-57.1	0.8	0.26	1552
SADIE A-11	A	I	49	40	304.4	S	24.1	L	9.8		-56.9	0.4	0.23	1557

SAMPLE	origin	type	vol %		Th_T (°C)		Th CO_2 (°C)		Tm cl (°C)	Tm ice (°C)	Tm CO_2 (°C)	NaCl (wt %)	XCO_2	P (bars)
BLACK CAP A-1	P	I	49	40	317.8	L	25.8	L	9.3		-57.0	1.4	0.22	1556
BLACK CAP A-2	P	II	28	40	293.0	V	26.5	V	9.7		-57.0	0.6	0.06	520
BLACK CAP A-3	P	II	32	40	317.8	V	26.0	V	8.9		-56.8	2.2	0.07	586
BLACK CAP A-4	P	II	40	40	330.2	V	25.9	V	6.2		-56.8	7.1	0.07	638
BLACK CAP A-5	P	III	40	R	362.9	L			7.2			5.4		
BLACK CAP A-6	P	I	50	40	318.2	L	25.3	L	8.7	-7.4	-56.9	2.6	0.24	1555
BLACK CAP A-7	P	II	55	40	323.6	S	22.9	V	9.4		-57.4	1.4		
BLACK CAP A-8	P	II	30	40	328.5	L	19.6	V	4.5		-56.8	9.8	0.05	556
BLACK CAP A-9	P	II	55	40	342.5	V	22.7	V	9.4		-57.5	1.4		
BLACK CAP A-10	P	I	70	40	302.7	L	22.6	L	9.3		-57.7	1.2		
LUCKY QUEEN-1	P	I	85	40	293.6	D	26.8	L	8.9		-57.4	2.2		
LUCKY QUEEN-2	P	I	36	40	300.9	S	27.3	L	8.8		-57.0	2.4	0.14	1562
LUCKY QUEEN-3	P	I	45	40	301.3	L	26.6	L	9.0		-57.2	2.0		
LUCKY QUEEN-4	P	II	27	40	288.0	L	27.0	V	10.0		-57.0	0.0	0.06	532
LUCKY QUEEN-6	P	II	30	40	313.8	L	25.8	V	9.1		-57.2	1.8	0.07	615
FLAME-MOTH-1	A	III	35	R	234.8	L				-13.3		17.3		
FLAME-MOTH-2	A	III	25	R	226.6	L				-0.8		1.4		
FLAME-MOTH -3a	A	III	30	R	311.8	L								
FLAME-MOTH -3b	A	III	20	R	294.9	L								
FLAME-MOTH -3c	A	III	30	R	307.5	L								
FLAME-MOTH -3d	A	III	40	R	310.0	L								
FLAME-MOTH -4	A	III	35	R	264.3	L				-5.4		8.4		
FLAME-MOTH -5	A	III	35	R	359.7	L				-0.5		0.9		
FLAME-MOTH -6	A	III	20	R	272.8	L				-2.6		4.3		

SAMPLE	origin	type	vol %		Th_T (°C)		$Th\ CO_2$ (°C)		Tm cl (°C)	Tm ice (°C)	$Tm\ CO_2$ (°C)	NaCl (wt %)	XCO_2	P (bars)
FLAME-MOTH -7	A	III	40	R	346.5	L				-7.6		11.2		
FLAME-MOTH -8	A	III	15	R	215.0	L								
FLAME-MOTH -9	A	III	40	R	316.8	L				-6.0		9.2		
FLAME-MOTH -10	A	III	45	R	359.8	L				-9.0		12.9		
FLAME-MOTH -11	A	III	40	40	355.0	L								
FLAME-MOTH -12	A	III	20	R	33.7	L				-2.4		4.0		
RUBY 1	A	I	85	40	307.7	V	24.8	L	9.6		-57.4	0.8		
RUBY-2	A	I	45	40	315.8	V	25.7	L	9.0		-57.4	2.0	0.20	1615
RUBY-3	A	II	30	40	305.0	V	25.2	V	9.1		-57.2	1.8		
RUBY-5	A	III	25	40	295.8	L				-7.0		10.5		
RUBY-6	A	II	46	40	315.8	V	24.7	L	8.0		-57.4	3.9	0.21	1655
RUBY-7	A	II	40	40	310.0	V	25.1	V	9.0		-57.3	2.0		
SILVER KING A-1	P	II	90	40	281.6	V	28.2	V	8.8		-58.6	2.4		
SILVER KING A-2	P	III	35	R	310.2	L			7.9		-59.0	4.1		
SILVER KING A-3	P	I	42	40	322.8	V	27.2	L	8.2		-59.2	3.6		
SILVER KING A-4	P	III	40	R	321.4	L			8.4		-58.8	3.4		
SILVER KING A-5	P	II	33	40	324.8	V	27.1	V	8.1		-57.9	3.8	0.08	639
SILVER KING A-6	P	III	45	R	309.4	L			9.1		-58.5	1.8		
SILVER KING A-7	P	VI	50	R	26.4	V	26.4	V			-57.7			
SILVER KING A-8	P	III	30	R	310.8	L			7.6		-58.1	4.7		
SILVER KING A-9	S	III	20	R	244.0	L				-1.1		2.0		

SAMPLE	origin	type	vol %		Th_T (°C)		Th CO_2 (°C)		Tm cl (°C)	Tm ice (°C)	Tm CO_2 (°C)	NaCl (wt %)	XCO_2	P (bars)
KENO 700-8	P	II	29	40	314.0	V	25.2	V	8.4		-57.0	3.4	0.06	638
KENO 700-9	P	II	28	40	312.9	S	24.8	V	8.7		-56.7	2.6	0.06	675
KENO 700-10	P	VI			25.8	V	25.8	V			-57.3			
KENO 700-11	P	III	20	R	291.0	L				-4.2		6.7		
KENO A-1	A	III	25	40	317.2	L			6.8		-57.7	6.1		
KENO A-2	S	III	20	R	267.3	L				-8.1		11.8		
KENO A-3	P	II	32	40	314.8	S	27.1	V	7.8		-57.1	4.3	0.07	583
KENO A-4	P	III	55	40	312.7	S			7.8		-57.0	4.3		
KENO A-5	P	VI	60	R	26.6	V	26.6	V	8.0		-58.4	4.0		
KENO A-6	P	VI			26.7	V	26.7	V			-58.2			
KENO A-7	P	III	25	R	336.3	L			7.2			5.4		
KENO A-8	A	II	29	40	314.0	V	25.2	V	8.4		-57.0	3.4	0.06	641
KENO A-9	A	II	45	40	312.9	S	24.8	V	8.7		-57.6	2.6		
KENO A-10	A	VI			25.8	V					-57.3			
KENO A-11	A	III	25	R	291.0	L	25.8	V		-4.2		6.7		
KENO B-1	P	I	43	40	311.2	V	25.5	L	9.6		-56.4	0.8	0.19	1661
KENO B-2	S	III	20	R	232.7	L			6.6			6.5		
KENO B-3	A	II	45	40	303.1	L	26.6	V	10.0		-56.8	0.0		
KENO B-4	P	I	43	40	322.7	V	27.8	L	9.6		-56.7	0.8	0.18	1562
KENO B-5	P	II	30	40	307.5	?	27.3	V	9.8		-56.6	0.4	0.07	639
KENO B-6	P	I	50	40	306.1	L	28.2	L						
KENO B-7	P	I	50	40	318.1	V	26.0	L						
KENO B-8	P	I	80	40	314.5	V	25.2	L						
KENO B-9	P	I	40	40	305.3	L	27.2	L						
KENO B-10	P	II	29	40	305.6	L	26.9	V	9.7		-56.6	0.6	0.07	668
KENO B-11	P	I	42	40	312.7	V	26.1	L	9.8		-56.3	0.4	0.18	1661

SAMPLE	origin	type	vol %		Th_T (°C)		Th CO_2 (°C)	Tm cl (°C)	Tm ice (°C)	Tm CO_2 (°C)	NaCl (wt %)	XCO_2	P (bars)
KENO ASP-1	S	III	15	R	233.2	L			-7.2		10.7		
KENO ASP-2	S	III	20	R	225.7	L			-6.2		9.3		
KENO ASP-3	S	III	20	R	226.9	L							
KENO ASP-4	S	III	25	R	216.9	L							
KENO ASP-5	S	III	15	R	179.8	L							
KENO ASP-6	S	III	15	R	218.1	L							
KENO ASP-7	S	III	20	R	188.0	L							
KENO ASP-8	S	III	15	R	188.5	L							
KENO ASP-9	S	III	15	R	188.6	L							
KENO ASP-10	S	III	25	R	284.6	L							
KENO ASP-11	A	III	30	R	299.9	L							
KENO ASP-12	A	III	30	R	313.1	L							
KENO ASP-13	A	III	35	R	304.3	L							
KENO ASP-14	A	III	25	R	283.7	L							
KENO ASP-15	A	III	30	R	303.8	L							
KENO ASP-16	P	III	55	R	303.1	L		11.8			0.0		
KENO ASP-17	P	III	35	R	298.5	L							
KENO ASP-18	A	III	40	R	289.5	L							
KENO ASP-19	P	III	50	R	326.7	V							
KENO ASP-20	P	III	35	R	310.5	L							
KENO ASP-21	P	III	30	R	312.7	L							
KENO ASP-22	P	III	55	R	312.8	V							
KENO ASP-23	P	III	25	R	306.8	L							

SAMPLE	origin	type	vol %		Th_T (°C)		$Th\ CO_2$ (°C)		Tm cl (°C)	Tm ice (°C)	$Tm\ CO_2$ (°C)	NaCl (wt %)	XCO_2	P (bars)
CARIBOU A5	A	III	25	R	256.0	L			4.4			10.0		
CARIBOU A6	A	III	20	R	252.7	L			5.1			8.9		
CARIBOU A7	A	III	25	R	257.0	L			4.1			10.4		
CARIBOU A8	A	III	20	R	255.7	L								
HECTOR 1	P	I	40	40	302.6	V	24.4	L	9.9		-57.1	0.2		
HECTOR 2	P	I	46	40	302.3	S	24.5	L	10.0		-56.7	0.0	0.21	1562
HECTOR 3	P	I	39	40	297.8	L	25.8	L	9.4		-56.6	1.2	0.17	1558
HECTOR 4	P	I	41	40	298.2	L	25.3	L	9.8		-57.0	0.4	0.18	1562
HECTOR 5	P	I	45	40	299.3	L	24.3	L	9.8		-57.0	0.4	0.21	1555
HECTOR 6	P	I	40	40	302.8	L	25.3	L	10.1		-57.6	0.0		
HECTOR 7	A	II	40	40	302.1	L	25.1	V	10.0		-57.5	0.0		
HECTOR 8	A	I	60	40	299.8	L	25.0	L	9.8		-57.3	0.4		
HECTOR 9	A	II	40	40	300.9	L	25.9	V	9.5		-57.1	1.0		
HECTOR 10	A	II	35	40	301.8	L	25.8	V	9.6		-57.0	0.8	0.06	574
SILVER BASIN 1	P	I	50	40	298.0	D	25.8	L	8.0		-57.2	3.9		
SILVER BASIN 2	P	I	51	40	311.1	L	23.8	L	7.8		-57.5	4.3	0.24	1557
SILVER BASIN 3	P	I	50	40	298.7	L	25.1	L	8.3		-57.2	3.4		
SILVER BASIN 4	P	I	30	40	303.4	L	25.2	L	7.9		-57.1	4.1		
SILVER BASIN 5	P	I	45	40	301.6	L	24.8	L	7.9		-57.4	4.1		
SILVER BASIN 6	P	I	52	40	314.8	L	23.0	L	8.0		-57.3	3.9	0.25	1641
SILVER BASIN 7	P	I	41	40	305.1	L	24.9	L	7.9		-57.0	4.1	0.18	1611
SILVER BASIN 8	P	I	50	40	307.8	L	25.0	L	8.3		-57.3	3.4		

SAMPLE	origin	type	vol %		Th_T (°C)		$Th\ CO_2$ (°C)	Tm cl (°C)	Tm ice (°C)	$Tm\ CO_2$ (°C)	NaCl (wt %)	XCO_2	P (bars)
BELLEKENO 1	S	III	20	R	265.1	D							
BELLEKENO 2	S	III	20	R	242.3	L			-9.2		13.1		
BELLEKENO 3	A	III	30	R	277.0	L			-9.4		13.3		
BELLEKENO 4	A	III	30	R	282.0	L			-8.6		12.4		
BELLEKENO 5	S	III	15	R	238.7	L							
BELLEKENO 6	S	III	20	R	233.5	L							
BELLEKENO 7	A	III	20	R	255.0	L			-9.4		13.3		
BELLEKENO 8	P	III	25	R	297.2	L							
BELLEKENO 9	P	III	25	R	315.1	L							
BELLEKENO 10	P	III	20	R	288.5	L							
BELLEKENO 11	A	III	15	R	255.7	L							
BELLEKENO 12	A	III	25	R	289.6	L			-7		10.5		
BELLEKENO 13	A	III	25	R	282.9	L							
BELLEKENO 14	A	III	25	R	323.5	L							
DIXIE A-1	P	III	20	R	286.0	L		5.6			8.1		
DIXIE A-2	P	III	25	R	295.7	L		5.3			8.6		
DIXIE A-3	S	III	10	R	257.3	L		8.0			3.9		
DIXIE A-4	P	III	30	R	297.4	L		4.7			9.5		
DIXIE A-5	P	III	20	R	282.0	L		5.9			7.6		
DIXIE B-1	P	III	40	R	286.7	L		7.4		-57.2	5.1		
DIXIE B-2	S	III	20	R	256.1	L		5.5			8.3		
DIXIE B-3	P	III	20	R	292.2	L		1.2			14.2		
DIXIE B-4	P	III	25	R	293.0	L		7.3			5.2		
DIXIE B-5	P	III	20	R	288.5	L		7.3			5.2		

SAMPLE	origin	type	vol %		Th_T (°C)		$Th\ CO_2$ (°C)	Tm cl (°C)	Tm ice (°C)	$Tm\ CO_2$ (°C)	NaCl (wt %)	XCO_2	P (bars)
DIXIE B-6	P	III	20	R	297.0	L		1.5			13.9		
DIXIE B-7	P	III	25	R	295.0	L		3.7			11.0		
DIXIE B-8	A	III	20	R	275.0	L		6.0			7.5		
DIXIE B-9	A	III	20	R	274.7	L							
DIXIE B-10	A	III	20	R	304.5	L							
DIXIE B-11	A	III			290.0	L							
BERMINGHAM 1	P	III	35	R	302.0	L		6.8			6.1		
BERMINGHAM 2	P	III	30	R	298.5	L		7.6			4.7		
BERMINGHAM 3	A	III	25	R	311.9	L		6.6			6.5		
BERMINGHAM 4	P	III	30	R	298.5	L		5.6			5.1		
BERMINGHAM 5	A	III	25	R	304.7	L		7.8			4.3		
BERMINGHAM 6	A	III	40	R	302.0	L		7.7			4.5		
BERMINGHAM 7	A	III	35	R	304.2	L							
BERMINGHAM 8	A	III	35	R	311.7	L							
BERMINGHAM 9	A	III	30	R	298.5	L							
BERMINGHAM 10	A	III	30	R	301.5	L							
BERMINGHAM 11	A	III	25	R	291.0	L							
BERMINGHAM 12	A	III	25	R	309.0	L							
BERMINGHAM 13	A	III	30	R	301.4	L							
BERMINGHAM 14	A	III	20	R	304.1	L							
BERMINGHAM 15	A	III	30	R	312.0	L							
BERMINGHAM 16	A	III	25	R	298.5	L							
BERMINGHAM 17	A	III	25	R	318.0	L							
BERMINGHAM 18	A	III	30	R	296.2	L							
BERMINGHAM 19	A	III	35	R	296.8	L							
BERMINGHAM 20	A	III	20	R	296.2	L							
BERMINGHAM 21	A	III	25	R	293.0	L							
BERMINGHAM 22	A	III	30	R	297.0	L							

SAMPLE	origin	type	vol %		Th_T (°C)		$Th\ CO_2$ (°C)	Tm cl (°C)	Tm ice (°C)	$Tm\ CO_2$ (°C)	NaCl (wt %)	XCO_2	P (bars)
CARIBOU 1	A	IV	15	R	225.1	L			-9.7		13.7		
CARIBOU 2	A	IV	25	R	280.1	L			-10.1		14.1		
CARIBOU 3	A	IV	20	R	256.1	L							
CARIBOU 4	A	IV	25	R	311.1	L							
BERMINGHAM 1	A	IV	15	R	267.0	L			-10.3		14.3		
BERMINGHAM 2	A	IV	15	R	269.8	L			-7.0		10.5		
BERMINGHAM 3	A	IV	20	R	274.2	L			-10.9		14.9		
BERMINGHAM 4	A	IV	30	R	262.5	L			0.0		0.0		
BERMINGHAM 5	A	IV	20	R	256.0	L			-16.2		19.8		
BERMINGHAM 6	A	IV	20	R	264.0	L			-0.3		0.5		
BERMINGHAM 7	A	IV	25	R	270.5	L							
BERMINGHAM 8	A	IV	30	R	265.7	L			0.0		0.0		
BERMINGHAM 9	A	IV	20	R	267.0	L			-0.5		0.9		
BERMINGHAM 10	A	IV	20	R	266.0	L			-10.1		14.1		
HECTOR 2	A	IV	20	R	267.0	L			-8.6		12.4		
HECTOR 3	A	IV	15	R	259.6	L			-8.4		12.2		
HECTOR 4	A	IV	30	R	276.0	L			-14.2		18.1		
HECTOR 5	A	IV	25	R	265.0	L			-10.0		14.0		
HECTOR 6	A	IV	15	R	243.0	L			-11.2		15.2		
HECTOR 7	A	IV	20	R	247.1	L			-8.2		11.9		
HECTOR 8	S	IV	20	R	233.2	L			-10.4		14.4		
HECTOR 9	A	IV	20	R	253.4	L			-8.7		12.5		
HECTOR 10	A	IV	20	R	266.3	L			-9.8		13.8		

SAMPLE	origin	type	vol %		Th_T (°C)		$Th\ CO_2$ (°C)	Tm cl (°C)	Tm ice (°C)	$Tm\ CO_2$ (°C)	NaCl (wt %)	XCO_2	P (bars)
KENO 1	P	IV	25	R	265.0	L							
KENO 2	P	IV	20	R	271.2	L		2.3			12.9		
KENO 3	P	IV	20	R	245.0	S							
KENO 4	P	IV	20	R	282.3	L		3.1			11.8		
KENO 5	P	IV	25	R	264.4	L		3.8			10.9		
KENO 6	P	IV	25	R	274.1	L		8.7			2.6		
KENO 7	P	IV	25	R	278.3	L							
KENO 8	P	IV	25	R	261.3	L		3.3			11.6		
KENO 9	P	IV	25	R	265.8	L		3.1			11.8		
KENO 10	P	IV	25	R	272.3	L		2.9			12.1		
KENO 11	P	IV	25	R	270.0	L		3.6			11.1		
KENO 12	P	IV	25	R	268.0	L		3.7			11.0		
KENO 14	P	IV	35	R	242.0	L		3.0			12.0		
SADIE LADUE 1	A	IV	30	R	280.7	L							
SADIE LADUE 2	A	IV	30	R	271.0	L			-9.6		13.5		
SADIE LADUE 3	A	IV	25	R	271.2	L			-10.2		14.2		
SADIE LADUE 4	A	IV	20	R	269.2	L			-7.3		10.9		
SADIE LADUE 5	A	IV	25	R	268.8	L			-9.9		13.9		
SADIE LADUE 6	A	IV	25	R	267.5	L			-7.8		11.5		
SADIE LADUE 7	A	IV	30	R	272.1	L			-8.5		12.3		
SADIE LADUE 8	A	IV	30	R	277.1	L			-9.6		13.5		
SADIE LADUE 9	A	IV	25	R	266.0	L			-9.0		12.9		
SADIE LADUE 10	A	IV	20	R	271.0	L			-8.8		12.6		

SAMPLE	origin	type	vol %		Th_T (°C)		$Th\ CO_2$ (°C)		Tm cl (°C)	Tm ice (°C)	$Tm\ CO_2$ (°C)	NaCl (wt %)	XCO_2	P (bars)
HUSKY R-224 1	A	V	25	R	243.0	L				-0.6		1.0		
HUSKY R-224 2	A	V	15	R	247.1	L				-0.1		0.2		
HUSKY R-224 3	A	V	10	R	226.8	L				-0.3		0.5		
HUSKY R-224 4	A	V	15	R	227.6	L				-0.4		0.7		
HUSKY R-224 5	A	V	20	R	225.4	L				-0.4		0.7		
HUSKY R-224 B-1	A	V	25	R	250.0	L			2.0			13.3		
HUSKY R-224 B-2	A	V	25	R	237.0	L								
HUSKY R-224 B-3	A	V	25	R	240.0	L			5.2	0.0		0.0		
HUSKY R-224 B-5	A	V	25	R	267.0	L				-0.2		0.3		
SILVER KING B 1	P	V	20	R	247.0	L				-2.8		4.6		
SILVER KING B 2	P	V	20	R	257.0	L				-1.0		1.7		
SILVER KING B 3	P	V	20	R	246.2	L				-0.5		0.9		
SILVER KING B 4	P	V	35	R	279.2	L				-0.1		0.2		
SILVER KING B 5	P	V	25	R	306.1	L				-1.1		1.9		
SILVER KING B 6	S	V	10	R	197.7	L								
SILVER KING B 8	S	V	10	R	207.0	L								
SILVER KING B 9	A	V	25	R	311.6	L				-0.3		0.5		
SILVER KING C 1	A	V	25	R	206.3	L				-1.8		3.1		
SILVER KING C 2	A	V	30	R	286.0	L			9.3			1.4		
SILVER KING C 3	A	V	35	R	153.7	L				-0.3		0.5		
SILVER KING C 4	A	V	15	R	152.2	L				-0.2		0.3		
SILVER KING C 5	A	VI			27.8	V	27.8	V			-56.8			
SILVER KING C 6	A	VI			27.8	V	27.8	V			-56.7			

SAMPLE	origin	type	vol %		Th_T (°C)		$Th\ CO_2$ (°C)	Tm cl (°C)	Tm ice (°C)	$Tm\ CO_2$ (°C)	NaCl (wt %)	XCO_2	P (bars)
SILVER KING C 7	A	V	20	R	237.4	L							
SILVER KING C 8	A	V	20	R	226.3	L			-0.3		0.5		
SILVER KING C 9	A	V	20	R	302.5	L							
SILVER KING C 10	A	V	15	R	210.3	L							
SILVER KING C 11	A	V	20	R	284.3	L							
SILVER KING C 12	A	V	15	R	191.1	L							
SILVER KING C 13	A	V	20	R	282.7	L			-0.4		0.7		
SILVER KING D1	S	V	25	R	187.0	L			-0.5		0.9		
SILVER KING D 2	S	V	10	R	161.0	L			-0.1		0.2		
SILVER KING D 3	S	V	30	R	222.0	L			-0.9		1.5		
SILVER KING D 4	S	V	20	R	222.8	L			-0.6		1.0		
SILVER KING D 5	P	V	15	R	194.1	L			-0.2		0.3		
SILVER KING D 6	P	V	20	R	171.8	L							
SILVER KING D 7	P	V	25	R	305.1	L			-1.0		1.7		
SILVER KING D 8	P	V	25	R	259.2	L			-2.5		4.2		
SILVER KING D 9	P	V	15	R	236.3	L			-1.0		1.7		
SILVER KING D 10	P	V	25	R	310.8	L			-1.1		1.9		
SILVER KING D 11	P	V	30	R	335.3	L			-0.4		0.7		
SILVER KING D 12	P	V	20	R	257.0	L			-0.8		1.4		
SILVER KING D 13	A	V	15	R	230.6	L			0.2		0.3		
SILVER KING D 14	A	V	15	R	232.0	L			0.3		0.5		
VN-15-A 1	P	III	70	R	474.4	V							
VN-15-A 2	P	III	35	R	337.5	L							
VN-15-A 3	P	III	45	R	510.0	D							

SAMPLE	origin	type	vol %		Th_T (°C)		$Th\ CO_2$ (°C)		Tm cl (°C)	Tm ice (°C)	$Tm\ CO_2$ (°C)	NaCl (wt %)	XCO_2	P (bars)
VN-15-B 1	S	I	35	R	297.0	L								
VN-15-B 2	S	I	25	R	300.4	L					-59.5	0.0		
VN-15-B 3	S	I	35	R	299.1	L					-59.2	0.0		
VN-15-B 4	P	I	30	R	314.5	L	14.6	L	12.8		-59.0	0.0		
VN-15-B 5	P	I	33	40	323.6	L	14.2	L	13.5		-59.3	0.0		
VN-15-B 6	S	I	25	R	293.6	L			10.1					
VN-15-B 7	P	I	30	40	330.5	L	18.4	L	12.5		-58.0	0.0		
VN-15-B 9	P	I	32	40	338.1	L	18.4	L	13.5		-58.1	0.0		
VN-15-C 1	A	I	25	40	316.2	L	18.7	L	13.0		-57.5	0.0		
VN-15-C 2	A	I	43	40	312.6	L	19.0	L	12.3		-57.5	0.0		
VN-15-C 3	A	I	20	40	313.4	L	18.7	L	12.9		-57.5	0.0		
VN-15-C 4	A	I	21	40	315.0	L	18.2	L	12.6		-58.0	0.0		
VN-15-C 5	A	I	40	40	311.4	L	19.1	L	12.8		-57.2	0.0		
VN-15-C 6	A	I	34	40	325.3	L	14.0	L						
VN-15-C 7	A	I	35	R	315.1	L	15.2	L						
VN-15-C 8	A	I	30	R	307.6	L	17.4	L						
VN-15-C 9	A	I	30	R	311.2	L	17.0	L						
VN-15-C 10	A	I					18.3	L						
VN-15-C 11	A	I					18.4	L						
VN-15-C 12	A	I					17.8	L						
VN-15-C 13	A	I					17.6	L						
VN-15-C 14	A	III	25	R	348.3	L				-0.2		0.4		
VN-15-C 15	A	III	30	R	368.4	L				-2.2		3.7		
VN-15-C 16	A	I	29	R	319.3	L	14.8	L	12.3		-58.8	0.0		
VN-15-C 17	A	I	33	R	329.1	L	13.6	L			-57.6	0.0		

SAMPLE	origin	type	vol %		Th_T (°C)		$Th\ CO_2$ (°C)		Tm cl (°C)	Tm ice (°C)	$Tm\ CO_2$ (°C)	NaCl (wt %)	P (bars)
VN-15-D 3	A	I	40	40	310.9	L	16.8	L	11.9		-58.3		
VN-15-D 4	A	III	35	40	403.4	L				-2.2			
VN-15-D 5	S	III	45	40	402.6	L				-3.1			
VN-15-D 6	S	III	25	40	305.8	L				-2.3			
VN-15-D 7	A	I	80	40	303.8	L	16.8	L	10.8		-58.0		
VN-15-D 8	A	I	50	40	321.4	L	17.5	L	11.0		-58.1		
VN-49 2	S	I	35	40	337.2	L	25.4	L	7.4		-57.3		
VN-49 3	A	I	45	40	314.7	L	26.7	L	9.7		-57.0		
VN-49 4	A	I	40	40	311.6	L	26.6	L	9.6				
VN-49 5	A	I	60	40	313.1	L	26.4	L	9.8				
VN-49 6	A	I	50	40	310.6	L	26.1	L	9.7		-57.3		
VN-49 7	A	I	45	40	315.2	L	26.4	L	9.8		-57.0		
VN-49 8	A	I	55	40	338.0	L	24.9	L	8.6				
VN-49 9	A	I	45	40	301.2	L	26.3	L	9.7				
VN-49 10	A	I	45	40	299.2	L	26.5	L	9.7				
VN-49 11	A	III	85	40	362.0	V			9.4				
VN-49 12	A	I	45	40	302.0	L	26.3	L	9.7				
VN-60 1	S	I	38	R	306.0	L	20.5	L			-58.0	1.0	
VN-60 2	A	II	20	R	303.3	L	20.6	V			-58.0	0.4	
VN-60 3	A	I	32	R	296.5	L	22.1	L					
VN-60 4	A	II	20	R	296.8	L	22.2	V					
VN-60 5	S	II	20	R	302.9	L	19.7	V					
VN-60 6	S	II	25	R	298.6	L	20.6	V					
VN-60 7	S	I	40	R	292.9	V	20.2	L					
VN-60 8	S	II			286.0	L							

SAMPLE	origin	type	vol %		Th_T (°C)		$Th\ CO_2$ (°C)		Tm cl (°C)	Tm ice (°C)	$Tm\ CO_2$ (°C)	NaCl (wt %)	XCO_2	P (bars)
VN-60 9	S	III			261.5	L								
VN-60 10	S	I			295.5	L								
VN-60 11	S	I			281.2	L								
VN-60 12	S	I			299.3	L	18.4	L						
VN-221 1	S	III	25	R	297.2	L			7.6			4.7		
VN-221 2	S	III	40	R	321.0	L			10.5			0.0		
VN-221 3	S	III	35	R	295.1	L								
VN-221 4	S	III	40	R	323.9	L			9.3			1.4		
VN-221 5	S	III	20	R	219.5	L								
VN-221 6	S	III	40	R	335.6	L								
VN-221 7	S	III	20	R	357.0	L				-11.5		15.5		
VN-221 8	A	III	25	R	305.5	L								
VN-221 9	A	III	35	R	315.4	L								
VN-221 10	A	III	40	R	368.5	L								
VN-221 11	A	III	35	R	402.2	L								
VN-221 12	A	III	40	R	352.9	L								
VN-221 13	A	III	35	R	398.0	L								
VN-221 14	A	III	30	R	358.3	L								
VN-221 15	A	III	35	R	358.8	L								
VN-25 1	P	III	30	R	381.5	L			11.7			0.0		
VN-25 2	P	III	40	R	452.9	V			11.7			0.0		
VN-25 3	P	III	25	R	455.0	V								
VN-25 4	P	III	35	R	478.4	V								
VN-25 5	A	III	35	R	367.5	V			9.4			1.2		
VN-25 6	A	III	50	R	534.5	V								
VN-25 7	A	III	25	R	358.4	L				-5.2		8.1		

SAMPLE	origin	type	vol %		Th_T (°C)		$Th\ CO_2$ (°C)		Tm cl (°C)	Tm ice (°C)	$Tm\ CO_2$ (°C)	NaCl (wt %)	XCO_2	P (bars)
VN-165 1	P	I	55	R	310.7	L	23.6	L	9.5		-58.5	1.0		
VN-165 2	P	I	45	R	315.0	L	23.7	L	8.7		-57.5	2.6		
VN-165 3	P	I	60	R	310.1	L	23.5	L	8.7		-57.9	2.6		
VN-165 4	P	I	40	R	312.2	L	23.8	L	9.0		-58.0	2.0		
VN-165 5	P	I	35	R	307.6	L								
VN-165 6	P	I	40	R	324.4	L								
VN-165 7	P	I	25	R	305.9	L								
VN-165 8	P	I	30	R	310.6	L								
VN-165 9	P	I	30	R	303.3	L								
VN-165 10	P	I	30	R	316.8	L								
VN-165 11	P	I	30	R	291.3	L								
VN-165 12	P	I	25	R	303.0	L								
VN-165 13	P	I	30	R	305.9	L								
VN-165 14	P	I	35	R	318.4	L								
VN-165 15	P	I	40	R	312.7	L								
VN-165 16	P	I	25	R	308.8	L								
VN-165 17	P	I	35	R	305.6	L								
VN-165 18	P	I	30	R	307.0	L								
VN-165 19	P	I	40	R	318.0	L								
VN-165 20	P	I	30	R	317.4	L								
VN-165 21	P	I	25	R	299.7	L								
VN-165 22	P	I	35	R	317.8	S								
VN-152 1	P	I	45	40	313.0	L	18.6	L	9.8		-57.0			
VN-152 2	P	I	90	40	310.0	V	23.5	L	10.7		-57.2			
VN-152 3	P	I	40	40	314.9	L	17.4	L	9.6		-56.9			
VN-152 4	P	I	35	40	313.3	L	20.1	L	10.5		-57.0			

SAMPLE	origin	type	vol %		Th_T (°C)		$Th\ CO_2$ (°C)		Tm cl (°C)	Tm ice (°C)	$Tm\ CO_2$ (°C)	NaCl (wt %)	XCO_2	P (bars)
VN-310 1	A	II	40	40	292.9	L	11.6	V	10.3		-57.4			
VN-310 2	A	II	60	40	313.8	L	17.3	V	10.2		-57.0			
VN-310 3	A	II	40	40	310.5	L	16.1	V	10.1		-57.0			
VN-310 4	A	II	35	40	320.1	L	18.1	V	9.9		-57.0			
VN-310 7	A	I	65	40	313.9	V	23.4	L	9.2		-58.8			
VN-310 8	A	II	55	40	317.9	L	19.7	V	9.8		-58.8			
VN-310 9	A	II	65	40	328.5	V	17.5	V	9.8		-58.8			
VN-310 10	A	II	70	40	319.4	V	21.9	V	10.2		-58.9			
VN-310 11	A	I	70	40	317.1	V	15.9	L	10.1		-58.5			

APPENDIX 2

DESCRIPTION AND USE OF COMPUTER PROGRAM FI-P-XCO_2

Appendix 2

Description and use of computer program FI-P-X_{CO_2}

This program estimates X_{CO_2} and pressure of entrapment, for three phase H_2O-CO_2-NaCl fluid inclusions, which have been trapped on the two phase immiscibility boundary. The program is written in Microsoft BASIC for a Macintosh Plus table top computer, but is adaptable to any BASIC compiler. A complete description of the method, and a listing of the equations used is given by W.T. Parry, (1986) ("Estimation of X_{CO_2}, P, and fluid inclusion volume from fluid inclusion temperature measurements in the system NaCl-CO_2-H_2O", Economic Geology, vol. 81, p. 1009-1013). The article also includes a table of measurements and results against which the program may be tested.

```
DEFDBL A-Z
PRINT "PROGRAM WRITTEN BY:        Greg Lynch
PRINT " "
PRINT "PROGRAM NAME:              FI-P-XCO2
PRINT " "
PRINT "PURPOSE: This is a BASIC computer program for calculating XCO2 and P"
PRINT "from 3 phase CO2-bearing fluid inclusions. For equations see:"
PRINT "PARRY, W.T., 1986, Economic Geology, Vol. 81, P. 1009-1013."
PRINT "    "
INPUT "CLATHRATE MELTING TEMPERATURE";A

W=15.52022-(1.02342*A)-(.05286*(A^2))          :'WT% NaCl

INPUT "HOMOGENIZATION TEMPERATURE ( C) OF CO2 INNER BUBBLE";B
INPUT "IF HOMOGENIZATION OF CO2 TO LIQUID TYPE 1, OR TO VAPOUR
      TYPE 2";C

IF C=1 THEN GOSUB LCO2 ELSE GOSUB VCO2   :'Calculate saturated CO2 density
E=W*.172 ' MOLALITY OF NaCl
F=(1000*.99164+58*E*.99164)/(1000+17.45*E*.99164+1.71*E^1.5*.99164+.04*E^2
   *.99164)  :'Density of H2O

INPUT "TEMPERATURE OF TOTAL HOMOGENIZATION";L
:'Calculation of parameters for Reidlich-Kwong equation

M=73030000#-71400!*L+21.57*L^2     :'aCO2
U=2.718281828459#^(-11.07+5943/(273.15+L)-
   2746000#/(273.15+L)^2+464600000#/(273.15+L)^3)
N=4.881243+.001823047#*L-.00001712269#*L^2+.000000006479419#*L^3
O=.02636494#-5.369939999999999D-04*L+.000002687074#*L^2-
   .000000004321741#*L^3
P=.006802827#-.0000948023#*L+.0000003770339#*L^2-.000000000507531 8#*L^3
Q=.00005235827#-.00000003505272#*L
R=111.3057+50.70083^(-.00982646#*L)
S=-8.05658^(-.00982646#*L)

INPUT "VOLUME % ESTIMATE OF CO2 (PREFERABLY AT 40 C)";G
INPUT "INITIAL P ESTIMATE (BARS)";Y
```

```
PRINT " "
PRINT "(note: if out of memory error is signalled, then your initial"
PRINT " pressure estimate is too far off of real value, try again)"

DD=D*44 :'converting CO2 in moles/cm3 to g/cm3 from subroutine
FOR JJ=1 TO 10  :'ten itterations to converge results to known 2-phase boundary

:'I,J,and K are used to help in initial XCO2 estimate, X

10   I=(G*DD)/44+2.3*(100-G)/1800

J=(100-G)/18
K=(J*W)*18/5800
X=I/(I+J+K)         :'XCO2 determination (Touret, 1977)

11    T=X^2*M+(1-X)^2*(R+W*S)*1000000!+2*X*(1-
X)*((46000000#*2.718281828459#^(N+W*O+(W^2)*P+W^3*Q)*1000000!)^.5+.5*8
3.12^2*(L+273.15)^2.5*U)
V=X*29.7+(1-X)*(14.6-W*.04420283#)
IF AA=1 THEN GOTO 80  :'itterations complete, proceed to final P determination
VOL=25  :'molar volume for first calculation
77  IF VOL=V THEN GOTO 90  :'error, division by 0
IF VOL=0-V THEN GOTO 91  :'error, division by 0
IF VOL=0 THEN GOTO 92  :'error, division by 0
PP=(83.12*(273.15+L))/(VOL-V)-T/((273.15+L)^.5*VOL*(VOL+V)):'pressure
IF (PP-Y)<0 THEN GOSUB LOWERV ELSE GOSUB ADDV:'adjust volume for correct
                                                          pressure
LOWERV:  'subroutine to decrease volume
VOL=VOL-.01
IF VOL=0 THEN VOL=.005
GOTO 77

ADDV:  'subroutine to increase volume
VOL=VOL+.01
IF PP-Y<=10 THEN GOTO 78 ELSE GOTO 77:'P calculation corresponds to P estimate
                                          within 10 bars
78  DI=(44*I+18*J+58*K)/(VOL*(I+J+K))
G=(DI-F)/(DD-F)*100
Y=PP

NEXT JJ:' itterate

AA=1
GOTO 10:'final XCO2 determination before final P determination
80   PP=(83.12*(273.15+L))/(VOL-V)-T/((273.15+L)^.5*VOL*(VOL+V))

PRINT "    "
PRINT "THE FOLLOWING VALUES HAVE BEEN CALCULATED"
PRINT "    "
PRINT "VOLUME % CO2", ,G
PRINT "XCO2", ,X
PRINT "PRESSURE", ,PP
PRINT "WT % NaCl", ,W
```

```
PRINT "MOL VOL (cm3/mol)",VOL
PRINT "DCO2", ,DD
PRINT "    "
PRINT "IF THESE VALUES DO NOT CORRESPOND TO ESTABLISHED
       EXPERIMENTAL"
PRINT "VALUES FOR SYSTEM, THEN RUN PROGRAM AGAIN USING THESE
       VALUES AS"
PRINT "INITIAL ESTIMATES"
END

90  PRINT "VOL=b"
 END
91  PRINT "VOL=-b"
 END
92  PRINT "VOL=0"
 END

LCO2:  'subroutine to calculate CO2(l) density
B=B+274.15
D=(.42897885#*(1-B/304.21)+.38225012#*(1-B/304.21)^(2/3)+1.9073793#*(1-
B/304.21)^.347+1)*.01059
RETURN

VCO2:  'subroutine to calculate CO2(g) density
B=B+274.15
D=(1.7739244#*(1-B/304.21)-.71728276#*(1-B/304.21)^(2/3)-1.7988929#*(1-
B/304.21)^.347+1)*.01059
RETURN
```

APPENDIX 3

COMPUTER PROGRAM FOR CALCULATING WATER-GRAPHITE EQUILIBRIA

APPENDIX 3

This is a computer program, written in Microsoft Basic for the MacIntosh, which calculates water-graphite equilibria for variable conditions of P, T, and fO_2. For a listing of the equations and thermodynamic data used, the reader is referred to:

Ohmoto, H., and Kerrick, D., 1977, Devolitization equilibria in graphitic systems. American Journal of Science, vol. 277, p. 1013-1044.

```
DEFDBL a-z
INPUT "TEMPERATURE (celcius)";T
INPUT "PRESSURE (bars)";P
INPUT "FUGACITY COEFFICIENTS FOR H2O, CO2, CH4";H2O,CO2,CH4
INPUT "FUGACITY COEFFICIENTS FOR H2S, CO, H2";H2S,CO,H2
INPUT "FUGACITY COEFFICIENTS FOR SO2, COS, S2, S8";SO2,COSS,S2,S8
INPUT "UPPER LOG fO2";UFO2
INPUT "LOWER LOG fO2";LFO2
INPUT "INCREMENTS OF LOG fO2";INC
T=273.15+T
P=P*1.013
FOR N=UFO2 TO LFO2 STEP INC
FO2=10^UFO2
K2=FO2/(CO2*P)*10^(20586/T+.0421+.028*(P/T-1/T))
K3=(CO2/(CO*FO2^.5))*(1/10^(14751/T-4.535))
K4=H2O/(10^(12510!/T-.979*(LOG(T)/LOG(10))+.483)*H2*FO2^.5)
K5=CO2*(H2O^2*P^2)/(CH4*FO2^2*10^(41997!/T+.719*(LOG(T)/LOG(10))-2.404))
K6=FO2*(18929/T-3.783)/(SO2*P*(10599/T-103750!/T^2-.015*(P-1)/T))
K7=CO*(4731/T-4.338)/(COSS*(10599/T-103750!/T^2-.015*(P-1)/T))
K8=10^(-81170!/T+.188*(LOG(T)/LOG(10))-.352)*H2O/(10^(10599/T-103750!/T^2-
.015*(P-1)/T)*(H2S*FO2^.5))
K9=1/((10599/T-103750!/T^2-.015*(P-1)/T)^2*S2*P)
K10=(21446/T-24.43)/((10599/T-103750!/T^2-.015*(P-1)/T)^8*S8*P)
a=K2*K5
b=K4+K8+1
c=K2*K3+K2+K6+K2*K3*K7+K9+K10-1
IF b^2-4*a*c<0 THEN GOSUB NEG
IF a=0 THEN GOSUB LIN
ROOT1=(-b+(b^2-4*a*c)^.5)/(2*a)
ROOT2=(-b-(b^2-4*a*c)^.5)/(2*a)
IF ROOT1<ROOT2 THEN XH2O=ROOT2 ELSE XH2O=ROOT1
5  XCO2=K2
XCO=K2*K3
XH2=K4*XH2O
XCH4=K2*K5*XH2O^2
XH2S=K8*XH2O
XSO2=K6
XCOS=K2*K3*K7
XS2=K9
XS8=K10
LPRINT "     "
LPRINT "LOGFO2", ,"XH2O", ,"XSO2"
LPRINT UFO2, XH2O,XSO2
```

```
LPRINT "XCO2", ,"XCH4", ,"XCOS"
LPRINT XCO2,XCH4,XCOS
LPRINT "XH2S", ,"XCO", ,"XS2"
LPRINT XH2S,XCO,XS2
LPRINT "XH2", ,"XS8"
LPRINT XH2,XS8
10  UFO2=UFO2+INC
NEXT N
T=T-273.15
LPRINT "TEMPERATURE";T
P=P/1.013
LPRINT "PRESSURE";P
END
NEG:
PRINT "SQUARE ROOT OF A NEGATIVE"
GOTO 10
LIN:
XH2O=(-1*c/b)
GOTO 5
```